

---

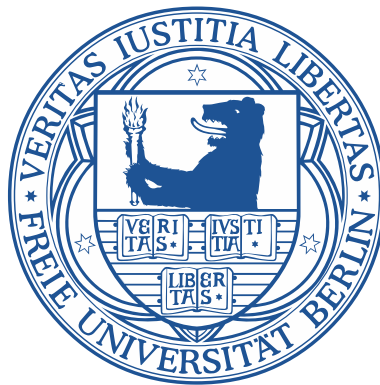
# Switching of Photochromic Molecules on Surfaces

---

Im Fachbereich Physik  
der Freien Universität Berlin eingereichte

## **DISSERTATION**

zur Erlangung des Grades  
**Doktor der Naturwissenschaften (Dr. rer. nat.)**



vorgelegt von

**Fabian Nickel**

Berlin, Juni 2018

---

Erstgutachter:	Prof. Dr. Wolfgang Kuch (Betreuer)
Zweitgutachter:	Prof. Dr. Martin Weinelt
Tag der Disputation:	15. November 2018

# Table of Contents

---

<b>Abstract</b>	<b>i</b>
<b>Kurzfassung</b>	<b>iii</b>
<b>List of Publications</b>	<b>v</b>
<b>1 Introduction</b>	<b>1</b>
<b>2 Spectroscopy of Adsorbed Molecules</b>	<b>7</b>
2.1 Core-Level Spectroscopies . . . . .	7
2.1.1 X-ray Absorption Spectroscopy . . . . .	7
2.1.2 X-ray Photoelectron Emission . . . . .	12
2.1.3 Density Functional Theory for Core-Level Excitations .	14
2.2 Differential Reflectance Spectroscopy . . . . .	16
2.3 Photochromic Molecules . . . . .	19
<b>3 Experimental Methods</b>	<b>21</b>
3.1 XA and XPS Measurements . . . . .	21
3.1.1 Synchrotron Radiation . . . . .	21
3.1.2 Experimental Setup . . . . .	22
3.1.3 XA Detection and Normalization . . . . .	23
3.1.4 Illumination Setup . . . . .	24
3.2 Optical Reflectance . . . . .	25
3.3 Sample Preparation . . . . .	25
3.4 Thickness Calibration . . . . .	26
<b>4 Photochromism on Surfaces</b>	<b>29</b>
4.1 Diarylethene on Surfaces . . . . .	29
4.2 Spiropyran on Bi(111) . . . . .	32
4.3 Spirooxazine on Bi(111) and Au(111) . . . . .	35
<b>5 Summary</b>	<b>39</b>

<b>6</b>	<b>Original Publications</b>	<b>43</b>
6.1	J. Phys.: Condens. Matter 29, 374001 (2017) . . . . .	43
6.2	Adv. Funct. Mater. 27, 1702280 (2017) . . . . .	65
6.3	Rev. Sci. Instrum. 89, 033113 (2018) . . . . .	87
6.4	J. Phys. Chem. C 122, 8031 (2018) . . . . .	99
	<b>Bibliography</b>	<b>117</b>
<b>A</b>	<b>DRS Setup Details</b>	<b>131</b>
A.1	Pictures of the Setup . . . . .	131
A.2	Software . . . . .	134
<b>B</b>	<b>XA Measurement Software</b>	<b>141</b>
B.1	XA Measurement Program . . . . .	141
B.2	Motor Control . . . . .	144
	<b>Acknowledgments</b>	<b>147</b>
	<b>Curriculum Vitae</b>	<b>149</b>
	<b>Selbstständigkeitserklärung</b>	<b>153</b>



# Abstract

---

In the context of this thesis, photochromic molecules of the groups spiropyranes (SPs), spirooxazines (SOs), and diarylethenes (DAEs) on solid surfaces were investigated. These molecular switches were prepared *in situ* in ultrahigh-vacuum by evaporation onto Au(111), Bi(111), and highly oriented pyrolytic graphite (HOPG) substrates. All coverages were below a saturated monolayer to measure molecules in direct contact with a surface. This preparation leads to a detailed picture of the molecule-surface interaction and an understanding of the surface-induced changes to non-decoupled molecules. Using x-ray absorption (XA) spectroscopy, x-ray photoelectron spectroscopy (XPS), and density functional theory (DFT), detailed pictures of the electronic configurations and geometric orientations of the systems are acquired.

First, a thiazol-diarylethene (T-DAE) switch was chosen for investigations on these surfaces. Switching from its open form to the closed form was achieved, but without the possibility for a reversible back-reaction. The stabilized switch on the surface was characterized. To find a fully reversible switch, previous measurements of SPs on surfaces were altered and the commonly used nitro-spiropyran was exchanged with spironaphthopyran (SNP). This modification led on the Bi(111) surface to a fully reversibly switchable system. The photoconversion to merocyanine (MC) took place using a UV LED at temperatures around 200 K. The resulting MC was thermally unstable so that by increasing the temperature above 250 K, back-switching to SNP could be invoked. Using this reversibility, time- and temperature-dependent measurements of the kinetics were performed and resulted in the discovery of an intermediate state. A model was found to explain and fit the behavior of the switching kinetic, which allows for determination of the energy barriers.

To gather a more detailed picture of the interaction between molecular switch and surface, the method of differential reflectance spectroscopy (DRS) was modified and built in a new setup to work with *in-situ*-prepared molecule-surface systems at various temperatures. This method enabled detection of the molecule-surface absorption bands in the UV and visible light range and allowed for a simple and straightforward alternative to measure switching kinetics of adsorbed switches in a lab. The high performance and various possibilities of this experiment were demonstrated by the characterization of the stability, noise level, and measurement modes.

Using DRS, the functionality of the spironaphthooxazine (SNO) photoswitch on Bi(111) was demonstrated. The energy barrier of this photoswitch's MC isomer was determined by DRS to be similar to the one in solution. With the support of DRS, XA, and DFT, SNO has been measured on Au(111), indicating the remarkable possibility of bi-directional photochromism. Using only UV and red-light illumination, a full control over the sample isomerization is achieved. Furthermore, the UV-induced switching is highly efficient, two orders of magnitude more than previously demonstrated.



# Kurzfassung

---

Im Rahmen dieser Arbeit wurden photochrome Moleküle der Gruppen Spiropyran (SP), Spirooxazin (SO) und Diarylethen (DAE) auf Festkörperoberflächen untersucht. Die molekularen Schalter wurden *in situ* im Ultrahochvakuum durch Verdampfung auf den Substraten Au(111), Bi(111) und hochorientiertem pyrolytischen Graphit (HOPG) präpariert. Es wurden Bedeckungen unterhalb einer vollständigen, kompletten Moleküllage gemessen. Dadurch wurde ein detailliertes Wissen über die Molekül-Oberflächen Wechselwirkung sowie ein Verständnis über die oberflächeninduzierten Veränderungen von nicht-entkoppelten Adsorbaten erlangt. Mit Hilfe von Röntgenabsorptionsspektroskopie (XA spectroscopy), Röntgenphotoelektronenspektroskopie (XPS) und Dichtefunktionaltheorie (DFT) wird ein zusammenhängendes Bild der elektronischen Konfigurationen und geometrischen Orientierungen der Moleküle gewonnen.

Im ersten Teil der Arbeit wurde ein Thiazol-Diarylethen (T-DAE) auf den genannten Oberflächen untersucht. Das Schalten von der offenen Form zum geschlossenen Isomer wurde erzielt, allerdings wurde keine Möglichkeit für das Zurückschalten gefunden. Um ein vollständig reversibles Schaltermolekül auf der Oberfläche zu finden, wurden Messungen mit Spiropyran durchgeführt. In der Literatur sind bereits erste Erfolge mit Nitro-Spiropyran erzielt worden. Zum Verbessern der Eigenschaften wurde dieses Molekül durch Spironaphthopyran (SNP) ersetzt. Dies führt zu einem vollständigen schaltenden System auf der Bi(111)-Oberfläche. Mittels einer UV-LED wird bei einer Temperatur von 200 K das SNO zu Merocyanin (MC) geschaltet. Das MC ist thermisch instabil, sodass durch eine Temperaturerhöhung auf über 250 K das Molekül zu SNP zurück geschaltet werden kann. Durch die Reversibilität wird die Bestimmung der involvierten Energiebarrieren ermöglicht. Zeit- und temperaturabhängige Messserien zeigen die Anwesenheit eines Zwischenzustandes. Ein Modell wird diskutiert, welches die Kinetik des Schaltverhaltens beschreibt und damit eine Bestimmung der Barrieren ermöglicht.

Um ein vollständigeres Bild der Wechselwirkung zwischen molekularen Schaltern und Oberfläche zu erhalten, wurde die Methode der differentiellen Reflexionsspektroskopie (DRS) modifiziert und ein neues Experiment zur Messung von DRS an *in-situ* präparierten Adsorbat/Substrat-Systemen bei variabler Temperatur ermöglicht. Dieses Experiment eignet sich zur Bestimmung der Absorptionsbanden des Molekül/Festkörper-Systems und erlaubt die Messungen der Schaltkinetik in einem vergleichsweise einfachen Laboraufbau. Die hohe Qualität der Messungen und die weitreichenden Möglichkeiten des Aufbaus werden demonstriert.

Mit DRS kann erfolgreiches Schalten des Moleküls Spironaphthooxazin (SNO) auf Bi(111) gezeigt werden. Die Energiebarrieren des Schaltens auf der Oberfläche sind ähnlich hoch wie bei Messungen in Lösungen. Mit Hilfe von DRS, XA und DFT wird gezeigt, dass SNO auf Au(111) einen vollständig lichtinduzierten Photochromismus aufweist. Eine Kontrolle über die Isomerisierung der Probe wird mit UV und rotem Licht erreicht. Dabei ist das UV-induzierte Schalten um zwei Größenordnungen effizienter als bei zuvor gemessenen Photoschaltern.



# List of Publications

---

This thesis is a cumulative work and consists of four publications briefly described below and reprinted in chapter 6.

- [FN 1] **F. Nickel et al., Journal of Physics: Condensed Matter 29, 374001 (2017):**  
*Light-induced Photoisomerization of a Diarylethene Molecular Switch on Solid Surfaces*  
A first approach to identifying the switching abilities of diarylethene derivatives on surfaces by x-ray methods is presented in this publication. A modified diarylethene, which is sensitive to soft x-ray absorption due to the presence of nitrogen, was evaporated on Bi(111) and highly oriented pyrolytic graphite (HOPG). In addition to characterization and comparison to density functional theory (DFT) simulations, a switching process was invoked by UV- and visible light illumination on both surfaces. *Reprinted on page 43.*
- [FN 2] **F. Nickel et al., Advanced Functional Materials 27, 1702280 (2017):**  
*Reversible Switching of Spiropyran Molecules in Direct Contact With a Bi(111) Single Crystal Surface*  
To find a fully controllable molecular switch on a surface, various substitutions of the spiropyran have been tested. This variation led to a fully functional molecular switch on a Bi(111) surface, where the reversibility has been demonstrated by UV light and temperature increase. Using x-ray absorption spectroscopy and temperature-dependent measurements, the most important energy barriers in the switching process were quantified. *Reprinted on page 65.*
- [FN 3] **F. Nickel et al., Review of Scientific Instruments 89, 033113 (2018):**  
*Optical Differential Reflectance Spectroscopy for Photochromic Molecules on Solid Surfaces*  
Since the x-rays were seen to influence some systems including photochromic molecules, a new approach was needed to investigate adsorption and switching of molecules on surfaces in the lab. This method was found with the differential reflectance spectroscopy (DRS). This publication describes our new experimental setup to perform DRS at various temperatures in ultrahigh vacuum. A demonstration of the potential is performed by quantification of the kinetics of a spirooxazine derivate on the Bi(111) surface. *Reprinted on page 87.*
- [FN 4] **F. Nickel et al., The Journal of Physical Chemistry C 122, 8031 (2018):**  
*Highly Efficient and Bidirectional Photochromism of Spirooxazine on Au(111)*  
With the help of the previously established DRS setup, the identification of a purely light-induced, reversible switching photochromic system of spirooxazine on a Au(111) surface was possible. Finally, the frequently-used gold surface can be utilized with a switch, with which the effective cross-section of photoconversion on the surface is increased by two orders of magnitude. *Reprinted on page 99.*

A complete list of publications, including the ones not related to this thesis, is provided on page 150.



# Introduction

## Towards the control of photochromic molecules on solid surfaces

Manipulation of material properties on the nanoscale is key to the research and development of novel materials [1]. As early as 1959, future Nobel prize laureate Richard Feynman noted in a lecture called “*There’s Plenty of Room at the Bottom*” the incredible number of possibilities for future devices to be still discovered down to the atomic scale [2]. Since then, a great many research fields have focused on minimization. Many of Feynman’s predicted technologies have already been realized, so that computing devices have been shrunk down very close to their physical limits; IBM, for example, has already achieved the fabrication of 5-nm-sized gates [3].

Recently, in 2016, the Nobel prize in chemistry was awarded to Jean-Pierre Sauvage, Sir James Fraser Stoddard, and Bernard Lucas Feringa for the design and synthesis of molecular machines [4]. The findings of these scientists represent a substantial leap forward in the realization of molecular motors, which can be utilized to spin a glass cylinder on top of a liquid crystal [5] or move a molecule, called a nanocar, on a copper surface [6].

To reach application-ready systems, different techniques have been explored. The classic computer processors in widespread use nowadays are manufactured in a top-down approach, by writing onto a chip using lithography. These lithography methods have improved over time but have also hit a limit, where production becomes incredibly expensive. In the so-called bottom-up approach for creating machines on the nanoscale, the smallest possible building blocks are produced by the functionalization of atoms or molecules [7, 8]. This promising technique has proven itself to be highly diverse but still exceedingly challenging. Despite the complexity of the bottom-up approach, this method in contrast with the top-down method is more versatile and allows for complex molecular logic devices. Furthermore, the production costs, which increase drastically for research and production of classical semiconductor devices, can potentially be minimized. Requirements of the building blocks include external control and handling on the nanoscale. Both of these requirements can be delivered by molecular

switches. Upon external stimuli, these molecules can be switched to another species. Therefore, those systems that allow for noninvasive and remote spatial and temporal control are of significant interest. Such stimuli can be provided by reaction to light, which is already utilized for triggering the release of drug delivery systems [9] and is present naturally for human vision [10, 11]. An important class of switches are photochromic molecules with the ability to switch by exposure to light between two different isomers. Many groups of photochromic molecules can be converted from an uncolored species to a colored form by ultraviolet (UV) light and back again using visible light. Through their intrinsic properties, these molecules can be directly used as building blocks. Not only does the absorption spectrum change upon switching, but additional chemical modifications also take place. Therefore, plenty of applications already include photochromic molecules. Besides utilization of the different optical absorption spectra in self-coloring sunglasses [12], more advanced functions have also been suggested. For example, data storage and logic circuits could be further improved [13, 14], since possible applications of optically accessible transistors [15], molecular memories [16] or logic modules [17] have recently been demonstrated.

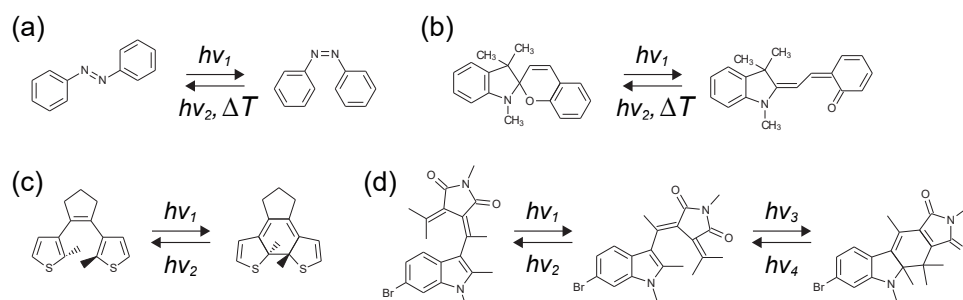


**Figure 1.1:** Isomers of four different groups of photochromic molecules and their photochromic reaction through light exposure or temperature increase. Illustrated are (a) azobenzene, (b) spiropyran, (c) diarylethene, and (d) fulgimide.

In the 20th century, many groups of photochromic molecules were found or invented. Nowadays, the majority of research in different fields is performed using the groups of (a) azobenzenes, (b) spiropyranes, (c) diarylethenes, and (d) fulgimides; a selection of such groups is presented in figure 1.1. Upon isomerization, these groups offer a broad range of change of chemical properties. Not only can their conformation switching be controlled [18], but also properties such as electric dipole moment [19], coordination properties [20], and conductance [21, 22]. These groups have distinct properties which led to famous applications such as optical



storage [23, 24] and light-powered motors [25] by azobenzene or force sensors [26] and photocontraction [27] by spiropyran. Diarylethene has also demonstrated a high potential to work as a switch for electron transport in single-molecule junctions [17, 28–30], or even in complex devices such as molecular transistors with distinct levels [16]. Furthermore, combinations of photochromic molecules were used to realize molecular logic gates by a fulgimide-porphyrin-diarylethene triad [31].

As part of the building blocks for the bottom-up approach to produce innovative molecular logic modules, molecules must be immobilized on a surface. Once the molecules are localized, either tuning the surface properties or using the intrinsic changes upon switching can be exploited. One approach to coat photochromic molecules onto surfaces is the self-assembled monolayers (SAMs), where linker groups on the organic molecule build a contact to the surface. Numerous important achievements have been realized using SAMs containing the above-mentioned groups of molecules on different surfaces [29, 32–38]. SAMs allow for a simple *ex-situ* preparation, but lead to a more complex chemical system and have drawbacks when targeting molecular electronics. Such molecular electronics might be realized by molecules in direct contact with metal surfaces, where the switching ability must persist. Direct contact with surfaces allows addressability by localized excitation, e.g., by a scanning tunneling microscope (STM) or by break junctions. For these experiments, several surfaces are suitable in principle, but have demonstrated drastically different properties in combination with adsorbed molecules. Great effort in theoretical and experimental physics has been made to understand or predict changes of chemical properties upon adsorption, but so far, no reliable method has been found. Therefore, the fully light-induced switching in direct contact with surfaces has not been achieved. In contrast, in a nanometer-thick spiropyran (SP) layer on MgO(100), switching has been reported [39]. For SP directly on the Bi(110) surface, a photostationary state upon illumination with blue light was demonstrated and attributed to bi-directional switching [40]. Most interestingly, it has been observed that for a SP derivate containing a nitro group in contact with a Au(111) surface the thermal stability is reversed [41]. For the group of azobenzenes, previous achievements include a deeper understanding of the adsorption energies and influences by surfaces [42–46], but did not lead to a reliable photo-control of the isomerization [45, 47–52].

Investigation of the targeted systems was mainly carried out by means of well-known surface science methods. Using these methods, recording

of small signals due to small coverages was possible and enabled progress in this field. Frequently, electron or x-ray-based methods such as low energy electron diffraction (LEED), x-ray absorption (XA) spectroscopy, or x-ray photoelectron spectroscopy (XPS) were used, but a particular issue with these methods is the damage caused by x rays or electrons. Beside exciting photoconversions, as seen with azobenzene on Bi(111) [53], triggering spin-crossover transitions [54] has also been observed. Molecules are also often destroyed by electron bombardment or x-ray influence, as seen in many studies, and therefore special attention was paid when investigating these systems [FN 4, 55]. Nevertheless, XA spectroscopy and XPS are powerful tools for investigating photochromic molecules on surfaces [41, 44, 56]. Isomers can be determined and characterized in a high quality and in contrast to other local methods, providing an average over the measurement spot size, which can be increased up to several square millimeters. These non-local observations lead to the possibility of observing the kinetics of a switching process and are therefore used for investigations presented in this work. XA spectroscopy can also be assisted by simulations using density functional theory (DFT), which helps in particular to identify isomers on the surface. The first working examples of one-directional photochromism on surfaces were rather inefficient, with cross-sections orders of magnitude below their potential efficiency determined by experiments in solution. Two important targets can be identified to advance progress in this field:

- (1) tailoring a system to switch bi-directionally at the same temperature by light-illumination as the only trigger.
- (2) improving the effective cross-sections to allow for a deeper investigation of the system, and later on, to lead to an application, e.g., in material science.

Finding a system which delivers such properties is complicated. Choosing from the most common groups of photochromic molecules, illustrated in figure 1.1, and identifying their changes on a surface is a good starting point. Diarylethene (DAE) is a robust switch in which ring-opening and ring-closing possesses a high fatigue resistance and can only be converted between each other by light. The switching also leads to two clear distinguishable states, so that for a nitrogen modified DAE derivate (T-DAE, 1,2-bis(5-methyl-2-phenylthiazol-4-yl)cyclopent-1-ene), studies on different surfaces were performed in the context of this thesis [FN 1] (reprinted on page 43). Since no reversible switching was achieved for DAEs, further investigations were performed on SPs, which demonstrated a promising photostationary state upon blue laser illumination on the Bi(110)

surface [40]. Using spironaphthopyran (SNP, 1,3,3-trimethylindolino- $\beta$ -naphthopyrylospiran) on a Bi(111) surface, a fully reversible switching was achieved, including determination of energy barriers, by performing temperature and time-dependent XA measurements [FN 2] (reprinted on page 65). To achieve a fully reversible light-induced switching, the SNP was modified to a spirooxazine derivate, more specifically spironaphthooxazine (SNO, 1,3,3-trimethylindolino-naphthospirooxazine). On a Au(111) surface, where previously a SP derivate revealed a thermally reversed behavior [41], a fully light-induced control of the sample isomerization was achieved [FN 4] (reprinted on page 99).

To improve studies on these potential photoswitch/surface candidates, avoiding the x-ray influence and simplification of the experimental setup are key challenges. With an experiment performed in a lab, the knowledge gathered by time-consuming and complex experiments using synchrotron radiation, such as XPS and XA spectroscopy, can be complementarily extended. One solution is the application of differential reflectance spectroscopy (DRS) for adsorbed photochromic switches. This method has already led to profound results in the field of alloys [57] or semiconductors treated by adsorbates [58] and is well known and described. For organic semiconductors, many properties were obtained and assisted research to tailor opto-electronics [59–63]. Contrary to the x-ray-based methods, visible and ultraviolet light is used for the spectroscopy. The absorption cross-section is very low; consequently, dealing with small signals rendered use of this method uncommon for surface science investigations until recent years when the quality of measurement equipment improved. Understanding of the interaction between molecules in direct contact or thicker layers on a surface can be obtained. These interactions include growth [60], charge transfer [62], or decoupling properties [63]. For SAMs, DRS measurements already led to promising results for systems measured at ambient conditions [35, 64, 65]. However, DRS of photochromic systems under ultrahigh-vacuum (UHV) conditions has not yet been performed. This method could create a valuable extension of common measurement methods for photochromic molecules, due to these molecules' strong change of optical properties upon isomerization.

Designing and building such a DRS system is part of this work. Two main properties for the application to photochromic molecules in very low coverages on solid surfaces were identified: 1) the temperature must be variable to study energy barriers and relaxation behavior at different temperatures and a monochromatic setup could potentially increase the usage

with highly efficient switching molecules; and 2) the influence of the measurement light must be kept at a minimum. Setup and results for the newly-built experiment are published in Ref. [FN 3] (reprinted on page 87) and parts of the theoretical background described in chapter 2 of this thesis.

Beside the brief presentation of the published results in chapter 4 and their reproduction (chapter 6), experimental details are also described in chapter 3 and a conclusive summary is provided in chapter 5.

# Spectroscopy of Adsorbed Molecules

Investigation of adsorbed molecules in submonolayers on surfaces requires advanced measurement techniques and environments. Due to low coverages, the effective signal of the molecules, compared to the background of the solid substrate, is very small. Surface-sensitive methods are necessary to identify changes of the geometry or the electronic properties of the organic switch. To begin this thesis, all used experimental and theoretical techniques are briefly described in this chapter. Complementary to this theoretical introduction, the experimental details are described in chapter 3.

## 2.1 Core-Level Spectroscopies

The following section presents the fundamental concepts and descriptions of the applied x-ray-related methods of XA spectroscopy by  $1s$  electrons, XPS, and DFT. DFT is explained with a special focus on the simulation of XA spectra.

These methods have been frequently applied to molecules on surfaces and have also been demonstrated to provide a high reliability and comprehensive amount of information. These methods utilize excitations of the core levels of a sample, which offers the valuable information about occupied and unoccupied electronic states. The angle dependence of XA even leads to conclusions on the geometry with respect to the surface. With the help of DFT simulations, a better understanding of the results can be gained.

### 2.1.1 X-ray Absorption Spectroscopy

XA spectroscopy, often also referred to as near-edge x-ray absorption fine-structure (NEXAFS), deals with the absorption of an x-ray photon with the

energy  $E_{\text{ph}} = \hbar\omega$  by a core level electron, leading to excitation to an unoccupied state. In the context of organic molecules,  $1s$  electrons are often measured using this technique and denoted as  $K$ -edges. Photon energies for these processes are typically in the soft x-ray regime below 2 keV and therefore, photoelectric absorption is the dominant type of interaction between x-rays and matter. A more detailed explanation of XA is offered by J. Stöhr [66].

To describe the absorption of a photon by matter, a quantum mechanical notation provided by the perturbation theory can be applied [66]. The probability  $\lambda_{i \rightarrow f}$  for a transition from an initial eigenstate  $|i\rangle$  to the final state  $\langle f|$  with a density  $\rho$  at the final state energy in a unit of time is described by Fermi's Golden Rule as:

$$\lambda_{i \rightarrow f} = \frac{2\pi}{\hbar} \rho |\langle f | H' | i \rangle|^2. \quad (2.1)$$

The incoming x-rays lead to the time-dependent harmonic perturbation  $H'$ . As mentioned above, initial states  $|i\rangle$  are core electron states, often of the  $1s$  shell. The final states  $\langle f|$  can be either bound or continuum states. The perturbation  $H'$  originates from the perturbation on an electron in a plane electromagnetic wave, with the vector potential  $\mathbf{A}$ . The Coulomb gauge<sup>1</sup> is applied and terms of higher order are neglected:

$$H' = \frac{-e}{2mc} \mathbf{A} \cdot \mathbf{p}. \quad (2.2)$$

This vector potential can be expressed as:

$$\mathbf{A}(\mathbf{r}, t) = e A_0 e^{i(\mathbf{k} \cdot \mathbf{r} - \omega t)}, \quad (2.3)$$

where  $\mathbf{k}$  is the wave vector and  $e$  a unit vector of the polarization.

At this point, an assumption already simplifies the physical problem. In the so-called electric dipole approximation, the wavelength of the x-rays is assumed to be much larger than the size of an atom<sup>2</sup>. Expanding the vector potential for  $\mathbf{k} \cdot \mathbf{r} \ll 1$  leads to only a time dependency remaining as  $\mathbf{A}(t) = e A_0 e^{-i\omega t}$  and therefore to a transition probability of

$$\lambda_{i \rightarrow f} = \frac{\pi}{\hbar} \frac{e^2}{2m^2 c^2} A_0^2 \rho |\langle f | e \cdot \mathbf{p} | i \rangle|^2. \quad (2.4)$$

<sup>1</sup>By using the Coulomb gauge, the divergence of the vector field vanishes:  $\nabla \cdot \mathbf{A}(\mathbf{r}, t) = 0$ .

<sup>2</sup>For example, for nitrogen ( $K$ -shell energies around 400 eV) the excitation wavelength is around 3.9 Å, whereas the core diameter as estimated by the Bohr radius is approximately 0.15 Å.

A more physical meaningful expression can be derived, taking the photon flux  $F_{\text{ph}}$  into account, replacing the linear momentum operator, and deriving the x-ray absorption cross-section as  $\sigma_{\text{x-ray}} = \lambda_{i \rightarrow f} / F_{\text{ph}}$  [66]:

$$\sigma_{\text{x-ray}} = \frac{4\pi e^2}{m^2 c \omega} \rho |\langle f | \mathbf{e} \cdot \mathbf{p} | i \rangle|^2 = \frac{4\pi e^2}{\hbar c} \rho \cdot \hbar \omega |\langle f | \mathbf{e} \cdot \mathbf{r} | i \rangle|^2. \quad (2.5)$$

When the photon energy  $\hbar\omega$  is close to the energy of a core level, excitations to unoccupied states are possible and described by the cross-section in equation (2.5). These strong absorptions close to an absorption edge can be utilized in an element-selective analysis of adsorbate properties. Figure 2.1 sketches the basic principle of XA spectroscopy on an abstract two-atomic molecule. A photon gets absorbed, e.g., by atom X, of which a core electron is excited to an unoccupied, bound molecular state. The photon energy must match the difference  $E = \hbar\omega = E_f - E_i$  between a final and the initial state. This absorption can in principle be monitored by detecting the transmitted photons behind a sample consisting of a thin foil, but typically a measurement of secondary electrons is simpler. In this work, the total electron yield (TEY) as explained in more detail for the experimental details in section 3.1.3 is used.

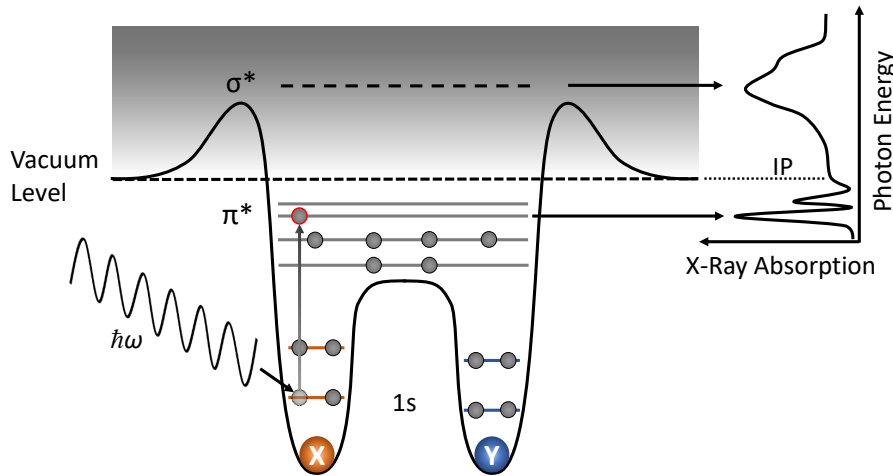


**Figure 2.1:** Illustration of the principle of x-ray absorption (XA) spectroscopy for the case of a diatomic molecule. A photon (energy  $\hbar\omega$ ) gets absorbed by a core level electron (e.g.  $1s$  shell). In the case of matching photon energy, the electron gets excited to an unoccupied molecule orbital, leading to an absorption signal, as illustrated in the spectrum on the right.

The resulting spectrum as illustrated in figure 2.1 can be described by different cases for the photon excitation energies. First, for  $E_{\text{ph}} \ll E_B$ , with



$E_B$  being the binding energy to excite the corresponding core electron to the vacuum, no photons are absorbed by the element  $X$ . For  $E_{ph} < E_B$ , the electron is excited from a core hole (the  $1s$  in the sketch) to an unoccupied molecular orbital (the lowest unoccupied molecular orbital (LUMO) in the sketch). These resonances are typically of  $\pi^*$ -nature and have a small natural linewidth around 0.1 eV for light elements such as nitrogen and oxygen [66, 67]. The experimental conditions such as resolution of the x-ray light cause additional broadening of the resonance.

Photon energies above the ionization potential (IP) of core electrons lead to the broad, so-called  $\sigma^*$  resonances. These excitations to virtual orbitals with very short life-times lead to a broad absorption signal. Close to the IP, a step-like absorption can be identified, but is experimentally not always fully visible. Importantly, when measuring for photon energies further above the  $\sigma^*$  resonances, only the absorption edge by ionization of core electrons is present. This value is proportional to the number of absorbing atoms and can therefore be used to determine amounts of atoms of specific elements on the surface when using a proper normalization and calibration.

The XA spectrum of a molecule can become quite complex, especially for larger molecules with a high density of unoccupied orbitals, to which can be excited to. A disentanglement by pure experimental observations is difficult, but may be carried out for identification of chemical groups with a very specific, known XA. This disentanglement has been performed in Ref. [68], where the absence of a phenanthroline group on a Au(111) surface was identified by independent investigation of the molecule moieties. For a more detailed understanding of molecule XA, theoretical methods are necessary, of which the most-applied one is DFT. Using DFT, in addition to the calculation of the electronic structure, a simulation of the XA spectrum is possible and explained in more detail in section 2.1.3.

XA spectroscopy is not only sensitive to the electronic configuration, but also to the orientation of molecular orbitals and polarization of light. As described by equation (2.5), the initial and final state both determine the absorption cross-section. The intensity  $I$  of a transition is hereby proportional to:

$$I \propto |e \cdot \langle f | \mathbf{r} | i \rangle|^2. \quad (2.6)$$

The incoming light is described by the polarization vector  $e$ , and the initial state of interest is a  $1s$  state. We consider the x rays to be purely linear and therefore exciting the electron by the electronic dipole selection rule  $\Delta l = \pm 1$  to a  $p$ -orbital only. The initial  $s$ -orbital has an isotropic charge distribution and, therefore, does not need to be taken into account for the angle dependence. For the description of the final state orbital, a



differentiation between vector- and plane-type orbitals must be performed [69]. For example, for a double bond, there exist two vector-type orbital directions  $\mathbf{O}$ ; one  $\sigma^*$  binding in direction of the molecule axis and, second, a  $\pi^*$ -orbital with direction orthogonal to the binding direction. For an aromatic ring, a  $\sigma^*$  plane-type orbital lies in-plane and a  $\pi^*$  vector-type orbital is directed out of the molecule plane, which is visualized in figure 2.2(b). The relevant orientations to the XA are described by the angle  $\alpha$  between the molecule orbital direction  $\mathbf{O}$  and the surface normal and the angle of the polarization vector  $\mathbf{e}$  to the surface normal<sup>3</sup>.

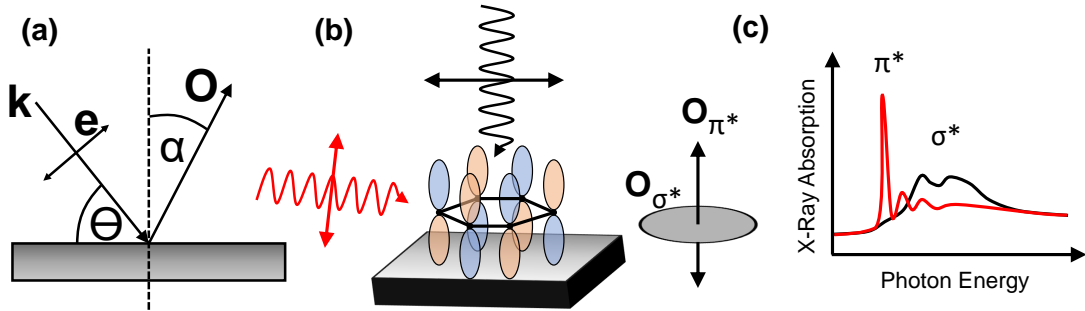


**Figure 2.2:** Schematic drawings for the determination of the angular orientation of orbitals. (a) The defined angles:  $\Theta$  between the wave vector and surface,  $\alpha$  between the orbital  $\mathbf{O}$  and the surface normal. (b) A benzene molecule on a surface with a representation of its  $p$ -orbitals. In red, the incoming x-ray wave in p-polarization in grazing incidence and in black, x-rays in normal incidence. The orbital's direction for the  $\pi^*$ -system is of vector type out-of-plane ( $\mathbf{O}_{\pi^*}$ ) and for the  $\sigma$ -orbitals (not sketched) a plane-type orbital  $\mathbf{O}_{\sigma^*}$ . (c) Different XA spectra for grazing p-polarized light (red) and normal incidence (black) in the case of benzene.

Figure 2.2(a) illustrates a scenario with an angle of incidence  $\Theta$  between the x-ray direction and the surface plane and a molecular orientation  $\mathbf{O}$  with an angle  $\alpha$  to the surface normal. The orientation and unit vector of polarization can be expressed using spherical coordinates (and including azimuth angles  $\varphi_{1,2}$ ) as:

$$\mathbf{e} = \begin{pmatrix} \cos \varphi_1 \sin \Theta \\ \sin \varphi_1 \sin \Theta \\ \cos \Theta \end{pmatrix}, \quad \mathbf{O} = \begin{pmatrix} \cos \varphi_2 \sin \alpha \\ \sin \varphi_2 \sin \alpha \\ \cos \alpha \end{pmatrix} \quad (2.7)$$

Aligning the coordinate system to the incoming wave's polarization vector simplifies the calculation and in the case of a threefold or higher

<sup>3</sup>The angle between  $\mathbf{e}$  and the surface normal is equal to the angle  $\Theta$  between the wave vector and surface as shown in figure 2.2(a).

substrate symmetry (which is the case for the used substrates) or random molecule orientations, the azimuthal angle can be removed by integration of the absorption intensity, following equation (2.6):

$$I \propto \frac{1}{2\pi} \int_0^{2\pi} d\varphi (e \cdot \mathbf{O})^2 = \cos^2 \Theta \cos^2 \alpha + \frac{1}{2} \sin^2 \Theta \sin^2 \alpha \quad (2.8)$$

This equation determines a proportionality of intensity as a function of angle of incidence  $\Theta$  and molecule orientation tilting angle  $\alpha$ . By measuring XA at two different angles, such as normal incidence (fixed as  $\Theta_{\text{normal}} = 90^\circ$ ) and grazing incidence  $\Theta_{\text{grazing}}$ , a determination of the intensity ratio  $R = I_{\text{grazing}}/I_{\text{normal}}$  of a resonance is possible. The average angle  $\alpha$  of the probed orbital orientations can thereby be calculated as:

$$\alpha(R) = \arccos \sqrt{1 - \frac{2 \cos^2 \Theta_{\text{grazing}}}{R - 1 + 3 \cdot \cos^2 \Theta_{\text{grazing}}}} \quad (2.9)$$

In the case of a flat adsorbed aromatic system on a surface, which is of high importance to this thesis, x-rays in normal incidence do not probe the  $\pi^*$  orbital out-of-plane, but probe the  $\sigma^*$  resonances at higher energy. Such an example is depicted in figure 2.2(c). The situation is reversed for (experimentally impossible) grazing incidence within the surface plane ( $\Theta_{\text{grazing}} = 0^\circ$ ). In the case of an angle  $\Theta_{\text{grazing}} = 54.7^\circ$ , no orbital orientation is present anymore ( $R = 1$ ) and the total isotropic absorption of a sample is probed.

Equation (2.9) is applied for single resonances; however, if a deconvolution of resonances is not possible or the orbitals exhibit a more complex behavior and are not localized on a certain group of the molecule, analysis of the orientation is only possible with the help of additional DFT calculations.

### 2.1.2 X-ray Photoelectron Emission

In addition to probing the unoccupied states by the previously described XA spectroscopy, probing the occupied states of a system is also valuable to obtain information about the electronic structure. One technique that allows the investigation of the occupied electronic states is XPS. The absorption of a photon with energy  $E_{\text{ph}} = \hbar\omega$  by a core-level electron with binding energy  $E_B$  leads in the simple single-electron picture to a release of the excited electron, if the photon energy is sufficiently high with  $E_{\text{ph}} > E_B$ . Contrary to XA spectroscopy, the measurement is not done by varying the incoming photon energy, but by scanning the energy of the released electrons.

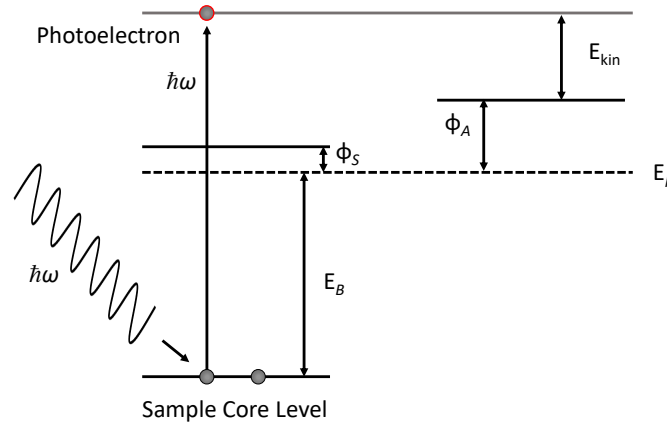


**Figure 2.3:** Illustration of the principle for x-ray photoelectron spectroscopy (XPS). A photon (of energy  $\hbar\omega$ ) is absorbed by a core level electron (e.g. 1s shell), which is excited and leaves the sample. This electron can be measured with a kinetic energy  $E_{kin}$  relative to the work function level of  $\Phi_A$  of the electron analyzer. The Fermi levels  $E_F$  of analyzer and sample are aligned to be able to calculate the core-electron binding energy  $E_B$ .

XPS in particular is useful to quantify elemental compositions in a system, because typical binding energies can be assigned to certain elements.

In the so-called photoelectric effect, the kinetic energy  $E_{kin}$  of the released electrons is determined by:

$$E_{kin} = \hbar\omega - E_B - \phi_A. \quad (2.10)$$

$\hbar\omega$  is again the incoming photon's energy,  $E_B$  is the binding energy of the electron in its initial state, and  $\phi_A$  is the work function of the analyzer. An energy scheme of the process is illustrated in figure 2.3, where a sample core electron is excited and the corresponding energies are denoted according to equation (2.10). Due to an electrical contact between analyzer and sample, their Fermi levels ( $E_F$ ) are aligned and knowing the value of the analyzer work function  $\Phi_A$  is sufficient. Binding energies are influenced by the electron's chemical environment. Chemical shifts may appear of the order of electron volts, depending on the interaction of the atom with its neighbors. In XPS, photoelectron measurement counts or count rates are typically plotted against the binding energy. Consequently, s-type orbitals lead to one peak, whereas the spin-orbit coupling for shells with an angular momentum  $l > 0$  leads to a peak splitting into a doublet. The quantitative analysis of the binding energies  $E_B$  through XPS allows for identification of state or element concentration in the recorded spectrum by comparing the areas after a background correction.

### 2.1.3 Density Functional Theory for Core-Level Excitations

As previously mentioned, a theoretical simulation of the core-electron levels and absorptions can assist the previously described methods significantly. The well-known and most-applied method of DFT allows for simulation of XA spectra and therefore a deeper interpretation of the electronic structure and geometric information. For the DFT analysis in this thesis, the StoBe code package has been used [70]. This package is described in more detail and has been applied to the identification of XA of various molecules in literature [56, 71–73]. It has been demonstrated that even an interpretation of large molecules such as porphines or porphyrines on surfaces is possible [74–76], even though the calculation does not include a surface. For photochromic molecules on surfaces, this package has previously been used to interpret the results of azobenzenes [44, 56] or spiropyranes [41]. This section provides a brief summary of DFT methods, particularly the application of the StoBe code.

In quantum mechanics, the electronic structure of a system can be described by the Schrödinger equation. In the case of a time-dependent, non-relativistic system for an arbitrary molecule this equation is given as:

$$(\hat{T}_e + \hat{V}_{ee} + \hat{V}_{en} + \hat{T}_n + \hat{V}_{nn})\psi = E\psi. \quad (2.11)$$

The kinetic energy contributions are represented by the operators  $\hat{T}$  and the potential energies by the operators  $\hat{V}$ .  $\psi$  is the quantum mechanical state as a function of all electrons and nuclei coordinates. Various contributions are included, namely from the kinetic energy of the electrons ( $\hat{T}_e$ ), electron-electron repulsion ( $\hat{V}_{ee}$ ), electron-nuclei attraction ( $\hat{V}_{en}$ ), nuclei kinetic energy ( $\hat{T}_n$ ), and the nuclei-nuclei repulsion ( $\hat{V}_{nn}$ ).

At this point, simplifications of the Schrödinger equation are already possible. The Born-Oppenheimer approximation states that the movements of nuclei are much slower than those of electrons, allowing for a separation of the electron and nuclei wave functions as  $\psi_{\text{total}} = \psi_{\text{electrons}} \times \psi_{\text{nuclei}}$ . The Hamiltonian in the Schrödinger equation in equation (2.11) simplifies to a so-called electronic Hamiltonian, where only the operators including electronic energies are present:

$$\hat{H}_{\text{elec}}\psi_{\text{elec}} = E_{\text{elec}}\psi_{\text{elec}}, \quad (2.12)$$

with  $\hat{H}_{\text{elec}}$  consisting of the sum of kinetic and potential energies [77]:

$$\hat{T}_e = -\frac{1}{2} \sum_{i=1}^N \nabla_i^2, \quad (2.13a)$$

$$\hat{V}_{ee} = - \sum_{i=1}^N \sum_{j>i}^N \frac{1}{|\mathbf{r}_i - \mathbf{r}_j|}, \quad (2.13b)$$

$$\hat{V}_{en} = - \sum_{i=1}^N \sum_{A=1}^M \frac{Z_A}{|\mathbf{R}_A - \mathbf{r}_i|}, \quad (2.13c)$$

where  $N$  is the number of electrons and  $M$  the number of nuclei.

The potential energy of nuclei-nuclei repulsion is only treated as a constant  $V_{nn}$  and the nuclear coordinates are not explicitly present in  $\psi_{\text{elec}}$ . The total energy of the system is in this case the sum of nuclear energies and electronic energies, given as  $E_{\text{tot}} = E_{\text{elec}} + E_{\text{nuclear}}$ . In principle, this equation is already possible to solve, e.g. by the variational principle [77]. However, an important drawback is the dimensionality of  $3N$  of the problem, which causes a too high demand on computational power for larger systems.

Using DFT, it is possible to overcome these limitations and drastically reduce the computational costs. Instead of treating every electron wave function as independent, the electron density  $\rho(\mathbf{r})$  (or more accurate, the probability density) is used and reduces the dimensionality of the problem to three. In 1964, Pierre Hohenberg and Walter Kohn stated in the Hohenberg-Kohn theorem that (1) the ground state electronic energy  $E_0$  and all properties are determined by the electron density  $\rho(\mathbf{r})$  and an external potential  $V_{\text{ext}}$ , and (2) according to the variational principle, the total energy is minimal for the real ground state density  $\rho_0$  [78].

To further reduce the problem, a combination of non-interacting single-electron functions leads to a simplification of the Schrödinger equation. These so-called Kohn-Sham orbitals solve the Schrödinger equation for single particles with wave functions  $\phi_i$  as:

$$H_{\text{KS}}\phi_i = \epsilon_i\phi_i. \quad (2.14)$$

The system of artificial non-interacting single-electron wavefunctions is connected to the real density, so that it equals the ground state density of the target system of interacting electrons:

$$\rho(\mathbf{r}) = \sum_{i=1}^{\text{occ}} \sum_{s=1}^{\text{spin}} |\phi_i(\mathbf{r}, s)|^2 = \rho_0(\mathbf{r}). \quad (2.15)$$

Using the Lagrange formalism [79], the Kohn-Sham equations can be solved as [77]:

$$\left( -\frac{1}{2}\nabla^2 - \sum_{A=1}^M \frac{Z_A}{|\mathbf{R}_A - \mathbf{r}|} + \int \frac{\rho(\mathbf{r}')}{|\mathbf{r} - \mathbf{r}'|} d\mathbf{r}' + V_{xc}[\rho(\mathbf{r})] \right) \phi_i = \epsilon_i \phi_i, \quad (2.16)$$

where  $V_{xc}[\rho(\mathbf{r})]$  is the exchange-correlation potential. This potential is the derivative of an exchange-correlation energy  $E_{xc}$  with respect to  $\rho$  and remains the only unknown in the equation (2.16). The Kohn-Sham principle is therefore in general a correct solution, which requires only an approximation for explicitly solving the density functional problem. Equation (2.16) is solved in DFT by applying an initial guess for the electron density and using well-tested approximations for the exchange-correlation functionals before optimization until a certain threshold of change is reached. In the context of this work, a revised exchange/correlation functional by Perdew, Burke, and Ernzerhof (RPBE) is applied [80, 81]. Details of the DFT simulation settings and procedures are noted in the supplementary information of the publications.

## 2.2 Differential Reflectance Spectroscopy

Even though the information gathered by core-level spectroscopy and its simulation is already comprehensive, there are some drawbacks as pointed out in the introduction. These drawbacks lead to the importance of using additional techniques such as DRS. This section explains the basic concepts of the interaction of visible light with organic-inorganic solid systems and this method's difference from well-known UV/Vis spectroscopy of solutions.

The signal of the DRS is defined as the wavelength-dependent change of a reflection  $R(\lambda)$  of a sample with an adsorbate at the wavelength  $\lambda$  compared to the reflection of the bare substrate  $R_0(\lambda)$  as:

$$\frac{\Delta R}{R}(\lambda) = \frac{R(\lambda) - R_0(\lambda)}{R_0(\lambda)}. \quad (2.17)$$

Using the Maxwell equations in homogeneous, linear, and isotropic media, the light can be described by two differential equations for the electric and magnetic field [82, 83]:

$$\nabla^2 \mathbf{E} = \frac{\tilde{\epsilon}}{c^2} \frac{\partial^2 \mathbf{E}}{\partial t^2}, \quad (2.18a)$$

$$\nabla^2 \mathbf{B} = \frac{\tilde{\epsilon}}{c^2} \frac{\partial^2 \mathbf{B}}{\partial t^2}. \quad (2.18b)$$

The complex dielectric function  $\tilde{\epsilon}$  is introduced to combine the real dielectric function  $\epsilon_r$  with a complex, dispersive term:

$$\tilde{\epsilon} = \epsilon_r - i \frac{\sigma}{\epsilon_0 \omega} \quad (2.19)$$

In the complex term, the electrical conductivity  $\sigma$  enters, leading to an absorption of the electromagnetic wave's energy by the medium. The differential equations for the electric and magnetic field can be solved by a general solution consisting of linear waves as:

$$\mathbf{E}(\mathbf{r}, t) = \mathbf{E}_0 \cdot e^{i(\omega t - \tilde{\mathbf{g}} \cdot \mathbf{r})}, \quad (2.20a)$$

$$\mathbf{B}(\mathbf{r}, t) = \mathbf{B}_0 \cdot e^{i(\omega t - \tilde{\mathbf{g}} \cdot \mathbf{r})}. \quad (2.20b)$$

Here, the complex wave vector  $\tilde{\mathbf{g}}$  is introduced and determined (with magnetic permeability of  $\mu_r = 1$ ) as:

$$\tilde{\mathbf{g}}^2 = \frac{\tilde{\epsilon} \cdot \omega^2}{c^2}. \quad (2.21)$$

An introduction of the complex index of refraction is possible, using  $|\tilde{\mathbf{g}}| = 2\pi/\lambda \cdot \tilde{n}$ . The complex index of refraction  $\tilde{n}$  has the form  $\tilde{n} = n - ik$ , which leads to:

$$\tilde{\epsilon} = \tilde{n}^2 = \underbrace{n^2 - k^2}_{\epsilon'} - i \cdot \underbrace{2nk}_{\epsilon''} \quad (2.22a)$$

$$\Rightarrow \epsilon' = n^2 - k^2, \quad (2.22b)$$

$$\Rightarrow \epsilon'' = 2nk. \quad (2.22c)$$

The solution of the complex dielectric function  $\tilde{\epsilon}$  with its real part  $\epsilon'$  and complex part  $\epsilon''$  now enables one to determine the desired substrate and adsorbate properties in terms of two properties only.

Investigating electromagnetic waves on interfaces of two media with different indexes of refraction is simplified by using the well-known Fresnel coefficients [82, 84]. With a deconvolution into two linear waves that are orthogonal to each other, coefficients for the complex reflective part in perpendicular ( $\perp$ ) and parallel ( $\parallel$ ) polarization can be given, using the



simplification of a non-absorbing medium 1, as:

$$\tilde{r}_{12,\perp} = \frac{n_1 \cos \alpha - \tilde{n}_2 \cos \tilde{\beta}}{n_1 \cos \alpha + \tilde{n}_2 \cos \tilde{\beta}}, \quad (2.23a)$$

$$\tilde{r}_{12,\parallel} = \frac{\tilde{n}_2 \cos \alpha - n_1 \cos \tilde{\beta}}{\tilde{n}_2 \cos \alpha + n_1 \cos \tilde{\beta}}, \quad (2.23b)$$

$$\tilde{t}_{12,\perp} = \frac{2n_1 \cos \alpha}{n_1 \cos \alpha + \tilde{n}_2 \cos \tilde{\beta}}, \quad (2.23c)$$

$$\tilde{t}_{12,\parallel} = \frac{2n_1 \cos \tilde{\beta}}{\tilde{n}_2 \cos \alpha + n_1 \cos \tilde{\beta}}. \quad (2.23d)$$

The angle  $\alpha$  is defined as the angle between the wave vector of the incoming wave and surface normal, whereas the angle  $\beta$  is defined as the vector of the wave inside the second medium and the normal direction. The complex angle  $\beta$  is utilized, originating from Snells' law as  $\sin \beta = \frac{n_1 \sin \alpha}{n_2 - ik_2}$ .

For DRS, the system of vacuum, adsorbate, and substrate can be calculated as a three-layer system with two interfaces. The incoming wave gets reflected and transmitted many times, a process known as the Fabry-Pérot interferometer. It is possible to calculate the wave phase change of each partial reflection [82, 85], allowing for the summation of a total reflected amplitude. A simplification and approximation of the total reflection of all three layers becomes possible for very thin layers, much smaller than the wavelength of the incoming beam [86]. Inserting the derived coefficients in equation (2.17) allows (after an extensive derivation) for a description of the measurement signal by the parts  $\epsilon'$  and  $\epsilon''$  of the complex dielectric function for the absorbing media (medium 2: adsorbate, medium 3: substrate) [83, 87, 88]. This signal results to:

$$\frac{\Delta R}{R} \approx -8\pi \frac{d}{\lambda} \frac{\epsilon_3''(\epsilon_2' - 1) + \epsilon_2''(1 - \epsilon_3')}{\epsilon_3'^2 + \epsilon_3''^2 - 2\epsilon_3' + 1}. \quad (2.24)$$

Equation (2.24) demonstrates that the measured signal is strongly dependent on both the adsorbate and substrate dielectric functions. The adsorbate can induce changes to the substrate's properties, e.g., through polarization. For only slightly coupled systems, properties for the substrate could be taken from references such as [89].

For the application of DRS to photochromic molecules in direct contact with surfaces, the main important property to observe is the switching ability. A change of absorption of medium 2 (by a change of  $\epsilon_2''$ ) leads to a change of the reflectance signal. Therefore, these complementary methods to the previously-explained core spectroscopies help to directly probe molecular properties using only a variation of well-known UV/Vis spectroscopy. The setup to acquire the signal is explained in section 3.2.



## 2.3 Photochromic Molecules

This section gives a brief overview about photochromism of molecular switches, in particular about the switching cross-section. Photochromism is a reversible transformation between two different states, such as isomers of a molecule. The reversibility is important, but does not necessarily need to be triggered by light and could also occur thermally.

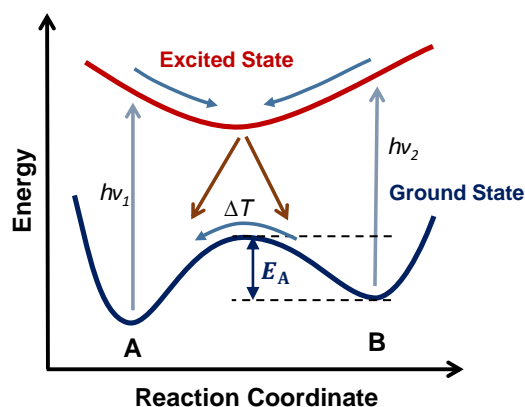


**Figure 2.4:** Scheme of a simple photochromic reaction. Two metastable states A and B of a molecule exist and conversion by light ( $h\nu_1$  and  $h\nu_2$ ) or temperature ( $\Delta T$ ) is possible.

A simple energy landscape of a photochromically switching system between two states A and B is shown in figure 2.4. In this illustration, a molecule can be switched between its two states by light, where an electron from each of the states can be excited by a photon ( $h\nu_1$  and  $h\nu_2$ ) and may relax to the other state. Thermal energy increases the probability to overcome the energy barrier  $E_A$  to switch from B to A. This temperature dependence of the thermal relaxation rate is modeled in a simple way by the Arrhenius equation. The switching rate  $k$  is temperature dependent as:

$$k = A \cdot e^{-\frac{E_A}{RT}}, \quad (2.25)$$

with  $R$  being the universal gas constant and  $A$  a pre-exponential factor mainly depending on the vibrational freedom of the molecule.

A part of this work deals with the kinetics of thermal- and light-induced switching processes. Identification of differences between molecules in solutions and on surfaces allow to conclude on surface-induced changes and to tailor the molecule's chemical groups. One of the main properties to compare is the quantum yield, which is defined as a probability for switching upon illumination of a photon by a single molecule. With methods

such as UV/Vis spectroscopy, properties like the quantum yield are typically compared to identify suitable molecules for further studies.

Since for experiments on solid surfaces, the total absorption of the light by the molecules is difficult to measure, a better quantity to compare is the cross-section. Similar to scattering theory, the incoming photons with a photon flux density  $\phi$  (in photons per area per time) interact with a layer of molecules which posses a density  $n$  (two-dimensional) in one of the states. The rate of change of the density of a particular state depends on the cross-section  $\sigma$ :

$$\frac{dn}{dt} = -\sigma\phi n. \quad (2.26)$$

The switching from one to the other state follows a single-exponential function with a time constant  $\tau$ :

$$n(t) = n \cdot e^{-\frac{t}{\tau}} \quad \rightarrow \quad \frac{dn}{dt} = -\frac{n}{\tau} \cdot e^{-\frac{t}{\tau}} \quad (2.27)$$

Comparing both rates in equations (2.26) and (2.27) results in a equation for the cross-section as:

$$\sigma = \frac{1}{\phi\tau}. \quad (2.28)$$

This cross-section does not fully apply to the experiments of adsorbed molecules on surfaces in this work. Due to the superposition of the incoming and reflected wave, the intensity is reduced in proximity to the surface. This is taken into account by using the effective cross-section as:

$$\sigma_{\text{eff}} = \sigma \cdot r_S, \quad (2.29)$$

with a reduction factor  $r_S$  on the surface defined as:

$$r_S = \frac{\text{photon flux density at surface}}{\text{photon flux density}} = \frac{\phi_S}{\phi} \quad (2.30)$$

In this thesis, the decrease of photon flux density on the surface is not explicitly taken into account and the effective cross-section is calculated as  $\sigma_{\text{eff}} = (\phi\tau)^{-1}$ . The reduction factor can be calculated using the electric field of the light as already derived before in equation (2.20a). For the reflected wave, the Fresnel coefficients in equations (2.23) can be utilized using optical properties of the substrates from literature. The superposition of both waves determines the intensity at the position of the molecules by using the optical properties of the substrates, which are available in literature. For bismuth and gold, the intensity is reduced by more than a factor of two [FN 2] and for HOPG about a factor of four [90]. For gold as used in [FN 4], a reduction of more than a factor of two for a wavelength of 365 nm and a factor of three for a wavelength of 625 nm can be calculated [91].

## Experimental Methods

In this chapter, the basic experimental details are explained. More detailed properties of experiments can be found in the methods section of each publication in chapter 6.

### 3.1 XA and XPS Measurements

The XA and XPS measurements presented in this thesis were performed at the synchrotron radiation source BESSY II of the Helmholtz-Zentrum Berlin (HZB). A customized UHV chamber owned by the AG Kuch (details in section 3.1.2) was used on the undulator beamline UE56/2-PGM-2. A detailed description of the beamline can be found in Refs. [92] and [93].

#### 3.1.1 Synchrotron Radiation

Synchrotron radiation provides x-rays of the highest brilliance<sup>1</sup>, as well as flexible properties such as energetic and temporal resolution. The principle of synchrotron radiation is based on deflection of charges. According to Maxwell's equations, accelerated charges emit electromagnetic radiation. In a synchrotron, electrons are accelerated and kept in a storage ring, which in the case of BESSY II has a perimeter of 240 m and is operated at an electron energy up to 1.7 GeV. Thirty-two deflection magnets keep the electrons on their trajectory and 11 so-called undulators deliver x rays in different energy regimes of the highest brilliance. Since the wavelengths of interest are in the soft x-ray regime, all parts of the storage ring and the beamline is kept at UHV.

Figure 3.1 depicts the principle of an undulator. Electrons with a velocity close to the speed of light enter the arrangement of permanent magnets arranged with opposite magnetization directions. Due to the Lorentz force, the electrons are forced on a periodical trajectory and emit radiation in the direction of the wave vector due to the resulting accelerations. The

---

<sup>1</sup>Brilliance is defined as photon flux per solid angle, source size, and bandwidth [94].

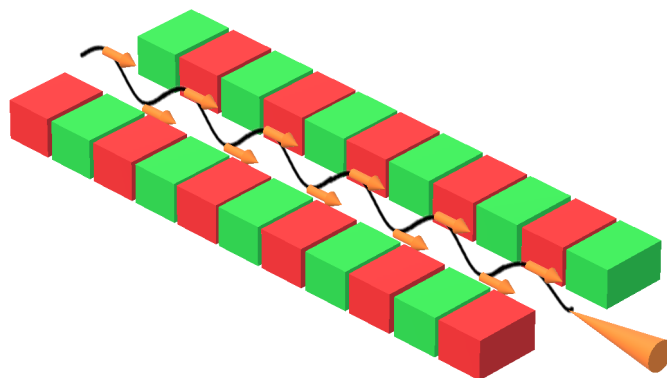


**Figure 3.1:** Schematic drawing of an undulator. Electrons are injected with a high velocity from the left side and move on periodical trajectories.

emitted photons superimpose in a constructive manner and lead to a polarization of the resulting x-ray wave. A degree of polarization above 99% is reached for linear polarized light. The wavelength is tuned by varying the gap opening between the magnets. Undulators, such as the one used at the UE56/2, in contrast to the schematic drawing consist of four rows of permanent magnets, so that the polarization of the x-rays can be varied, e.g., to circular or vertical polarized light. To measure the angular orientation of molecules, the sample was kept in a fixed position in grazing incidence and only the polarization was varied between horizontal and vertical linear. In the beamline right behind the undulator, a plane grating monochromator (PGM) is installed to monochromize the resulting (already discrete) undulator spectrum and leads to a very high spectral resolution [92].

### 3.1.2 Experimental Setup

All measurements and preparations were carried out in UHV. The pressure was in the order of  $10^{-9}$  mbar or below. At higher pressures, significant contaminations by residual gases would appear. To achieve the UHV pressure regime, the chambers were equipped with different types of pumps. The chamber used for synchrotron radiation measurements consisted of various equipment. For the preparation of the samples, a sputter gun was used, and LEED and Auger systems enabled pre-characterization of the clean substrate. In addition, a quick exchange of samples through a storage and a load-lock was possible. The load-lock enabled cleaving of HOPG through ripping a carbon tape off of the surface under high vacuum ( $10^{-7}$  mbar) conditions.

XPS and XA measurements were performed using the sample holder of the manipulator equipped with a liquid helium flow cryostat. Samples were mounted on Omicron sample plates. To control the temperature, a heating filament was mounted on the temperature exchange block. A boron nitride heater was installed behind the sample. Thermocouples were mounted above and below the holder. Using liquid helium, temperatures as low as 60 K could be achieved, but in the context of this thesis temperatures were usually kept between 130 K and room temperature. The sample can be moved and rotated in five axes, enabling a change of the x-ray beam incidence angle.

The electron analyzer was mounted with an angle of  $45^\circ$  with respect to the incoming x-rays. For detection of the XPS, a hemispherical analyzer of the type Phoibos 100 by SPECS GmbH was used. Evaporators were mounted behind valves in various positions, depending on the exact type of experiment being performed. Most often, evaporators were placed orthogonal to the x-ray beam direction, to enable evaporation and measurement in grazing incidence geometry at the same time.

Further details on the experimental setup as used for synchrotron radiation measurements are published elsewhere [52, 95, 96] and summarized, including more detailed description, in each publication as reprinted later in this thesis. Additionally, to improve acquisition speed and reliability, a motorization of the setup was built, which is described in appendix B.2.

### 3.1.3 XA Detection and Normalization

Detection of XA of solids is possible by different methods, such as x-ray fluorescence, x-ray-induced Auger electrons, and x-ray total electron yield (TEY) [66]. TEY has particular advantages due to its simple principle: The drain current of the sample to ground is measured. After photoabsorption of the x-rays, avalanches of electrons are generated inside the solid, in which some electrons with sufficiently high energy can overcome the work function of the surface. In this way, TEY is also very surface sensitive due to the limited mean free path of electrons in solids.

To detect the very small currents in the order of picoampere, the sample must have a resistance to ground in the high gigaohm range. Additionally, high care must be taken in the mechanical and electrical stability of the environment to reduce noise in the measurements. The pre-amplification of currents was achieved by using variable sub-femtoampere amplifier DDPCA-300 by Femto Messtechnik GmbH. They amplify and convert to a

voltage with gain of (mostly used)  $10^{10} \text{ V A}^{-1}$ . Readout was performed using Keithley electrometers of type Model 6514.

Upstream of the experiment as described in the previous section, a gold grid was mounted. A gold electron-beam evaporator enables coating of the grid with a fresh gold film. Therefore, absorption of pure gold can be used for normalization of the beam intensity. This signal is denoted as  $I_{\text{grid}}$ , whereas the pure sample drain current is assigned to  $I_{\text{sample}}$ . To identify the contributions of the XA signal which are originating from the adsorbate only, reference measurements of the clean substrate were also taken and denoted as  $I^{\text{reference}}$ . The measurements of the signal of adsorbate and substrate together are denoted as  $I^{\text{adsorbate}}$ . The presented XA spectra are calculated by:

$$I = \frac{I_{\text{sample}}^{\text{adsorbate}} / I_{\text{grid}}^{\text{adsorbate}}}{I_{\text{sample}}^{\text{reference}} / I_{\text{grid}}^{\text{reference}}} \quad (3.1)$$

To further normalize the spectra, they have been divided by their intensity on the pre-edge (some eV before the first  $\pi^*$  resonance), leading to a presentation of the relative change of signal by the adsorbate.

### 3.1.4 Illumination Setup

For illumination of the samples by ultraviolet (UV) and visible light for synchrotron measurements, different setups were used. The setup using a xenon-mercury arc lamp has only been applied for [FN 1] and is described there.

Most experiments were executed using LED setups. Various LEDs of wavelengths (in brackets the Thorlabs article numbers) 365 nm (M365LP1), 365 nm (M365L2), 405 nm (M405LP1), 455 nm (M455L2), 530 nm (M530L2), 565 nm (M565L3), 590 nm (M590L2), 625 nm (M625L3), and 850 nm (M850L3) were installed on the UHV chambers to achieve a highly powerful illumination. Due to rather slow switching effects, improving the illumination power was necessary. Behind the LEDs, an achromatic lens was mounted to collimate the beam. For focusing on the sample, UV-fused silica lenses were directly mounted on the UHV chamber windows. All illuminations were performed in measurement position, to enable simultaneous measurements.

For calculation of the effective cross-sections of the switching processes, measurement of the illumination power in sample position is necessary. For these measurements, the exact positions have been set up *ex situ* and a thermal power sensor of type S302C by Thorlabs was used to measure the illumination power. In order to have comparable values in all publications, the photon flux density in photons/s/mm<sup>2</sup> was calculated.

## 3.2 Optical Reflectance

The description of the newly-built setup for measuring DRS is published in a *Review of Scientific Instruments* article, which is reprinted on page 87. Further information, such as pictures of the setup or details of the software components, can be found in appendix A.

## 3.3 Sample Preparation

To clean single-crystal substrates in UHV, the sputter gun was used. This tool accelerates  $\text{Ar}^+$  ions onto the surface using a high voltage between 0.6 kV and 2 kV. Due to an angle between the gun and sample surface, the impurities are kicked away from the surface. Afterwards, an annealing is necessary to achieve an atomically flat surface. This was accomplished in the annealing process by heating to high temperatures, but staying below the melting temperature, such as 350 K for Bi(111) and 900 K for Au(111). The sputtering and annealing was repeated alternately until no contamination in XPS and XA was visible and sharp LEED spots were obtained. HOPG was prepared by cleaving off a carbon tape in high vacuum in a dedicated home-made cleaving stage. The HOPG was purchased in highest grade (ZYA) from Structure Probe Inc.

Deposition of molecules was performed for nearly all experiments at substrate temperatures around 200 K. There has been evidence that over a long time at room temperature only weakly bound molecules can desorb from inert surfaces such as Bi(111) and HOPG. Molecules were evaporated from a Knudsen cell using a home-made evaporator (described in Ref. [95]). Except for thiazol-diarylethene, all molecules used in this work are commercially available, e.g., at *TCI Chemicals*. The evaporators were equipped with a quartz microbalance, which can be used for measuring the number of evaporated molecules after a calibration. The change of the eigenfrequency of a quartz was measured. To stabilize this frequency against external influences and improve the sticking rate of molecules, the quartz was cooled by ice water.



### 3.4 Thickness Calibration

To calibrate the previously explained quartz microbalance with coverages in terms of fractions of fully closed layers (monolayers), calibration measurements have been performed using XA and DRS. The principle is identical for both methods. The molecules were evaporated onto the substrate step-wise with recording of spectra in between. This has been performed in a similar way for azobenzene on the Au(111) surface before using XPS [50]. For weakly bound molecules, only one saturated layer sticks on the surface. This layer's signal can be identified using either the total edge jump of the XA of an element or by observing a certain absorption band in DRS. In this PhD work, calibrations were measured for spironaphthopyran and spironaphthooxazine on Bi(111) using XA and DRS, respectively. In figure 3.2, the calibration using XA is provided. On the carbon *K* edge, a total edge jump of 17% is fitted by an exponential function. Due to different structure and bending of the spectra, a direct comparison with the last spectrum in figure 3.2 (a virtually saturated layer) is a straightforward option to identify coverages. This calibration can easily be transferred to other molecules, substrates or elements. In the same beamtime with same conditions, it is feasible to subtract (instead of divide, see equation (3.1)) the XA background signals and compare absolute sample drain currents for the adsorbate signals. For other molecules with different amounts of carbon atoms and different packing on the surface, assumptions can be included and therefore estimations can be carried out. This calibration was cross-checked and verified with various calibrations determined in previous theses [50, 95, 96].

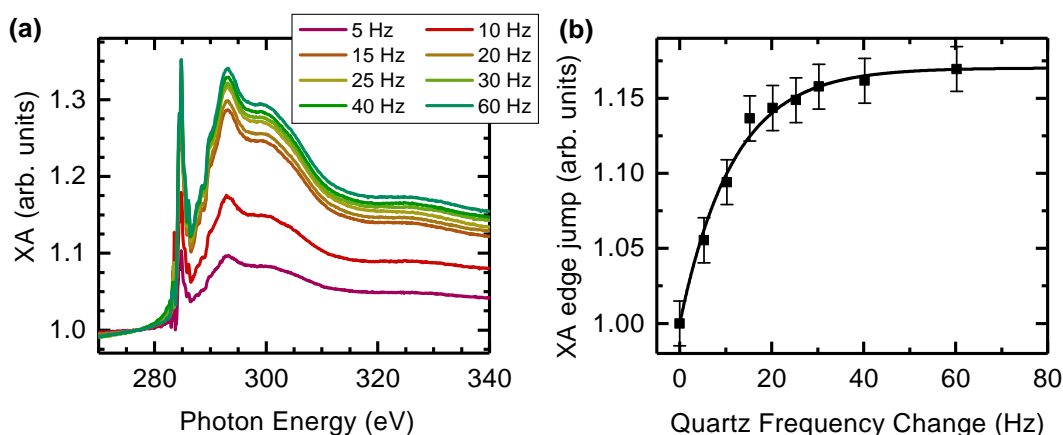


**Figure 3.2:** (a) XA of spironaphthopyran on Bi(111) after different evaporation steps at room temperature. (b) Evaluation of the total edge jump (4 eV average at 338 eV) for different changes of frequency of the quartz microbalance.



The same type of calibration has been carried out for DRS. Spironaphthooxazine was evaporated on Bi(111) at room temperature, with the DRS measured after each step. The result is presented in figure 3.3 and the saturation is evaluated to be at a DRS signal of -0.061 at 245 nm. The difference of change of frequency between both methods presumably originates from a drastically different distance of the evaporator to the sample. In DRS, the distance is much larger, since the evaporator is not used with a shutter, but placed behind a valve. This difference could also be explained by different quartz geometries or different sticking coefficients of the molecules.

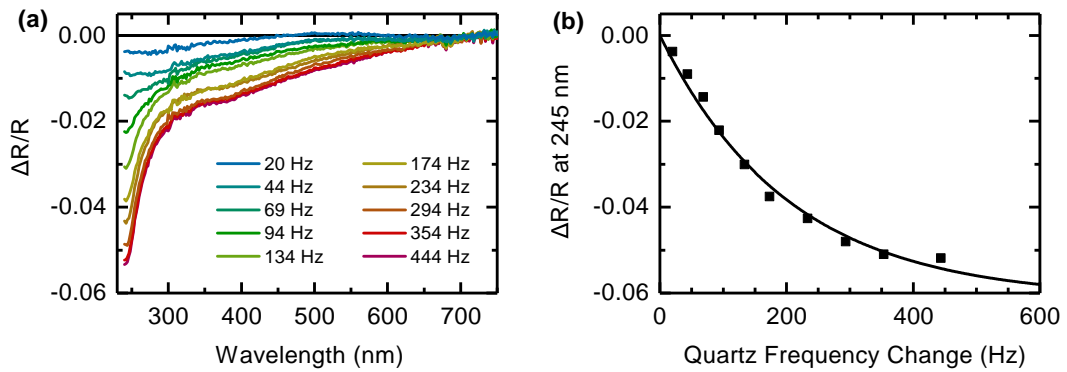


**Figure 3.3:** (a) DRS of spironaphthooxazine on Bi(111) after different evaporation steps at room temperature. (b) Signal at 245 nm as a function of the microbalance frequency change. Taken from [FN 3]. © 2018 AIP Publishing.



## Photochromism on Surfaces

This chapter provides an overview of the experiments and results published in [FN 1], [FN 2], and [FN 4]. Basic properties of the systems are introduced and the important milestones of each publication are summarized.

### 4.1 Diarylethene on Surfaces

Diarylethene is a versatile molecular switch which attracted attention in various systems [14]. This switch's high fatigue resistance of photoresponsive ring-closing and ring-opening is of great interest. Additionally, the reversible switching from closed form to open form can not be invoked by thermal energy. Especially on surfaces, the thermal stability of switches can differ drastically from their behavior in solutions [41, 53].

In collaboration with the working group of Prof. Dr. Stefan Hecht of the Humboldt University of Berlin, a derivate synthesized by this group has been chosen for investigation on different surfaces using XA and XPS. The selected molecule thiazol-diarylethene (T-DAE, 1,2-bis(5-methyl-2-phenylthiazol-4-yl)cyclopent-1-ene) is illustrated in figure 4.1. This molecule

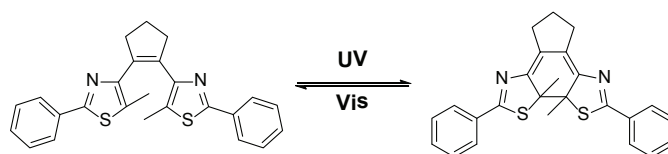


**Figure 4.1:** Chemical structure of T-DAE in its open isomer (left) and closed isomer (right). Ring opening and ring closure can take place in solutions using ultraviolet and visible light.

is well-studied in solutions and by DFT [97, 98] and has a very important advantage for use with XA and XPS: it contains two nitrogen atoms close to the switching unit, in order to identify switching processes by changes of the nitrogen chemical properties.

The target of the investigations was to find a suitable surface to reversibly switch the molecule light-controlled in both directions. The surfaces Bi(111),

HOPG, and Au(111) were considered and studied, but led to problems on the Au(111) surface. As indicated in previous experiments, sulfur may react quite intensely when exposed to x-rays on the gold surface [99, 100].

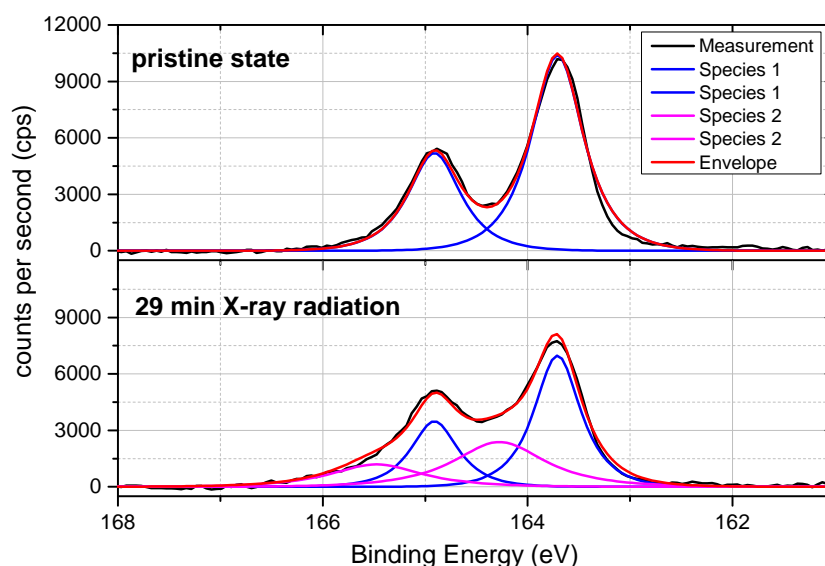


**Figure 4.2:** XPS of 0.69(5) ML of T-DAE on Au(111). Top panel: pristine after evaporation. Bottom panel: same measurement spot, but after 29 minutes of recording XPS.

Figure 4.2 depicts the XPS of the sulfur  $2p$  electrons of 0.69(5) ML of T-DAE on Au(111) and in particular (bottom panel) the change upon 29 minutes of x-ray radiation. The doublets stem from the spin-orbit splitting, which results in  $2p_{1/2}$  and  $2p_{3/2}$  sulfur peaks. Before illumination, only one species (blue line) was present, meaning that all molecules were present in the same state. Upon 29 minutes of x-ray radiation, a newly emerging sulfur species with a doublet at higher binding energy (magenta lines) with a  $2p_{3/2}$  peak at 164.3 eV is present. Similar blue shifts have been previously observed for destructed sulfur-containing molecules [100]. And also in the case of T-DAE on Au(111) originate presumably from a destructed molecule induced by the x rays.

The results on HOPG and Bi(111) are published in [FN 1]. A switching from the ring-opened form to the ring-closed form by strong UV and UV/visible light was achieved. Figure 4.3 presents the time dependence of such a switching process using XA and the fitting by the linear combination of the first and last spectrum of each intermediate spectrum. The effective cross-section for this process is  $\sigma_{\text{eff}} = 1.3(2) \times 10^{-22} \text{ cm}^2$ . The same value has been obtained for T-DAE on Bi(111). By using DFT for gas phase isomers of T-DAE, a clear assignment of the present T-DAE isomer on the surface to a

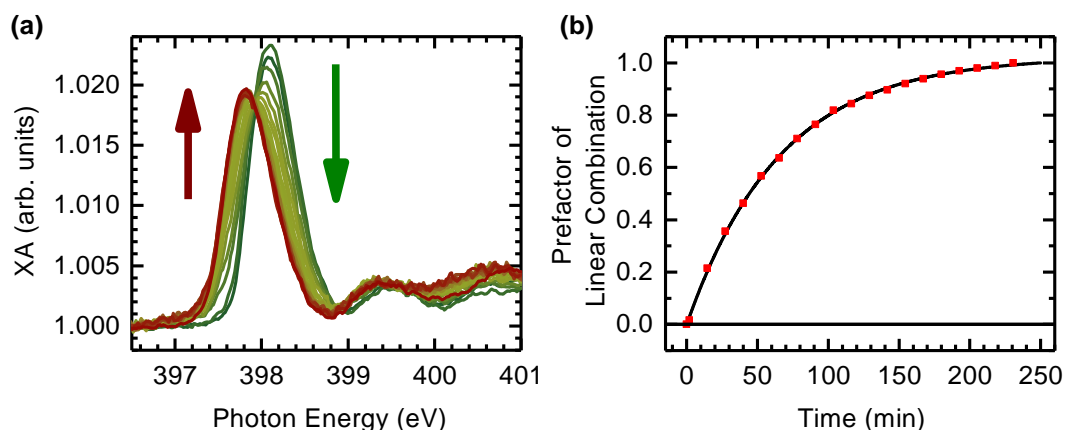


**Figure 4.3:** (a) XA of the nitrogen *K* edge of a submonolayer T-DAE on HOPG recorded in grazing incidence ( $20^\circ$ , p-polarized light). Beginning with the green spectrum, a broadband UV/Vis illumination for 231 minutes led to the red spectrum. (b) For each spectrum, the superposition of first and last spectrum from (a) has been fitted. Plotted is the prefactor for the linear combination of the last spectrum versus the illumination time. Taken from [FN 1]. © IOP Publishing Limited.

ring-closed form can be made; however, the exact nature of the resulting isomer has not been determined. Three possible ring-closed isomers were calculated by DFT and through comparison to experimental nitrogen XA, no clear results could be given. For the light-induced ring-closure reactions on both surfaces, upon light illumination a change of mean angular orientation of the molecule by  $5^\circ$  towards a flatter lying isomer was also found. This discovery indicates a ring-closure as well. XPS revealed a newly emerging sulfur species with a shift of binding energy by  $-0.6$  eV, which is close to values reported in literature [55]. In addition, for the illuminated sample, a species with a strong shift by  $2.2$  eV of sulfur  $2p$  binding energy was also observed and attributed to a light/x-ray induced chemisorption of the T-DAE [FN 1].

Upon illumination, the resulting isomers on Bi(111) and HOPG could not be switched further. This finding could point towards a distorted closed-form isomer, which no longer exhibits switching functionality. If present, the photoinduced back-reaction would have an effective cross-section below  $10^{-22}$  cm<sup>2</sup>, as determined by intense illumination with different light sources for more than 75 minutes each. The switching time constants in the order of 12 hours to days would not be experimentally observable by the applied methods.

## 4.2 Spiropyran on Bi(111)

SP is one of the most used photochromic molecules [14, 101, 102]. Its most prominent change of property upon isomerization is the substantial difference in electric dipole moment. SP and close relatives are intensely studied in different environments [103–109].

To find a molecule that can reversibly switch while in direct contact with a surface, SP derivatives were investigated. Of particular success were the investigations of spironaphthopyran (see figure 4.4) on Bi(111).

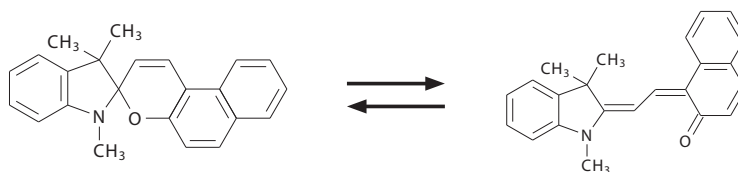


**Figure 4.4:** Chemical structure of SNP in its spiropyran form (left) and merocyanine (MC) form (right). Photoconversion can take place in solutions using ultraviolet and visible light. Switching from MC to SNP is also possible using thermal energy.

SP has been chosen for investigations on surfaces, since promising results have already been achieved [40, 41, 110]. Most often, the trimethyl-6-nitrospiropyran (named as nitro-spiropyran in this work) was used. It was found that in the case of nitro-spiropyran on Au(111), even the thermal stability was reversed, and upon heating above 300 K, the SP converts without further influence to its merocyanine (MC) form [41]. On the other hand, on Bi(110) a photostationary state was reached using a blue laser illumination [40]. Since no reversible switching was achieved and the back-reaction from MC to SP in particular could not be achieved in direct contact with surfaces, the nitro-spiropyran was exchanged to the spironaphthopyran. Instead of the electron-withdrawing nitro group, a naphtho group was added to the spiropyran, leading through its electron-donating nature to a destabilization of the MC form. To have a less interacting surface, the semimetallic Bi(111) was chosen instead of Au(111). The density of states at the Fermi level of Bi(111) is low [111–113] and therefore a reduced van-der-Waals interaction is expected.

Both modifications led to a reversible switching of SNP on Bi(111), as published in [FN 2]. Using a combination of XA and DFT, the UV-induced ring-opening was proven and by heating the sample to temperatures above 250 K, reversibility to SNP was achieved. Since the effect is also easily reproducible, investigations of the energetic barriers are likewise feasible.

By varying the temperature and assuming simple Arrhenius-like behaviors, a model was established. The Arrhenius equation states a temperature-dependent rate  $k$  as product of an pre-exponential factor  $A$  and an exponential function including the activation energy  $E_A$  as:  $k(T) = Ae^{\frac{-E_A}{RT}}$ . The final model enables an explanation of the experimental data. Figure 4.5 presents one of the important results of this work. Panel (a) shows a sketch of the proposed energy landscape of SNP and MC. Panel (b) provides the notation for the mathematical description of the differential equations.

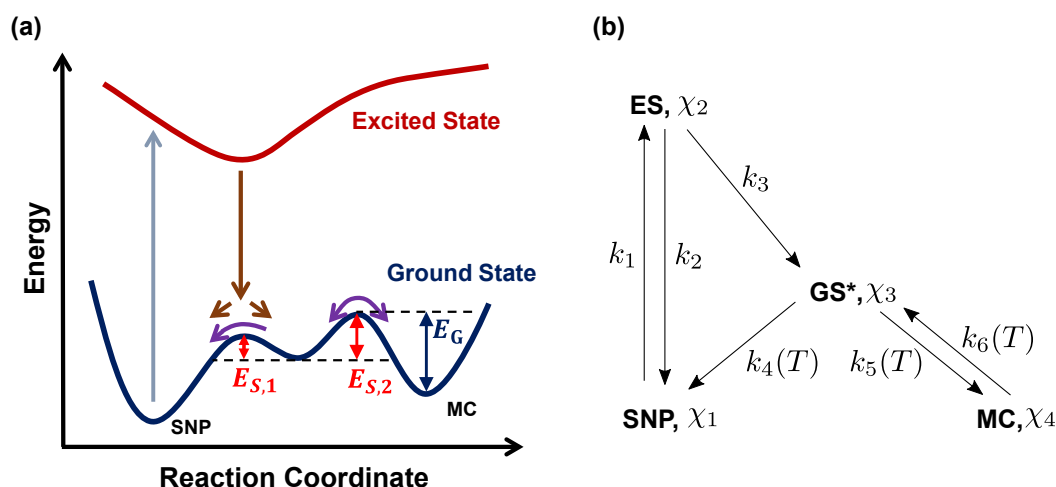


**Figure 4.5:** (a) Schematic visualization of the proposed energy landscape for the photoinduced and thermal switching between SNP and MC. Suggested is an intermediate state with the energy barrier  $E_{S,1}$  to the SNP isomer and  $E_{S,2}$  to the MC isomer. The MC isomer is at a local minimum adjoining to the barrier  $E_G$ . (b) Mathematical notation for the fitting of the experimental data to the proposed energy landscape as denoted in (a). Taken from [FN 2]. © 2017 WILEY-VCH Verlag GmbH & Co. KGaA, Weinheim

After excitation of the SNP state to some excited state (rate  $k_1$ ), a relaxation takes place (rate  $k_3$ ) back to the ground state. The present state is presumably a ring-opened MC in a *cis* configuration.<sup>1</sup> The most-stable MC configurations were found to have the carbon bonds in a *trans* configuration. In this configuration, the molecule can either undergo a back-relaxation to the SP form by passing the energy barrier  $E_{S,1}$  (rate  $k_4$ ) or relax to the metastable MC configuration by overcoming the barrier  $E_{S,2}$  (rate

<sup>1</sup>Depending on the conformation of the alkene-bridge segments of the MC, eight different possible MC isomers exist. The terms *cis* or *trans* isomers denote the configuration of the central bridge.

$k_5$ ). The thermal relaxation from MC to SNP is included by overcoming the energetic barrier  $E_G$  (rate  $k_6$ ).

According to figure 4.5(b), the rates for  $k_4$ ,  $k_5$ , and  $k_6$  are:

$$k_4(T) = A_S e^{-E_{S,1}/(RT)}, k_5(T) = A_S e^{-E_{S,2}/(RT)}, k_6(T) = A_G e^{-E_G/(RT)}. \quad (4.1)$$

The prefactors  $A_S$  and  $A_G$  are attempt frequencies for switching in each direction. Using the initial conditions, the differential equation for the fraction  $\chi_{MC}$  of MC molecules is [FN 2]:

$$\frac{d\chi_{MC}}{dt} = (1 - \chi_{MC}) \cdot k_{SNP \rightarrow MC} - \chi_{MC} \cdot k_{MC \rightarrow SNP}, \quad (4.2)$$

with the switching coefficients as:

$$k_{MC \rightarrow SNP} = -A_G e^{-E_G/(RT)} \frac{1}{1 + e^{-\Delta E_S/(RT)}}, \quad (4.3a)$$

$$k_{SNP \rightarrow MC} = \sigma(\lambda) \phi_{UV} \Phi_1 \frac{1}{e^{\Delta E_S/(RT)} + 1}. \quad (4.3b)$$

$\sigma(\lambda)$  is the cross-section of one molecule absorbing a photon of wavelength  $\lambda$ ,  $\phi_{UV}$  is the photon flux density, and  $\Phi_1$  is the quantum yield for the excited state. For fitting, the energy barrier difference  $\Delta E_S = E_{S,2} - E_{S,1}$  is taken into account and the prefactors for  $k_{SNP \rightarrow MC}$  are combined as  $k_S = \sigma(\lambda) \phi_{UV} \Phi_1$ . The obtained prefactors and energy barrier values are:  $E_G = 79(2) \text{ kJ mol}^{-1}$ ,  $\Delta E_S = 16(2) \text{ kJ mol}^{-1}$ ,  $A_G = 10^{15.4(4)} \text{ s}^{-1}$ , and  $k_S = 7(2) \text{ s}^{-1}$ . Of special interest in these values is the thermal stability  $E_G$  of the MC state. This value is slightly higher than observed in polar solutions, where the value is at  $75 \text{ kJ mol}^{-1}$  [107].

The origin of the barrier is not fully assigned. In literature, various theoretical and experimental results indicate this barrier in the ground state, which is attributed to the *cis-trans-isomerization* of the carbon bonds upon ring opening [107, 114–116]. However, for other photochromic molecules, barriers in the excited state have been observed [117]. They cannot be ruled out for SNP on Bi(111), since their mathematical description would also well match to the experimental data.

The finding of a fully reversible switching with a high effective cross-section allows for a deep insight into the switching process on the surface. Bistability is still observed on the surface, in contrast to previous results, e.g. on a Au(111) surface. Still, a redesign of photochromic molecules when transferred to surfaces is necessary and a systematic investigation of the redesign is needed.



### 4.3 Spirooxazine on Bi(111) and Au(111)

Spirooxazine (SO) is closely related to SP. For the work on SO in this thesis, the spironaphthooxazine (SNO, 1,3,3-trimethylindolinonaphthospirooxazine) molecule was chosen. This molecule is commercially used in phototropic glasses, which are glasses that darken when exposed to light and return to their transparent state in the absence of light [118, 119]. An illustration of the molecule with its MC form is provided in figure 4.6.

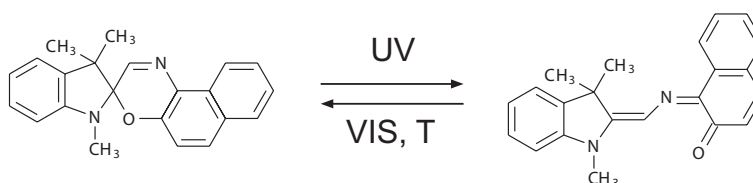


**Figure 4.6:** Chemical structure of SNO in its spiropyran form (left) and merocyanine (MC) form (right). Photoconversion in solutions can take place using ultraviolet and visible light. Switching from MC to SNO is also possible using thermal energy.

To gain more insight into photochromism on surfaces, a new experiment has been built and benchmarked using SNO on Bi(111) [FN 3]. The DRS offers a superior tool to investigate temperature-dependent switching and stability of adsorbed molecules on surfaces. As a highlight from reference [FN 3], the result of temperature-dependent relaxation of SNO on Bi(111) is reprinted in figure 4.7.

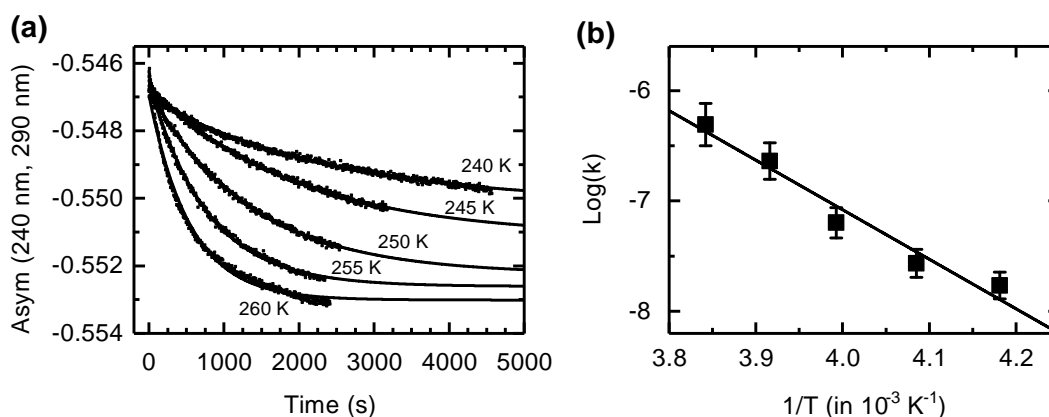


**Figure 4.7:** (a) Time-dependent measurements of the asymmetry of saturated MC-isomerized samples at different temperatures. (b)  $1/T$ -plot of the corresponding relaxation rates and a fit to determine the energy barrier in an Arrhenius model. Taken from [FN 3]. © 2018 AIP Publishing.

Figure 4.7(a) presents the time dependence of the thermal relaxation of the *asymmetry signal*<sup>2</sup> of MC to SNO at temperatures between 240 and 260 K. At higher temperatures, the SNO state is reached in a shorter period of time. This behavior can be fitted using an Arrhenius description of the rates. The energy barrier of the MC state relaxing to SNO can be obtained from the Arrhenius plot shown in figure 4.7(b). An energy barrier of  $E_A = 37(4) \text{ kJ mol}^{-1}$  was obtained for SNO on Bi(111) [FN 3], which is reduced compared to measurements in solution, where the barrier was found to be between 61 and 78  $\text{kJ mol}^{-1}$  [103, 120].

The reduced stability of the MC isomer of SNO on the Bi(111) surface compared to the MC of SNP on Bi(111) (see previous section 4.2) offers a new perspective: enabling bistability of a photochromic switch on Au(111). As explained previously, nitro-spiropyran was found stabilized on Au(111) [41], but for SNO this is no longer the case [FN 4]. Instead, a highly efficient light-induced bidirectional photochromism is enabled. Figure 4.8 contains the DRS asymmetry measurements of SNO on Au(111). Using only UV and red LED illuminations, a control of the SNO isomerization in a submonolayer is achieved. Beginning from an MC state, five consecutive switching cycles are presented. The time constants can be determined with this method as 1074(57) s (1st red), 16(1) s (2nd UV, first blue line), 872(21) s (2nd red), 14(1) s (3rd UV), and 836(27) s (3rd red). The significant decrease of time constants could suggest a process that is trained through repeated cycles. A possible explanation for such behavior is a rearrangement of molecules.

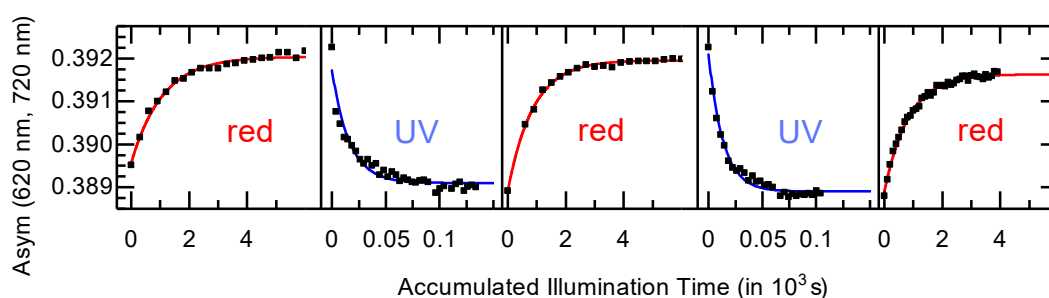


**Figure 4.8:** Switching cycles of SNO on Au(111) as measured by DRS at a temperature of 200 K. Taken from [FN 4]. © 2018 American Chemical Society.

The calculated effective cross-sections for the most efficient switching series are  $\sigma_{\text{eff,UV}} = 2.3(6) \times 10^{-19} \text{ cm}^2$  and  $\sigma_{\text{eff,red}} = 1.4(3) \times 10^{-21} \text{ cm}^2$ , which in the case of UV switching is ~2 orders of magnitudes more efficient than previously measured systems [FN 2, 40, 110]. There is still a high potential

<sup>2</sup>a defined measure, to identify both isomers in DRS.

for further optimization since the cross-section in solutions are still orders of magnitude higher than cross-sections measured on surfaces [107, 108].

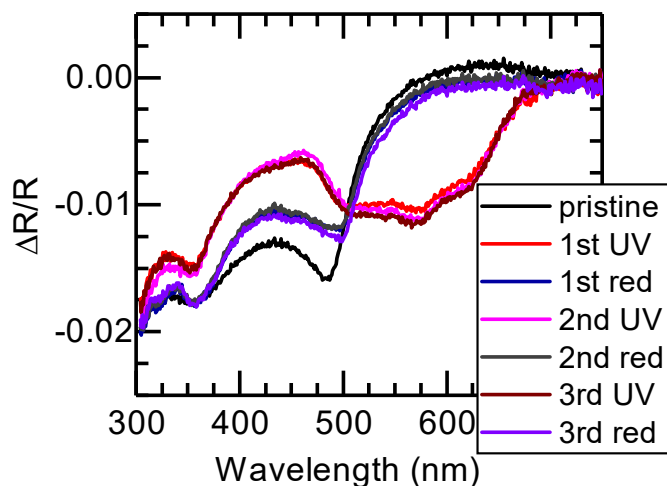


**Figure 4.9:** DRS of a submonolayer of SNO on Au(111) at a temperature of 200 K for the pristine state and six states upon subsequent illumination by UV and red light. Taken from [FN 4]. © 2018 American Chemical Society.

The DRS spectra of pristine and photostationary states are presented in figure 4.9 and provide interesting details about the system. The spectrum of the pristine sample does not exactly match the spectra after red illumination, even though the same isomers should be present. This difference is attributed to a reorganization of the molecules on the surface and, therefore, to a different influence on the Au(111) surface states. In addition, the shape of the DRS is comparable to the shape of UV/Vis measurements of SNO and its MC form in solution [121].

The results of SNO on Bi(111) and Au(111) constitute the next step in research on photochromic systems on surfaces, which is enabled by DRS. With SNO on surfaces, a highly efficient and in the case of the Au(111) surface even bidirectional pure light-induced switching is achieved. Further steps will be to identify the changes of properties such as the electric dipole moment on the surface and to tailor the molecules to function at room temperature.



## Summary

In this work, detailed studies of photochromic molecules on different surfaces have been presented. To find a system of molecular switch and suitable surface, preferably a single-crystal substrate, various combinations have been investigated. The substrates Au(111), Bi(111), and HOPG were utilized. A T-DAE, SPs, and SOs were analyzed by XA spectroscopy and XPS. To support the core-level spectroscopies, DFT simulations of XA spectra were carried out. These methods deliver a comprehensive picture of the chemical and electronic states, but are inefficient when systematic and time-consuming studies are required because they rely on an x-ray source such as a synchrotron radiation beamline. To achieve a deeper understanding and tailoring of the photochromic switches, a new method was transferred for application with such systems; the DRS was built in a lab-based setup to be used with a standard UHV chamber.

The DRS setup was optimized for the use of lowest possible light exposures, to avoid influencing the state of photochromic switches. Furthermore, high mechanical requirements were met to enable measurements at variable temperatures between 100 and 460 K with constant conditions over hours. Using photomultipliers (PMTs), the noise level was reduced by a factor of three compared to other setups, which brought the noise level close to the shot noise threshold. To allow for an investigation of highly efficient photoswitches, the light exposure was reduced compared to typical CCD-based setups by at least four orders of magnitude. The application and potential for research of kinetics was demonstrated for a sub-monolayer of a SO switch on Bi(111) [FN 3]. The setup allows for a thorough investigation of the optical reflectance of photochromic molecules on surfaces, even for only very small coverages below a fully closed molecular layer. Computer-controlled temperature and highly reproducible automated measurements, including light-illumination, are a key to progress in the field of adsorbed functional molecules in direct contact with surfaces.

All molecules were evaporated *in situ*, to achieve a clean analysis of molecules in sub-monolayers on surfaces. From previous experiments in

literature, it was already known that the molecular properties change drastically when in contact with surfaces. Therefore, finding a system with low interaction between surface and adsorbates was a target. Investigations were performed mainly at temperatures around 200 K, since a higher stability of all isomerization states is expected at this temperature. In first experiments, using XPS, XA, and DFT, the successful light-induced ring-closure of T-DAE was demonstrated [FN 1]. The process is inefficient with an effective cross-section of  $\sigma_{\text{eff}} = 1.3(2) \times 10^{-22} \text{ cm}^2$ , which is comparable to previous experiments with photoswitches on surfaces. The resulting species of the T-DAE cannot conclusively be determined, since invocation of a back-reaction was not achieved; two other possible closed-form isomers, a T-DAE with the methyl groups on the same side of the molecule and a by-product which is described in literature were simulated. These isomers also describe the observed XA and XPS changes. Furthermore, XPS reveals a sulfur species which is not explainable by an isomer of the T-DAE. A partial chemisorption with the substrate induced by the illumination is suggested.

The research with SP led to promising results using the SNP switch. On the semimetallic Bi(111) substrate, a reversibly switchable system was found and investigated [FN 2]. For the first time, a fully reversible control of the isomerization of a photochromic molecule directly on a surface was demonstrated. The UV-induced ring-opening to MC and MC-to-SNP switching by temperature increase allowed to quantitatively determine energy barriers involved in the switching process. Temperature-dependent XA measurements of the kinetics of the reaction revealed the presence of an intermediate state. Including this state in a model and fitting it to the time- and temperature-dependent experimental data led to the determination of the energy barrier for the MC and of the difference in energy between both barriers adjoining the intermediate state. The thermal stability of MC on the Bi(111) surface is not significantly changed compared to solution measurements, rendering research with SNP or the bismuth substrate a highly interesting subject for further experiments. The light-induced SNP-to-MC switching at 223 K was more efficient than the T-DAE conversion with an effective cross-section of  $\sigma_{\text{eff}} = 1.1(3) \times 10^{-20} \text{ cm}^2$ , but at this temperature already the thermal back-reaction sets in.

A further goal was achieved using SNO. On the Bi(111) surface, it was possible to demonstrate that the thermal stability of the MC was reduced compared to solution experiments. The corresponding energy barrier of  $E_A = 37(4) \text{ kJ mol}^{-1}$  was determined, which is reduced by about a factor of two compared to values in solutions [FN 3]. For a utilization of this change, the SNO was investigated on the Au(111) surface, where previously

nitro-spiropyran was identified to possess a drastically increased stability of the MC state, leading to a reversed thermal behavior. SNO was found to exhibit a highly efficient photoconversion to MC using a UV-LED and, vice versa, a bi-directional switching from MC to SNO using a red-light LED illumination [FN 4]. The effective cross-section for both reactions are  $\sigma_{\text{eff,UV}} = 2.3(6) \times 10^{-19} \text{ cm}^2$  and  $\sigma_{\text{eff,red}} = 1.4(3) \times 10^{-21} \text{ cm}^2$ . The UV-induced switching efficiency was strongly increased by  $\sim 2$  orders of magnitude compared to previously-determined cross-sections for SPs. The decrease of switching time constants by repeated illumination cycles and the significant difference between the DRS of the pristine evaporated SNO and the one after red-light illumination point towards a reorganization of the lateral structure of the adsorbed molecules.

The results achieved in this work are the basis for further tailoring of photochromic systems. Modification of a previously used nitro-spiropyran to the spironaphthooxazine enabled the bi-directional light-driven photoconversion on the frequently-used Au(111) surface. By further investigation and changes of molecule substitutions, an increase of the effective cross-section, up to the efficiency as seen in solutions, is the next target. The DRS method provides the necessary tool to address the candidates that possess the potential to act as building blocks for molecular electronics. Studying the cooperation of photochromic switches with inorganic molecules or (supra)molecular networks on surfaces could help to achieve the next milestone for applications.





## Original Publications

This chapter presents the original publications. The contributions for each publication are explained in the corresponding section. Fabian Nickel is first author and main contributor for each publication with supervising postdoctoral researcher Dr. Matthias Bernien as second author. All work (except the synthesis of molecules) was performed under supervision and in the research group of Prof. Dr. Wolfgang Kuch at the Freie Universität Berlin in the department of experimental physics.

### 6.1 J. Phys.: Condens. Matter 29, 374001 (2017)

By Fabian Nickel, Matthias Bernien, Martin Herder, Sandro Wrzalek, Pantelis Chittas, Kai Kraffert, Lucas M. Arruda, Lalminthang Kipgen, Dennis Krüger, Stefan Hecht, and Wolfgang Kuch

**Light-induced photoisomerization of a diarylethene molecular switch on solid surfaces**

Published August 2017

DOI: <https://doi.org/10.1088/1361-648X/aa7c57>

© 2017 IOP Publishing Limited

#### **Contributions:**

FN and MB planned and supervised the XAS and XPS experiments. FN, MB, SW, PC, KK, LMA, LK, DK performed the XAS and XPS experiments. FN analyzed the XAS data. SW and FN analyzed the XPS data. MH synthesized the molecule. FN carried out the DFT simulations. FN prepared and wrote the manuscript with corrections by MB, WK, MH, SH. All authors discussed the results. WK supervised the study.



# Light-induced photoisomerization of a diarylethene molecular switch on solid surfaces

Fabian Nickel<sup>1</sup>, Matthias Bernien<sup>1</sup>, Martin Herder<sup>2</sup>, Sandro Wrzalek<sup>1</sup>, Pantelis Chittas<sup>1</sup>, Kai Kraffert<sup>1</sup>, Lucas M Arruda<sup>1</sup>, Lalminthang Kipgen<sup>1</sup>, Dennis Krüger<sup>1</sup>, Stefan Hecht<sup>2</sup> and Wolfgang Kuch<sup>1</sup>

<sup>1</sup> Institut für Experimentalphysik, Freie Universität Berlin, Arnimallee 14, 14195 Berlin, Germany

<sup>2</sup> Institut für Chemie, Humboldt-Universität zu Berlin, Brook-Taylor-Str. 2, 12489 Berlin, Germany

E-mail: [fabian.nickel@fu-berlin.de](mailto:fabian.nickel@fu-berlin.de)

Received 28 April 2017, revised 19 June 2017

Accepted for publication 28 June 2017


Published 10 August 2017



## Abstract

Diarylethenes are molecular switches, the state of which can efficiently be controlled by illumination with ultraviolet or visible light. To use the change in the molecular properties when switching between the two states for a specific function, direct contact with solid surfaces is advantageous as it provides immobilization. Here we present a study of a diarylethene derivate (T-DAE, 1,2-bis(5-methyl-2-phenylthiazol-4-yl)cyclopent-1-ene) in direct contact with highly ordered graphite as well as with semimetallic Bi(111) surfaces by x-ray photoelectron spectroscopy, x-ray absorption spectroscopy and simulated spectra based on density functional theory. On both surfaces, the molecule can be switched from its open to its closed form by 325–475 nm broadband or ultraviolet illumination. On the other hand, back isomerization to the ring-open T-DAE was not possible.

Keywords: diarylethene, molecular switch, surfaces, photochromism, adsorbed molecules, x-ray spectroscopy

 Supplementary material for this article is available [online](#)

(Some figures may appear in colour only in the online journal)

## 1. Introduction

Molecular switches have triggered the development of plenty of innovative and powerful devices in recent years [1–3]. Photochromism allows these molecules to be switched in a controlled manner between two isomeric forms by using ultraviolet/visible light as external stimuli. Diarylethenes (DAEs) are a class of molecular switches that can be reversibly inter-converted between a ring-open and a ring-closed isomer. The strong change of their electrical conductance upon isomerization renders DAEs promising candidates for molecular electronics on the smallest possible level. A vast number of investigations have been performed on DAEs [4, 5]. In particular the combination of the drastic change in conductance accompanied by only a small geometry alteration is of interest for the use as functional molecular unit in the solid state.

The transition from pure solid-state organic devices to organic-inorganic hybrid systems opens many new opportunities. For example, spatial control of functional units can be achieved by adsorption on inorganic surfaces. However, in contrast to several experiments in solution, the switching function becomes mostly quenched in the adsorbed state [6–8]. While photoswitchable thin films on gold surfaces have been realized [9], the first layer of the molecules is chemisorbed on the Au(111) surface via their sulfur atoms, leading to a loss of bistability. The switching behavior could be recovered upon decoupling the diarylethene from the gold surface via proper linkers to thiol anchoring groups [10]. Many studies of DAEs in direct contact with surfaces have been performed. On the Ag(111) surface, no chemisorption was found by scanning tunneling microscopy (STM) and excitation with the STM tip did lead to switching, but a reversible isomerization was not

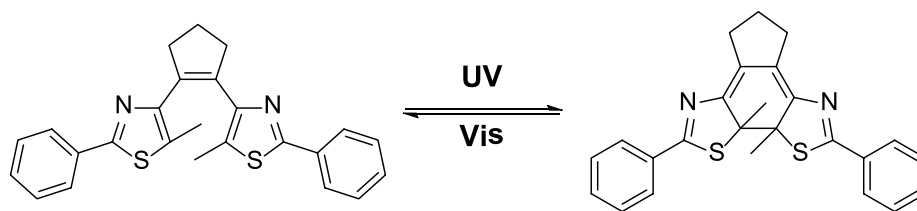


**Figure 1.** Chemical structure of T-DAE as open (left) and closed (right) isomer. Switching in solution can be induced by ultraviolet and visible light. [14]

shown [6]. Modifying the usually sulfur-containing switching unit of the DAEs by an oxygen unit prevents a chemisorption on the Au(111) surface and rises the possibility of a reversible switching by an STM tip [11]. Also in contact with organic semiconductors [12] or in between break junctions [13], the photochromic properties of DAEs were successfully demonstrated.

Here, we investigate the thiazole-containing DAE (T-DAE, figure 1), for which reversible photoswitching has been demonstrated in solution [14], by means of x-ray absorption (XA) and x-ray photoelectron spectroscopy (XPS) on highly oriented pyrolytic graphite (HOPG) and Bismuth(111) surfaces, accompanied by density functional theory using the StoBe code. T-DAE was chosen as it possesses photochromic properties similar to the well-known thiophene-containing analogues [14] and at the same time enables XA measurements using the nitrogen *K*-edge. The focus is on the adsorption of molecules in submonolayers with direct contact to the substrate and their light-induced isomerizations. After adsorption, the open-form isomer can be identified on both surfaces and switching can be induced by light.

## 2. Methods

All experiments were performed in an ultrahigh vacuum (UHV) chamber with a base pressure of  $p = 5 \times 10^{-10}$  mbar. The Bi(111) surface was prepared *in situ*, while preparation of the HOPG surface was carried out in high vacuum at  $p = 5 \times 10^{-7}$  mbar by cleaving with the help of a carbon tape. Bi(111) was cleaned by subsequent sputter and annealing cycles with  $\text{Ar}^+$  ions of 600 eV. Annealing was carried out for 15 min at 350 K. After cleaning of the substrates, no contamination was present in XPS and sharp low-energy electron diffraction (LEED) spots were observed for Bi(111) while a sharp ring-shaped LEED pattern was observed for HOPG.

X-ray measurements were performed at the BESSY II synchrotron radiation source of the Helmholtz-Zentrum Berlin by using linearly p-polarized x-rays of the undulator beamline UE56/2 PGM2, with a degree of polarization of about 99% and an energy resolution of approximately 150 meV. The x-ray absorption spectra were measured by means of the total electron yield method and normalized by the signal of a gold grid upstream to the measurement chamber as well as the corresponding background spectra of clean substrates. Thicknesses were defined by comparing to reference measurements of a spiropyran derivate [15] in a submonolayer on Bi(111), where the saturation of the first layer was monitored by XA at the carbon *K* edge. This calibration

is expected to give sufficient accuracy to confirm that the molecule coverage is below a saturated monolayer and the individual molecules have contact with the substrate. In case of a lower packing density of T-DAE, an error up to 20% to the defined value can be considered. The calibration on the HOPG surface was carried out by subtracting the absolute signal of the background and comparing the total nitrogen absorption with that of the molecules on the bismuth surface. A thickness of 69(5)% of a saturated layer, the latter defined as a monolayer (ML), has been determined for the samples presented here.

XPS was measured by a SPECS Phoibos 100 electron analyzer, at an energy resolution of 600 meV with 20 eV pass energy and at normal emission under 45° incidence. Excitation energies of 260 eV and 345 eV were used with an energy resolution of 200 meV. Binding energies have been calibrated to the Bi  $4f_{5/2}$  literature value of 162.3 eV. For the measurements on HOPG, the S 2*p* spectra measured with an excitation energy of 260 eV were calibrated to an S 2*p* spectrum recorded with an excitation energy of 345 eV that was referenced to a C 1*s* spectrum with 345 eV. The 345-eV-excitation S 2*p* spectrum was shifted according to the observed shift of the 284.4 eV C 1*s*  $\text{sp}^2$  peak [16, 17].

Molecules were evaporated from a Knudsen cell at a temperature of 393 K onto the substrate, kept at a temperature of around 200 K. The measurement spot was varied on the sample to reduce the amount of defragmentation of the molecules by the x-rays. Since an influence on the switching speed by the x-ray radiation has been seen for time-dependent measurements, the position of the x-ray spot was not varied and the condition of the molecules was checked after the illumination series. A more detailed discussion on the radiation influence is given in the results section. The syntheses and further details of the T-DAE molecules can be found in [14] and [18]. Details about the density functional theory (DFT) simulation by means of the StoBe code can be found in the supplementary data ([stacks.iop.org/JPhysCM/29/374001/mmedia](https://stacks.iop.org/JPhysCM/29/374001/mmedia)).

For the illumination by UV and visible light, a 1000 W xenon-mercury arc lamp was used. The light was collimated and an FM204 UV cold mirror with a reflection >90% between 325 and 475 nm was used to filter a UV and blue part of the light spectrum ('broadband'). Furthermore, a 30 cm focal length fused silica lens was used to focus the light through a fused silica window onto the sample surface inside the UHV chamber. For illumination during XPS measurements, an additional UG11 filter was used, leading to an intense UV illumination with the highest intensity at 325 nm and no light above 400 nm ('UV'). The photon flux density

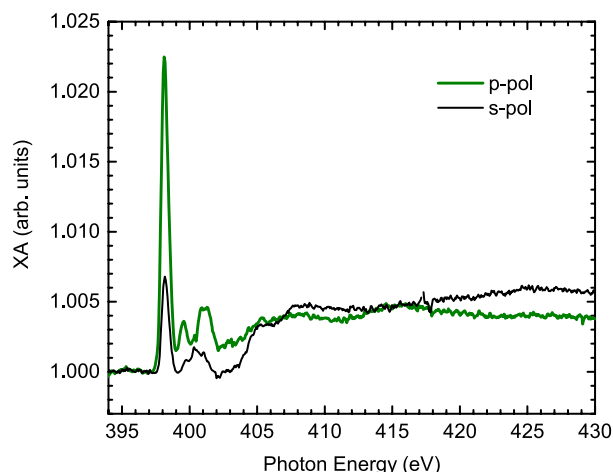


**Figure 2.** Polarization-dependent T-DAE XA after evaporation on to HOPG at  $T = 202$  K measured under  $20^\circ$  incidence.

was around  $\phi_{\text{broadband}} = 2.0(3) \cdot 10^{16}$  photons  $\text{s}^{-1}\text{mm}^{-2}$  and  $\phi_{\text{UV}} = 2.5(3) \cdot 10^{15}$  photons  $\text{s}^{-1}\text{mm}^{-2}$  in the two different illuminations, respectively.

### 3. Results and discussion

We investigated T-DAE on highly oriented pyrolytic graphite (HOPG) and a Bi(111) single crystal by means of XAS, XPS, and DFT simulations to identify the isomeric state of the adsorbed molecule and to switch it by *in situ* illumination in UHV.

#### 3.1. Adsorption on HOPG

Figure 2 shows the XA of 0.69(5) ML T-DAE on HOPG, for p- and s-polarization (green and black line, respectively) of the x-rays. Both polarizations were measured with an incidence angle of  $20^\circ$  between the surface and the k vector of the x-rays. A strong  $\pi^*$  resonance at 398.1 eV is visible for both, p- and s-polarized light. It is attributed to the excitation to the LUMO localized on the thiazole moieties, as shown in the supplementary data. From the ratio of the intensities for p- and s-polarized light, the mean angle of this LUMO can be determined [19]. The measured ratio of 3.3(2) leads to an angle of  $37(1)^\circ$  between the molecular orbital and the surface plane. The second and third peak at 399.6 and 401.0 eV, respectively, for the p-polarized light are less intense in the s-polarized spectrum. In contrast, a peak at 400.6 eV is more intense. In the supplementary data, orbitals presumably representing the p-polarized XA are shown. Due to the low XA signal in this photon energy range, a clear determination of the orbital orientations is not feasible. The 400.6-eV peak for s-polarized light may originate from an orbital (or combination of orbitals) that is more vertical on the surface than the magic angle ( $54.7^\circ$ ).

The energetically lowest configuration is the open-form isomer, therefore an adsorption in this isomerization state is assumed and later on discussed in more detail. DFT

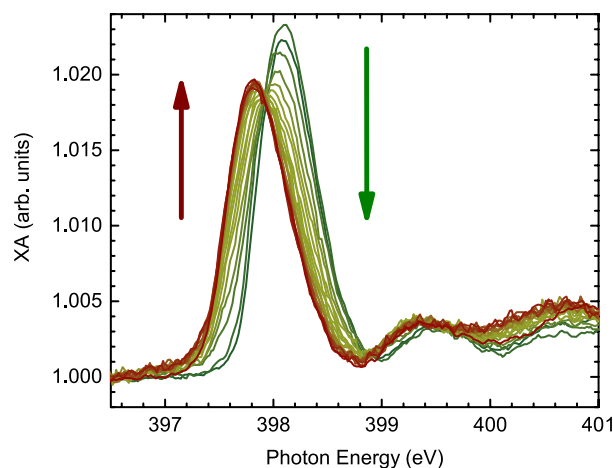


**Figure 3.** Measurements of the N K XA of T-DAE on HOPG under *in situ* illumination by the 'broadband' illumination setup (cf Methods section). Green is the beginning of the series and red is after 231 min of illumination. The spectra were taken by p-polarized light at  $20^\circ$  angle of incidence.

simulations (see supplementary data) for the free open-form molecule reveal an angle of around  $50^\circ$  between the two symmetric moieties. Since absorption by equivalent orbitals on both moieties of the T-DAE from the two nitrogen atoms contributes to that peak, the smallest determined angle by polarized XA for a flat-lying, unbent molecule would be on average  $25^\circ$ . The exact topology remains unclear, but it is known that flat-lying molecules on surfaces tend to interact strongly with the surface and therefore might prevent the switching ability.

#### 3.2. Light-induced switching

Illumination of T-DAE on HOPG was carried out by the UV/blue illumination as described in the experimental methods ('broadband'). The molecules, the spectra of which after adsorption are shown in figure 2, were illuminated *in situ* while in parallel measuring the p-polarized N K absorption. To gain insight into the kinetics of the switching process, shorter spectra of the first  $\pi^*$  resonance with higher point density were consecutively taken. The first spectrum (green) in figure 3 was measured before illumination. Afterwards the illumination was turned on until a saturation of the effect was nearly reached (red spectrum). The total illumination time was 231 min. To analyze the time dependence, all spectra were fitted as a superposition of the one of the pristine sample, with the  $\pi^*$  resonance at 398.1 eV, and the nearly saturated spectrum with a resonance at 397.8 eV. The intensity of the newly emerging peak is shown in figure 4 as a function of illumination time. Fitting a simple exponential function to the data, a time constant of  $\tau = 65.9(8)$  min for the process is acquired. Since the saturation of the exponential function would be reached for a prefactor of 1.03(1), the process is not completely saturated. Therefore a small amount of molecules is not yet switched, but there is no indication for molecules being unable to switch to the closed form. The corresponding effective cross section  $\sigma_{\text{eff}} = (\phi\tau)^{-1} = 1.3(2) \cdot 10^{-22}$  cm<sup>2</sup> is comparable to other photochromic processes on surfaces. Azobenzenes exhibit a *trans/cis* photoisomerization with an

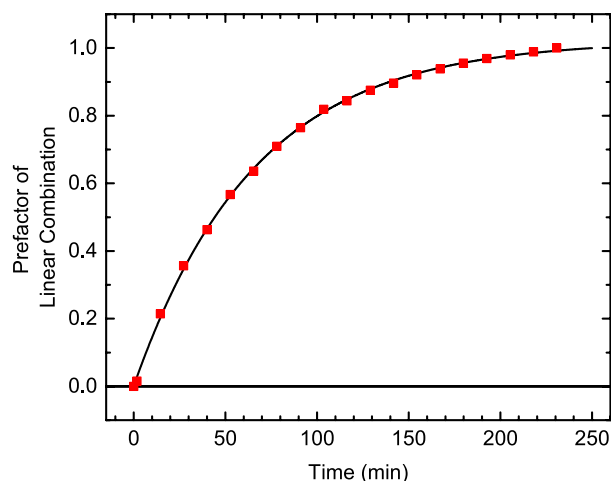


**Figure 4.** Exponential time dependence of the switching process as obtained from the fit of the spectra shown in figure 3.

effective cross section of around  $2 \cdot 10^{-24} \text{ cm}^2$  on Bi(111) [20], and around  $6 \cdot 10^{-20} \text{ cm}^2$  on Cu(111) [21]. Spiroyrans on bismuth accomplish switching with a cross section for conversion from spiropyran to merocyanine between  $2 \cdot 10^{-20} \text{ cm}^2$  [15] and  $4 \cdot 10^{-22} \text{ cm}^2$  [7]. However, all these effective cross sections represent rather inefficient switching processes, since in solution cross sections in the order of  $10^{-17} \text{ cm}^2$  can be achieved. The presence of a surface already reduces the light intensity due to the superposition of incoming and reflected waves. For HOPG this leads to an intensity reduction of about a factor of 4 [22]. The remaining difference must be attributed to the influence of the surface. Several reasons for lowering the switching ability of molecules on surfaces can be expected. An interaction between molecules and surface could lead to a strongly reduced lifetime of the excited states by additional de-excitation channels, so that the switching process cannot take place. Also, steric hindrance by the reduced degree of freedom in the switching pathway is another possibility of lowering the cross section on surfaces.

The polarization-dependent spectra for the N *K* XA are shown in figure 5. These data were recorded after the switching series from figure 3. The major change compared to figure 2 is the already mentioned shift of the first  $\pi^*$  resonance from 398.1 eV to 397.8 eV. The ratio between the same  $\pi^*$  resonances for both polarizations is now 4.8(2) and therefore, the average angle between molecular plane and the surface changes from  $37(1)^\circ$  to  $32(1)^\circ$ . This is a rather small change in angle and does not allow for a clear identification of the resulting form on the surface.

### 3.3. XPS

To identify the T-DAE isomers on the surface, XPS has been performed on the sulfur *2p* photoelectrons. The results (a) before and (b) after illumination are shown in figure 6. The setup for *in situ* ‘UV’ illumination during XPS is described in the experimental methods section. Before the illumination, a clear doublet of  $2p_{1/2}$  and  $2p_{3/2}$  photoelectrons can be identified, with a  $2p_{3/2}$  peak at 163.9 eV and the typical

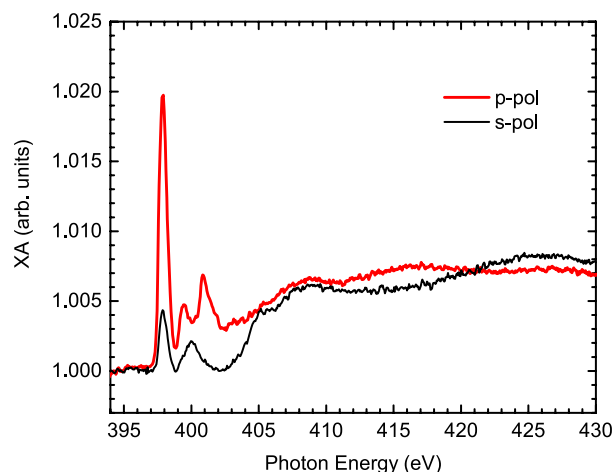


**Figure 5.** Polarization-dependent T-DAE XA after ‘broadband’ illumination for 231 min at  $T = 202 \text{ K}$ .

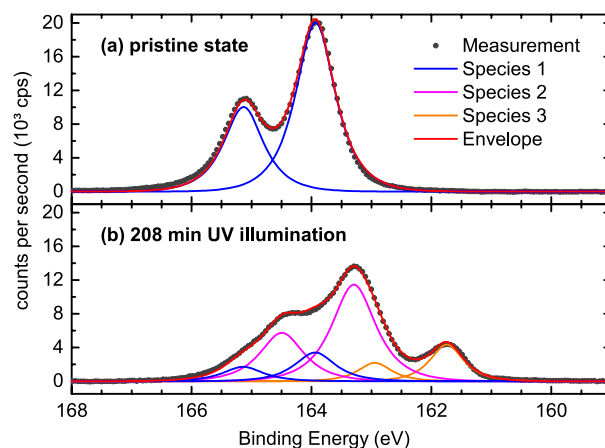


**Figure 6.** XPS of the S *2p* photoelectrons. In panel (a) the pristine sample is shown and fitted with a doublet. Panel (b) shows a convolution into three species of the T-DAE XPS after 208 min ‘UV’ illumination.

difference of 1.16 eV to the  $2p_{1/2}$  peak due to spin-orbit splitting. This binding energy is in good accordance to XPS of a self-assembled monolayer of DAE on a gold surface, where for the open form the sulfur photoelectrons are measured at 163.7 eV [23] and originating from the thiophene groups of an open-form isomer. The absence of a strong shift indicates a weak interaction of the molecule with the HOPG surface since that would probably lower the sulfur binding energies due to partial screening by the substrate [9]. After switching, three different sulfur species are needed to fit the experimental data. The pristine doublet is still present with an integrated intensity of 17(1)%, and two new species are emerging with their  $2p_{3/2}$  peaks at 163.3 eV and 161.7 eV, respectively. The former is attributed to a closed-form isomer with a shift of -0.6 eV with respect to the pristine form. The relative intensity of this species is 64(1)%. For a DAE switch in thin films on Au(111), a change of -0.8 eV has been reported [9]. The reason that the switching effect is not completely saturated, in contrast to the XA measurements, might be due to slight differences in illumination, since XPS is not measured on the same spot as



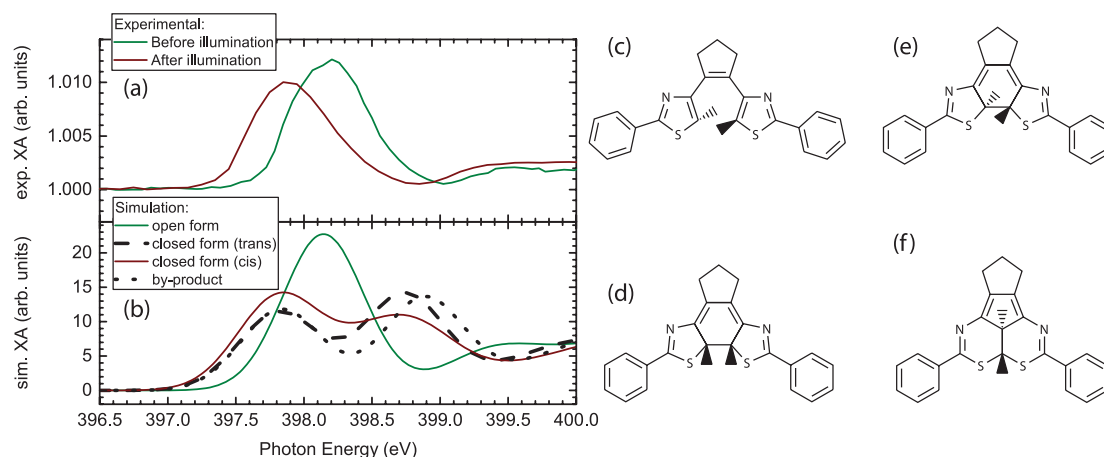


**Figure 7.** Comparison of the experimental isotropic N *K* edge XA of T-DAE on HOPG directly after adsorption and after illumination for 231 min (a) with the simulations for a free standing T-DAE molecule in the open form and three different closed-form isomers (b). The structures for the different isomers are shown on the right: (c) ring-open isomer, (d) ring-closed isomer with methyl groups in *cis* configuration, (e) ring-closed isomer with methyl groups in *trans* configuration, (f) by-product.

XA on the sample. In case of T-DAE on Bi(111) presented in the supplementary data and explained in the next section, the corresponding  $2p_{3/2}$  peak at 164.5 eV nearly vanishes at a fresh position on the sample. The origin of the latter species, the third sulfur species at 161.7 eV, remains unknown. This species cannot be attributed to a T-DAE isomer. A fraction of 19(1)% of the sulfur atoms is present in this state. A similar energy as for this species has been seen for dithienylethene on Au(111) [9], and has been assigned to chemisorbed sulfur. However, chemisorption on a HOPG surface is unlikely and therefore a decomposition due to the strong illumination by UV light is also a possible explanation. Due to the strong difference in binding energy, it can be assumed that this contribution originates from a strongly chemically modified compound.

### 3.4. T-DAE on Bi(111)

Similar to the results in previous sections, T-DAE was investigated on the Bi(111) surface. A detailed evaluation of this is given in section S2 of the supplementary data. XA was recorded in the same way as on HOPG. The submonolayer at 200 K showed a similar time dependence of the switching process with a time constant of 66.2(8) min. A clear distinction of the sulfur contributions in the XPS is not possible due to an overlying Bi  $4f_{5/2}$  peak. The pristine T-DAE sulfur is shifted by 0.6 eV to higher binding energies, but the relative shift in binding energy upon switching has nearly the same value. From the XPS time dependence during *in situ* illumination, a time constant of 33(1) min and an effective cross section of  $2.1(2) \cdot 10^{-21} \text{ cm}^2$  are determined. This is, as mentioned before, in a range that has been observed for several photochromic molecules on surfaces and is a bit higher than for the 'broadband' illumination. The deviation to the time constant as determined by XA measurements can be attributed to a higher x-ray photon flux and different optical setups. A comparable time constant for the 'UV' and for the 'broadband' illumination leads to the conclusion that UV light provokes the ring closing, as expected from UV/Vis measurements in solution [14]. The saturation of the effect is already reached

at 68(1)%, indicating a rather efficiently emerging by-product with x-ray illumination, whereas on a virgin sample position without previous x-ray exposure with 92(1)% a much higher percentage of closed-form T-DAE is determined.

### 3.5. Identification by DFT

Since from the experiment alone it remains unknown which T-DAE isomers are present on the surface, simulations for different structures for free molecules have been carried out by means of the StoBe code [24]. Figure 7 compares the experimental and simulation results. Panel (a) shows the experimental spectra for isotropic XA of T-DAE on HOPG at 202 K before and after illumination. The isotropic absorption before UV illumination was obtained by a measurement at an angle of  $54.7^\circ$  with p polarization. The corresponding spectrum after UV illumination is calculated from the polarization-dependent data shown in figure 5 according to [19]. Simulated spectra using the StoBe code are shown in panel (b). These spectra have been shifted by 2 eV to match the experimental results. Further details on the simulation and structures of the optimized molecules are given in the supplementary data. A very good accordance between the simulated spectrum of the ring-open isomer (structure shown in panel (c)) and the spectrum before switching is observed (both plotted in green colour). Only one absorption peak at around 398.1 eV for both, the simulated and experimental spectra, is visible. For the simulation of a ring-closed form, three different structures have been calculated: (d) an isomer with methyl groups in *cis* configuration; (e) an isomer with methyl groups in *trans* configuration; (f) a by-product that has been observed before [14, 18]. All three simulations give the same shift in absorption energy after the switching process with a new  $\pi^*$  resonance at 397.8 eV. Like in the experiment, this peak is reduced in intensity compared to the absorption before switching. The closed isomer with a *cis* configuration as shown in panel (d) fits slightly better to the experiment, but with a deviation at a photon energy around 398.8 eV. Such *cis* isomer is not expected, since it does not occur as a product during irradiation experiments in solution

and is not predicted by the Woodward–Hoffmann rules. All three simulations exhibit a double-peak structure that is not present in the experiment. The second peak is less intense for the *cis* product than for the *trans* form and the by-product. In the supplementary data, the orbitals that contribute to that second peak in the DFT simulations are presented for each configuration.

Due to the poor accordance of the XA spectrum after the switching reaction with the simulations, a distinct assignment of the resulting state is not possible. A possible deformation of the T-DAE due to surface interaction could lead to a change in the experimental XA and therefore to a deviation to the simulated spectra. However, all isomers show a similar shift of the first nitrogen resonance as observed in the experiment, which indicates that a ring closure was achieved on both surfaces, HOPG and Bi(111).

### 3.6. Possible stabilization of the ring-closed isomer

The reversibility of the switching process of molecules adsorbed on solid surfaces is self-evidently of huge importance for applications. During our investigations, several attempts have been carried out to reversibly switch T-DAE on HOPG and Bi(111) from the closed form to its open-form isomer. For example, illumination with an *FM203 visible cold mirror* in combination with a *GG400* filter, leading to an illumination spectrum between 400 nm and 650 nm with a photon flux density that is in the order of  $10^{16}$  photons  $\text{s}^{-1}\text{mm}^{-2}$ , did not lead to any visible backswitching in the XA spectra in a time span over 110 min, and for XPS even for 180 min. Illumination with a green LED was also carried out for a submonolayer of ring-closed T-DAE on HOPG. With a photon flux density of  $2.7(5) \cdot 10^{15}$  photons  $\text{s}^{-1}\text{mm}^{-2}$  for 75 min, also no reversibility was observed. This leads to the conclusion that the cross section for a reversible switching process would be far below  $10^{-22}$   $\text{cm}^2$ . Dissolved in acetonitrile, the quantum yield for ring-opening is around 0.02, whereas the ring-closing isomerization has a quantum yield of 0.56 [18]. Taking into account this difference in quantum yield, clearly a slower switching process would be expected, but it could even be quenched on the surface. A reversible switching could only be seen if the efficiency for the backreaction would increase strongly on the surface, otherwise time constants would lie in the order of several hours.

## 4. Conclusion

Using x-ray spectroscopies we prove that T-DAE adsorbs on solid surfaces in submonolayers in the expected open form. The molecules are tilted with an average angle of  $37(1)^\circ$  with respect to the surface plane. When illuminating with a broad-band UV and blue illumination, switching can be identified from the nitrogen XA. The effective cross section for this process is  $1.3(2) \cdot 10^{-22}$   $\text{cm}^2$ . XPS reveals two new species of sulfur, one of which is attributed to a closed-form isomer. However, distinct assignment of the switched state of the molecule by DFT simulations of the XA spectra is not possible. The

light-triggered backreaction could not be induced, pointing to a rather low efficiency or complete quenching of the process.

## Acknowledgments

This work was financially supported by the DFG through Sfb 658. LMA received funding from CAPES (No. 9469/13-3). We thank the HZB for the allocation of synchrotron radiation beamtime and B Zada and W Mahler for their technical support during the measurements at BESSY II in Berlin. Computing time on the high-performance cluster of the Zentraleinrichtung für Datenverarbeitung (ZEDAT) at the Freie Universität Berlin is gratefully acknowledged.

## References

- [1] Leydecker T, Herder M, Pavlica E, Bratina G, Hecht S, Orgiu E and Samor P 2016 *Nat. Nanotechnol.* **11** 769–75
- [2] Ragazzon G, Baroncini M, Silvi S, Venturi M and Credi A 2015 *Nat. Nanotechnol.* **10** 70–5
- [3] Zhao H, Sen S, Udayabhaskararao T, Sawczyk M, Kučanda K, Manna D, Kundu P K, Lee J W, Král P and Klajn R 2016 *Nat. Nanotechnol.* **11** 82–8
- [4] Uchida K, Yamanoi Y, Yonezawa T and Nishihara H 2011 *J. Am. Chem. Soc.* **133** 9239–41
- [5] Irie M, Fukaminato T, Matsuda K and Kobatake S 2014 *Chem. Rev.* **114** 12174–277
- [6] Wirth J, Hatter N, Drost R, Umbach T R, Barja S, Zastrow M, Rück-Braun K, Pascual J I, Saalfrank P and Franke K J 2015 *J. Phys. Chem. C* **119** 4874–83
- [7] Schulze G, Franke K J and Pascual J I 2012 *Phys. Rev. Lett.* **109** 026102
- [8] Krüger A, Bernien M, Hermanns C F and Kuch W 2014 *J. Phys. Chem. C* **118** 12916–22
- [9] Mendoza S M, Lubomska M, Walko M, Feringa B L and Rudolf P 2007 *J. Phys. Chem. C* **111** 16533–7
- [10] Kudernac T, van der Molen S J, van Wees B J and Feringa B L 2006 *Chem. Commun.* 3597–9
- [11] Reece G, Lotze C, Sysoiev D, Huhn T and Franke K J 2016 *ACS Nano* **10** 10555–62
- [12] Wang Q, Frisch J, Herder M, Hecht S and Koch N 2017 *ChemPhysChem* **18** 722–27
- [13] Kim Y *et al* 2012 *Nano Lett.* **12** 3736–42
- [14] Herder M, Eisenreich F, Bonasera A, Grafl A, Grubert L, Pätzelt M, Schwarz J and Hecht S 2017 *Chem. Eur. J.* **23** 3743–54
- [15] Nickel F, Bernien M, Krafft K, Krüger D, Arruda L M, Kipgen L and Kuch W 2017 in preparation
- [16] Brühwiler P A, Maxwell A J, Puglia C, Nilsson A, Andersson S and Mårtensson N 1995 *Phys. Rev. Lett.* **74** 614–7
- [17] Mérel P, Tabbal M, Chaker M, Moisa S and Margot J 1998 *Appl. Surf. Sci.* **136** 105–10
- [18] Herder M, Schmidt B M, Grubert L, Pätzelt M, Schwarz J and Hecht S 2015 *J. Am. Chem. Soc.* **137** 2738–47
- [19] Stöhr J and Outka D A 1987 *Phys. Rev. B* **36** 7891–905
- [20] Bronner C, Priewisch B, Rück-Braun K and Tegeder P 2013 *J. Phys. Chem. C* **117** 27031–8
- [21] Bazarnik M, Henzl J, Czajka R and Morgenstern K 2011 *Chem. Commun.* **47** 7764–6
- [22] Bernien M *et al* 2015 *ACS Nano* **9** 8960–6
- [23] Pijper T C, Ivashenko O, Walko M, Rudolf P, Browne W R and Feringa B L 2015 *J. Phys. Chem. C* **119** 3648–57
- [24] Hermann K, Pettersson L G M, Casida M, Daul C, Goursot A, Koester A, Proynov E, St-Amant A and Salahub D R 2014 StoBe-deMon, version 3.3 ([www.fhi-berlin.mpg.de/KHsoftware/StoBe/](http://www.fhi-berlin.mpg.de/KHsoftware/StoBe/))



## Supplementary data

### Light-induced ring closure of a diarylethene molecular switch on solid surfaces

**Fabian Nickel<sup>1</sup>, Matthias Bernien<sup>1</sup>, Martin Herder<sup>2</sup>, Sandro Wrzalek<sup>1</sup>, Pantelis Chittas<sup>1</sup>, Kai Kraffert<sup>1</sup>, Lucas M. Arruda<sup>1</sup>, Lalminthang Kipgen<sup>1</sup>, Dennis Krüger<sup>1</sup>, Stefan Hecht<sup>2</sup>, Wolfgang Kuch<sup>1</sup>**

<sup>1</sup> Institut für Experimentalphysik, Freie Universität Berlin, Arnimallee 14, 14195 Berlin, Germany

<sup>2</sup> Institut für Chemie, Humboldt-Universität zu Berlin, Brook-Taylor-Str. 2, 12489 Berlin, Germany

E-mail: [fabian.nickel@fu-berlin.de](mailto:fabian.nickel@fu-berlin.de)

Submitted to: *J. Phys.: Condens. Matter*

## S1. Details of the StoBe simulations

Theoretical simulations by DFT have been carried out using the StoBe code package [1]. This package has been used for several XA simulations of gas phase molecules. For not strongly coupled molecules, the simulation fits very well even for molecules on surfaces [2–4].

Figure S1 shows T-DAE after relaxation in the four states used for the simulation of the XA spectra.

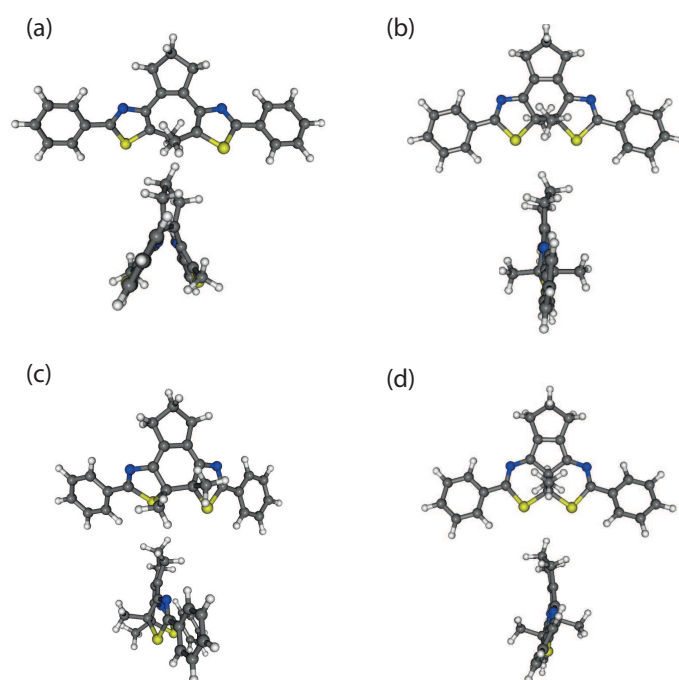


**Figure S1.** DFT derived structures of T-DAE optimized by the StoBe code in the TZVP basis set. The top part of each panel shows the front and the bottom part the side view of: (a) ring-open isomer, (b) ring-closed isomer (*trans* configuration), (c) ring-closed isomer (*cis* configuration), (d) by-product.

A gradient-corrected RPBE (revised Perdew-Burke-Ernzerhof) exchange correlation functional [5, 6] has been used for both, geometry optimization and XA simulation. A triple-zeta valence plus polarization (TZVP) basis set was chosen according to [7] with field-induced polarization (FIP) functions for the hydrogen atoms [8]. *K* edge absorption spectra are simulated by the Slater transition state (TS) method [9, 10]. For that, in the core-excited states, IGLO-III basis sets [11] are used on the center of excitation, whereas remaining atoms of the same element are described by an effective core potential as given in [12]. The double-basis-set technique by adding a large diffuse [19s, 19p, 19d] basis on the center of excitation is used [13]. To compare the resulting simulations with the experiment, all spectra were shifted by 2.0 eV to lower energies. Gaussian broadening was applied to the discrete transition energies. The full width at half maximum (FWHM) for the Gaussian was set to 0.7 eV for transitions below the ionization potential and then linearly increased to a FWHM of 4.5 eV up to a photon energy of 10 eV above the ionization potential.

Figure S2 shows the orbitals that are predominant in the simulated nitrogen XA for the T-DAE molecule in its open form. The orbitals are acquired by using the transition state calculations as included in the StoBe code. Their transition excitation energies are given in the caption.

In analogy, figure S3 shows the transition state orbitals for the three closed-form isomers. The LUMO and LUMO+1 transitions for each configuration are given to explain the excitations as shown in the paper in figure 7.

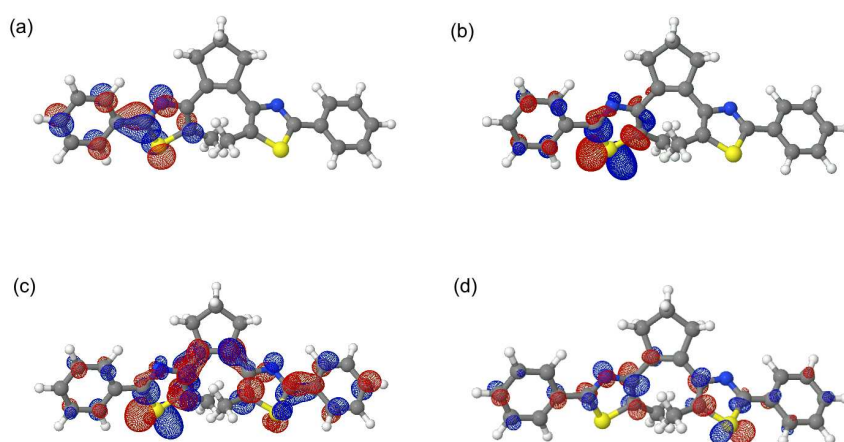


**Figure S2.** Orbitals of the T-DAE open-form isomer that are presumably most intense in XA. All orbitals as determined by the Slater transition-state method with an excitation on the nitrogen atom on the left-hand side are depicted.

(a) LUMO (398.1 eV);

(b) LUMO+4 (400.0 eV);

(c) superposition of the excitations at 399.3, 399.5, and 400.0 eV;

(d) LUMO+8 (400.9 eV)

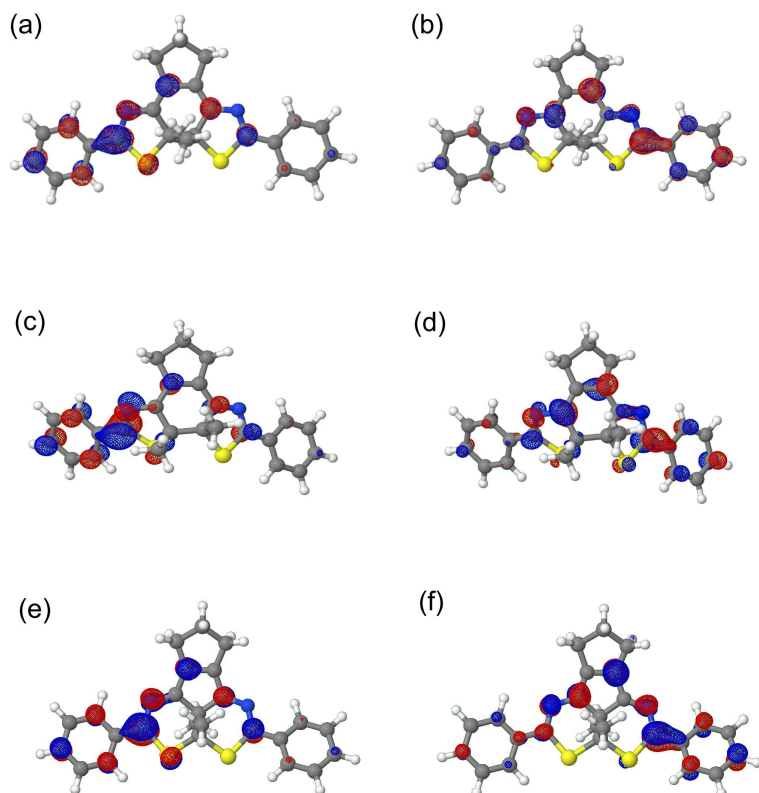


**Figure S3.** Orbitals of the T-DAE closed-form isomers that are presumably most intense in XA. All orbitals as determined by the Slater transition-state method with an excitation on the nitrogen atom on the left-hand side are depicted.

(a), (b): ring-closed isomer with methyl groups in *trans* configuration, with (a) LUMO (397.8 eV), (b) LUMO+1 (398.7 eV);

(c), (d): ring-closed isomer with methyl groups in *cis* configuration, with (c) LUMO (397.8 eV), (d) LUMO+1 (398.6 eV);

(e), (f): by-product, with (e) LUMO (397.8 eV), (f) LUMO+1 (398.9 eV).

## S2. T-DAE on Bi(111)

### S2.1. XA of T-DAE on Bi(111)

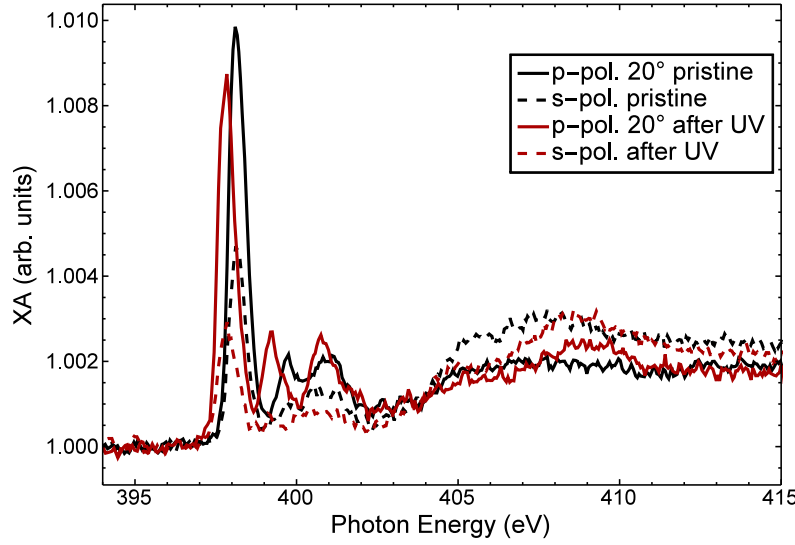


**Figure S4.** Polarization-dependent T-DAE XA after evaporation onto Bi(111) at  $T = 200$  K (pristine, shown in black). After illumination, the peaks shift to lower absorption energies (shown in red).

T-DAE on Bi(111) has been investigated in the same way as on HOPG. Figure S4 presents the polarization-dependent XA of a submonolayer at  $T = 200$  K before and after "broadband" light illumination for 208 min. In black the XA before and in red color the XA after the switching process are shown. The average orientation of the molecules on the Bi(111) surface changes from  $43(1)^\circ$  to  $38(1)^\circ$  between the molecules and the surface plane. The change in angle is the same as on the HOPG surface, but with a bit steeper angle before and after illumination. Also the peak positions are the same, with 398.1 eV before switching and 397.8 eV after switching. Figure S5 shows the time evolution of the first  $\pi^*$  resonances of the N  $K$  absorption edge recorded with p-polarized light. The time constant of  $\tau = 66.2(8)$  min is essentially the same as for the switching on graphite. This leads again to the same low cross-section of  $\sigma_{eff} = (\phi\tau)^{-1} = 1.3(2) \cdot 10^{-22}$  cm<sup>2</sup>. The time dependence of the switching is therefore very much the same as on HOPG in the main paper (figures 3 and 4). The error in the determination of the cross-section is dominated by the uncertainties in the flux density due to different alignments of the illumination setup on the UHV chamber.

In contrast to the HOPG surface, the polarization dependence of the carbon  $K$

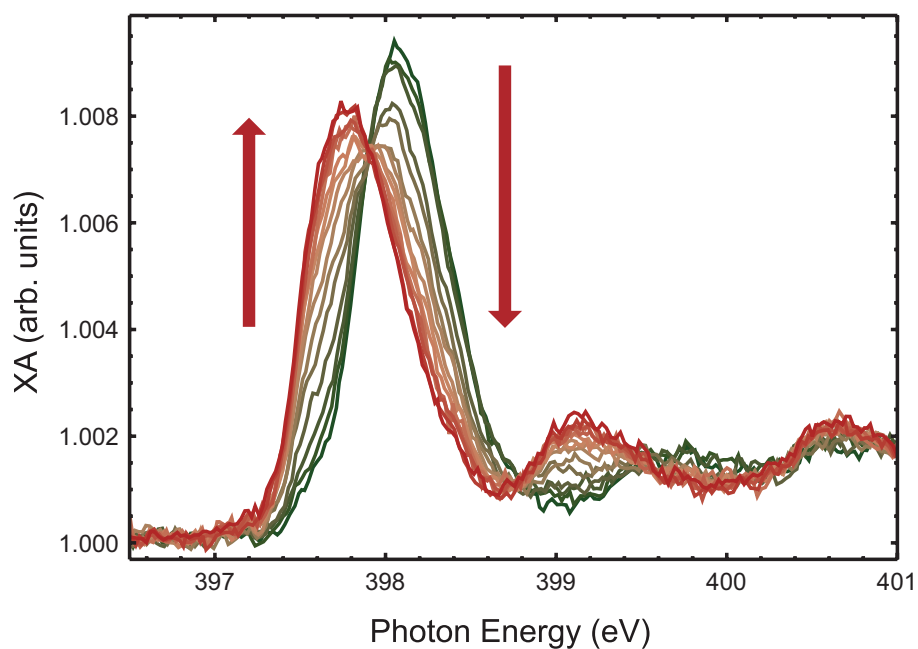


**Figure S5.** Measurements of the N *K* XA of T-DAE on Bi(111) by p-polarized light under 20° incidence with *in-situ* illumination by the described illumination setup. The spectra are shown for 208 minutes illumination.

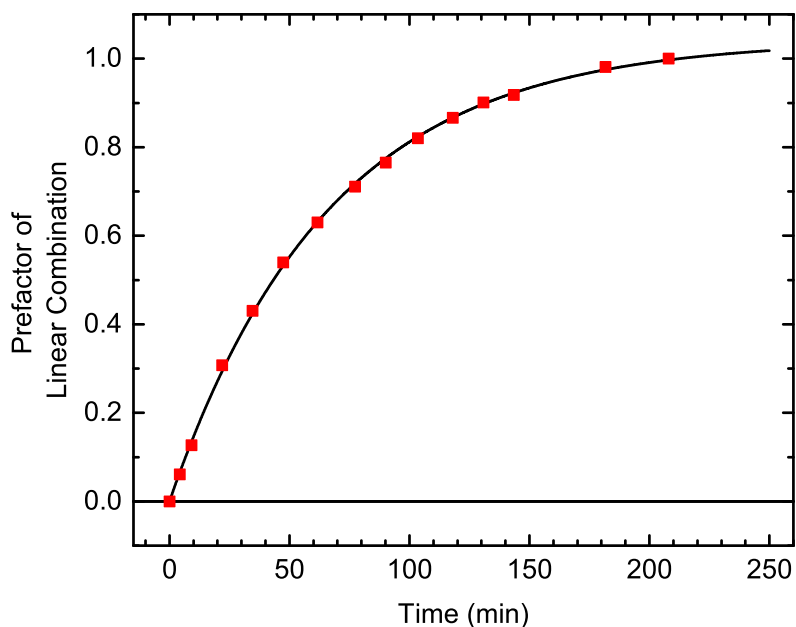


**Figure S6.** Prefactor of each spectrum for the linear combination of first and last spectrum from figure S5. A prefactor of 0 means no contribution from the switched closed form isomer and at a prefactor of 1, mainly the closed-form isomer is present.

edge absorption signal of the molecules can also be identified by XA. In figure S7, the carbon XA (a) before and (b) after illumination is shown in analogy to the nitrogen XA in figure S4. Due to low x-ray intensity (originating from beamline contamination) and several changes on the carbon XA, a determination of molecule angles or direct comparison to DFT results is not useful.

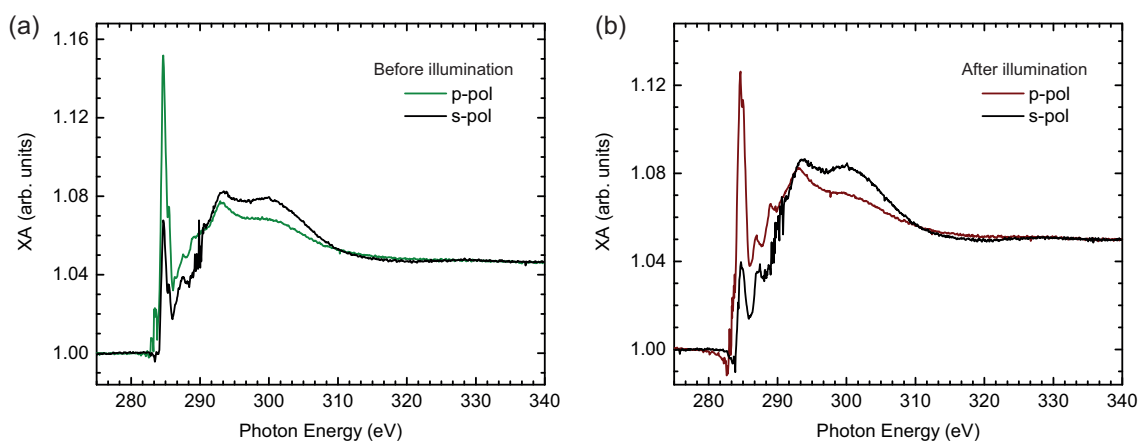


**Figure S7.** XA on the carbon *K* edge. (a) before illumination and (b) after illumination by the broadband light.

## S2.2. XPS of T-DAE on Bi(111)

XPS of the S 2*p* photoelectrons of T-DAE on the Bi(111) surface was performed with an excitation energy of 260 eV. Unfortunately, the Bi 4*f*<sub>5/2</sub> peak at 162.3 eV is overlapping with the sulfur signal coming from the molecules. Nonetheless, before switching, one distinct species with a 2*p*<sub>3/2</sub> peak at 164.5 eV is identifiable. This is shown in the top left panel of figure S8 for the pristine sample. Subsequently, *in-situ* illumination by "UV" light (as described in the Methods section in the paper) in XPS position was performed. The energy of the sulfur doublet from the pristine sample was kept fixed during the fit while its amplitude was treated as a free parameter. Fitting the newly emerging component of a sulfur species with its S 2*p*<sub>3/2</sub> peak at 163.8 eV enables to monitor the time dependence of the switching as well during the XPS measurements. Of course, by doing that, one ignores the contribution of a possible third species as it was observed on HOPG. This potential contribution is obscured by the 162.3 eV bismuth peak. Compared to HOPG, the pristine T-DAE sulfur binding energies are shifted by 0.6 eV to higher binding energies. The species, emerging with UV illumination, is as well shifted by 0.5 eV in the same direction such that the relative shift is very similar to the one measured on HOPG. This points again towards a very similar behaviour of T-DAE on HOPG and Bi(111).

Evaluation of the time dependence of the conversion of T-DAE from the XP measurements shown in figure S8 is possible by the determination of the areas of all observed species. A complete transfer of the area of the peak of the pristine species to the one of the new emerging species is assigned to a completely switching sample. The first seven panels are plotted in figure S9 and fitted by a simple exponential model. The data is well described by the fit yielding an extrapolated saturation of switched molecules of 68(1)%. This is very close to the value of 64(1)% as seen on HOPG and points towards the existence of a third sulfur species, again at lower binding energies. The time constant for this switching process is  $\tau = 33(1)$  min. Together with the reduced photon flux for the "UV" illumination, this leads to an effective cross section of  $\sigma_{eff} = (\phi\tau)^{-1} = 2.1(2) \cdot 10^{-21}$  cm<sup>2</sup>, which is one order of magnitude higher than the one of the illuminations with the "broadband" light, indicating that the ring-closure of T-DAE is probably triggered by UV light only. It is not clear why the switching under "UV" illumination is faster on the absolute time scale. The most likely explanation is a different alignment of the light source, but the possibility of a back reaction cannot be fully excluded for the case of "broadband" illumination.

XPS in the last panel on the bottom right is taken at a completely virgin (no previous x-ray illumination) and long-time UV-illuminated position on the sample. The amount of switched molecules with 92(1)% does not fit anymore to the time-dependence presented in figure S9. This can be explained by the formation of the third sulfur species by x-ray radiation and indicates that all of the molecules can perform a ring-closure. The third species of sulfur does not contribute to the fraction of closed form isomers in case of the fitting for the figure S6. It is not possible to determine if there is a third



sulfur species present on the Bi(111) surface. In case there is not, it would probably lead to a completely switched T-DAE molecule layer on the surface.

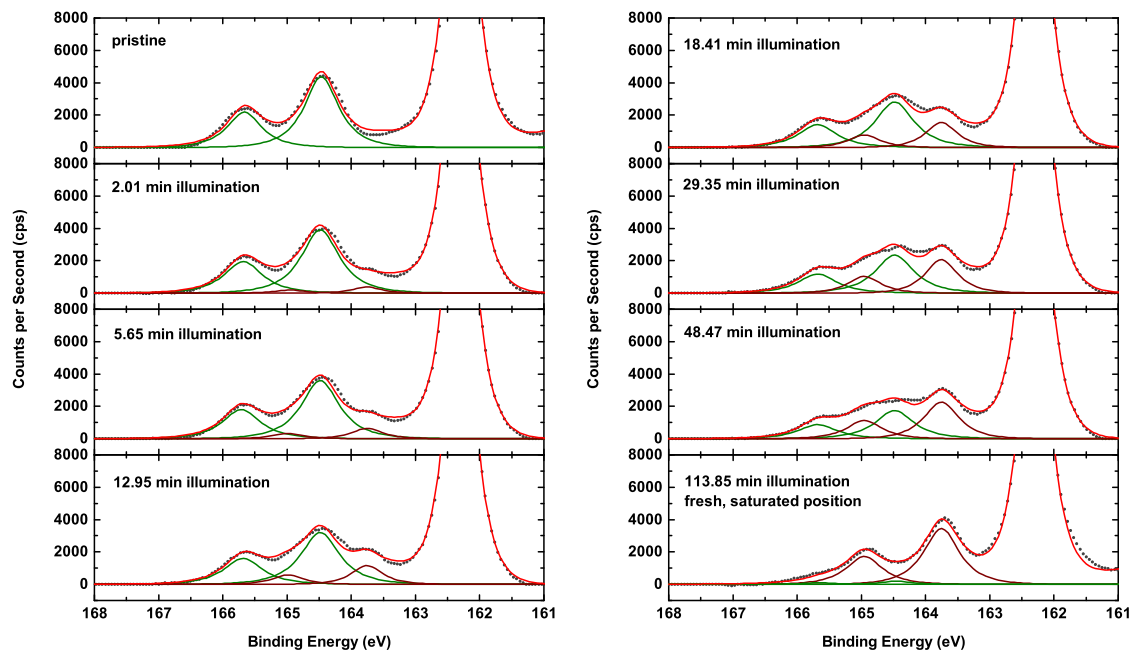


**Figure S8.** XPS for different "UV" illumination times of T-DAE on Bi(111). The last panel on the bottom right shows the XPS on a fresh and nearly saturated sample position.

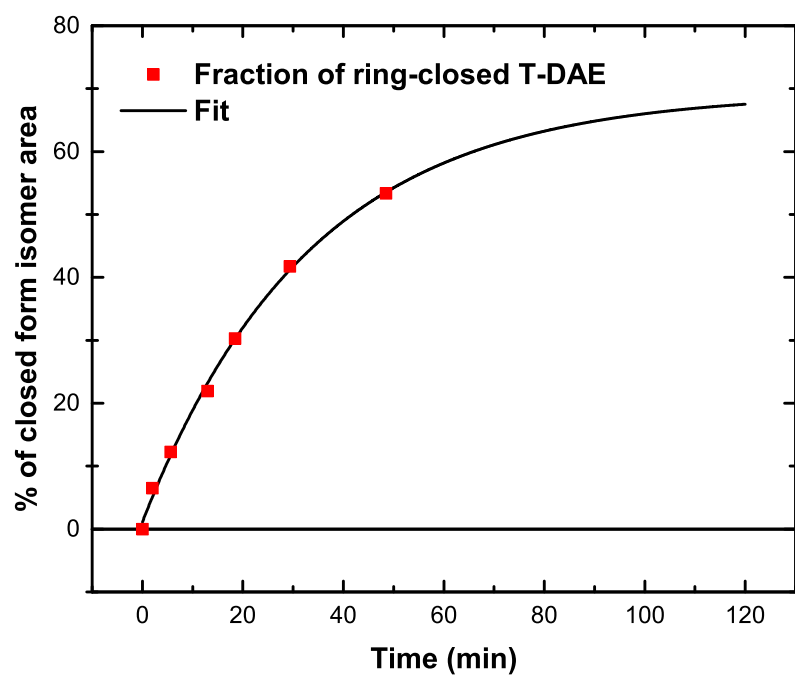


**Figure S9.** Percentage of area of the closed-form T-DAE determined from figure S8. 100% of switched molecules corresponds to a complete transfer of the area of the S  $2p_{3/2}$  peak at 164.5 eV to the sulfur species with the S  $2p_{3/2}$  peak at 163.8 eV.

### S2.3. Comparison to StoBe simulations

Figure S10 shows the comparison of the measurements before and after switching of the nitrogen XA with the theoretical simulations using the StoBe code. The simulations are the same as shown in the article but on a larger energy scale. Panel (a) shows the isotropic absorption of T-DAE on the Bi(111) surface. Panel (b) presents the simulation of the open-form T-DAE, which shows a very good accordance to the adsorbed molecule. Below are the shown: (c) experimental data of T-DAE after 208 min "broadband" illumination, (d), (e), (f), simulations for gas phase isomers in *trans*, *cis*, and by-product conformation, respectively.

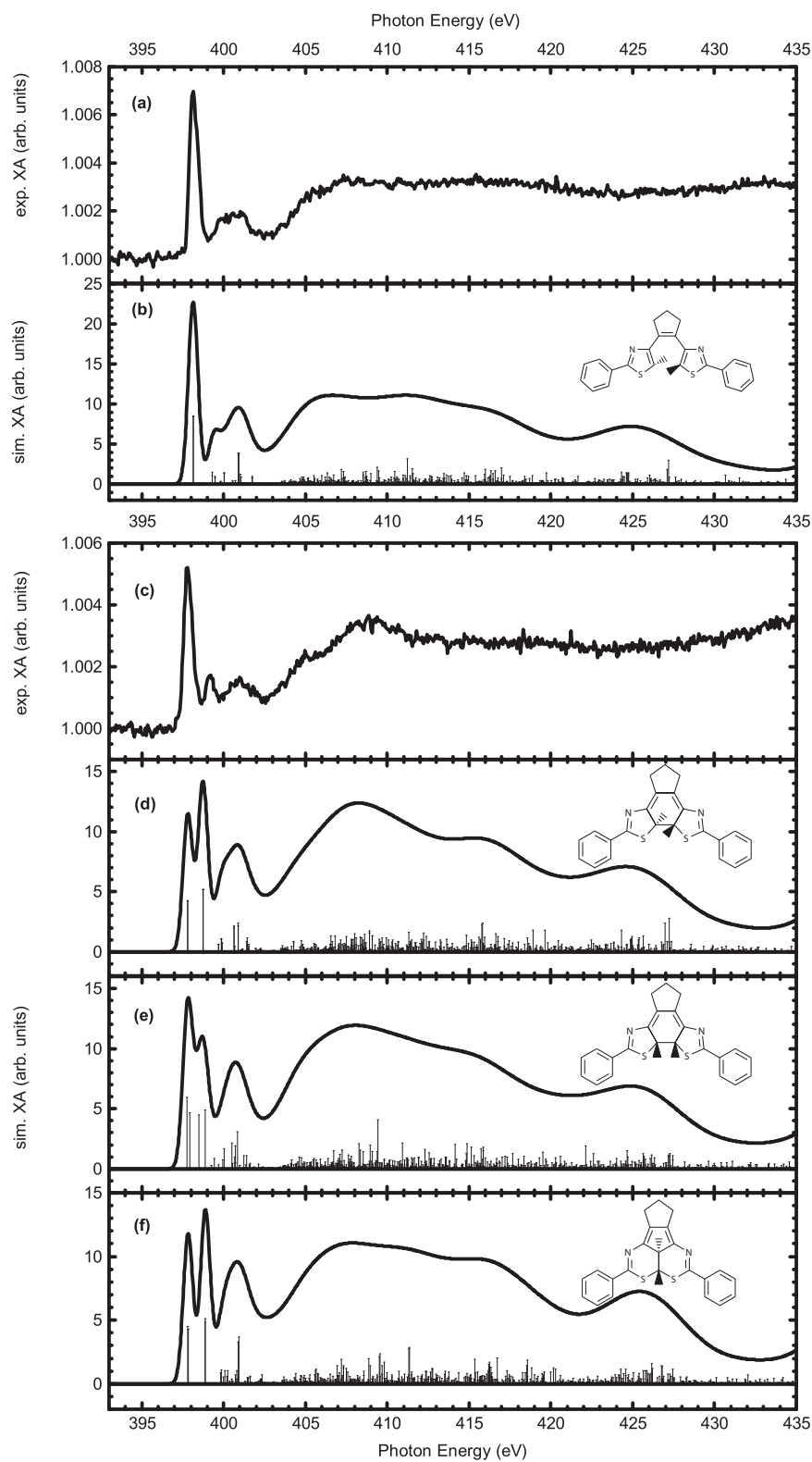


**Figure S10.** Comparison of the N *K* edge XA on Bi(111): both top panels give the pristine nitrogen XA (a) and the simulated one of the corresponding open-form isomer (b). Below is the T-DAE XA on Bi(111) after switching (c) and simulations for three possible isomers (d), (e), (f), as shown in the insets.

## Bibliography

- [1] Hermann K, Pettersson L G M, Casida M, Daul C, Goursot A, Koester A, Proynov E, St-Amant A and Salahub D R 2014 StoBe-deMon, version 3.3
- [2] Piantek M, Schulze G, Koch M, Franke K J, Leyssner F, Krüger A, Navío C, Miguel J, Bernien M, Wolf M, Kuch W, Tegeder P and Pascual J I 2009 *J. Am. Chem. Soc.* **131** 12729–12735
- [3] Piantek M, Miguel J, Krüger A, Navío C, Bernien M, Ball D K, Hermann K and Kuch W 2009 *J. Phys. Chem. C* **113** 20307–20315
- [4] Guo C S, Sun L, Hermann K, Hermanns C F, Bernien M and Kuch W 2012 *J. Chem. Phys.* **137** 194703
- [5] Perdew J P, Burke K and Ernzerhof M 1996 *Phys. Rev. Lett.* **77** 3865–3868
- [6] Hammer B, Hansen L B and Nørskov J K 1999 *Phys. Rev. B* **59** 7413–7421
- [7] Godbout N, Salahub D R, Andzelm J and Wimmer E 1992 *Can. J. Chem.* **70** 560–571
- [8] Guan J, Duffy P, Carter J T and Chong D P 1993 *The Journal of Chemical Physics* **98** 4753–4765
- [9] Slater J C 1972 Statistical Exchange-Correlation in the Self-Consistent Field *Advances in Quantum Chemistry* vol 6 ed Löwdin P O (Academic Press) pp 1–92
- [10] Slater J C and Johnson K H 1972 *Phys. Rev. B* **5** 844–853
- [11] Kutzelnigg W, Fleischer U and Schindler M 1990 The IGLO-Method: Ab-initio Calculation and Interpretation of NMR Chemical Shifts and Magnetic Susceptibilities *Deuterium and Shift Calculation (NMR Basic Principles and Progress* no 23) (Springer Berlin Heidelberg) pp 165–262 ISBN 978-3-642-75934-5 978-3-642-75932-1
- [12] Pettersson L G M, Wahlgren U and Gropen O 1987 *J. Chem. Phys.* **86** 2176–2184
- [13] Ågren H, Carravetta V, Vahtras O and Pettersson L G M 1997 *Theor. Chem. Acta.* **97** 14–40



## 6.2 Adv. Funct. Mater. 27, 1702280 (2017)

By Fabian Nickel, Matthias Bernien, Kai Kraffert, Lucas M. Arruda, Lalminthang Kipgen, and Wolfgang Kuch

### Reversible Switching of Spiropyran Molecules in Direct Contact With a Bi(111) Single Crystal Surface

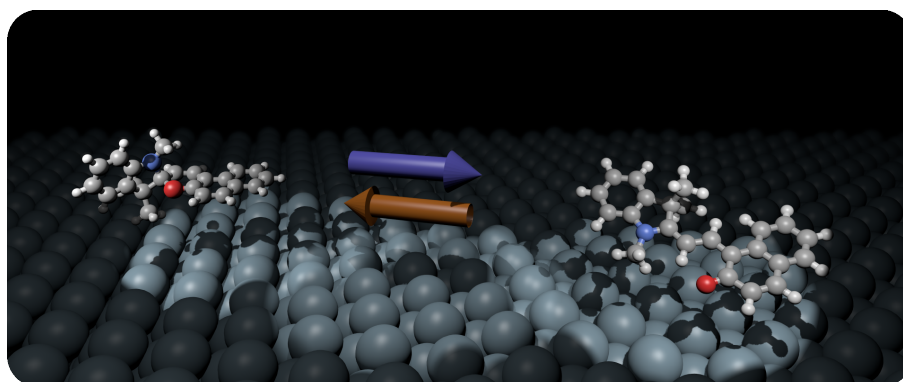
Published online November 2017

DOI: <https://doi.org/10.1002/adfm.201702280>

© 2017 WILEY-VCH Verlag GmbH & Co. KGaA, Weinheim

#### Contributions:

FN, MB and WK planned and supervised the XAS experiments. FN, MB, KK, LMA, LK performed the XAS experiments. FN analyzed the XAS data. FN and MB created the model and performed the fits. FN carried out the DFT simulations. All authors discussed the results. FN prepared and wrote the manuscript with corrections by MB and WK. WK supervised the study.







# Reversible Switching of Spiropyran Molecules in Direct Contact With a Bi(111) Single Crystal Surface

Fabian Nickel, Matthias Bernien,\* Kai Kraffert, Dennis Krüger, Lucas M. Arruda, Lalminthang Kipgen, and Wolfgang Kuch

Photochromic molecular switches immobilized by direct contact with surfaces typically show only weak response to optical excitation, which often is not reversible. In contrast, here, it is shown that a complete and reversible ring-opening and ring-closing reaction of submonolayers of spironaphthopyran on the Bi(111) surface is possible. The ring opening to the merocyanine isomer is initiated by ultraviolet light. Switching occurs in a two-step process, in which after optical excitation, an energy barrier needs to be overcome to convert to the merocyanine form. This leads to a strong temperature dependence of the conversion efficiency. Switching of the merocyanine isomer back to the closed form is achieved by a temperature increase. Thus, the process can be repeated in a fully reversible manner, in contrast to previously studied nitro-spiropyran molecules on surfaces. This is attributed to the destabilization of the merocyanine isomer by the electron-donating nature of the naphtho group and the reduced van der Waals interaction of the Bi(111) surface. The result shows that molecules designed for switching in solutions need to be modified to function in direct contact with a surface.

## 1. Introduction

Molecules that can be switched by external stimuli in a reversible manner have attracted tremendous scientific interest since they allow for the manipulation of materials on the nanoscale. In biological systems, they are crucial for the realization of complex functions like, e.g., sight<sup>[1]</sup> or cell regulation.<sup>[2]</sup> Over the last century, chemists have designed many molecules that can, for example, switch their conformation,<sup>[3]</sup> electric dipole moment,<sup>[4]</sup> magnetic moment,<sup>[5]</sup> conductance,<sup>[6,7]</sup> or trigger a unidirectional motion in molecular machines.<sup>[8,9]</sup> If such molecular switches are used to represent information, they have the potential to boost the density in data storage or information processing.<sup>[10,11]</sup> To use individual switchable molecules as functional units of data storage or processing devices, they need to be immobilized and contacted. This requires to bring the molecules into contact with a surface. However, molecules

that are designed to show a certain functionality in solution may lose this property if they are adsorbed on a surface. Several reasons can be identified as the cause for a quenching of their switching behavior in contact with a surface: A chemical reaction with the substrate may take place that changes the molecular properties;<sup>[12]</sup> the lifetime of the excited state reached by the stimulus may be reduced on the surface due to additional de-excitation channels;<sup>[13]</sup> the interaction with the surface may shift total energies and result in a destabilization of one of the two metastable ground states.<sup>[14]</sup> Especially in densely packed molecular layers, steric hindrance and intermolecular interaction are additional causes for suppression of switching functionality.

Spiropyran (SP) is a molecular switch that can be controlled by light. It undergoes a ring opening reaction to its merocyanine (MC) form upon UV light exposure. The initial SP state can be restored by visible light or thermal activation, as illustrated in **Figure 1a**. The ring-opening reaction is accompanied by a change in electronic conjugation, which can be used to switch the electrical conductance. The strong difference between the electric dipole moments of the two molecular states is useful, for example, to optically control the electrostatic properties of a surface.<sup>[15]</sup> The ring-opening from SP to MC and the ring-closing back reaction are widely investigated in solutions,<sup>[16–21]</sup> but a reversible switching of SP molecules in direct contact with solid surfaces has not yet been achieved. Switching was only reported in nanometer-thick films of SP containing a nitro group on MgO(100)<sup>[22]</sup> and in self-assembled molecules on nanoparticles.<sup>[23,24]</sup> Directly adsorbed submonolayers (sub-MLs) on Au(111) showed ground-state energies that are reversed compared with solution.<sup>[14]</sup> The MC state is thereby stabilized by the formation of an image dipole at the surface, increased van der Waals interaction due to its planar geometry, and the formation of molecular dimers by hydrogen bonds. Heating above room temperature led to a thermally activated, irreversible transition from the SP to the MC state.<sup>[14]</sup> On Bi(110), a light-induced ring opening of SP has been observed but no thermal- or light-induced back reaction could be shown.<sup>[25]</sup> Here, we investigate sub-MLs of a spironaphthopyran (SNP, see **Figure 1a**) on Bi(111). Compared with the former experiments, the electron-withdrawing nitro group is replaced by an electron-donating naphtho group in order to destabilize the MC

F. Nickel, Dr. M. Bernien, K. Kraffert, D. Krüger, L. M. Arruda,  
L. Kipgen, Prof. W. Kuch  
Institut für Experimentalphysik  
Freie Universität Berlin  
Arnimallee 14, Berlin 14195, Germany  
E-mail: matthias.bernien@fu-berlin.de

The ORCID identification number(s) for the author(s) of this article can be found under <https://doi.org/10.1002/adfm.201702280>.

DOI: 10.1002/adfm.201702280

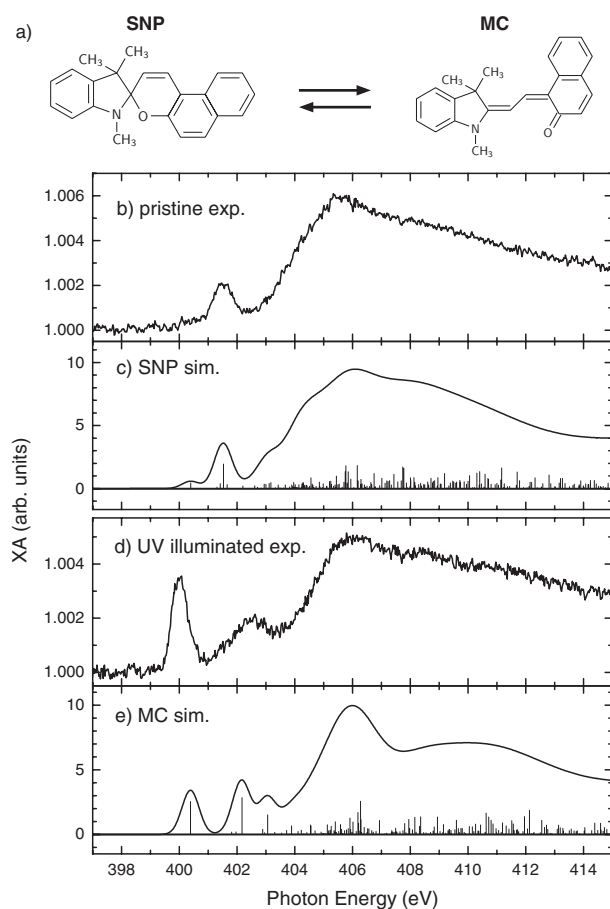


**Figure 1.** a) Sketches of the spironaphthopyran (SNP, left) and merocyanine isomer (MC, right, in a TTC-configuration) molecules. Isomerization in solution from SNP to MC can be triggered by UV light and vice versa by visible light or temperature. b) Measurement of the N K XA of a sub-ML SNP on Bi(111) recorded at the magic angle, c) simulation of N K XA of free SNP by means of the StoBe code, d) N K absorption spectrum after the illumination of the sample by a UV LED for 90 min at 194 K, e) simulation of the N K XA signal of free MC.

state. To reduce van der Waals interaction, we use a semimetallic Bi(111) substrate that, compared with metal substrates like Au(111) or Cu(111), exhibits a low density of states at the Fermi level.<sup>[26–28]</sup> Both effects are suitable to counteract the surface-induced stabilization of the MC state that was found by previous studies.<sup>[14,29]</sup> With these modifications, we achieve a virtually complete and fully reversible switching of SNP in direct contact with a Bi(111) surface. Illumination with UV light at a temperature of 200 K induces the transition from SNP to MC. Heating up to 245 K fully resets the SNP state.

## 2. Results and Discussion

### 2.1. Adsorption

To investigate the isomerization of the SP derivate, X-ray absorption (XA) measurements at the N and O K edges were performed.

For the former, the results are shown in Figure 1b for an isotropic absorption measured at the magic angle (54.7°), at which the influence of the orientation of the molecules on the spectra cancels. O K edge XA can be found in the Supporting Information. Figure 1b shows the N K XA of 0.69 MLs of SNP at a sample temperature of 200 K on the Bi(111) surface directly after deposition. A weak  $\pi^*$  absorption at 401.5 eV and a broad absorption maximum at 404.5 eV originating from  $\sigma^*$  states are present. Density functional theory (DFT) calculations of the absorption spectrum of the free gas phase SNP molecule shown in panel c agree well with the spectrum of the pristine form. The simulations were performed by means of the StoBe code,<sup>[30]</sup> which has been successfully applied to a variety of molecules.<sup>[12,14,31]</sup> Further details are presented in the Supporting Information. The energetic distance between the most intense  $\pi^*$  absorption and the  $\sigma^*$  maximum matches quite well to the experiment as well as the ratio of their intensities. A significant accordance in line shape between experiment and theory for the SP form is reached.

### 2.2. UV-Induced Ring-Opening Reaction

The ring-opening reaction was monitored at the N K edge. For the light-induced isomerization, the UV LED was used which illuminated the sample continuously for about 90 min with an initial temperature of 194 K (cf. Supporting Information), until no further change in the spectrum was observed. The resulting isotropic XA at the nitrogen K edge is shown in Figure 1d. A clear difference to the pristine spectrum is present. The most significant change is the new  $\pi^*$  absorption peak at 400.0 eV. The spectral shape is similar to that of a MC derivative with a nitro group on the Au(111) surface after irreversible temperature-induced isomerization.<sup>[14]</sup> The simulated spectrum of free MC in Figure 1e with carbon bonds in trans–trans–cis (TTC) isomerization is in good agreement with the experimental spectrum. Theory clearly reproduces the shift of the first  $\pi^*$  resonance from SNP to MC. The overall line shape of the spectrum also agrees, except for the second  $\pi^*$  resonance that appears stronger in the simulation. This is likely caused by the absence of a surface in the calculation and has been seen in many systems before.<sup>[12,14,32]</sup>

There are two indicators that all of the SNP molecules undergo switching and contribute to the spectral changes shown in Figure 1d. One is the very low interaction of SNP with the Bi(111) surface that even leads to desorption of the molecules above room temperature. The second is that the observed intensity ratio of the 400.0 eV peak to the maximum of the  $\sigma^*$  resonances around 406.0 eV is even higher than for the theoretical simulations of the free MC molecule shown in Figure 1e.

In literature, a similar isomerization has also been reported for nitro-SP on the Bi(110) surface.<sup>[25]</sup> In contrast to,<sup>[25]</sup> we excite the molecule with a wavelength that lies in the typical absorption band in solution<sup>[18,21]</sup> and such reach a larger amount of switched molecules with a higher effective cross-section, as will be discussed in the context of the activation barriers.

### 2.3. Reversibility

After UV illumination, the MC configuration can be switched back to SNP in a reversible manner. **Figure 2** shows N K XA

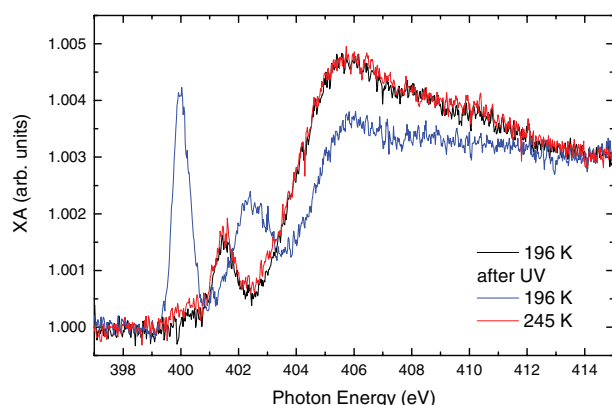


**Figure 2.** XA measurements of the N K edge by p-polarized light ( $20^\circ$  angle of incidence) for a sub-ML of SNP on Bi(111). The molecules are first in the pristine SNP form at 196 K (black), and then present in the MC configuration after UV illumination (blue). After heating up, the molecules relax back to SNP at 245 K (red).

spectra measured with p-polarized light under  $20^\circ$  angle of incidence. SNP is present at 196 K after evaporation (black line). Upon UV illumination for 1 h 47 min at an initial temperature of 196 K, it is switched to MC (blue line). Heating up to 245 K leads to a relaxation of the molecules, and the XA spectrum (red line) matches very well the one of the freshly evaporated molecules. No molecules are blocked in the MC configuration and fully reversible switching is possible.

#### 2.4. Activation Barriers

In order to get a more detailed and quantitative view of the photoisomerization mechanism of SNP on Bi(111), several illumination series were carried out. Measurements at different initial temperatures, using the same optical photon flux, offer the possibility to determine energy barriers. During illumination, consecutive measurements of the N K edge in  $20^\circ$  grazing incidence with p-polarized X-rays were taken. The grazing-incidence spectra have a stronger signal at the 400.0 eV  $\pi^*$  resonance compared with the magic-angle-incidence due to the orientation of the SNP on the surface. Further details on the angle-resolved measurements are briefly discussed in the Supporting Information.

The peak area of the 400 eV-peak was determined by integrating from 399.4 to 400.3 eV for each of the spectra after background correction by subtracting the signal of the pristine SNP state. This peak area is directly proportional to the fraction of MC molecules present on the surface, since the SNP isomer has no XA at this energy. The result of three illumination series is shown in Figure 3a. After each series, the molecules were switched back to the MC configuration by heating up to 245 K and waiting for thermal relaxation as shown in Figure 2. The saturation fraction of MC strongly depends on the temperature, leading to the conclusion that a thermal back reaction must take place. Not only the saturation is changing, but also the speed of the switching process. At higher temperature (223 K, ■), saturation was achieved after nearly 1000 s, whereas for 184 K (▲),

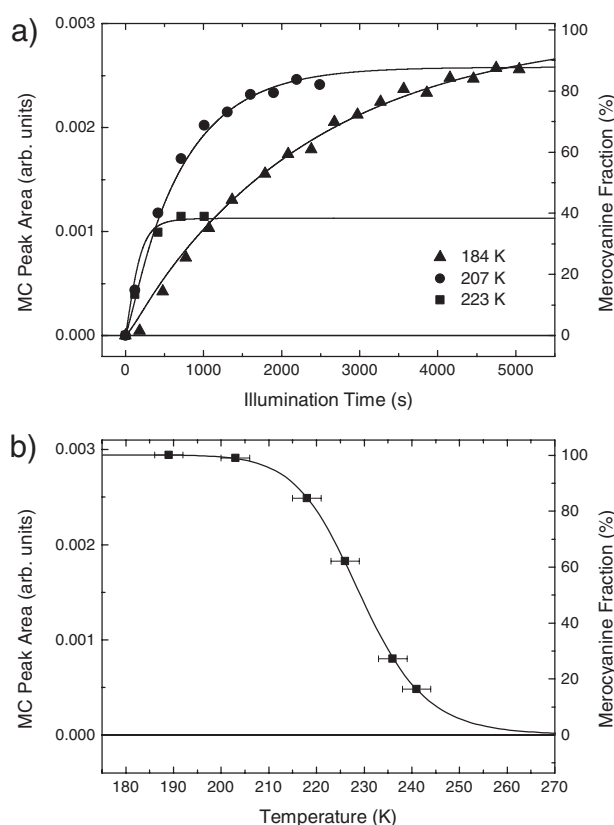


**Figure 3.** a) Evaluation of the peak area of the resonance at 400.0 eV as a function of the UV illumination time. Three different series were taken at initial sample temperatures of 184, 207, and 223 K. b) Temperature-dependent evaluation of the MC saturation during UV illumination from the 400.0 eV peak area. The temperature has been corrected by an offset due to heating by the UV LED (see Supporting Information). The same sample as for (a) was used and both data sets were fitted simultaneously to the model to obtain a well-defined set of parameters.

saturation is still not achieved after more than 5000 s. Measurements of the saturated fraction of switched molecules under UV illumination as a function of temperature are shown in Figure 3b. Here, the amount of MC has been saturated at lower temperatures using the UV LED and then the temperature was increased step-by-step under continuing illumination.

A scheme of a potential energy landscape is shown in Figure 4. It includes three different energy barrier heights in the ground state to explain the temperature dependence of the switching rates and the fraction of MC in saturation as measured in the experiment. The model assumes an intermediate state in the ground state after ring opening by UV excitation. From this state,  $E_{S,2}$  needs to be overcome to reach the metastable MC configuration.  $E_{S,1}$  describes the barrier from the intermediate state to the SNP configuration and has to be sufficiently small since we have observed no signature of an intermediate state by XA at lower temperatures. The barrier  $E_C$  needs to be overcome to switch from the MC configuration back to SNP and describes the thermal relaxation. The coexistence of these three energy barriers leads to different photo- and thermostationary states.

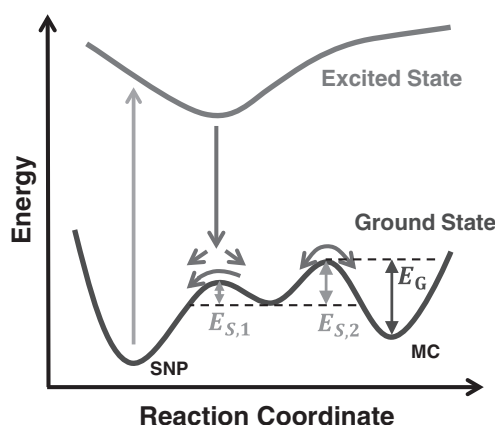


**Figure 4.** A schematic representation of the proposed energy barriers in the potential energy surfaces that are involved in the switching process. Our data suggest an energy barrier  $E_{S,2}$  in the switching path, leading to a temperature dependence on the switching efficiency from SNP to MC. The ground-state energy barrier  $E_G$  determines the thermal back-switching rate from MC to SNP.

In terms of rate equations, these observations can be expressed by a differential equation for the fraction  $\chi_{MC}$  of MC molecules as

$$\frac{d\chi_{MC}}{dt} = -\chi_{MC}k_{MC \rightarrow SNP} + (1 - \chi_{MC})k_{SNP \rightarrow MC} \quad (1)$$

$k_{SNP \rightarrow MC}$  and  $k_{MC \rightarrow SNP}$  are the rates for both isomerization directions, independent of their mechanism. In such a two-state model, the transient states, i.e., the excited state and the intermediate state, are not included explicitly assuming that the life times are small and their populations negligible. The temperature dependence of the two switching rates is described by using Arrhenius equations and derived in the Supporting Information as

$$k_{MC \rightarrow SNP} = A_G e^{-E_G/(RT)} \frac{1}{1 + e^{-\Delta E_S/(RT)}} \quad (2)$$

$$k_{SNP \rightarrow MC} = \sigma(\lambda) \phi_{UV} \Phi_1 \frac{1}{e^{\Delta E_S/(RT)} + 1} \quad (3)$$

Here,  $\sigma(\lambda)$  is the cross-section of one SNP molecule absorbing a photon,  $\phi_{UV}$  is the photon flux density of the UV LED, and  $\Phi_1$  is the quantum yield of the excited state to relax to the intermediate state after photoabsorption.  $A_G$  is a preexponential factor that depends on the vibrational freedom of the MC molecules, and  $\Delta E_S = E_{S,2} - E_{S,1}$  is the difference of the barriers confining the intermediate state. Full rate equations for a four-state model and the derivation of the rates in the effective two-state model are given in the Supporting Information.

To fit simultaneously the data from Figure 3a,b, the differential Equation (1) is evaluated using the prefactors  $A_G$  and  $k_S = \sigma(\lambda) \phi_{UV} \Phi_1$ , the difference of the energy barriers of the intermediate state  $\Delta E_S$  and the energy barrier  $E_G$  together with a common scaling factor as fitting parameters. Due to heating by the LED, the temperature of the sample is time dependent

during UV illumination, which has been included as  $T = T_0 + \Delta T (1 - e^{-t/\tau})$ , with  $\Delta T = 9.46(1)$  K,  $\tau = 147(1)$  s, and  $T_0$  the initial sample temperature (cf. Supporting Information). For the photo- and thermostationary state (Figure 3b),  $\frac{d\chi_{MC}}{dt}$  was set to 0 in Equation (1) and solved for constant temperature given as  $T_0 + \Delta T$ . Values of  $E_G = 79(2)$  kJ mol<sup>-1</sup>,  $\Delta E_S = 16(2)$  kJ mol<sup>-1</sup>,  $A_G = 10^{15.4(4)}$  s<sup>-1</sup>, and  $k_S = 7(2)$  s<sup>-1</sup> are determined. The fit identifies the photo- and thermostationary states as 38(1)%, 88(1)%, and 99(1)% for initial sample temperatures of 223, 207, and 184 K, respectively.

The activation energy  $E_G = 79(2)$  kJ mol<sup>-1</sup> for the thermal relaxation from MC to SNP is slightly higher than the activation energy of the same compound in polar solutions such as ethanol (75 kJ mol<sup>-1</sup>).<sup>[18]</sup> For less polar solvents such as methylcyclohexane the activation energy is lower, being around 65 kJ mol<sup>-1</sup>.<sup>[18]</sup>

The preexponential factor on Bi(111) of  $A_G = 10^{15.4(4)}$  s<sup>-1</sup> is as well slightly higher than the preexponential factor for polar solvents and even higher than for weakly polar solvents.<sup>[18]</sup> Temperature-dependent experiments have shown that nitro-SP is more stable in its MC configuration on Au(111) and Bi(110).<sup>[14,25]</sup> The activation energy of SNP on Bi(111) is rather high compared with solutions, but still low enough to have a thermal relaxation of the molecule at temperatures above 245 K.

Directly after breaking the SNP C–O bond by UV excitation, the indole and naphthopyran moieties of the open molecule are still perpendicular to each other. The cleavage of the C–O bond was found to be ultrafast, faster than 100 fs, afterward the bond can be reformed within 180 fs or a transition from near-perpendicular configuration to the planar MC state can occur within several picoseconds.<sup>[33]</sup> This has been extensively studied in solution by time-resolved UV–vis spectroscopy to determine possible pathways for the isomerization processes.<sup>[18,33,34]</sup> Studies using ultrafast pump–probe experiments on SPs found no temperature dependence of the quantum yield from the excited state to the intermediate state,<sup>[33,35]</sup> showing that in solution no barrier is present in the excited state. We propose a similar mechanism here. However, on the basis of our data, we cannot exclude the possibility of a barrier in the excited state. The proposed rate equation does not rely on a barrier in the ground state. A barrier in the excited state would lead to a rate equation similar to Equation (1). Results from theoretical work<sup>[34,36]</sup> and time-resolved spectroscopy<sup>[18,35]</sup> indicate that after ring opening, the molecules are present in a cis-isomerized intermediate state. Accordingly, the perpendicularly oriented MC isomer directly after photoexcitation needs to undergo an unfolding process to a planar TTC configuration. Such a process may be supported by the presence of a surface since a planar MC configuration maximizes van der Waals interactions. For the switching from SNP to MC on the Bi(111) surface, the experimentally determined energy barrier difference is  $\Delta E_S = 16(2)$  kJ mol<sup>-1</sup>. This is of the same order of magnitude as the energy barrier seen for various SPs in solution, which is attributed to the unfolding of the perpendicularly oriented rings of the molecule after ring opening to a metastable MC configuration.<sup>[34,35]</sup>

The conversion efficiency to reach the photo- and thermostationary state in Figure 3a is temperature-dependent



and varies with time constants from 2500(150) to 260(30) s for the switching series with initial temperatures of 184 and 223 K, respectively. Switching at an initial temperature of 223 K is therefore efficient with an effective cross-section of  $\sigma_{\text{eff}} = (\phi\tau)^{-1} = 1.1(3) \times 10^{-20} \text{ cm}^2$  and  $\phi$  being the photon flux density of the UV LED of  $3.5(8) \times 10^{15} \text{ photons s}^{-1} \text{ mm}^{-2}$ . This is more than one order higher than for the light-induced ring opening of a nitro-SP on Bi(110).<sup>[25]</sup> The cross-section of the photoisomerization of an azobenzene derivative in a ML on the same Bi(111) surface<sup>[37]</sup> is found as  $3.4(3) \times 10^{-23} \text{ cm}^2$  and therefore even much lower than for the ring opening of SP. Switching of SNP on Bi(111) is thus efficient, compared with other photochromic molecules on surfaces. On the other hand, even when considering that the light intensity is reduced by more than a factor of 2 in the proximity of the surface<sup>[38]</sup> due to the superposition of the incoming and reflected light wave, the effective cross-section is still orders of magnitude smaller than in solution, where it is around  $10^{-16} \text{ cm}^2$ .<sup>[18,20]</sup> This indicates that there exists a variety of relaxation channels of the photoexcited molecule or that through, e.g., van der Waals interaction the degree of freedom on the surface is reduced and the quantum yield of the conversion is lowered.

### 3. Conclusion

Using in situ XA spectroscopy, we have demonstrated a reversible switching of SNP molecules in contact with a bismuth surface. Irradiation with UV light switches the molecules from SNP to its MC isomer. This reaction has a high cross-section compared with similar experiments on surfaces. For the photoswitching from the SNP to the MC isomer, a temperature-dependent quantum yield is found, leading to a higher switching efficiency at higher temperatures, since at lower temperatures the excited molecules relax more likely back to SNP after UV excitation. The thermal kinetics reveals that the energy barrier in the ground state, responsible for the bistability of the molecules in solution, is preserved on the surface with a height of 79(2) kJ mol<sup>-1</sup>. This is important for the reversibility of the process, since an unfavorably stabilized MC isomer, which was previously observed on surfaces, suppresses the ring-closing back reaction. In our case, the back reaction can be triggered by a temperature increase. Molecular functional units for information processing need to possess bistability, addressability, and reversible switching controlled by external stimuli. Molecules that have been designed to switch well in solution, however, may not provide these properties on a surface. They thus need to be redesigned, for example, by tuning of molecular end groups, taking into account the interaction with the particular surface.

### 4. Experimental Section

All experiments and sample preparations were carried out in situ in an ultrahigh vacuum (UHV) system with a base pressure of  $p = 8 \times 10^{-10} \text{ mbar}$ . The Bi(111) single crystal has been prepared by repeated sputtering-annealing cycles. Sputtering with Ar<sup>+</sup> ions of 600 eV and annealing at 350 K were carried out until no contamination of the surface was present in X-ray photoelectron spectra, and sharp LEED

patterns were observed. XA measurements were performed by using linearly p-polarized X-rays of the undulator beamline UE56/2-PGM2 at BESSY II of the Helmholtz-Zentrum Berlin. The degree of polarization was about 99%. The incidence angle between the X-ray wave vector and the surface was set to 54.7° for magic angle measurements and 20° for grazing angle measurements, respectively. Absorption spectra were acquired by the total electron yield method, measuring the sample drain current as a function of X-ray photon energy. A freshly prepared gold grid upstream the experiment, and measurements of the clean Bi(111) substrate were used for normalization of the signal. To reduce possible defragmentation of the molecules by the X-rays, the UHV chamber was moved out of the focus of the X-ray beam to minimize the X-ray flux density, and the exposure time was kept as short as possible. Subsequent measurements of the same XA spectrum did not show any visible changes in neither of the isomerization states in a reasonable experimentation time. Furthermore, the measurement spot was moved on the sample surface for different experiments to obtain identical conditions.

In all experiments, 1,3,3-trimethylindolino- $\beta$ -naphthopyrrolospiran molecules (spironaphthopyran, SNP, purchased from TCI Europe) were evaporated directly onto the substrate kept in UHV. The molecules were evaporated at a temperature of 380 K from a tantalum Knudsen cell and deposited onto the substrate held at temperatures around 200 K to avoid thermal desorption from the surface. The deposition rate was monitored by a quartz microbalance and calibrated by the total carbon K edge XA signal. A reference measurement had been performed with continuous evaporation of the same molecule onto a Bi(111) substrate held at room temperature. The exponential saturation of the carbon K edge jump observed at room temperature had been assigned to a completely saturated ML. Samples with a sub-ML coverage of 0.56(5) ML were used for the determination of the energy barriers (Figure 3), 0.64(5) ML for the reversible switching (Figure 2), and 0.69(5) ML for the comparison with simulations (Figure 1).

Illumination of the samples was performed in the measurement position by different LEDs. In order to collimate the LED light, a coated aspherical lens was used with a focal length of 32 mm. A 300 mm spherical lens was mounted in front of a fused silica window on the chamber (transmission > 90%). UV illumination was performed with a wavelength of  $\lambda = 365 \text{ nm}$  and a full width at half-maximum of 7.5 nm. The approximate spot size of the light on the sample was  $5 \times 7 \text{ mm}^2$ . By means of a power meter, the photon flux density at the sample position was determined as  $\phi_{\text{UV}} = 3.5(8) \times 10^{15} \text{ photons s}^{-1} \text{ mm}^{-2}$ . The initial sample temperatures during synchrotron-radiation experiments were measured on the sample holder and not directly on the sample. During illumination, these temperatures were lower than the temperature on the crystal. To identify the real sample temperature, a calibration measurement with a thermocouple glued to the bismuth crystal had been performed. A temperature increase of 9.46(1) K with a time constant of 147(1) s for the UV illumination had been determined. The data are presented in the Supporting Information. This time-dependent temperature had been taken into account when fitting the model to the UV illumination data.

### Supporting Information

Supporting Information is available from the Wiley Online Library or from the author.

### Acknowledgements

Financial support by the DFG through Sfb 658 is gratefully acknowledged. L.M.A. received funding from CAPES (No. 9469/13-3). The authors thank P. Chittas and S. Wrzalek for their support during the beamtimes. The authors thank the HZB for the allocation of synchrotron radiation beamtime and B. Zada and W. Mahler for their technical

support during the measurements at BESSY II. The authors gratefully acknowledge the computing time on the high-performance cluster of the Zentraleinrichtung für Datenverarbeitung (ZEDAT) at the Freie Universität Berlin.

## Conflict of Interest

The authors declare no conflict of interest.

## Keywords

molecular switches, photochromism, spiropyran, surfaces, X-ray absorption spectroscopy

Received: April 28, 2017

Revised: August 25, 2017

Published online: November 6, 2017

- [1] R. R. Rando, *Angew. Chem., Int. Ed.* **1990**, 29, 461.
- [2] C. Li, K. Wurst, S. Jockusch, K. Gruber, M. Podewitz, K. R. Liedl, B. Kräutler, *Angew. Chem., Int. Ed.* **2016**, 55, 15760.
- [3] T. Hugel, N. B. Holland, A. Cattani, L. Moroder, M. Seitz, H. E. Gaub, *Science* **2002**, 296, 1103.
- [4] M. Elbahri, A. U. Zillohu, B. Gothe, M. K. Hedayati, R. Abdelaziz, H. J. El-Khozondar, M. Bawa'aneh, M. Abdelaziz, A. Lavrinenko, S. Zhukovsky, S. Homaeigohar, *Light: Sci. Appl.* **2015**, 4, e316.
- [5] L. Bogani, W. Wernsdorfer, *Nat. Mater.* **2008**, 7, 179.
- [6] A. H. Flood, J. F. Stoddart, D. W. Steuerman, J. R. Heath, *Science* **2004**, 306, 2055.
- [7] M. del Valle, R. Gutiérrez, C. Tejedor, G. Cuniberti, *Nat. Nanotechnol.* **2007**, 2, 176.
- [8] G. Ragazzon, M. Baroncini, S. Silvi, M. Venturi, A. Credi, *Nat. Nanotechnol.* **2015**, 10, 70.
- [9] A. Saywell, A. Bakker, J. Mielke, T. Kumagai, M. Wolf, V. García-López, P.-T. Chiang, J. M. Tour, L. Grill, *ACS Nano* **2016**, 10, 10945.
- [10] J. E. Green, J. Wook Choi, A. Boukai, Y. Bunimovich, E. Johnston-Halperin, E. Delonno, Y. Luo, B. A. Sheriff, K. Xu, Y. Shik Shin, H.-R. Tseng, J. F. Stoddart, J. R. Heath, *Nature* **2007**, 445, 414.
- [11] C. P. Collier, E. W. Wong, M. Belohradský, F. M. Raymo, J. F. Stoddart, P. J. Kuekes, R. S. Williams, J. R. Heath, *Science* **1999**, 285, 391.
- [12] M. Piantek, J. Miguel, A. Krüger, C. Navío, M. Bernien, D. K. Ball, K. Hermann, W. Kuch, *J. Phys. Chem. C* **2009**, 113, 20307.
- [13] C.-Q. Wu, J.-X. Li, D.-H. Lee, *Phys. Rev. Lett.* **2007**, 99, 038302.
- [14] M. Piantek, G. Schulze, M. Koch, K. J. Franke, F. Leyssner, A. Krüger, C. Navío, J. Miguel, M. Bernien, M. Wolf, W. Kuch, P. Tegeder, J. I. Pascual, *J. Am. Chem. Soc.* **2009**, 131, 12729.
- [15] Q. Shen, Y. Cao, S. Liu, M. L. Steigerwald, X. Guo, *J. Phys. Chem. C* **2009**, 113, 10807.
- [16] E. Pottier, R. Dubest, R. Guglielmetti, P. Tardieu, A. Kellmann, F. Tübel, P. Levoir, J. Aubard, *Helv. Chim. Acta* **1990**, 73, 303.
- [17] A. K. Chibisov, H. Görner, *J. Phys. Chem. A* **1997**, 101, 4305.
- [18] A. K. Chibisov, H. Görner, *Phys. Chem. Chem. Phys.* **2001**, 3, 424.
- [19] H. Görner, *Chem. Phys.* **1997**, 222, 315.
- [20] H. Görner, *Phys. Chem. Chem. Phys.* **2001**, 3, 416.
- [21] N. A. Voloshin, A. V. Chernyshev, A. V. Metelitsa, I. M. Raskita, E. N. Voloshina, V. I. Minkin, *Russ. Chem. Bull.* **2005**, 54, 705.
- [22] M. Karcher, C. Rüdte, C. Elsässer, P. Fumagalli, *J. Appl. Phys.* **2007**, 102, 084904.
- [23] P. K. Kundu, D. Samanta, R. Leizrowice, B. Margulis, H. Zhao, M. Börner, T. Udayabhaskararao, D. Manna, R. Klajn, *Nat. Chem.* **2015**, 7, 646.
- [24] P. K. Kundu, S. Das, J. Ahrens, R. Klajn, *Nanoscale* **2016**, 8, 19280.
- [25] G. Schulze, K. J. Franke, J. I. Pascual, *Phys. Rev. Lett.* **2012**, 109, 026102.
- [26] C. R. Ast, H. Höchst, *Phys. Rev. Lett.* **2001**, 87, 177602.
- [27] P. Hofmann, *Prog. Surf. Sci.* **2006**, 81, 191.
- [28] S. Xiao, D. Wei, X. Jin, *Phys. Rev. Lett.* **2012**, 109, 166805.
- [29] C. Bronner, G. Schulze, K. J. Franke, J. I. Pascual, P. Tegeder, *J. Phys.: Condens. Matter* **2011**, 23, 484005.
- [30] K. Hermann, L. G. M. Pettersson, M. Casida, C. Daul, A. Goursot, Koester, E. Proynov, A. St-Amant, D. R. Salahub, *StoBe-deMon, version 3.3*, Fritz-Haber-Institut (Berlin, Germany) **2014**.
- [31] C. S. Guo, L. Sun, K. Hermann, C. F. Hermanns, M. Bernien, W. Kuch, *J. Chem. Phys.* **2012**, 137, 194703.
- [32] C. Kolczewski, F. J. Williams, R. L. Cropley, O. P. H. Vaughan, A. J. Urquhart, M. S. Tikhov, R. M. Lambert, K. Hermann, *J. Chem. Phys.* **2006**, 125, 034701.
- [33] J. Z. Zhang, B. J. Schwartz, J. C. King, C. B. Harris, *J. Am. Chem. Soc.* **1992**, 114, 10921.
- [34] S. Prager, I. Burghardt, A. Dreuw, *J. Phys. Chem. A* **2014**, 118, 1339.
- [35] N. P. Ernsting, T. Arthen-Engeland, *J. Phys. Chem.* **1991**, 95, 5502.
- [36] F. Liu, K. Morokuma, *J. Am. Chem. Soc.* **2013**, 135, 10693.
- [37] C. Bronner, P. Tegeder, *New J. Phys.* **2014**, 16, 053004.
- [38] H.-J. Hagemann, W. Gudat, C. Kunz, *J. Opt. Soc. Am.* **1975**, 65, 742.

# ADVANCED FUNCTIONAL MATERIALS

## Supporting Information

for *Adv. Funct. Mater.*, DOI: 10.1002/adfm.201702280

### Reversible Switching of Spiropyran Molecules in Direct Contact With a Bi(111) Single Crystal Surface

*Fabian Nickel, Matthias Bernien,\* Kai Kraffert, Dennis Krüger, Lucas M. Arruda, Lalminthang Kipgen, and Wolfgang Kuch*

## Supporting Information

# Reversible Switching of Spiropyran Molecules in Direct Contact With a Bi(111) Single Crystal Surface

Fabian Nickel, Matthias Bernien, Kai Kraffert, Dennis Krüger,  
Lucas M. Arruda, Lalminthang Kipgen, and Wolfgang Kuch

Institut für Experimentalphysik, Freie Universität Berlin,  
Arnimallee 14, 14195 Berlin, Germany

## S1 Details of the DFT Simulations

To obtain theoretical simulations of the  $K$  edge XA spectra, quantum chemical calculations on a density functional theory (DFT) basis were performed. The StoBe code package [1] was used, which has been successfully applied to a variety of different molecules before, including spiropyran [2–4]. Consistency with Ref. 2 was preserved by doing a two-step geometry optimization for the electronic ground states of both forms, the closed and the open form, of the spironaphthopyran molecule. First, a calculation with a standard local spin density (LSD) exchange functional [5] and an LSD correlation functional [6] was performed and the result

S-1



taken for further optimization by a gradient-corrected RPBE (revised Perdew-Burke-Ernzerhof) exchange correlation functional [7, 8]. All calculations have been performed in a triple-zeta valence plus polarization (TZVP) basis set [9], where one  $d$  function is added for carbon, nitrogen, and oxygen. For the simulation of  $K$  edge absorption spectra by the StoBe code, the Slater transition state (TS) method is used [10, 11]. Core-excited states were calculated by an IGLO-III [12] basis set on the center of excitation, and remaining atoms of the same element were described by an effective core potential (ECP) [13]. On the center of the excitation, a large diffuse [19s,19p,19d] basis set [14] was added in the so-called double basis set technique to improve the description of excitations to unbound states in the excited core region.

The spectra were shifted by 1.3 eV to lower energies to match the experimental peaks. The discrete transitions below the ionization potential were broadened with a full width at half maximum (FWHM) of 0.7 eV and 1.0 eV for N and O, respectively. This broadening was linearly increased to 4.5 eV (for N) and 6 eV (for O) up to an energy of 10 eV above the ionization potential and kept fixed for higher photon energies.

## S2 XA and Simulation of the Oxygen *K* Edge

The simulation of the x-ray absorption of the oxygen atom in the SNP molecule and the corresponding experimental spectra are shown in figure S1. Panels a) and b) are the experimental and simulated spectra for the pristine SNP form, respectively. As already presented for the nitrogen *K* edge, also these simulations fit very well in peak ratio, position, and overall line shape. After switching, the MC isomer is assumed to be present on the surface. The simulation proves this as well, as shown in panel c) for the experiment and d) for the simulation of a free MC.

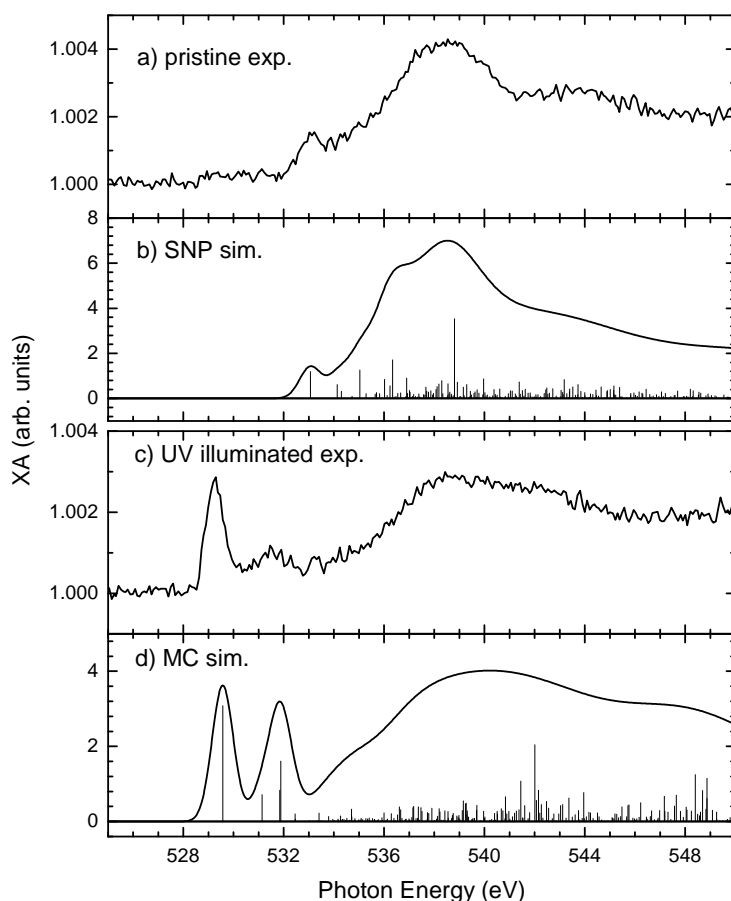


Figure S1: a) Measurement of the O *K* XA of a submonolayer SNP on Bi(111) under the magic angle, b) simulation of O *K* XA of free SNP by means of the StoBe code, c) O *K* absorption spectrum after the illumination of the sample by a UV LED for 90 min at 194 K, d) simulation of the O *K* XA signal of free MC.

### S3 Angle-Resolved NEXAFS

Except for figure S3, all the spectra in the paper were taken under the magic angle of incidence and are therefore not influenced by the orientation of the molecules. Measuring with p-polarized light under  $20^\circ$  angle of incidence between surface normal and E-field vector and with s-polarized light of the undulator beamline leads to different excitation probabilities from the spherical 1s electron distribution to the unoccupied orbitals. Due to the lack of significant strong  $\pi^*$  resonances for the SNP molecule and the 3-dimensional nature of this molecule, it is not feasible to determine the orientation of the molecule quantitatively. However, the MC molecule is a nearly completely flat molecule and the first strong  $\pi^*$  resonance belongs to a conjugated orbital which spreads over the molecule. A determination of the average angle to the surface is therefore possible. The corresponding transition orbital of MC in a TTC configuration, used in the Slater transition state method, is shown in figure S2.

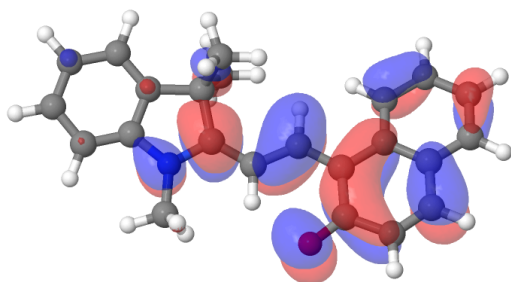


Figure S2: Transition orbital of the nitrogen 1s transition state of MC (half filled shell) in the StoBe code.

In figure S3 the polarization-resolved N  $K$  absorption spectra for SNP (upper panel) and MC (lower panel) are shown. For the SP, no angle dependence is present. This is due to the nature of the orthogonal arrangement of the moieties of the SP, which is therefore likely to have a random distribution on the surface. After the switching, the average tilt-angle of all MC molecules under azimuthal integration [15] is determined to be  $36(2)^\circ$ . It is reasonable that MC molecules

are not completely flat-lying on the surface because of the corrugation of the Bi(111) surface [16] as well as of the two out-of-plane oriented methyl groups of the molecule.

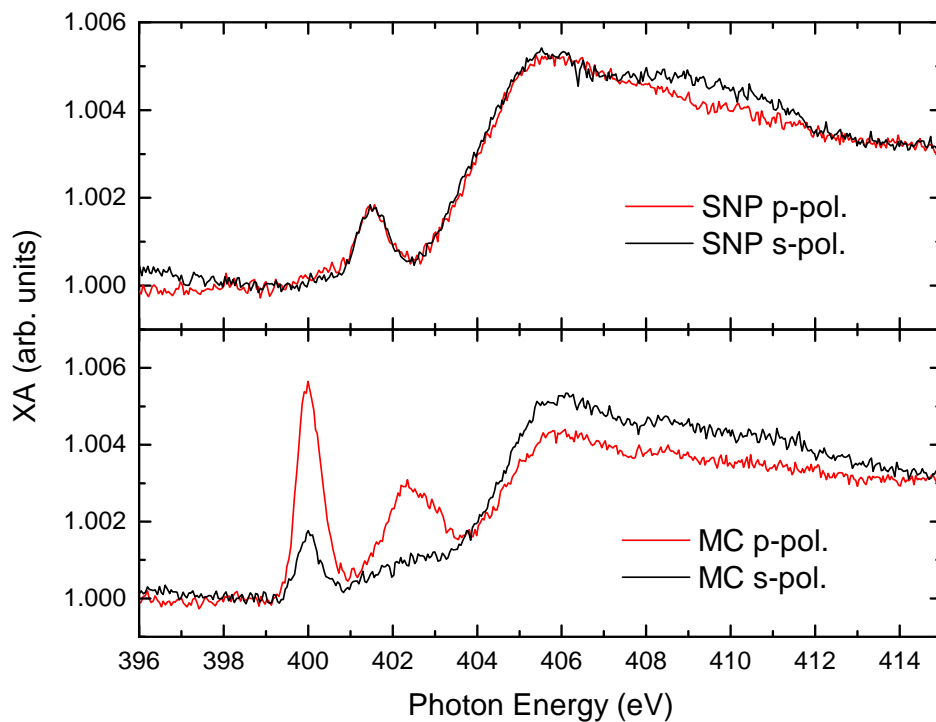


Figure S3: Angle-resolved XA measurements of the N  $K$  edge for a submonolayer of SNP on Bi(111) at a sample temperature of 194 K. The upper panel is for the pristine SNP before illumination. No angle dependence is present. After 90 min illumination by a UV LED, most of the SNP are switched to MC and shown for both polarizations in the lower panel. A clear polarization dependence is present with an average angle of the molecules of  $36(2)^\circ$  to the surface.

## S4 Influence of the Illumination on the Sample Temperature

During the XA measurements, the sample temperature has been monitored and controlled by thermocouples on the sample holder. In thermal equilibrium this temperature is identical to the one of the substrate. However, during illumination, differences can occur due to the strong light flux coming from the LED. To give a precise temperature of the sample during LED illumination, a K-type thermocouple has been glued directly to the side of the bismuth substrate after the synchrotron-radiation experiments and the temperature increase with controlled sample-holder temperature has been measured. Figure S4 shows the temperature increase during illumination by the UV LED (left panel) and blue LED (right panel). Simple exponential fits yield time constants of 147(1) s for the UV LED and 144.8(5) s for the blue LED, respectively, and a saturated bismuth temperature change of 9.46(1) K for UV and 24.9(1) K for blue light. These have been used in the model described by equation (1) of the article to account for the temperature increase due to illumination during the switching.

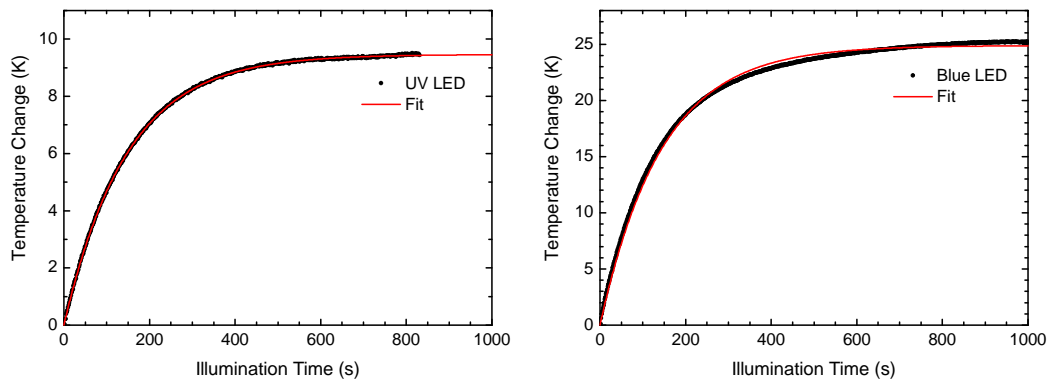


Figure S4: Left panel: Temperature change of the bismuth crystal under illumination by the UV LED in measurement condition. Right panel: Temperature change by the blue LED. The initial temperature was 194 K for both series.

## S5 Derivation of the Rate Equation

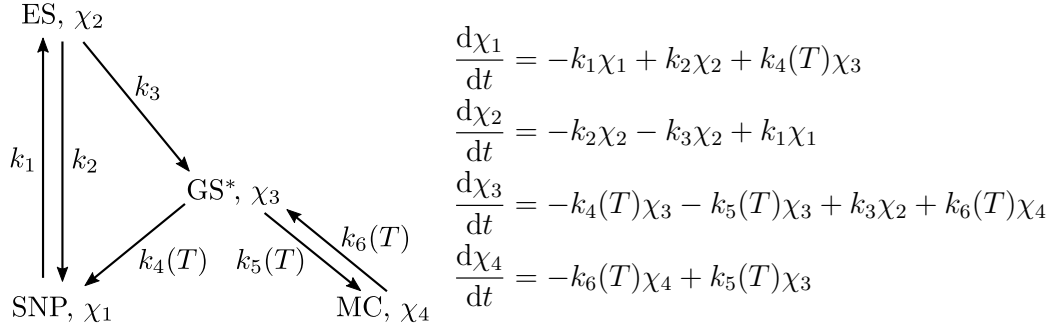


Figure S5: Scheme (left) and rate equations (right) for a four-state model with the states  $\chi_1$  as SNP ground state,  $\chi_2$  as photo-excited state,  $\chi_3$  as intermediate state,  $\chi_4$  as MC ground state. A Arrhenius temperature behavior is taken into account for the rates  $k_4$ ,  $k_5$ , and  $k_6$ .

For a detailed view on the temperature dependence of the switching kinetics, a four-state model is sketched in figure S5. The four different states, labeled  $\chi_1$  as SNP ground state,  $\chi_2$  as photo-excited state,  $\chi_3$  as intermediate state,  $\chi_4$  as MC ground state and the corresponding rate equations are included. The temperature dependence of the rate constants  $k_4$ ,  $k_5$ , and  $k_6$  is given by Arrhenius equations as

$$k_4(T) = A_S e^{-E_{S,1}/(RT)}, k_5(T) = A_S e^{-E_{S,2}/(RT)}, k_6(T) = A_G e^{-E_G/(RT)}$$

where  $A_S$  and  $A_G$  are the attempt frequencies in the switching and the MC ground state, respectively. The energy barrier between the switching state and the SNP state is  $E_{S,1}$ . The energy barrier from the switching state to the MC state is denoted as  $E_{S,2}$  and for the back reaction as  $E_G$ .

The differential equations of this four-state model can be solved numerically and it can be fitted to the experimental data. However, the fit would be under-determined because the experimental data represents only the comparably slow dynamics of the spiropyran and merocyanine states, whereas the fast dynamics of the transient states is not accessible for this low coverages. It is instructive to

convert the four-state model to an effective two-state model by assuming that the dynamics of the two transient states is very fast and can be neglected on the time scale of the experiment. This means that the occupations of the transient states are negligible. The conversion is done by setting  $\frac{d\chi_2}{dt} = 0$  and  $\frac{d\chi_3}{dt} = 0$  together with the initial conditions  $\chi_2(0) = 0$  and  $\chi_3(0) = 0$ . We obtain:

$$\begin{aligned}\frac{d\chi_4}{dt} &= -k_6(T) \frac{k_4(T)}{k_4(T) + k_5(T)} \chi_4 + k_1 \frac{k_3}{k_2 + k_3} \frac{k_5(T)}{k_4(T) + k_5(T)} \chi_1 \\ &= -A_G e^{-E_G/(RT)} \frac{1}{1 + e^{(E_{S,1}-E_{S,2})/(RT)}} \chi_4 + \sigma(\lambda) \phi_{UV} \Phi_1 \frac{1}{e^{(E_{S,2}-E_{S,1})/(RT)} + 1} (1 - \chi_4)\end{aligned}$$

with  $\chi_1 = 1 - \chi_4$ ,  $k_1 = \sigma(\lambda) \phi_{UV}$ , and  $\Phi_1 = \frac{k_3}{k_2 + k_3}$ . Here,  $\sigma(\lambda)$  is the cross section of one SNP molecule absorbing a photon,  $\phi_{UV}$  the photon flux density of the UV LED, and  $\Phi_1$  the quantum yield of the excited state to relax to the switching state after photoabsorption.

We can see that with this assumptions the number of free parameters is reduced. To fit the model to the experimental data we define the switching rate  $k_S = \sigma(\lambda) \phi_{UV} \Phi_1$  and the difference in the energy barriers of the switching state  $\Delta E_S = E_{S,2} - E_{S,1}$  and use them together with  $A_G$  and  $E_G$  as fitting parameters. The temperature is time-dependent during LED illumination and described as  $T(t) = T_0 + \Delta T \cdot (1 - e^{-t/\tau})$  (*cf.* section S4), which is taken into account when solving the differential equation and fitting the experimental data.

## S6 Effect of Blue-Light Illumination

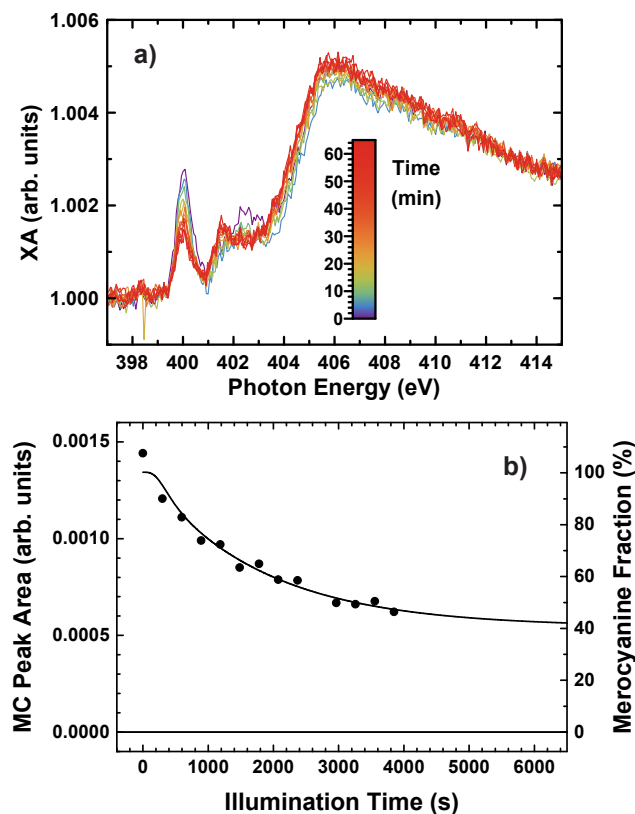


Figure S6: a) N *K* edge XA spectra of a submonolayer of SNP on Bi(111) under the magic angle of 54.7°. Continuous illumination at an initial sample temperature of 195 K by the blue LED ( $\lambda = 455$  nm) leads to a reduction of the 400.0 eV  $\pi^*$  resonance of the MC isomer. The color gradient from blue to red corresponds to the illumination time from 0 to 62 minutes. b) Area of the first resonance as a function of illumination time (solid circles) and fit of the experimental data (solid line, see text).

It is interesting to investigate whether the ring-closing reaction converting MC to SNP can be induced not only by temperature but also by visible light as it is known in solutions. Figure S6 a) shows an illumination series at the N *K* edge with an initial temperature of 195 K. It reveals that illumination of the sample by the blue LED ( $\lambda = 455$  nm and a FWHM of 20 nm) triggers a MC to SNP conversion. The photon flux density at the sample position was  $\phi_{\text{blue}} = 5.4(9) \cdot 10^{15} \text{ photons s}^{-1} \text{ mm}^{-2}$  with an approximate spot size of  $10 \times 12 \text{ mm}^2$ .



The experiment was executed under the same conditions as the switching from SNP to MC, but measured under the magic angle. Again, the integrated area from 399.4 to 400.3 eV is used to determine the kinetics and the peak areas are plotted as a function of illumination time in figure S6 b). A single exponential fit to determine the time constant (not shown) leads to  $\tau_{\text{MC} \rightarrow \text{SNP}} = 1.4(2) \cdot 10^3$  s. This would correspond to an effective cross section for that reaction of  $1.3(5) \cdot 10^{-21}$  cm<sup>2</sup>. A stationary fraction of 40(1)% of MC molecules is found. However, illumination with the blue LED also leads to a significant increase in sample temperature (*cf.* section S4). This poses the question whether the conversion can be explained by assuming blue-light induced photoisomerization only from SNP to MC and a thermal back-relaxation. The data in figure S6 b) is fitted with the model presented in the article in equation (1) using the thermal parameters of the blue LED and fixing the other parameters to the values obtained by the fit of the UV illumination data (figure 3). The switching rate  $k_S$  and an overall scaling factor were used as fitting parameters. The fit yields  $k_S = 1.2(2)$  s<sup>-1</sup>. This shows that the data can be well explained without assuming a photo-induced back-reaction from MC to SNP.

## References

- [1] K. Hermann, Lars G. M. Pettersson, M.E. Casida, C. Daul, A. Goursot, A. Koester, E. Proynov, A. St-Amant, and D. R. Salahub. StoBe-deMon, version 3.3, 2014.
- [2] Marten Piantek, Gunnar Schulze, Matthias Koch, Katharina J. Franke, Felix Leyssner, Alex Krüger, Cristina Navío, Jorge Miguel, Matthias Bernien, Martin Wolf, Wolfgang Kuch, Petra Tegeder, and José Ignacio Pascual. Reversing the Thermal Stability of a Molecular Switch on a Gold Surface: Ring-Opening Reaction of Nitrospiropyran. J. Am. Chem. Soc., 131(35):12729–12735, September 2009.
- [3] M. Piantek, J. Miguel, A. Krüger, C. Navío, M. Bernien, D. K. Ball, K. Hermann, and W. Kuch. Temperature, Surface, and Coverage-Induced Conformational Changes of Azobenzene Derivatives on Cu(001). J. Phys. Chem. C, 113(47):20307–20315, November 2009.
- [4] C. S. Guo, L. Sun, K. Hermann, C. F. Hermanns, M. Bernien, and W. Kuch. X-ray absorption from large molecules at metal surfaces: Theoretical and experimental results for Co-OEP on Ni(100). J. Chem. Phys., 137(19):194703, November 2012.
- [5] P. a. M. Dirac. Note on Exchange Phenomena in the Thomas Atom. Math. Proc. Cambridge, 26(03):376–385, July 1930.
- [6] S. H. Vosko, L. Wilk, and M. Nusair. Accurate spin-dependent electron liquid correlation energies for local spin density calculations: A critical analysis. Can. J. Phys., 58(8):1200–1211, August 1980.
- [7] John P. Perdew, Kieron Burke, and Matthias Ernzerhof. Generalized Gradient Approximation Made Simple. Phys. Rev. Lett., 77(18):3865–3868, October 1996.

- [8] B. Hammer, L. B. Hansen, and J. K. Nørskov. Improved adsorption energetics within density-functional theory using revised Perdew-Burke-Ernzerhof functionals. Phys. Rev. B, 59(11):7413–7421, March 1999.
- [9] Nathalie Godbout, Dennis R. Salahub, Jan Andzelm, and Erich Wimmer. Optimization of Gaussian-type basis sets for local spin density functional calculations. Part I. Boron through neon, optimization technique and validation. Can. J. Chem., 70(2):560–571, February 1992.
- [10] John C. Slater. Statistical Exchange-Correlation in the Self-Consistent Field. In Per-Olov Löwdin, editor, Advances in Quantum Chemistry, volume 6, pages 1–92. Academic Press, 1972.
- [11] J. C. Slater and K. H. Johnson. Self-Consistent-Field  $x\alpha$  Cluster Method for Polyatomic Molecules and Solids. Phys. Rev. B, 5(3):844–853, February 1972.
- [12] Werner Kutzelnigg, Ulrich Fleischer, and Michael Schindler. The IGLO-Method: Ab-initio Calculation and Interpretation of NMR Chemical Shifts and Magnetic Susceptibilities. In Deuterium and Shift Calculation, number 23 in NMR Basic Principles and Progress, pages 165–262. Springer Berlin Heidelberg, 1990.
- [13] Lars G. M. Pettersson, Ulf Wahlgren, and Odd Gropen. Effective core potential parameters for first- and second-row atoms. J. Chem. Phys., 86(4):2176–2184, February 1987.
- [14] Hans Ågren, Vincenzo Carravetta, Olav Vahtras, and Lars G. M. Pettersson. Direct SCF direct static-exchange calculations of electronic spectra. Theor. Chem. Acta., 97(1-4):14–40, October 1997.

- [15] J. Stöhr and D. A. Outka. Determination of molecular orientations on surfaces from the angular dependence of near-edge x-ray-absorption fine-structure spectra. Phys. Rev. B, 36(15):7891–7905, November 1987.
- [16] H. Mönig, J. Sun, Yu. M. Koroteev, G. Bihlmayer, J. Wells, E. V. Chulkov, K. Pohl, and Ph. Hofmann. Structure of the (111) surface of bismuth: LEED analysis and first-principles calculations. Phys. Rev. B, 72(8):085410, August 2005.

## 6.3 Rev. Sci. Instrum. 89, 033113 (2018)

By Fabian Nickel, Matthias Bernien, Uwe Lipowski, and Wolfgang Kuch

### Optical differential reflectance spectroscopy for photochromic molecules on solid surfaces

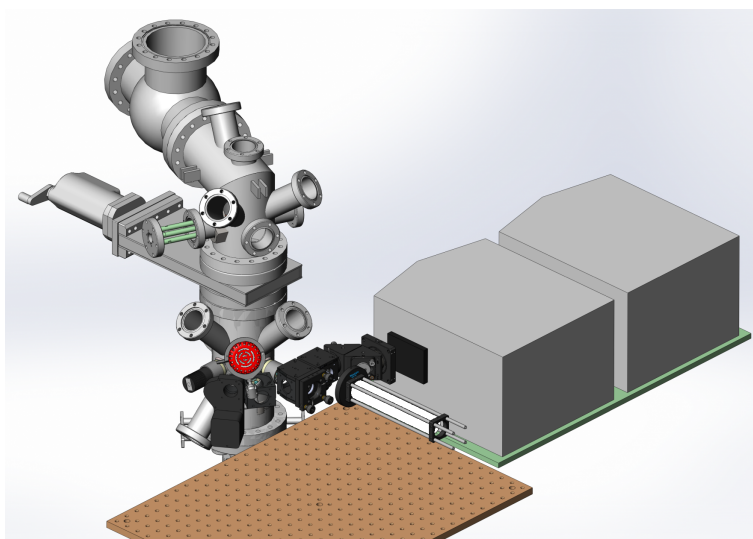
Published March 2018

DOI: <https://doi.org/10.1063/1.5019415>

© 2018 AIP Publishing

#### Contributions:

FN, MB, and WK planned the project. FN set up the UHV chamber including all measurement equipment. FN designed and built all necessary electronic parts. FN designed and programmed all used software components. UL designed the UHV parts in discussion with FN and MB and under supervision of WK. FN conceived, performed and analyzed all measurements. FN, MB and WK discussed the scientific results. FN wrote the manuscript with corrections from all authors. All authors discussed the design and results. WK supervised the study.



Simplified drawing of the designed DRS experiment.



# Optical differential reflectance spectroscopy for photochromic molecules on solid surfaces

Fabian Nickel,<sup>a)</sup> Matthias Bernien, Uwe Lipowski, and Wolfgang Kuch

*Institut für Experimentalphysik, Freie Universität Berlin, Arnimallee 14, 14195 Berlin, Germany*

(Received 14 December 2017; accepted 1 March 2018; published online 28 March 2018)

Optical reflectance of thin adsorbates on solid surfaces is able to reveal fundamental changes of molecular properties compared to bulk systems. The detection of very small changes in the optical reflectance required several technical improvements in the past decades. We present an experimental setup that is capable of high-quality measurements of submonolayers and ultrathin layers of photochromic molecules on surfaces as well as quantifying their isomerization kinetics. By using photomultipliers as detectors, an enhancement of the signal-to-noise ratio by a factor of three with a total reduction of light exposure on the sample by at least four orders of magnitude is achieved. The potential of the experimental setup is demonstrated by a characterization of the photoswitching and thermal switching of a spirooxazine derivative on a bismuth surface. *Published by AIP Publishing.*

<https://doi.org/10.1063/1.5019415>

## I. INTRODUCTION

Optical differential reflectance spectroscopy (DRS) compares the reflectance of a clean substrate with one that has been modified.<sup>1</sup> Possible modifications are, e.g., gas or molecule adsorption. The relative change of the reflectance gives indirect information on the change of the surface properties or, in case of molecules, of the inorganic-organic system. For investigation of adsorbates on surfaces, typically characterization methods such as low-energy electron diffraction (LEED), scanning tunneling microscopy (STM), x-ray absorption spectroscopy (XAS), or x-ray photoelectron spectroscopy (XPS) are used. The main difference to optical methods is the smaller penetration depth, which renders them highly surface sensitive. These methods have certain drawbacks, e.g., electrons and x rays can strongly interact with the adsorbate, which can even lead to a total destruction. STM, on the other hand, only gives local properties and limited information on the chemical structure.

The optical method of DRS has been applied since decades, e.g., for alloys<sup>2</sup> or the change of semiconductor properties after treating by adsorbates.<sup>3</sup> More recently, DRS has been used for the investigation of *in-situ*-grown organic semiconductors, for example, 3,4,9,10-perylene-tetracarboxylic dianhydride (PTCDA) on surfaces such as mica, highly oriented pyrolytic graphite (HOPG), KCl(100), or Au(111).<sup>4–9</sup> Growth and crystallization of these systems lead to a strong influence on the optical absorption and make DRS a highly universal method to measure adsorbates on surfaces. With this tool, a deeper understanding of the interaction, growth,<sup>7</sup> charge transfer of molecules,<sup>10</sup> as well as decoupling from solid surfaces<sup>8</sup> has been obtained. Clarification of these effects is crucial for realization of true molecular electronics.

Besides the application to organic semiconductors on surfaces, also investigations of self-assembled monolayers

(SAM) of photochromic molecules by DRS have been carried out.<sup>11,12</sup> There, the focus is not on the growth since these systems were prepared *ex situ*, but the important key property is the optical change upon illumination by various light sources. Photochromic molecules consist of two metastable states, which can be converted to each other by illumination with light of different wavelengths or changes in temperature. For material application, an immobilization of photochromic molecules on surfaces is essential. When in contact with a solid surface, switching properties are often found to be quenched and only partial or not fully reversible switching has been shown. Several species of different photoswitches have been investigated on surfaces, but so far no molecule in direct contact with a surface has been found that can be switched efficiently and reversibly by light only: For example, diarylethenes on HOPG and Bi(111) did not show reversibility after photoisomerization to a closed-form<sup>13</sup> and a spiropyran containing a nitro group is even reversing its thermal stability on an Au(111) surface.<sup>14</sup> On the other hand, systems using a bismuth substrate have been reported with promising results. Azobenzenes on Bi(111) can be switched to one state by x rays and to the other by thermal energy.<sup>15</sup> Spiropranes on Bi(110) were found in a photostationary state upon blue-light illumination,<sup>16</sup> and spironaphthopyran on a Bi(111) surface can be reversibly switched by using a UV LED and thermal energy.<sup>17</sup> From UV/Vis-spectroscopy in solution, the absorption bands of these molecules are already well known, but when in contact with a surface, the optical reflection represents a combination of the electronic and optical properties of the full system including the substrate. Therefore, DRS is a very suitable method to determine and quantify the ability to switch photochromic molecules on a surface. Explanation and characterization of the optical absorption even for molecules that do not show switching properties on the surface might lead to a deeper understanding of the switching process in proximity to the substrate.

The DRS setups for investigating organic semiconductors,<sup>5,9,18,19</sup> SAMs,<sup>11,12,20</sup> or polymers<sup>21,22</sup> have a typical

<sup>a)</sup>Electronic mail: fabian.nickel@fu-berlin.de

white-light setup in common. A white-light source illuminates directly or via an optical fiber the sample surface, and the reflectivity is measured by a spectrometer. A typical advantage of this is the fast acquisition time and the flexibility. A huge drawback to measure photochromic molecules is their potential conversion by light absorption. In solution, quantum yields of photoswitchable molecules nearly reach 100%, which means that upon measurement by white-light illumination a significant amount of molecules would be switched. In addition, the contrast within a spectrum is limited by the dynamic range of the spectrometer. A strong reflection in the visible part of spectra often leads to an increased noise in the UV or infrared range. Most photochromic molecules do not exhibit any absorption in the visible range in one of their states, which makes it necessary to have a good spectral quality over the whole UV/Vis range.

Here, we present an experimental setup that is capable of measuring photoisomerization of *in-situ*-deposited molecules in a UHV environment at variable temperature. It is designed to measure the change of the optical reflection and the switching kinetics during illumination. Using a monochromatic measurement beam in combination with photomultipliers (PMT) leads to a minimum light exposure of the molecules. In addition, this enables time-dependent measurements at single wavelengths such that the acquisition speed can be increased with less total light exposure. To maximize the signal-to-noise ratio (SNR), a reference beam can be used. Special effort was spent to optimize the setup in the UV range since, as mentioned before, photochromic molecules often do not exhibit absorption in the visible range. Therefore a dual-lamp with a deuterium and halogen source as well as UV-optimized optics is used. As a demonstration of the potential of our setup, measurements of the photochromic switch spironaphthooxazine (SNO) on the Bi(111) surface are presented. Besides the DRS of both isomerization states, the kinetics of the UV photoisomerization to the merocyanine state (MC) is quantified. By temperature-dependent measurements of the relaxation, activation barriers between the two metastable states are determined within an Arrhenius model.

## II. DIFFERENTIAL REFLECTANCE SPECTROSCOPY SETUP

### A. Measurement principle

Using the optical reflection of a surface-adsorbate system, the signal consists of contributions from the surface and adsorbate. Comparing the optical reflection of the hybrid system to the signal of the bare substrate enables one to extract information on the absorption of the adsorbate. This method allows for a very sensitive investigation of the change of the optical properties of the surface. The DRS signal is defined by the reflection  $R(\lambda)$  at a certain wavelength  $\lambda$  compared to the substrate reflection  $R_0(\lambda)$  as

$$\frac{\Delta R}{R}(\lambda) = \frac{R(\lambda) - R_0(\lambda)}{R_0(\lambda)}. \quad (1)$$

To account for noise originating from the lamp and optical setup, a reference is introduced and the reflection is measured

as

$$R(\lambda) = \frac{I_S(\lambda)}{I_R(\lambda)}, \quad (2)$$

with the sample and reference PMT currents  $I_S$  and  $I_R$ , respectively. Such a normalization has been already utilized in the literature and increases the signal-to-noise (SNR) ratio significantly.<sup>19</sup>

The change  $\Delta R/R(\lambda)$  is not only originating from the optical absorption of the adsorbate but also from the change of optical constants of the surface. Therefore a direct inference to the properties of the adsorbing film is not feasible. By linearization of the Fresnel equations for the reflection of a layered system of vacuum, adsorbate, and semi-infinite substrate, an approximation for the complex dielectric functions of adsorbate and substrate can be given,<sup>23</sup> but only for the case of highly transparent substrates, further simplifications to determine optical constants of adsorbates are possible.<sup>5</sup> By applying models or using the Kramers-Kronig relation, optical constants can also be determined for opaque substrates, e.g., gold or HOPG.<sup>24</sup> Separation of the optical constants of molecule and substrate is not necessarily required for the investigation of photochromic systems, in particular, if the focus of interest lies on the kinetics of the switching process. Only a weak change of each optical constant is expected if there is no strong interaction between surface and switch. A detailed deconvolution into the contributions from the refractive index and extinction coefficient as described in the literature<sup>1,24,25</sup> is thus not in the scope of the experiment presented here. The important property to identify in these systems is the ability to switch reversibly and efficiently.

### B. UHV setup

In surface science, entire sample handling under UHV conditions is necessary. Therefore, the presented DRS setup consists of a UHV chamber with a base pressure of  $2 \times 10^{-10}$  mbar. A sample load-lock to quickly exchange substrates as well as a device to cleave surfaces (e.g., HOPG) is mounted on this chamber. For preparation of single-crystal surfaces, a sputter gun and heating stage are present. In Fig. 1(a), the main UHV body based on a CF100 T-piece is shown. Due to the small diameter (100 mm) of this chamber body, the distances between the sample and windows are reduced to only 62 mm. This makes the use of in-vacuum lenses unnecessary. Six fused silica CF16 windows with an inner diameter of 16 mm are mounted and enable high optical transmission between 190 and 2500 nm. The flanges of the two innermost windows on the horizontal axis are cut to reduce the angle for near-normal incidence to 11.5° to the surface normal axis. The two outer windows on the horizontal axis offer the possibility for polarization-dependent measurements. The angle between these windows is 90°. The sample holder is directly mounted from the bottom of the CF100 T-piece and enables fast exchange and adjustment. The sample holder is shown in panel (b) of Fig. 1. For a stable operation of DRS, highest mechanical stability is required. When using a manipulator, mechanical oscillations or translations may occur. Therefore, a fixed sample holder was built. An *ex situ* manipulation of five axes (all except for azimuthal rotation) is available to adjust



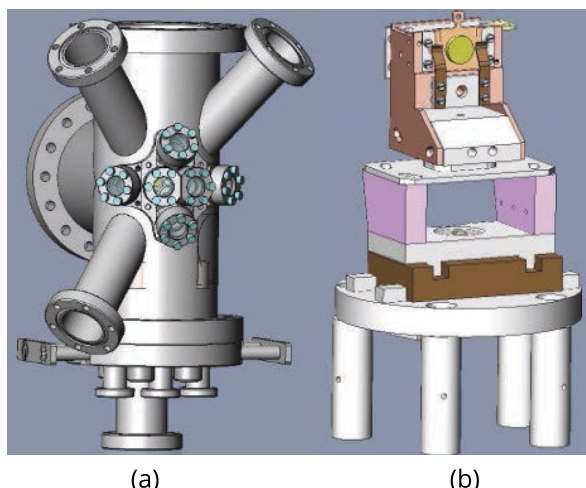


FIG. 1. (a) UHV chamber for *in situ* DRS measurements. The optical components are directly mounted on the CF16 windows in the center; three CF40 ports for evaporators are pointing toward the sample. (b) Sample holder designed for highest stability with the possibility of *ex situ* five-axis adjustment.

the optical setup. The sample is pressed strongly against an oxygen-free high thermal conductivity (OFHC) copper block by two spring bronze plates. A boron nitride heater plate is mounted on the top of this block for sample heating. For cooling, a liquid-nitrogen-cooled heat exchanger is connected to the main block by copper strands. The strands are required to decouple the sample holder from possible nitrogen boiling disturbances. Thermal insulation of the copper block is achieved by using two polyimide blocks as a connection to the *x-y* manipulation of the socket. This leads to a very low thermal conductivity and a minimal temperature limited by thermal radiation. The temperature of the main block is measured by a LakeShore DT-670B-CO silicon diode. An accurate control of the temperature is achieved by PID-control of the heating power by a home-made LabView program. With that, stable temperatures with oscillations below 0.1 K were reached between 100 and 460 K.

The three CF40 ports in Fig. 1(a) are pointing to the sample and enable mounting of different additional equipment with direct view on the sample. For investigations of photochromic molecules, a home-made Knudsen-cell evaporator with a quartz microbalance is mounted behind a valve.

### C. Optical setup

Figure 2 presents a sketch of the optical components of the DRS setup. A nearly normal incidence has been chosen for the measurement of photochromic molecules on opaque substrates. In contrast to recent publications of similar setups, white-light illumination of the sample is not used. A double monochromator in combination with two photomultiplier tubes (PMTs) measures the reflectance.

A Bentham ILD-D2-QH lamp provides highly intense light from 200 to 300 nm with a low-noise deuterium ( $D_2$ ) lamp and 300 to 2000 nm by a quartz halogen (QH) lamp. The illumination source is selected by a flip mirror (M1), which is controlled by the home-made measurement software.

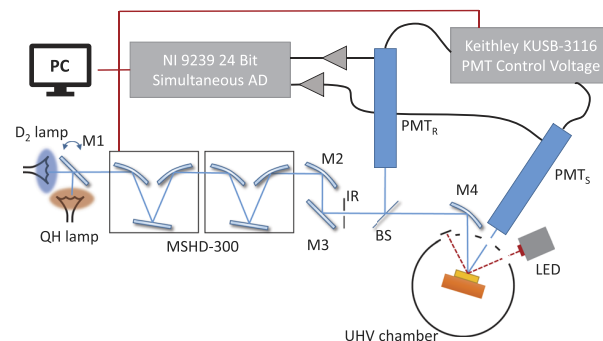


FIG. 2. Illustration of the optical setup: Light from a Deuterium/Quartz-Halogen source (selection by flip-mirror M1) is monochromatized by a double monochromator. The beam is collimated by mirror M2. A fused silica beam-splitter (BS) redirects a fraction of the light to the reference PMT<sub>R</sub>, whereas the mirror M4 focuses the beam into the UHV chamber. Detection of the reflected light from the sample is done by the sample PMT<sub>S</sub>. Both PMT gains are controlled by a Keithley KUSB-3116, and the photocurrents are amplified by FEMTO amplifiers and subsequently digitized by a National Instruments 9239 AD converter. *In situ* LED illumination is possible through various windows on the chamber.

The broadband light is monochromatized by a MSHD-300 double monochromator purchased from LOT-QuantumDesign GmbH. A double monochromator has been chosen over a single one since the estimated change of reflection of sub-monolayers of molecules upon isomerization can be of the order of only  $10^{-3}$ . Stray light of a single monochromator can be of the same order of magnitude, which would lead to incorrect conclusions. Besides that, a low light exposure of the photochromic molecules is required to not interfere with the desired LED-illumination effect. A double monochromator minimizes the relative stray light down to  $10^{-6}$ . Three gratings are mounted in each of the monochromators to allow for broad range and detailed measurements in different regions of the spectrum from UV to NIR. For the spectra presented later on, a grating with 1200 l/mm and a blaze wavelength of 300 nm has been used, which provides sufficient intensity from 240 to 750 nm. With a 2400 l/mm holographic 250 nm blaze grating, measurements down to 200 nm are possible, whereas for the infrared region a 1200 l/mm grating with a blaze of 750 nm is mounted. Additionally, filters blocking light below 350, 430, and 725 nm are introduced automatically between the two monochromators depending on the selected wavelength to suppress light of higher orders.

The slits of the monochromator can be adjusted between 0.05 and 8 mm width, where theoretical bandwidths between 0.07 and 11 nm are reached. Behind the exit slit of the double monochromator, an  $f/4$  focal length focussing mirror (M2) is placed. The collimated beam is directed by mirror M3 to an iris aperture (IR), to limit the beam diameter. Uncoated fused silica is used as a beamsplitter. This beamsplitter has about 4% reflectance to split a reference beam into the reference photomultiplier PMT<sub>R</sub>. The sample beam is focused again with a UV-enhanced off-axis parabolic mirror (M4) with a focal length of 15.2 mm. Therefore, the focus is behind the sample, enabling for a smaller spot on the exit window than on the entrance window. This is intended to reduce the eventuality of

clipping of the beam. Such a clipping would lead to a vulnerability to increased noise. The whole beam path is covered by a tube system and black-anodized aluminum foil to block all ambient light from the experiment.

Photomultipliers from Hamamatsu of the type H10426-01 are used. Their advantage is a rather broad spectral sensitivity (185–850 nm) and a very large sensitive area with a diameter of 25 mm. This enables detection of the whole reflected beam when mounted behind the CF16 vacuum window (diameter 16 mm). Typical spectrometers as used in white-light setups employ CCD chips to measure DRS. In Ref. 19, an NMOS-type Si diode array (Hamamatsu S3904) is used, which has a spectral response between 0.05 and 0.25 A/W. Compared to this, the Hamamatsu PMTs exhibit a sensitivity in the range between 10 and 70 mA/W. Together with a gain of, e.g.,  $10^5$  (the gain can be controlled between  $10^3$  and  $10^7$ ), the PMT is around four orders of magnitude more sensitive at a wavelength of 600 nm. A further advantage compared to a white-light setup is the reduced exposure to light during the measurement. Assuming a sample consisting of photochromic switches that are switching equally effective as in solution (cross sections around  $10^{-17}$  cm<sup>2</sup>),<sup>26</sup> conventional DRS white-light setups would lead to a switching of the molecules with time constants in the range of several 100 s. This would interfere with typical measurement times for the different isomerization states of the molecule-surface systems. In contrast to that, our setup allows measurement times of several days since the light flux is orders of magnitude below that needed for CCD-based detectors.

Both PMTs are equipped with computer-controlled shutters (Thorlabs SH1/M for the sample and SHB1 for the reference). The shutters are operated by two different safety interlocks, to close either when the current exceeds a certain limit or when an LED for sample illumination is operated. Hereby, the sample illumination is possible by different LEDs, mounted on CF16 windows. Typically, two different LEDs are mounted for experiments with photochromic molecules to allow for possible bi-directional light-induced switching. Additional optics can be used to increase the intensity further by focussing to a smaller area.

Several variations of the optical setup can be imagined. For investigations of the optical anisotropy, the outer windows can be used for DRS. The polarization dependency can be analyzed by a Glan-Thompson polarizing prism as, for example, described by Navarro-Quezada *et al.*<sup>27</sup>

#### D. Acquisition and software

The data acquisition and control are done by a National Instruments (NI) 9239 analog-digital converter and Keithley KUSB-3116 digital-analog converter, respectively. A very stable control voltage for the Hamamatsu PMT is required for an accurate internal high voltage generation. This control voltage is supplied by the Keithley device, which was found to deliver the most stable operation over long times. Any instability of the 0.4–1.4 V control voltage directly influences the measurement. The detection of the signals is realized by amplifying the currents in the order of microamperes with a FEMTO DDPCA-300 current amplifier for each PMT and then logged

to the personal computer (PC) by the NI 9239 converter. Especially in the case of light sources with a high frequency noise, such as xenon arc lamps, a fast and simultaneous signal acquisition of the reference and sample is necessary. To account for this, NI 9239 uses independent AD converters, which are triggered simultaneously and convert with an accuracy of up to 24 bit and 50 kS/s.

Automation is of high importance for the measurement of photochromic systems since typically cross sections for photoswitching on surfaces are reduced by several orders of magnitude<sup>13,17</sup> and result in extensive measurement times. To determine suitable combinations of molecules and substrates, experiments in a reproducible and reliable manner are required. As mentioned before, the temperature control is automatized, which enables recording of temperature ramps and systematic studies. Measurements are executed and controlled by a home-made LabView program. A spectrum can hereby be split into parts with different PMT control voltages, therefore increasing the dynamical range of a spectrum by orders of magnitude. For the sake of fast acquisition, presented spectra are taken with an integration time of 700 ms per point and a step width of 2 nm. For the demonstrated application, besides taking full spectra, also other types of measurements are necessary. Measuring the kinetics of switching processes is possible by only recording certain points of a spectrum to increase the speed of measurement. For a time-dependent measurement without additional illumination, either only a certain wavelength can be recorded or different wavelengths alternatingly. For a highly accurate and drift-resistant investigation of switching kinetics, a point on an absorption peak and one on a more or less constant area can be measured. Rates can be determined by taking the asymmetry of an absorption peak by

$$\text{asym}(\lambda_1, \lambda_2) = \frac{R(\lambda_1) - R(\lambda_2)}{R(\lambda_1) + R(\lambda_2)}. \quad (3)$$

In that way, a time-dependent measurement of temperature or light-induced switching is possible with an accurate determination of rate constants. By taking full spectra before and after the switching series, the asymmetry can be related to the amount of switched molecules.

Since the use of additional LED illumination is not possible while scanning with the PMTs, the shutters of the PMTs need to be closed and their high voltage shut down for intense LED illumination. Therefore, recording the asymmetry of an absorption peak and light-exposure are done alternatingly.

#### E. Noise and drift

For a fast acquisition, the noise needs to be minimized. Typical noise deviations in a white-light setup of the  $\Delta R/R$  signal due to instability of lamps without using a reference signal were often found to be in the order of  $10^{-2}$ , while with reference this could be around  $3 \times 10^{-4}$  for long integration times of 6 s.<sup>19</sup>

Figure 3 presents time-dependent recordings of the reflection of a clean Au(111) substrate and reference at a wavelength of 500 nm. Each point has been taken with an integration time of 1 s, and the points are normalized to the first point before subtracting a value of 1. The red dots represent the signal of the sample PMT; the black dots represent that of the reference

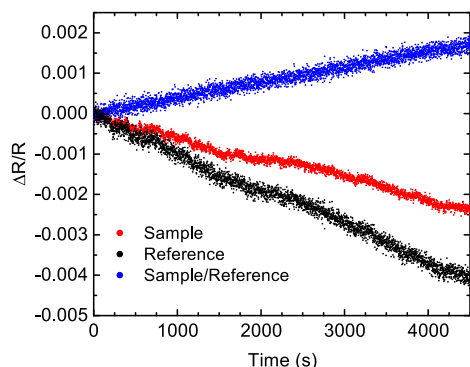


FIG. 3. Time-dependent measurement of the photocurrents of both PMTs (red dots for the sample and black for the reference) and normalized to the first data point for each PMT. A clean Au(111) substrate was used, and the reflection was measured at  $\lambda = 500$  nm at room temperature.

PMT, and the blue dots represent that of the sample/reference normalized signal, respectively. Photocurrents are  $2.5 \mu\text{A}$  for the sample PMT and  $2.1 \mu\text{A}$  for the reference PMT, respectively. The temperature was left at room temperature. Different drifts are apparent in the measurement. The overall nearly linear drift to smaller reflected intensity for both PMTs is presumably originating from a combination of light-source and gain drift.

The standard deviation, calculated from the data of Fig. 3 by subtracting straight lines for each series, is  $7 \times 10^{-5}$  for the sample PMT,  $1 \times 10^{-4}$  for the reference PMT, and thus  $1 \times 10^{-4}$  as well for the normalized signal. Utilizing PMTs for recording DRS therefore leads to a reduced noise level in our setup. Compared to the noise level reported in Ref. 19, it is improved by at least a factor of three for the normalized signal using a reference. Without reference, the improvement is even higher, more than two orders of magnitude.<sup>19</sup> A noise level better than  $10^{-4}$  is crucial for the measurements. The noise is dominated by the shot noise of the PMT. Using the photocurrents, gains ( $10^4$  for sample,  $2 \times 10^5$  for reference), and integration time a shot noise of  $4 \times 10^{-5}$  for the sample PMT and  $1 \times 10^{-4}$  for the reference PMT is calculated, respectively.<sup>28</sup> Besides the linear drift, shorter drifts are visible around 1700 s at both PMTs, most likely originating from a drift of the light source. Instabilities of the light source and other influences such as vibrations of the monochromator can efficiently be separated by normalizing to the reference signal, hence leading to a stable measurement. Remaining long-term drifts over time spans of hours can be corrected by later data treatment as explained in the context of the application.

### III. APPLICATION TO PHOTOCHROMIC MOLECULES

#### A. Experiment with spironaphthooxazine

As a demonstration of the various possibilities for application of the described setup, results of the photochromic spironaphthooxazine (SNO, full chemical name 1,3,3-trimethylindolinonaphthospirooxazine) on a Bi(111) surface will be shown. SNO is shown in Fig. 4 and can be converted by UV-light illumination to merocyanine (MC). A conversion backwards to SNO is possible in solution by

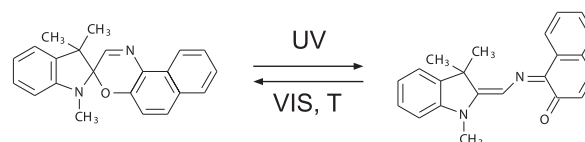


FIG. 4. Scheme of the molecular switch spironaphthooxazine (SNO), which can be converted in solution by UV illumination to merocyanine (MC) and reversibly back by either visible-light illumination or increase of temperature.

either visible-light illumination (often red) or a temperature increase.

The Bi(111) surface was prepared by standard sputter and annealing cycles. For sputtering, 600 eV  $\text{Ar}^+$  ions were used, and for annealing, the crystal was kept for 15 min slightly above 350 K. The base pressure of the UHV chamber was  $2 \times 10^{-10}$  mbar. SNO molecules, purchased from TCI Chemicals, were evaporated from a home-built evaporator with a Knudsen cell at a temperature of about 363 K with a pressure of  $5 \times 10^{-9}$  mbar. The substrate temperature was kept at 200 K for evaporation, to increase the rate of adsorption on the surface. Prior to the measurements, all optical components have been warmed up for several hours to reduce drifts of the signal. The settings were adjusted for an optimized acquisition speed. Hereby, 700 ms integration time per point and 2 nm step width were used. The slits were set to 1 mm with a theoretical bandwidth of 1.35 nm. A measurement spot of  $3 \times 7 \text{ mm}^2$  on the Bi(111) was used.

#### B. Adsorption on Bi(111)

Figure 5 shows the measurement of adsorbed SNO on Bi(111). It is important to care about correction and thickness calibration of the DRS in detail. Panel 5(a) shows the DRS of the freshly adsorbed SNO on Bi(111) of the pristine sample (black line) and after 5:30 h of experiments (red line) without normalization to the reference PMT. By the already-described drift of the DRS, the signal changes by 0.01. Beside that, noise in the range of  $1 \times 10^{-3}$  is visible as well as a spike from the change of the illumination source at 300 nm. Spikes and remaining noise originate from instabilities of the optical setup, e.g., grating vibrations or inaccuracies. In panel (b), the reference PMT has been used for normalization and in addition a simple correction for the drift is applied. For the latter, a sensitivity drift was calculated, which is defined as the factor between the photocurrents for each PMT in the pure-substrate spectrum and the one in the recorded spectrum at a certain wavelength. A wavelength of 720 nm is chosen for this correction since there is no absorption by the adsorbate expected and a good signal can be acquired. The calculated factor is applied to the whole spectrum. This drift could originate from changes in the PMTs or drift of the control voltage for the internal high voltage generation of the PMTs. Applying this factor leads to well-matching spectra, even over long time spans. By using the reference signal, the noise is strongly reduced without further adjustments. The drift of the PMTs, as shown in Sec. II E, dominates the results.

In contrast to the low-temperature measurements, molecules do not permanently stick after completion of the first layer on a Bi(111) surface. Therefore, to determine the

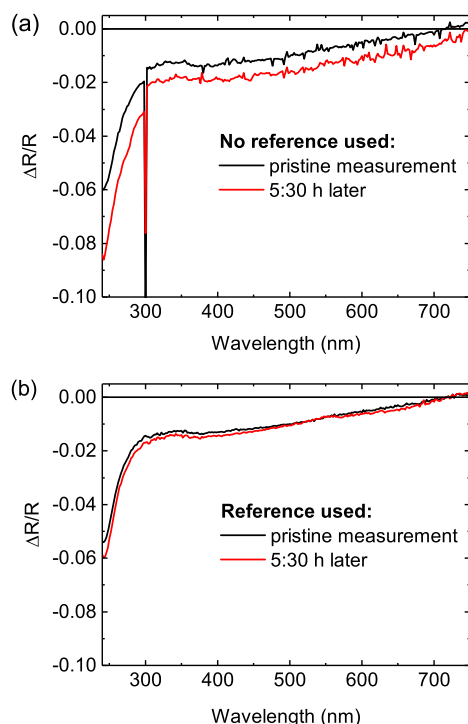


FIG. 5. DRS of SNO on Bi(111) (a) without using the reference directly after evaporation (black line) and after 5:30 h (red line). (b) Exactly the same measurements including the use of the reference beam and correcting for a gain drift by referencing to the 720 nm intensity. Measurements were taken at  $T = 200$  K.

amount of molecules on the surface, measurements at room temperature were carried out. For the similar molecule spiro-naphthopyran on the same surface, this has been done before by x-ray absorption spectroscopy.<sup>17</sup> Figure 6 shows the thickness calibration for SNO on Bi(111). A quartz microbalance mounted in the evaporator provides a measure proportional to the amount of molecules arriving at the sample surface during evaporation. The quartz is cooled by ice water to improve sticking of the molecules. Since the adsorbate does not form a permanent second layer on Bi(111) at room temperature, the coverage saturates exponentially. To measure and fit this saturation, different steps of evaporation were carried out successively with recording DRS in between. Panel (a) of Fig. 6 shows the corresponding DRS spectra, whereas panel (b) plots the intensity at 245 nm for each evaporation step. The fit leads to a saturation of the DRS signal at  $-0.061$  for one monolayer (ML). Due to inaccuracies of this method and drifts of the setup, such a calibration has an estimated error of around 10%. The following experiments were carried out with a 245-nm signal of around  $-0.055$  which corresponds to a coverage of 0.9(1) ML.

### C. UV-induced switching

To demonstrate the ability of the DRS setup for detecting the photochromism of molecules on a surface, a submonolayer of SNO on Bi(111) was illuminated by a UV LED with a wavelength of 365 nm and a photon flux density of  $\phi = 2.8(5) \times 10^{15}$  photons  $\text{s}^{-1} \text{mm}^{-2}$  at the surface (measured by means of

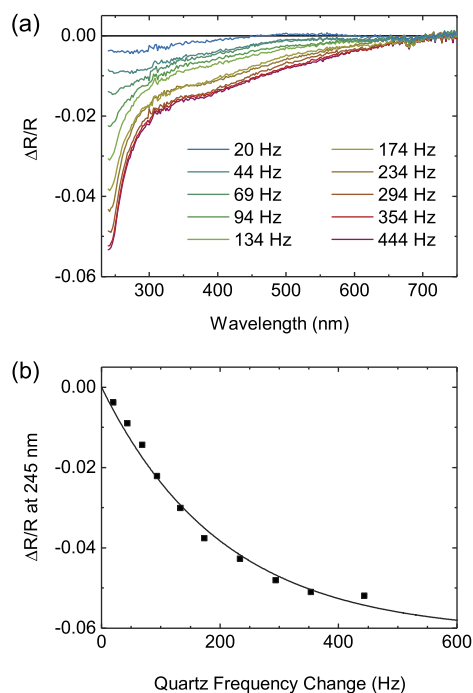


FIG. 6. Stepwise evaporation of SNO on Bi(111) with DRS measurements after each step. (a) DRS spectra for different coverages. The frequency change of the quartz microbalance serves as a measure of the evaporated amount of molecules. (b) Signal at 245 nm as a function of the microbalance frequency change.

a power meter). The illumination spot has approximately a size of  $9 \times 9 \text{ mm}^2$  with a rectangular shape and is therefore larger than the measurement spot of the DRS setup. Experiments were carried out at a temperature of 200 K with a coverage slightly below one ML (cf. Sec. III B). With this illumination, the molecules can be very quickly switched in solution from SNO to MC because of a quantum yield of up to 0.41.<sup>26</sup> Due to the high sensitivity of the DRS, evaluation of the changes for short LED illumination times is possible.

Figure 7 shows in panel (a) the total change between the DRS after evaporation (black line) and after 94 s of accumulated UV LED illumination (red line). In panel (b), the asymmetry, as defined in Eq. (3), between the intensity at 240 and 290 nm is plotted for each illumination step. The change in DRS between the pristine and the UV-illuminated sample can be compared to UV/Vis spectra of the SNO and MC form in solution. Spiropyrans and SNO have been investigated intensely. Their absorption spectra reveal for SNO nearly no absorption in the visible part of the spectrum and for MC a peak around 600 nm.<sup>26,29</sup> This 600-nm peak has often a double-peak structure, depending on the configuration of the carbon bonds.<sup>29</sup> We can identify a very similar change of the DRS spectrum, even though here the signal is a combination of substrate and adsorbate properties. The intensity of the reflectance in the UV region increases, whereas there is more absorption around a maximum at 625 nm. Knowing the change of absorption of the adsorbate/substrate system is highly important to identify candidates and wavelengths for the reversible switching. Reverse photoisomerization has not yet been achieved for this system. With deeper knowledge through



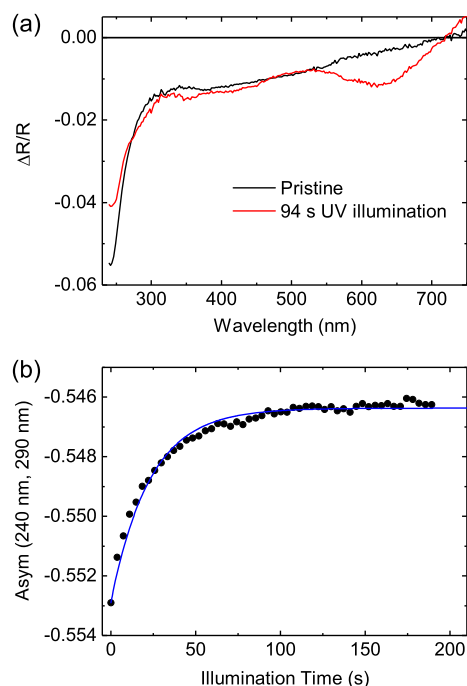


FIG. 7. (a) SNO on Bi(111) in the pristine state and after 94 s UV illumination. (b) Time dependence of the effect: stepwise illumination for 3.7 s and recording of the asymmetry of the 240 and 290 nm reflectance.

comparison of different photochromic molecules on surfaces, it will be possible to tailor systems to reach this important milestone.

The rate for the SNO-to-MC conversion can be measured by the DRS setup as well. To do so, the pristine SNO has been subjected to 3.7-s illumination steps and alternating recordings of the asymmetry. The advantage of this method is that the measurement of the clean substrate is not taken into account, other than for the DRS. Therefore it is independent of long-term drifts, but the asymmetry cannot be directly related to DRS intensity. An exponential function with a time constant of 24(1) s fits to the measurement, as presented in Fig. 7(b). Hereby, the first point without illumination has been determined with higher accuracy and kept fixed for the fit, resulting in a systematic deviation from a single-exponential function. The origin of this effect remains unclear but may be attributed to a more complex behavior of the switching kinetics, e.g., different adsorption sites or cooperative effects.

By the measured photon flux density, the effective cross section can be calculated as  $\sigma_{\text{eff}} = (\phi\tau)^{-1} = 1.4(3) \times 10^{-19} \text{ cm}^2$ . Compared to literature values for cross sections of photochromic switching on surfaces, this is a highly effective process. In solutions, typically cross sections orders of magnitude higher are measured.<sup>30,31</sup> Hence there is still a high potential to increase the switching efficiency while in contact with a surface. So far, in direct contact with surfaces, cross sections that are by orders of magnitude lower than those for experiments in solutions have been observed. The spironaphthopyran-to-MC conversion on Bi(111) exhibited a cross section in the order of  $10^{-20} \text{ cm}^2$  for elevated temperatures and even below  $10^{-21} \text{ cm}^2$  at 200 K.<sup>17</sup> Other photochromic molecules

were measured with even lower effective cross sections such as  $10^{-23} \text{ cm}^2$  for azobenzenes in thin films on the Bi(111) surface.<sup>32</sup>

Switching back by a red-light source was not possible for this system, but by heating the substrate to higher temperatures such as 250 K, the molecules relax back to the SNO form.

#### D. Determination of the activation energy

The temperature relaxation at slightly elevated temperatures can be used to identify the heights of the energy barriers in a simple Arrhenius model. The energetics of molecules on surfaces can be drastically different compared to those in solution. For example, a nitro-containing spiropyran was found to be stabilized in the open merocyanine form on the Au(111) surface.<sup>14</sup> Investigating the energy barriers involved in the switching process and comparing them to their solution values lead to the possibility of tailoring the properties on the surface. We determine here the energy barrier leading to the temperature-dependent relaxation of MC to SNO.

Figure 8 shows the result of temperature-dependent relaxation measurements. Panel (a) presents relaxation curves of the 240-to-290-nm asymmetry as a function of time for five different temperatures from 240 to 260 K. The corresponding logarithms of the rate over  $1/T$  are shown in panel (b). In an Arrhenius model with an energy barrier  $E_A$ , the rate is  $k(T) = A \times e^{-E_A/(RT)}$ , with  $R$  being the gas constant and  $A$  being a pre-exponential factor depending on the vibrational freedom, which is in the order of  $10^9$ – $10^{14} \text{ s}^{-1}$  for measurements in solutions.<sup>26,33</sup> Each relaxation series has been fitted with a single exponential function but different zero lines to determine the switching rate. Due to the different temperature, changes of

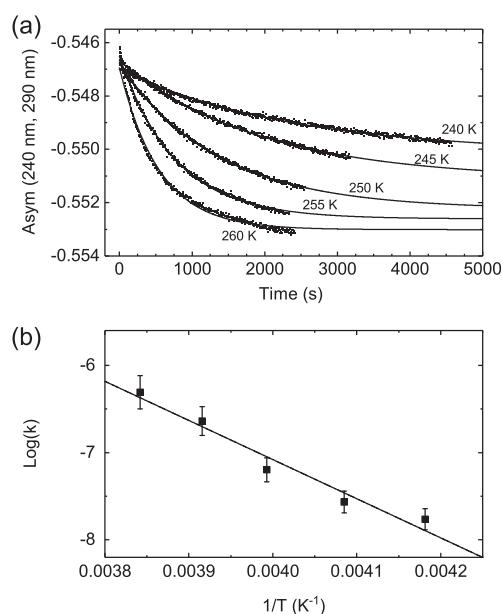


FIG. 8. Measurement of thermal relaxation of SNO on Bi(111). (a) Time dependence of the asymmetry at different temperatures and their fits by single exponential functions (solid lines) and (b) evaluation of the rates by a simple Arrhenius behavior and a fit to determine the energy barrier (solid line).

the substrate reflectance are likely and lead to a different magnitude of the observed effect. The fits reproduce the data well, with a small deviation for the highest temperature at 260 K. From the data, it is not clear whether a drift has an impact on the fit or an additional relaxation channel is available at higher temperatures. Fitting the data in panel (b) to the Arrhenius behavior results in  $E_A = 37(4)$  kJ mol<sup>-1</sup> and  $A = 5(1) \times 10^5$  s<sup>-1</sup>. For this molecule in different solutions, barriers between 61 and 78 kJ mol<sup>-1</sup> have been found.<sup>26,33</sup> The difference can be explained with a strong influence of the substrate on the switching process. The deviation from the fit in Fig. 8(b) hints toward a more complex behavior than a simple Arrhenius-like energy barrier. It is remarkable that the prefactor is much lower compared to typical values found in solution. This could be explained by the reduced freedom of the molecule on the surface but could also originate from a deficiency of the model. Nevertheless, the variation of temperature allows for a deeper analysis of the switching kinetics. Additional measurements of the kinetics for UV illumination at different temperatures might lead to a determination of the barriers in a more advanced energy scheme, as has been done in Ref. 17 by using x-ray absorption spectroscopy.

#### IV. CONCLUSION

A DRS setup suitable for the investigation of photochromic molecules on solid surfaces at low coverages has been presented. Hereby, monochromatic light is used and the reflectance is detected by PMTs, in order to keep the light exposure of the molecules at a minimum. The stable mechanical setup and PID-controlled temperature enable reliable measurements between 100 and 460 K. A low noise of the spectra and measurement of switching kinetics allow systematic investigations of photochromic molecules on opaque substrates. As a demonstration, a monolayer of spironaphthooxazine molecules on a Bi(111) surface has been measured. The measurement of the highly efficient conversion to merocyanine is shown together with an evaluation of the activation energy for the thermal back-relaxation.

#### ACKNOWLEDGMENTS

Financial support from DFG through Sfb 658 is gratefully acknowledged. The authors thank Lukas Kemmler and Janina Drauschke for their assistance during first experiments with the presented setup. Ivar Kumberg is acknowledged for proofreading of the manuscript. The precision mechanics workshop of the Department of Physics of the Freie Universität Berlin is acknowledged for manufacturing the UHV chamber and most of the vacuum parts.

<sup>1</sup>R. Forker, M. Gruenewald, and T. Fritz, "Optical differential reflectance spectroscopy on thin molecular films," *Annu. Rep. Sect. C: Phys. Chem.* **108**, 34–68 (2012).

<sup>2</sup>R. E. Hummel, "Differential reflectometry and its application to the study of alloys, ordering, corrosion, and surface properties," *Phys. Status Solidi A* **76**, 11–44 (1983).

<sup>3</sup>D. E. Aspnes and A. A. Studna, "Anisotropies in the above-band-gap optical spectra of cubic semiconductors," *Phys. Rev. Lett.* **54**, 1956–1959 (1985).

<sup>4</sup>H. Proehl, T. Dienel, R. Nitsche, and T. Fritz, "Formation of solid-state excitons in ultrathin crystalline films of PTCD: From single molecules to molecular stacks," *Phys. Rev. Lett.* **93**, 097403 (2004).

<sup>5</sup>H. Proehl, R. Nitsche, T. Dienel, K. Leo, and T. Fritz, "In situ differential reflectance spectroscopy of thin crystalline films of PTCD on different substrates," *Phys. Rev. B* **71**, 165207 (2005).

<sup>6</sup>R. Forker, T. Dienel, T. Fritz, and K. Müllen, "Optical evidence for substrate-induced growth of ultrathin hexa-peri-hexabenzocoronene films on highly oriented pyrolytic graphite," *Phys. Rev. B* **74**, 165410 (2006).

<sup>7</sup>T. Dienel, C. Loppacher, S. C. B. Mannsfeld, R. Forker, and T. Fritz, "Growth-mode-induced narrowing of optical spectra of an organic adlayer," *Adv. Mater.* **20**, 959–963 (2008).

<sup>8</sup>R. Forker, D. Kasemann, T. Dienel, C. Wagner, R. Franke, K. Müllen, and T. Fritz, "Electronic decoupling of aromatic molecules from a metal by an atomically thin organic spacer," *Adv. Mater.* **20**, 4450–4454 (2008).

<sup>9</sup>R. Forker and T. Fritz, "Optical differential reflectance spectroscopy of ultrathin epitaxial organic films," *Phys. Chem. Chem. Phys.* **11**, 2142–2155 (2009).

<sup>10</sup>A. Baby, M. Gruenewald, C. Zwick, F. Otto, R. Forker, G. van Straaten, M. Franke, B. Stadtmüller, C. Kumpf, G. P. Brivio, G. Fratesi, T. Fritz, and E. Zojer, "Fully atomistic understanding of the electronic and optical properties of a prototypical doped charge-transfer interface," *ACS Nano* **11**, 10495–10508 (2017).

<sup>11</sup>T. Moldt, D. Brete, D. Przyrembel, S. Das, J. R. Goldman, P. K. Kundu, C. Gahl, R. Klajn, and M. Weinelt, "Tailoring the properties of surface-immobilized azobenzenes by monolayer dilution and surface curvature," *Langmuir* **31**, 1048–1057 (2015).

<sup>12</sup>T. Moldt, D. Przyrembel, M. Schulze, W. Bronsch, L. Boie, D. Brete, C. Gahl, R. Klajn, P. Tegeder, and M. Weinelt, "Differing isomerization kinetics of azobenzene-functionalized self-assembled monolayers in ambient air and in vacuum," *Langmuir* **32**, 10795–10801 (2016).

<sup>13</sup>F. Nickel, M. Bernien, M. Herder, S. Wrzalek, P. Chittas, K. Krafft, L. M. Arruda, L. Kipgen, D. Krüger, S. Hecht, and W. Kuch, "Light-induced photoisomerization of a diarylethene molecular switch on solid surfaces," *J. Phys.: Condens. Matter* **29**, 374001 (2017).

<sup>14</sup>M. Piantek, G. Schulze, M. Koch, K. J. Franke, F. Leyssner, A. Krüger, C. Navío, J. Miguel, M. Bernien, M. Wolf, W. Kuch, P. Tegeder, and J. I. Pascual, "Reversing the thermal stability of a molecular switch on a gold surface: Ring-opening reaction of nitrospiropyran," *J. Am. Chem. Soc.* **131**, 12729–12735 (2009).

<sup>15</sup>A. Krüger, M. Bernien, C. F. Hermanns, and W. Kuch, "X-ray-induced reversible switching of an azobenzene derivative adsorbed on Bi(111)," *J. Phys. Chem. C* **118**, 12916–12922 (2014).

<sup>16</sup>G. Schulze, K. J. Franke, and J. I. Pascual, "Induction of a photostationary ring-opening–ring-closing state of spiropyran monolayers on the semimetallic Bi(110) surface," *Phys. Rev. Lett.* **109**, 026102 (2012).

<sup>17</sup>F. Nickel, M. Bernien, K. Krafft, D. Krüger, L. M. Arruda, L. Kipgen, and W. Kuch, "Reversible switching of spiropyran molecules in direct contact with a Bi(111) single crystal surface," *Adv. Funct. Mater.* **27**, 1702280 (2017).

<sup>18</sup>U. Heinemeyer, K. Broch, A. Hinderhofer, M. Kytka, R. Scholz, A. Gerlach, and F. Schreiber, "Real-time changes in the optical spectrum of organic semiconducting films and their thickness regimes during growth," *Phys. Rev. Lett.* **104**, 257401 (2010).

<sup>19</sup>H. Zaglmayr, C. G. Hu, L. D. Sun, and P. Zeppenfeld, "Optical referencing in differential reflectance spectroscopy," *Meas. Sci. Technol.* **25**, 115603 (2014).

<sup>20</sup>C. Weber, L. Pithan, A. Zykov, S. Bommel, F. Carla, R. Felici, C. Knie, D. Bléger, and S. Kowarik, "Multiple timescales in the photoswitching kinetics of crystalline thin films of azobenzene-trimers," *J. Phys.: Condens. Matter* **29**, 434001 (2017).

<sup>21</sup>C. Weber, T. Liebig, M. Gensler, L. Pithan, S. Bommel, D. Bléger, J. P. Rabe, S. Hecht, and S. Kowarik, "Light-controlled 'molecular zippers' based on azobenzene main chain polymers," *Macromolecules* **48**, 1531–1537 (2015).

<sup>22</sup>C. Weber, T. Liebig, M. Gensler, A. Zykov, L. Pithan, J. P. Rabe, S. Hecht, D. Bléger, and S. Kowarik, "Cooperative switching in nanofibers of azobenzene oligomers," *Sci. Rep.* **6**, 25605 (2016).

<sup>23</sup>J. D. E. McIntyre and D. E. Aspnes, "Differential reflection spectroscopy of very thin surface films," *Surf. Sci.* **24**, 417–434 (1971).

<sup>24</sup>R. Nitsche and T. Fritz, "Determination of model-free Kramers-Kronig consistent optical constants of thin absorbing films from just one spectral

- measurement: Application to organic semiconductors,” *Phys. Rev. B* **70**, 195432 (2004).
- <sup>25</sup>A. B. Djurišić, T. Fritz, and K. Leo, “Modeling the optical constants of organic thin films: Application to 3,4,9,10-perylenetetracarboxylic dianhydride (PTCDA),” *Opt. Commun.* **183**, 123–132 (2000).
- <sup>26</sup>A. K. Chibisov and H. Görner, “Photoprocesses in spirooxazines and their merocyanines,” *J. Phys. Chem. A* **103**, 5211–5216 (1999).
- <sup>27</sup>A. Navarro-Quezada, M. Aiglinger, E. Ghanbari, T. Wagner, and P. Zeppenfeld, “Polarization-dependent differential reflectance spectroscopy for real-time monitoring of organic thin film growth,” *Rev. Sci. Instrum.* **86**, 113108 (2015).
- <sup>28</sup>Hamamatsu, *Photomultiplier Tubes: Basics and Applications*, 3rd ed. (Hamamatsu Photonics K.K., Hamamatsu, 2007).
- <sup>29</sup>F. Maurel, J. Aubard, A. Samat, M. Rajzmann, and R. Guglielmetti, “Interplay between theory and experiment in organic photochromism: Example of spirooxazine ring opening/closing equilibrium,” *Mol. Cryst. Liq. Cryst.* **430**, 221–226 (2005).
- <sup>30</sup>A. K. Chibisov and H. Görner, “Photochromism of spirobenzopyranindolines and spironaphthopyranindolines,” *Phys. Chem. Chem. Phys.* **3**, 424–431 (2001).
- <sup>31</sup>H. Görner, “Photochromism of nitrospiropyrans: Effects of structure, solvent and temperature,” *Phys. Chem. Chem. Phys.* **3**, 416–423 (2001).
- <sup>32</sup>C. Bronner and P. Tegeder, “Photo-induced and thermal reactions in thin films of an azobenzene derivative on Bi(111),” *New J. Phys.* **16**, 053004 (2014).
- <sup>33</sup>E. Pottier, R. Dubest, R. Guglielmetti, P. Tardieu, A. Kellmann, F. Tfibel, P. Levoir, and J. Aubard, “Effets de substituant, d’hétéroatome et de solvant sur les cinétiques de décoloration thermique et les spectres d’absorption de photomérocyanines en série spiro[indoline-oxazine],” *Helv. Chim. Acta* **73**, 303–315 (1990).





## 6.4 J. Phys. Chem. C 122, 8031 (2018)

By Fabian Nickel, Matthias Bernien, Dennis Krüger, Jorge Miguel, Andrew J. Britton, Lucas M. Arruda, Lalminthang Kipgen, and Wolfgang Kuch

### Highly Efficient and Bidirectional Photochromism of Spirooxazine on Au(111)

Published online March 2018

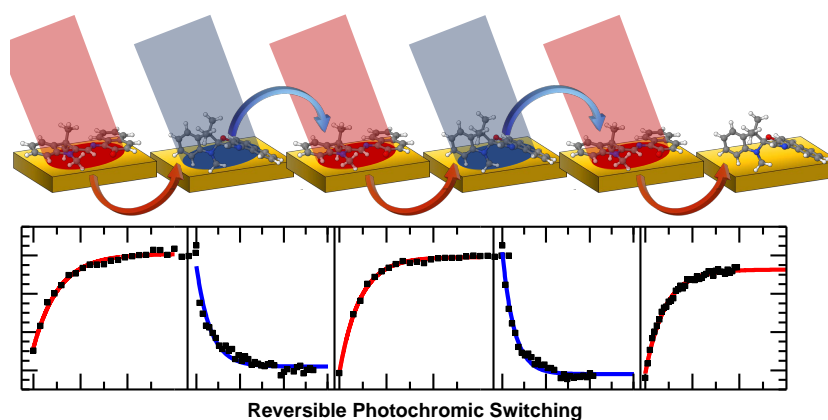
DOI: <https://doi.org/10.1021/acs.jpcc.8b02220>

Reprinted with permission from J. Phys. Chem. C 122, 8031 (2018). Copyright 2018 American Chemical Society.

ACS article on request available at: <http://pubs.acs.org/articlesonrequest/AOR-dcrTSFrZZ3gePdqSd6d6>

#### Contributions:

FN and MB planned and supervised the XAS experiments. FN, MB, DK, JM, AJB, LMA, LK performed the XAS experiments. FN analyzed the XAS data. FN planned, performed, and analyzed the DRS experiments. FN and WK interpreted the results. All authors discussed the results. FN prepared and wrote the manuscript with corrections by MB, LK, and WK. WK supervised the study.





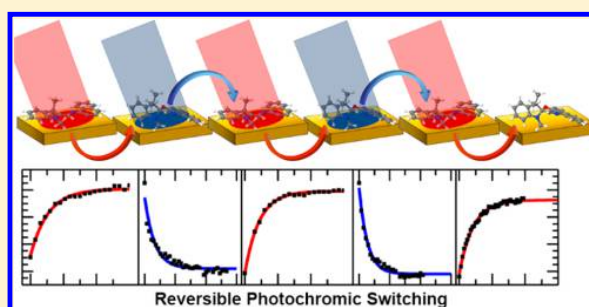
# Highly Efficient and Bidirectional Photochromism of Spirooxazine on Au(111)

Fabian Nickel, Matthias Bernien,<sup>1</sup> Dennis Krüger, Jorge Miguel, Andrew J. Britton, Lucas M. Arruda, Lalminthang Kipgen, and Wolfgang Kuch<sup>\*,1</sup>

Institut für Experimentalphysik, Freie Universität Berlin, Arnimallee 14, 14195 Berlin, Germany

## Supporting Information

**ABSTRACT:** Controlling molecules in direct contact with surfaces is central to molecular electronics. Photochromic molecules immobilized and contacted by a surface promise to provide remote control on the molecular level using light. Combining X-ray absorption spectroscopy, differential reflectance spectroscopy, and density functional theory, we demonstrate highly efficient and bidirectional photochromism of a spirooxazine molecular switch in direct contact with a Au(111) surface. The ring-opening reaction by UV light is 2 orders of magnitude more efficient than previously reported for other surface-adsorbed systems, and even more importantly, the red-light-induced ring-closing is accessible even in contact with a metal surface. This opens new prospects for applications by utilizing the gold surface with directly adsorbed functional units consisting of molecular photochromic switches.



## INTRODUCTION

Photochromism of molecules, a well-known and ubiquitous effect, enables one to remotely control systems on the molecular level by illumination only. Excitation with light of different wavelengths leads to a bidirectional switching of the molecules. In addition to having distinct absorption spectra, the resultant isomers also exhibit drastically different physical and chemical properties, for example, in the electric dipole moment.<sup>1,2</sup> Different groups of photochromic molecules cover a diverse and broad range of current and future applications. Possible applications can be found in nature, where fundamental functions, e.g., the activation of the retinal molecule,<sup>3</sup> can be linked to photoinduced processes. Furthermore, the implementation of tailored molecular switches is not limited to biological systems, but compounds designed for molecular electronics may lead to a significant improvement in data storage and logic circuits.<sup>4,5</sup> The possibility of optically accessible transistors<sup>6</sup> or even memories<sup>7</sup> as well as logic modules<sup>8</sup> has recently been demonstrated using molecular switches. Of particular interest for applications is the group of spiropyranes (SPs) and spirooxazines (SOs). Their drastic change of chemical reactivity, electric dipole moment, and geometry upon isomerization attracted great attention of scientists. In solution, they share the ability for highly efficient light-induced interconversion to the corresponding merocyanine (MC) forms. Modifications of SPs and SOs have been studied to a large extent, leading to many examples of SP-based materials<sup>2</sup> and (a still incomplete) understanding of the complex isomerization process of SP/SOs.<sup>9–13</sup> For utilization in nanoscale systems such as for molecular electronics,

immobilization on a surface is required. The switching ability needs to persist on the surface, which is challenging for photochromic molecules.<sup>14–19</sup> Due to additional effects such as hybridization of electronic states, fast relaxation of excited states, or steric hindrance, the switching is quenched in proximity to a surface in most systems. To overcome these limitations, attempts to decouple molecules from the surface in self-assembled monolayers (SAMs) led to promising results of efficient and reversibly switching layers.<sup>20–24</sup> When in direct contact to a surface, as is required for molecular electronics, the isomerization of photochromic molecules was found to be strongly suppressed,<sup>25</sup> nonexistent,<sup>14,16</sup> or energetically reversed.<sup>15</sup> With the availability of a fully reversible system in contact with a conducting surface, new prospects would evolve for future devices, such as embedding molecular switching units in networks, controlling the current through molecular wires, or influencing magnetic properties of adsorbed molecules.

For photochromic molecules on surfaces, irreversible thermal switching from SP to MC was observed on Au(111).<sup>15</sup> In refs 26 and 27, optical switching from SP/SO to MC was demonstrated and reversibility was achieved through thermal backswitching. The key to enable a reversible isomerization was to exchange the frequently used electron-withdrawing nitro group on the pyran moiety by an electron-donating naphtho group. This leads to a destabilized MC configuration and thus a thermally reversible process.<sup>26</sup> However, so far no photo-

Received: March 6, 2018

Revised: March 16, 2018

Published: March 19, 2018



ACS Publications

© 2018 American Chemical Society

8031

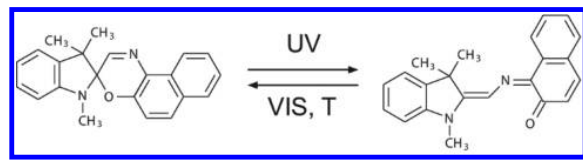
DOI: 10.1021/acs.jpcc.8b02220  
*J. Phys. Chem. C* 2018, 122, 8031–8036

induced backswitching has been shown in direct contact with solid surfaces. This lack of optical control over electrically contacted molecules hampers the implementation in applied systems. Gold is often the preferred choice of substrate or metal electrode for single molecules or in assembling molecular layers<sup>20,28,29</sup> due to its inert surface, high electrical and thermal conductivity, their well-known vacuum cleaning procedure, and frequently investigated surfaces.<sup>30–34</sup> On gold, the famous unidirectional molecular motor has been immobilized<sup>35</sup> and phenyl-spacer-group linked diarylethenes were found to be able to switch their conductance.<sup>34</sup>

Here, we show the fully reversible and light-only driven photoisomerization of a SO derivate in less than one layer of molecules on a Au(111) surface. By exchanging the previously used spironaphthopyran derivate<sup>26</sup> to spironaphthooxazine (SNO), a change in the energy landscape enables repeatable control of the isomerization states using only UV and red light-emitting diode (LED) illumination. We prove this by a combination of X-ray absorption (XA) spectroscopy, density functional theory (DFT) simulations, and differential reflectance spectroscopy (DRS). DRS, a direct and nondestructive method for probing the mean isomerization state on the surface, provides also a quantification of the corresponding effective cross sections of the switching processes.

The photoinduced reaction is sketched in Scheme 1. A colorless spironaphthooxazine (SNO, 1,3,3-trimethylindolino-

**Scheme 1. Spironaphthooxazine (SNO, Left) Can Be Converted to Merocyanine (MC) by UV Light and Reversibly Back to SNO by Visible Light or Temperature Increase**



naphthospirooxazine, purchased from TCI Chemicals) can be converted to the colored merocyanine (MC) by UV light and reversibly back by visible light or temperature increase. This is a well-known photoconversion, intensely studied in various solutions,<sup>36,37</sup> gels,<sup>38</sup> or thin films.<sup>39,40</sup>

## EXPERIMENTAL SECTION

All sample preparations have been carried out in ultrahigh vacuum (UHV). Standard sputter and annealing cycles were applied by using Ar<sup>+</sup> ions with an energy of 1 kV and subsequent annealing slightly above 900 K for 15 min. The SNO has been evaporated from a home-built Knudsen cell evaporator at a temperature of 363 K onto the substrate maintained at a temperature of 200 K. Coverages were estimated for the X-ray measurements by comparing the total absorption of the carbon K-edge to the calibration as carried out in ref 26. The estimated coverage is 0.70(5) monolayer (ML) for the X-ray absorption (XA) studies. For the calibration of the coverage of the samples used in the differential reflectance spectroscopy (DRS) setup, the procedure is presented in detail in ref 27. A saturation of one layer of molecules has been measured on a Bi(111) surface. With this, the change of frequency of an ice-water-cooled quartz microbalance can be related to the amount of molecules on the surface. Exactly the same setup has been used for all DRS measurements, and with the explained calibration, layer thicknesses of 0.7(1) ML were investigated.

XA measurements were carried out at the synchrotron radiation facility BESSY II of the Helmholtz-Zentrum Berlin at the beamline UE56-2/PGM-2 with a home-built UHV chamber. This undulator beamline exhibits a degree of linear polarization of ~99%. The energy resolution was set to 150 meV for the measurement of the nitrogen K-edge. The base pressure was  $8 \times 10^{-10}$  mbar for all XA experiments. The signal was acquired with the total electron yield method by measuring the amplified sample current via a FEMTO DDP-300 subfemtoampere amplifier. A freshly prepared gold grid upstream of the experimental chamber was used to normalize the X-ray beam intensity. To extract XA signals arising only from the molecules, all measurements are normalized to that measured from a clean substrate. An incidence angle of 25° with respect to the surface plane was used for measuring spectra with *p*- and *s*-polarized light. Magic-angle spectra for identification of the isotropic absorption were acquired at an angle of 54.7° and using *p*-polarized light.

To reduce the influence of X-rays on the sample, the chamber was moved out of the focus of the beamline. By that, an X-ray spot of about  $1 \times 1$  mm<sup>2</sup> illuminated the sample, leading to an estimated photon flux density of  $\sim 10^{13}$  photons s<sup>-1</sup> cm<sup>-2</sup>. Except for the time evolution of the nitrogen K-edge in panel (b) of Figure 1, all spectra have been measured on virgin positions. A longer exposure for >30 min leads to a small

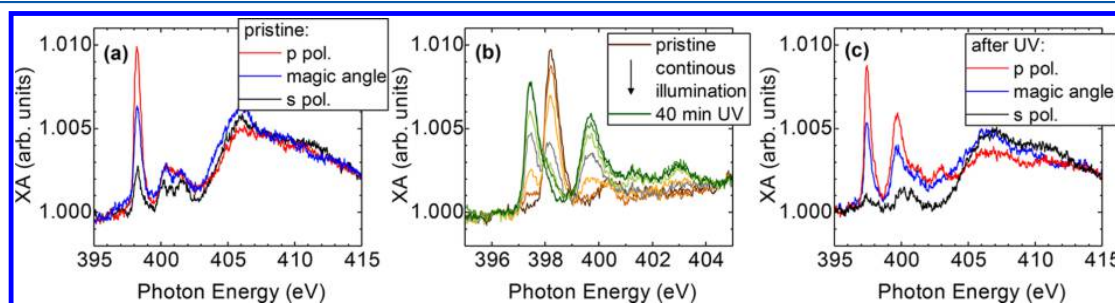


**Figure 1. Nitrogen K-edge XA of a sub-ML SNO on Au(111).** (a) Pristine state after evaporation for *p* and *s* polarizations measured at 25° angle of incidence and at the magic angle (probing the isotropic absorption at 54.7° angle of incidence). (b) Consecutive recording of *p*-polarized spectra for 40 min during in situ UV illumination. (c) XA after 40 min UV illumination for both polarizations and the magic angle.

reduction of absorption intensity on the first  $\pi^*$  resonances, presumably by destruction of molecules. Additionally, an influence of X-ray exposure on the switching itself is also observed. This has been reported for different switchable molecules before.<sup>17,41</sup> Hence, the XA data is not used for a quantification of the switching process, and the favorable method of DRS is applied instead. The details of the DRS experiments and DFT simulations can be found in the Supporting Information.

## RESULTS AND DISCUSSION

Figure 1 shows the results of the XA investigations of SNO on Au(111). With a coverage of 70% of a fully covered monolayer (ML), direct contact of the molecules with the surface is expected. Figure 1a presents the XA at the nitrogen *K*-edge of a freshly evaporated sample at a sample temperature of 200 K. An intense  $\pi^*$  resonance is present at an energy of 398.2 eV. The angle dependence, obtained from the comparison of the *p*-polarized spectrum (measured at 25° angle of incidence) and the *s*-polarized spectrum, enables the determination of the mean angle of the corresponding orbital for all probed molecules.<sup>42</sup> The magic-angle spectrum is measured at an angle of 54.7° to the surface and represents the isotropic absorption. Quantitative analysis of the angle dependence yields a mean angle of 35(1)° between the orbital and the surface normal. In DFT calculations, this orbital is localized on the naphthooxazine moiety of the SNO (cf. Supporting Information). Using a UV LED, a very clear change to the XA spectrum can be induced, as shown in Figure 1b. After 40 min of UV illumination, the 398.2 eV peak vanished and a new  $\pi^*$  resonance at 397.4 eV evolved (green line). In addition, a new resonance appears at 399.7 eV. For different SP derivatives, such as nitro-BIPS<sup>15</sup> or spironaphthopyran,<sup>26</sup> a similar new resonance was found and attributed to the MC form. The XA at the nitrogen *K*-edge of MC differs strongly from that of the pristine state. As can be seen in Figure 1c, beside the different energies of the  $\pi^*$  resonances, the intensity ratio between *p*- and *s*-polarized spectra increases upon UV-light illumination. This signifies an on average more flat-lying molecule, with a mean angle of 23(1)° to the surface. The optimization of the geometric structure of the free molecule in DFT simulations and previous results in literature point toward a flat MC configuration.<sup>15</sup>

To interpret the changes of the observed nitrogen *K*-edge XA resonances, DFT calculations on both isomers were carried out. The StoBe code package<sup>43</sup> has been used, which had been successfully applied to many photochromic molecules previously to identify isomerization states, even by comparing the simulated free-molecule XA to the one measured on the surface.<sup>15,25,26,44</sup> For the spectrum of the pristine state in Figure 1a, a clear agreement with Figure 2 is visible for the SNO isomer (black line). The calculation yields a prominent  $\pi^*$  resonance at 398.2 eV and two less intense resonances at 399.6 and 401.1 eV. The 398.2 eV resonance originates from the nitrogen of the oxazine compound, which is the most obvious difference compared to the spectra of spironaphthopyran.<sup>26</sup> The simulation of the corresponding MC species in the most-observed trans–trans–cis configuration of the carbon and nitrogen (of the oxazine moiety) bonds (as sketched in Scheme 1), is represented by the red line in Figure 2. The shift of 0.8 eV of the first  $\pi^*$  resonance in the experimental data is consistent with the shift of 1.0 eV to lower energies in the simulated spectrum. The overall spectral shape of the experimental

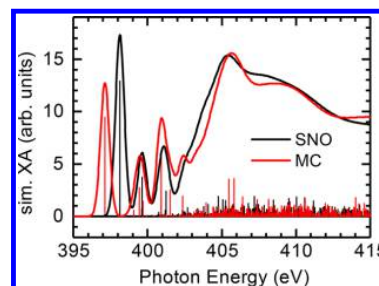


Figure 2. Simulation of the XA spectra of SNO and MC for a free molecule by means of DFT (cf. Supporting Information).

spectrum after UV illumination agrees well with the simulated MC spectrum.

For the X-ray measurements, radiation-induced changes have been observed, and therefore, virgin sample positions were chosen to measure the spectra in each of the panels in Figure 1. This is clearly not possible for an accurate determination of the switching kinetics and attempts to reversibly switch the sample isomerization over a longer time span. To investigate and demonstrate the control of the isomerization, we thus utilize DRS.<sup>27</sup> DRS allows one to identify changes of the optical reflectance of adsorbate/solid hybrid systems by comparing the reflection  $R(\lambda)$  of a system as a function of the wavelength  $\lambda$  with the reflection  $R_0(\lambda)$  of the substrate only. This is calculated as

$$\Delta R(\lambda)/R(\lambda) = R(\lambda)/R_0(\lambda) - 1.$$

To acquire DRS with very low noise and minimum light exposure during the measurement as well as a very precise control over the temperature, a special setup was built to investigate photochromic molecules on solid surfaces. Details of this experiment are described briefly in the Supporting Information and in ref 27. DRS does not relate directly to the reflection of the adsorbate because the complex optical constants of the surface also contribute to the signal. For only slightly bound or even decoupled molecules, clear assignments of the absorption bands can be attained.

Figure 3 shows the DRS of a sub-ML (coverage around 0.7 ML) SNO on Au(111). The molecules have been evaporated onto the Au(111) crystal kept at 200 K, and all illuminations were performed at this temperature by a 365 nm UV LED and a 625 nm red LED (cf. Supporting Information). Clearly, a

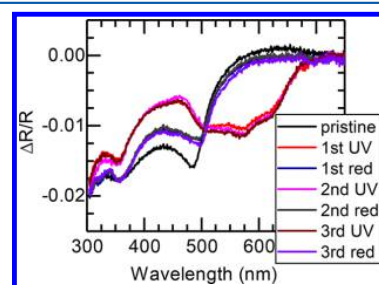
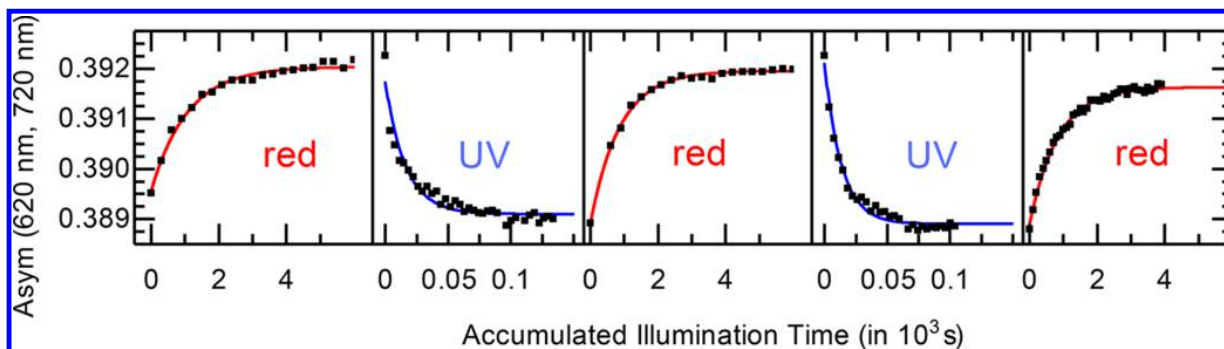


Figure 3. DRS of a sub-ML SNO on Au(111) at  $T = 200$  K. The pristine state after evaporation and six further illumination steps, alternatingly by UV and red LEDs, are shown. Total illumination time for UV and red light was more than 100 and 4000 s, respectively. Negative DRS corresponds to a stronger absorption of the organic–inorganic system compared to the clean substrate.





**Figure 4.** Detailed investigation of the switching kinetics leading to the final isomerization states shown in Figure 3. The asymmetry of the 620 and 720 nm reflectance intensities is recorded as a function of illumination time at a temperature of 200 K. The illumination time before each measurement point for UV illumination was 3.7 s, while in the case of red-light illumination it was 300 s for the first two series and 100 s for the last illumination series.

bidirectional photochromism using both LEDs is achieved. The spectra reproduce completely after the first UV illumination. The pristine spectrum (black line) features a peak at 485 nm and one at 350 nm. Except for the 485 nm peak, the overall spectral shape of the change in reflectance has similarities with SNO measured in ethanol solution, where only a peak at 360 nm is present.<sup>40</sup> The 485 nm peak presumably originates from the change of surface properties induced by molecule adsorption, because gold has a strong change of absorption at this wavelength and no SNO or MC absorption is expected from solution results.<sup>40</sup> A similar peak is also observed for alkanethiolate SAMs on Au(111).<sup>20</sup> In addition, the same SNO molecule did not feature such a peak on a Bi(111) substrate.<sup>27</sup> After the first UV illumination, a strong change of the overall spectral shape of the DRS is achieved (red line). The main differences are new peaks at 570 and 625 nm, a reduction of the intensity of the 485 nm peak, and a shift to 505 nm. By comparing these changes of reflectance to UV/vis spectra of MC in solution, the presence of a MC isomer on the surface can be clearly stated with its absorption close to reported wavelengths in solution.<sup>40</sup> MC, recorded in ethanol solution, shows a double peak at 570 and 620 nm. The DRS upon UV illumination on Au(111) shows a remarkable resemblance with peaks at the same wavelength. The double-peak structure stems from either a vibronic shoulder or an aggregation of MC molecules,<sup>45</sup> but due to the complex interaction of the optical properties, it is not feasible to analyze the aggregation in DRS.

Illumination of the MC isomer on Au(111) with red light leads to a relaxation of the sample back to the SNO isomer (blue line). A pronounced difference to the pristine state, especially in the region of 485 nm, where the surface-attributed peak is slightly lowered and shifted to 500 nm, is observed. We attribute this to a rearranging of the SNO molecules, because the difference of the SNO states is dominated by increased reflectance at the 485 nm peak. The overall remaining difference in DRS intensity does not show the shape of the MC/Au(111) DRS and suggests that, for the photostationary state by the red light, all MC isomers were converted back to SNO. On the Bi(111) surface, DRS attributed to the MC isomer was found to have a peak at 625 nm as well, but, as previously mentioned, no light-induced photoconversion from MC to SNO could be observed.<sup>27</sup>

The same sample was switched by three UV illuminations from SNO to MC and three times by red light from MC to SNO. Except for the difference between the first two SNO

states, all further illumination steps led to very reproducible spectra. To quantify the switching kinetics, DRS can be utilized as well. The highest reliability was achieved by using the DRS asymmetry, more specifically by comparing the reflectance at two different wavelengths (cf. Supporting Information and ref 27). This asymmetry is defined as

$$\text{asym}(\lambda_1, \lambda_2) = (R(\lambda_1) - R(\lambda_2)) / (R(\lambda_1) + R(\lambda_2))$$

Figure 4 shows the time-resolved asymmetry measurements leading to molecule isomerization of which the DRS spectra are shown in Figure 3. Starting from a MC configuration, red-light illumination was carried out alternating with recordings of the asymmetry (red lines). For each point, 300 s red-light illumination was applied using a 625 nm LED with a full width at half maximum (fwhm) of 18 nm. A clear increase of the asymmetry signifies the switching from MC to SNO. Because the MC-to-SNO conversion can be induced by either red-light illumination or temperature, it is necessary to identify the origin of the effect. We conclude that the MC-to-SNO switching as shown in Figure 4 originates from red-light illumination: The temperature on the sample is well-known from the silicon temperature diode. As described in ref 27, the sample is pressed to a thick copper block which is proportional–integral–derivative (PID)-controlled with an accuracy of 0.1 K. The complete sample plate is in contact with the copper block by pressing it with two strong phosphorus bronze springs. The measurement data do not allow for a full exclusion of an additional temperature-induced relaxation, but different observations emphasize the conclusion of light-induced switching:

(1) Red-light-induced switching at 130 K (cf. Supporting Information section 3) is possible whereas thermal stability at higher temperatures (165 K by the same asymmetry measurement, >3 h of measurement time at 200 K) has been observed.

(2) The thermal relaxation (cf. Supporting Information section 4) reveals the barriers of the MC-to-SNO relaxation. Assuming an Arrhenius behavior, the corresponding necessary temperature for the switching of the 130 K illumination as a pure thermal effect would be >230 K. If such a temperature increase would take place, attempts of illumination at room temperature would have led to a direct desorption of the molecules, because they start desorbing above room temperature.

(3) In the case of a bad thermal contact, the thermal equilibrium would need longer time to settle (e.g., measured

with a time constant around 145 s in ref 26). This would lead to a strongly different average temperature for the measurement with different illumination times, compared to the one shown in Figure 3 for the third red-light illumination (100 s illumination steps instead of 300 s). After each measurement point, the asymmetry is recorded for  $\sim 60$  s. In case of the 100 s illumination time steps, the average temperature would be lower, leading to slower switching speeds, which has not been observed.

(4) SNO on Bi(111) was not possible to switch reversibly back by red light in the same setup with the same temperatures and very similar relaxation barriers.<sup>27</sup>

In Figure 4, the following UV-light illuminations for 3.7 s each point (blue lines, using a 365 nm LED with a fwhm of 9 nm) present a significantly faster process. This is expected, because the quantum yield of the photocoloration is  $\sim 0.4$  in solution,<sup>37</sup> about 2 orders of magnitude above the one for decoloration.<sup>1</sup> The last MC-to-SNO switching series with illumination steps of 100 s is saturated slightly below the other two red illuminations, but this might be considered an artifact, due to possible experimental drifts.<sup>27</sup>

A closer look into the time dependence reveals the high efficiency of the process: The time constants as determined by the single-exponential fits are 1074(57) s (1st red), 16(1) s (2nd UV, first blue line), 872(21) s (2nd red), 14(1) s (3rd UV), and 836(27) s (3rd red). This is potentially a process that can be trained by illumination cycles, and therefore the switching efficiencies after each step increase slightly. A rearrangement as assumed for the initial UV/red light cycles of the molecules is likely. Additionally, the fits for UV illumination are not completely fitting to the experimental data. Beside the possibility of experimental drifts, also a more complex behavior such as cooperativity might be present. For the fastest UV and red illuminations, effective cross sections can be calculated using the photon flux density and switching time constant by  $\sigma_{\text{eff}} = (\phi\tau)^{-1}$  as  $\sigma_{\text{eff,UV}} = 2.5(6) \times 10^{-19} \text{ cm}^2$  and  $\sigma_{\text{eff,red}} = 1.4(3) \times 10^{-21} \text{ cm}^2$ . The process is highly efficient compared to previous findings on similar molecules on surfaces, where effective cross sections were lower by  $\sim 2$  orders of magnitude.<sup>16,26</sup> There is still a high potential for further increase of the efficiency, because in solution cross sections up to  $10^{-16} \text{ cm}^2$  have been determined.<sup>1,37</sup> The improved effective cross section compared to spironaphthopyran or nitro-BIPS could originate from the formation of a singlet state instead of a triplet state upon UV excitation, as has been discussed for SOs in gels or films.<sup>38,39</sup> Our findings show that an efficient photochromism can also be achieved on the surface without a decoupling layer, which enhances the amount of possible applications and reduces the complexity of the system. This and the enhanced effective cross section of the SNO-to-MC conversion constitute a huge leap forward in realization of photochromic molecular devices on solid surfaces.

## CONCLUSIONS

In conclusion, we demonstrate a functional photochromic molecular switch directly adsorbed on a Au(111) surface, which had previously been found to stabilize MC isomers. XA measurements reveal an intact SNO that can be converted to MC by UV illumination. The fully reversible, purely light-driven process in molecules immobilized on a surface is demonstrated by DRS using UV and red LEDs for the control of the isomerization. In contrast to previous studies of photochromic molecules on surfaces, the effective cross section

for the SNO-to-MC photoconversion is increased by nearly 2 orders of magnitude. This opens new horizons for applications of photochromic molecules, e.g., in assemblies with networks or inorganic molecules.

## ASSOCIATED CONTENT

### Supporting Information

The Supporting Information is available free of charge on the ACS Publications website at DOI: 10.1021/acs.jpcc.8b02220.

Further experimental (DRS) and theoretical (DFT) details; visualization of orbitals upon X-ray excitation; experiments of red-light illumination at 130 K; determination of the thermal stability (PDF)

## AUTHOR INFORMATION

### Corresponding Author

\*E-mail: kuch@physik.fu-berlin.de.

### ORCID

Matthias Bernien: 0000-0002-1734-1800

Wolfgang Kuch: 0000-0002-5764-4574

### Notes

The authors declare no competing financial interest.

## ACKNOWLEDGMENTS

We acknowledge financial support by the DFG through Sfb 658. L.M.A. thanks CAPES for funding (no. 9469/13-3). The Helmholtz-Zentrum Berlin is acknowledged for the allocation of beamtime at BESSY II. The authors thank B. Zada and W. Mahler for their technical support during the beamtimes and I. Kumberg for proofreading the manuscript. The high-performance cluster of the Zentraleinrichtung für Datenverarbeitung (ZEDAT) of Freie Universität Berlin is gratefully acknowledged for computing time.

## REFERENCES

- (1) *Molecular Switches*, second ed.; Feringa, B. L., Browne, W. R., Eds.; Wiley-VCH: Weinheim, Germany, 2001.
- (2) Klajn, R. Spiropyran-Based Dynamic Materials. *Chem. Soc. Rev.* **2014**, *43*, 148–184.
- (3) Palczewski, K.; Kumasaka, T.; Hori, T.; Behnke, C. A.; Motoshima, H.; Fox, B. A.; Le Trong, I.; Teller, D. C.; Okada, T.; Stenkamp, R. E.; et al. Crystal Structure of Rhodopsin: A G Protein-Coupled Receptor. *Science* **2000**, *289*, 739–745.
- (4) Aviram, A. Molecules for Memory, Logic, and Amplification. *J. Am. Chem. Soc.* **1988**, *110*, 5687–5692.
- (5) Irie, M. Photochromism: Memories and Switches - Introduction. *Chem. Rev.* **2000**, *100*, 1683–1684.
- (6) Gemayel, M. E.; Börjesson, K.; Herder, M.; Duong, D. T.; Hutchison, J. A.; Ruzié, C.; Schweicher, G.; Salleo, A.; Geerts, Y.; Hecht, S.; et al. Optically Switchable Transistors by Simple Incorporation of Photochromic Systems into Small-Molecule Semiconducting Matrices. *Nat. Commun.* **2015**, *6*, 6330.
- (7) Leydecker, T.; Herder, M.; Pavlica, E.; Bratina, G.; Hecht, S.; Orgiu, E.; Samori, P. Flexible Non-Volatile Optical Memory Thin-Film Transistor Device with over 256 Distinct Levels Based on an Organic Bicomponent Blend. *Nat. Nanotechnol.* **2016**, *11*, 769–775.
- (8) Meng, F.; Hervault, Y.-M.; Shao, Q.; Hu, B.; Norel, L.; Rigaut, S.; Chen, X. Orthogonally Modulated Molecular Transport Junctions for Resettable Electronic Logic Gates. *Nat. Commun.* **2014**, *5*, 3023.
- (9) Ernsting, N. P.; Arthen-Engeland, T. Photochemical Ring-Opening Reaction of Indolinespiropyrans Studied by Subpicosecond Transient Absorption. *J. Phys. Chem.* **1991**, *95*, 5502–5509.

- (10) Ernsting, N. P.; Dick, B.; Arthen-Engeland, T. The Primary Photochemical Reaction Step of Unsubstituted Indolino-Spiropyran. *Pure Appl. Chem.* **2009**, *62*, 1483–1488.
- (11) Zhang, J. Z.; Schwartz, B. J.; King, J. C.; Harris, C. B. Ultrafast Studies of Photochromic Spiropyran in Solution. *J. Am. Chem. Soc.* **1992**, *114*, 10921–10927.
- (12) Kaiser, C.; Halbritter, T.; Heckel, A.; Wachtveitl, J. Thermal, Photochromic and Dynamic Properties of Water-Soluble Spiropyran. *ChemistrySelect* **2017**, *2*, 4111–4123.
- (13) Kohl-Landgraf, J.; Braun, M.; Özçoban, C.; Gonçalves, D. P. N.; Heckel, A.; Wachtveitl, J. Ultrafast Dynamics of a Spiropyran in Water. *J. Am. Chem. Soc.* **2012**, *134*, 14070–14077.
- (14) Maurer, R. J.; Reuter, K. Bistability Loss as a Key Feature in Azobenzene (Non-)Switching on Metal Surfaces. *Angew. Chem., Int. Ed.* **2012**, *51*, 12009–12011.
- (15) Piantek, M.; Schulze, G.; Koch, M.; Franke, K. J.; Leyssner, F.; Krüger, A.; Navio, C.; Miguel, J.; Bernien, M.; Wolf, M.; et al. Reversing the Thermal Stability of a Molecular Switch on a Gold Surface: Ring-Opening Reaction of Nitrospiropyran. *J. Am. Chem. Soc.* **2009**, *131*, 12729–12735.
- (16) Bronner, C.; Schulze, G.; Franke, K. J.; Pascual, J. I.; Tegeder, P. Switching Ability of Nitro-Spiropyran on Au(111): Electronic Structure Changes as a Sensitive Probe during a Ring-Opening Reaction. *J. Phys.: Condens. Matter* **2011**, *23*, 484005.
- (17) Krüger, A.; Bernien, M.; Hermanns, C. F.; Kuch, W. X-Ray-Induced Reversible Switching of an Azobenzene Derivative Adsorbed on Bi(111). *J. Phys. Chem. C* **2014**, *118*, 12916–12922.
- (18) Bronner, C.; Priewisch, B.; Rück-Braun, K.; Tegeder, P. Photoisomerization of an Azobenzene on the Bi(111) Surface. *J. Phys. Chem. C* **2013**, *117*, 27031–27038.
- (19) Wirth, J.; Hatter, N.; Drost, R.; Umbach, T. R.; Barja, S.; Zastrow, M.; Rück-Braun, K.; Pascual, J. I.; Saalfrank, P.; Franke, K. J. Diarylethene Molecules on a Ag(111) Surface: Stability and Electron-Induced Switching. *J. Phys. Chem. C* **2015**, *119*, 4874–4883.
- (20) Moldt, T.; Brete, D.; Przyrembel, D.; Das, S.; Goldman, J. R.; Kundu, P. K.; Gahl, C.; Klajn, R.; Weinelt, M. Tailoring the Properties of Surface-Immobilized Azobenzenes by Monolayer Dilution and Surface Curvature. *Langmuir* **2015**, *31*, 1048–1057.
- (21) Garling, T.; Tong, Y.; Darwish, T. A.; Wolf, M.; Campen, R. K. The Influence of Surface Potential on the Optical Switching of Spiropyran Self Assembled Monolayers. *J. Phys.: Condens. Matter* **2017**, *29*, 414002.
- (22) Schulze, M.; Utecht, M.; Hebert, A.; Rück-Braun, K.; Saalfrank, P.; Tegeder, P. Reversible Photoswitching of the Interfacial Nonlinear Optical Response. *J. Phys. Chem. Lett.* **2015**, *6*, 505–509.
- (23) Smaali, K.; Lenfant, S.; Karpe, S.; Oçafraïn, M.; Blanchard, P.; Deresmes, D.; Godey, S.; Rochefort, A.; Roncali, J.; Vuillaume, D. High On–Off Conductance Switching Ratio in Optically-Driven Self-Assembled Conjugated Molecular Systems. *ACS Nano* **2010**, *4*, 2411–2421.
- (24) Ivashenko, O.; van Herpt, J. T.; Feringa, B. L.; Rudolf, P.; Browne, W. R. UV/Vis and NIR Light-Responsive Spiropyran Self-Assembled Monolayers. *Langmuir* **2013**, *29*, 4290–4297.
- (25) Nickel, F.; Bernien, M.; Herder, M.; Wrzalek, S.; Chittas, P.; Krafft, K.; Arruda, L. M.; Kipgen, L.; Krüger, D.; Hecht, S.; et al. Light-Induced Photoisomerization of a Diarylethene Molecular Switch on Solid Surfaces. *J. Phys.: Condens. Matter* **2017**, *29*, 374001.
- (26) Nickel, F.; Bernien, M.; Krafft, K.; Krüger, D.; Arruda, L. M.; Kipgen, L.; Kuch, W. Reversible Switching of Spiropyran Molecules in Direct Contact With a Bi(111) Single Crystal Surface. *Adv. Funct. Mater.* **2017**, *27*, 1702280.
- (27) Nickel, F.; Bernien, M.; Lipowski, U.; Kuch, W. Optical Differential Reflectance Spectroscopy for Photochromic Molecules on Solid Surfaces. *Rev. Sci. Instrum.* **2018**, *89*, 033113.
- (28) Moldt, T.; Przyrembel, D.; Schulze, M.; Bronsch, W.; Boie, L.; Brete, D.; Gahl, C.; Klajn, R.; Tegeder, P.; Weinelt, M. Differing Isomerization Kinetics of Azobenzene-Functionalized Self-Assembled Monolayers in Ambient Air and in Vacuum. *Langmuir* **2016**, *32*, 10795–10801.
- (29) Katsonis, N.; Vicario, J.; Kudernac, T.; Visser, J.; Pollard, M. M.; Feringa, B. L. Self-Organized Monolayer of Meso-Tetradecylporphyrin Coordinated to Au(111). *J. Am. Chem. Soc.* **2006**, *128*, 15537–15541.
- (30) Nazin, G. V.; Qiu, X. H.; Ho, W. Visualization and Spectroscopy of a Metal-Molecule-Metal Bridge. *Science* **2003**, *302*, 77–81.
- (31) Mohn, F.; Repp, J.; Gross, L.; Meyer, G.; Dyer, M. S.; Persson, M. Reversible Bond Formation in a Gold-Atom-Organic-Molecule Complex as a Molecular Switch. *Phys. Rev. Lett.* **2010**, *105*, 266102.
- (32) Quek, S. Y.; Venkataraman, L.; Choi, H. J.; Louie, S. G.; Hybertsen, M. S.; Neaton, J. B. Amine–Gold Linked Single-Molecule Circuits: Experiment and Theory. *Nano Lett.* **2007**, *7*, 3477–3482.
- (33) Kronemeijer, A. J.; Akkerman, H. B.; Kudernac, T.; van Wees, B. J.; Feringa, B. L.; Blom, P. W. M.; de Boer, B. Reversible Conductance Switching in Molecular Devices. *Adv. Mater.* **2008**, *20*, 1467–1473.
- (34) Katsonis, N.; Kudernac, T.; Walko, M.; van der Molen, S. J.; van Wees, B. J.; Feringa, B. L. Reversible Conductance Switching of Single Diarylethenes on a Gold Surface. *Adv. Mater.* **2006**, *18*, 1397–1400.
- (35) van Delden, R. A.; ter Wiel, M. K. J.; Pollard, M. M.; Vicario, J.; Koumura, N.; Feringa, B. L. Unidirectional Molecular Motor on a Gold Surface. *Nature* **2005**, *437*, 1337.
- (36) Marevtsev, V. S.; Zaichenko, N. L. Peculiarities of Photochromic Behaviour of Spiropyran and Spirooxazines. *J. Photochem. Photobiol., A* **1997**, *104*, 197–202.
- (37) Chibisov, A. K.; Görner, H. Photoprocesses in Spirooxazines and Their Merocyanines. *J. Phys. Chem. A* **1999**, *103*, 5211–5216.
- (38) Biteau, J.; Chaput, F.; Boilot, J.-P. Photochromism of Spirooxazine-Doped Gels. *J. Phys. Chem.* **1996**, *100*, 9024–9031.
- (39) Krohm, F.; Kind, J.; Savka, R.; Alcaraz Janßen, M.; Herold, D.; Plenio, H.; Thiele, C. M.; Andrieu-Brunsen, A. Photochromic Spiropyran- and Spirooxazine-Homopolymers in Mesoporous Thin Films by Surface Initiated ROMP. *J. Mater. Chem. C* **2016**, *4*, 4067–4076.
- (40) Siddiqui, M. K.; Corthey, G.; Hayes, S. A.; Rossos, A.; Badali, D. S.; Xian, R.; Murphy, R. S.; Whitaker, B. J.; Miller, R. J. D. Synchronised Photoreversion of Spirooxazine Ring Opening in Thin Crystals to Uncover Ultrafast Dynamics. *CrystEngComm* **2016**, *18*, 7212–7216.
- (41) Kipgen, L.; Bernien, M.; Nickel, F.; Naggert, H.; Britton, A. J.; Arruda, L. M.; Schierle, E.; Weschke, E.; Tuzcek, F.; Kuch, W. Soft-x-Ray-Induced Spin-State Switching of an Adsorbed Fe(II) Spin-Crossover Complex. *J. Phys.: Condens. Matter* **2017**, *29*, 394003.
- (42) Stöhr, J.; Outka, D. A. Determination of Molecular Orientations on Surfaces from the Angular Dependence of Near-Edge x-Ray-Absorption Fine-Structure Spectra. *Phys. Rev. B: Condens. Matter Mater. Phys.* **1987**, *36*, 7891–7905.
- (43) Hermann, K.; Pettersson, L. G. M.; Casida, M. E.; Daul, C.; Goursot, A.; Koester, A.; Proynov, E.; St-Amant, A.; Salahub, D. R. *StoBe-DeMon*, version 3.3; Fritz-Haber-Institut: Berlin, 2014.
- (44) Püttner, R.; Schmidt-Weber, P.; Kampen, T.; Kolczewski, C.; Hermann, K.; Horn, K. Identification of Isomers in the Gas Phase and as Adsorbates by Near-Edge X-Ray Absorption Fine Structure Spectroscopy: Cis- and Trans-Stilbene. *J. Electron Spectrosc. Relat. Phenom.* **2017**, *215*, 16–21.
- (45) Würthner, F. Dipole–Dipole Interaction Driven Self-Assembly of Merocyanine Dyes: From Dimers to Nanoscale Objects and Supramolecular Materials. *Acc. Chem. Res.* **2016**, *49*, 868–876.



**Supporting Information:**

**Highly Efficient and Bidirectional Photochromism  
of Spirooxazine on Au(111)**

Fabian Nickel, Matthias Bernien, Dennis Krüger, Jorge Miguel, Andrew J.  
Britton, Lucas M. Arruda, Lalminthang Kipgen, and Wolfgang Kuch\*

*Institut für Experimentalphysik, Freie Universität Berlin, Arnimallee 14, 14195 Berlin,  
Germany*

E-mail: kuch@physik.fu-berlin.de

# 1 Details of the DFT simulations

Similar to the XA measurements, the DFT simulations were carried out in the same way as already successfully applied in reference S1. Hence, the derived XA spectra for the free molecules can be compared between the spironaphthopyran from reference S1, spironaphthoxazine in this article, and the experimental XA data. To shortly sum up the configuration used for the DFT calculations: The StoBe code package<sup>S2</sup> has been used for simulation of nitrogen *K* edge XA spectra. This package works on a DFT basis and has been applied to a huge variety of molecules.<sup>S3-S6</sup> Consistency to references S1 and S6 is obtained by using the same two-step geometry optimization. In the final optimization step, a gradient-corrected RPBE (revised Perdew-Burke-Ernzerhof) exchange correlation functional is used.<sup>S7,S8</sup> The calculations were performed using a slightly modified TZVP basis set,<sup>S9</sup> where one *d* function is added for the contained chemical elements. The Slater transition-state (TS) method<sup>S10,S11</sup> is applied in the very same way as for the references given above. To obtain a final comparison to the experimental spectra, the spectra were shifted by 2.0 eV to lower energies. A broadening by gaussians was applied with a full width at half maximum (FWHM) of 0.7 eV for transitions below the ionization potential (IP), linearly increasing the FWHM up to 4.5 eV at 10 eV above the IP, and a constant FWHM of 4.5 eV above.

To map simulated resonances to orbitals, the strongest three  $\pi^*$  resonances for both isomers in the Slater TS method are visualized in Figure S1. All the most visible peaks seen in Figure 2 of the article originate from these resonances. The exact energies, center of excitations, and oscillator strengths are given in Tables S1 and S2.

**Table S1: Energies for SNO nitrogen *K* edge x-ray excitations.**

Energy (eV)	Center of Excitation	Orbital	Relative Strength	Figure
398.1	oxazine nitrogen	LUMO	12.8	S1 (a)
399.6	oxazine nitrogen	LUMO +1	3.8	S1 (b)
401.2	oxazine nitrogen	LUMO +6	2.4	S1 (c)

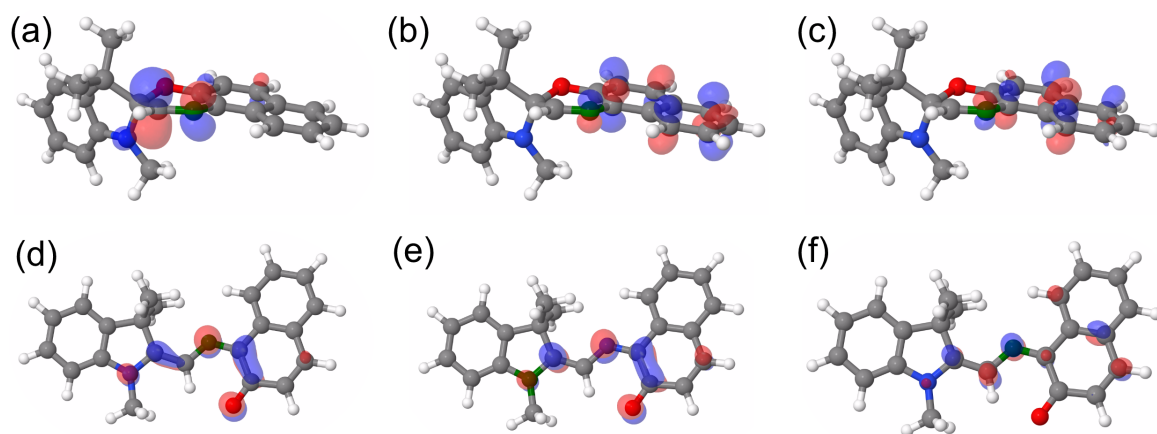


Figure S1: Orbitals of the three strongest  $\pi^*$  excitations as simulated by means of the StoBe code in the TS method. The center of excitation is marked in green. Table S1 and S2 list the values for each excitation.

**Table S2: Energies for MC nitrogen *K* edge x-ray excitations.**

Energy (eV)	Center of Excitation	Orbital	Relative Strength	Figure
397.1	imine nitrogen	LUMO	9.5	S1 (d)
399.5	indoline nitrogen	LUMO	2.7	S1 (e)
400.9	imine nitrogen	LUMO +8	6.1	S1 (f)

## 2 Details of the DRS Measurements

The DRS has been recorded in a new home-built experimental setup in a near-normal incidence configuration. Details of the setup, which is focused on the kinetics of photochromic processes on surfaces, are published in reference S12.

In contrast to other DRS setups, a monochromatic light-beam is used. By detecting the reflection with photomultipliers (PMTs), the sensitivity is maximized and therefore the total light-exposure to the sample is minimized, avoiding switching by the measurement beam. This leads to highly accurate measurements close to the shot-noise limit. To account for instabilities and certain drifts of the optical setup and light sources, a reference beam is integrated in the optical path. A fused silica glass splits about 4% of the light to the reference PMT. A very stable PID-control of the temperature is possible between 100 and 460 K to gain insights of temperature-dependent switching kinetics.

The optical setup consists of a dual-lamp with a deuterium and halogen source. For monochromization a MSHD-300 double-monochromator is used with 1200 l/mm gratings and a blaze wavelength of 300 nm to reach high intensity also in the UV region. The slits were set to 1 mm for a theoretical bandwidth of 1.35 nm. The optical path for focusing the beam to the sample consists of mirrors only, to avoid chromatic aberration. Evaporation on an atomically flat and clean single crystal takes place in the measurement position. At a short distance of about 62 mm, six CF16 vacuum windows are present to measure and illuminate the sample. The angle between the innermost windows, as used for near-normal incidence DRS, and the surface normal is  $11.5^\circ$ . In our measurements, a spot size of  $3 \times 7 \text{ mm}^2$  is set up and for fast acquisition time, spectra are acquired with a step-width of 1 nm and an integration time of 1000 ms per point. Further details can be found in reference S12. To correct for drifts in the data, originating from gain drifts of the PMTs, a procedure as described and analyzed in reference S12 has been applied. A gain factor is calculated and multiplied to the whole spectrum: The reflectance at a wavelength of 720 nm is divided through the intensity for the corresponding background spectrum at the same wavelength,

providing a gain drift factor. However, remaining drifts in spectra were found in the range of 0.001, which is sufficiently small compared to the signal.

Two LEDs are mounted with the possibility to illuminate the sample in the measurement position: A UV LED with a wavelength of 365 nm and a red LED with a wavelength of 625 nm. Both LEDs exhibit an illumination spot size of about  $9 \times 9 \text{ mm}^2$  at the sample, larger than the DRS measurement spot. The photon flux densities, as measured by a Thorlabs S302C thermal power sensor, are  $\phi_{\text{UV LED}} = 2.8(5) \times 10^{15} \text{ photons s}^{-1} \text{ mm}^{-2}$  and  $\phi_{\text{red LED}} = 8(1) \times 10^{15} \text{ photons s}^{-1} \text{ mm}^{-2}$ .

To measure time-dependent illumination series, a stepwise measurement needs to be applied, since the LEDs and PMTs can not operate simultaneously. In addition, drifts of the PMTs and lamp might also have an impact on the measurement data quality, so that a reference has to be introduced. Therefore we define as a measure of switched molecules the asymmetry as:<sup>S12</sup>

$$\text{asym}(\lambda_1, \lambda_2) = \frac{R(\lambda_1) - R(\lambda_2)}{R(\lambda_1) + R(\lambda_2)} \quad (1)$$

This leads to a good measure for the fraction of SNO or MC molecules, when taking one reflectance on a peak position (minimum in the DRS) and one on a more or less constant position in the spectrum, using the latter as a reference point. For the presented asymmetry recordings, the reference beam has not been taken into account.

### 3 Red-light illumination at 130 K

Also investigations at other temperatures were carried out, since the DRS setup is capable of variation of the temperature between 100 and 460 K. Activation energies in the energy landscapes have been observed, e.g., for the SP-to-MC switching process by UV-light of a spironaphthopyran on a Bi(111) surface.<sup>S1</sup> To see if the red-light-induced conversion from MC to SNO still takes place at lower temperatures, we illuminated with red light at a temperature of 130 K. Figure S2 shows the DRS asymmetry of the 620 and 720 nm intensity as a function

of time (■ symbols, with red line as single-exponential fit). The temperature stability of the MC isomer is shown in the same plot by data for an increased temperature of 165 K without illumination (grey circles, corrected for a small temperature-dependent constant offset to match the data at 130 K). It is obvious that the red-light-induced switching is slower than at

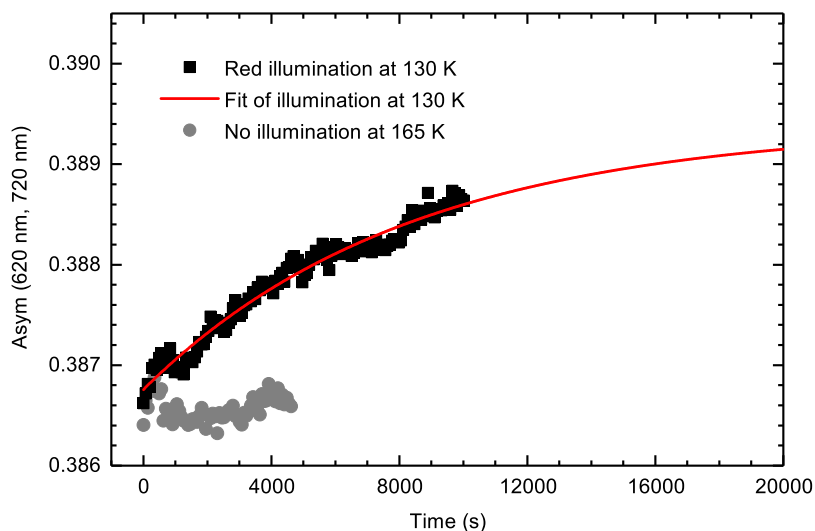


Figure S2: Red-light illumination ( $\lambda = 625$  nm) of a MC isomerized sample (switched before at a temperature of 200 K) at a temperature of 130 K (■ symbols) with a single-exponential fit (red line). In grey circles, the stability at a temperature of 165 K is shown.

200 K. The time constant for this switching at 130 K is 8300(800) s. This corresponds to an effective cross-section of  $1.4 \times 10^{-22}$  cm<sup>2</sup>, about a factor of 8 smaller than at a temperature of 200 K. The photoisomerization of SNO and MC is known to be temperature-dependent. In addition to the ring closure, also *trans-cis* isomerizations takes place. The barriers for these processes induce a temperature dependence on the switching and therefore a reduced speed at lower temperatures is expected.

## 4 Relaxation by temperature

Information about the thermal stability of the MC isomer can be gathered by measuring the thermal relaxation as, e.g., performed for a spin-crossover relaxation in reference S13.

Using an Arrhenius model and assuming a barrier  $E_a$  leads to a relaxation rate of  $k(T) = A \cdot e^{-E_a/(RT)}$ , with  $A$  being a preexponential factor and  $R$  the gas constant. When ramping the temperature, the time-dependent fraction of MC molecules can be fitted by:<sup>S13</sup>

$$\gamma_{\text{MC}}(t) = e^{-A \int_0^t e^{-E_a/(RT(t))} dt} . \quad (2)$$

To evaluate the former equation, continuous measurements of the asymmetry as a function of time were performed by using a constant temperature ramp of 1 K/min. The corresponding data is shown in Figure S3 (a). Before fitting equation (2), the data has been corrected for a small linear drift (as can be seen for the first and last 20 K on the x-axis), presumably originating from a temperature dependence of the reflectance. Afterwards, the data can be fitted very well as shown in panel (b). The fit leads to values of  $E_A = 44(1)$  kJ mol<sup>-1</sup> and  $A = 9(2) \times 10^5$  s<sup>-1</sup>. These values are close to those of the same molecule on a Bi(111) surface measured by DRS by a different method.<sup>S12</sup>

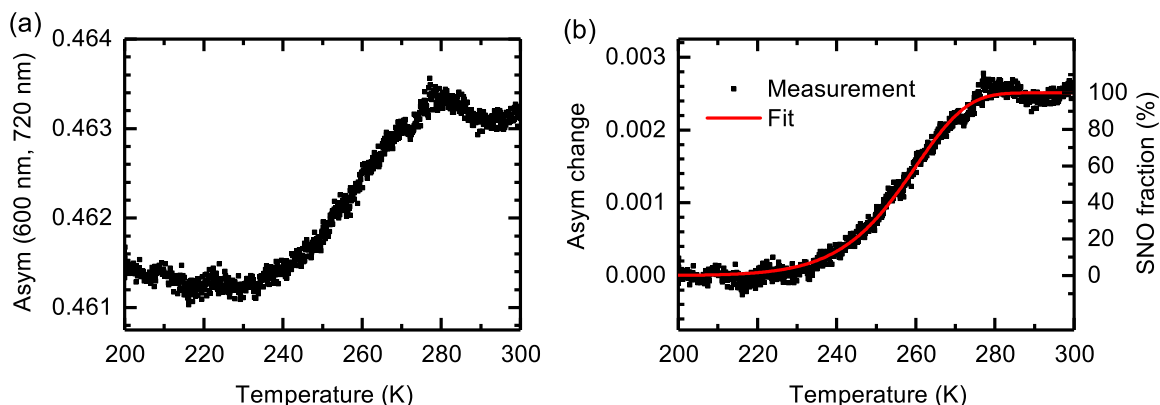


Figure S3: (a) Temperature-dependent measurement of the asymmetry between the 600 and 720 nm reflectance. (b) Drift-corrected data with fit according to an Arrhenius model.

After the heating series as shown in Figure S3, the sample was further warmed up to 330 K to compare with the reversed thermal stability as reported in reference S6. There, nitro-BIPS was fully switching to MC at a temperature of 330 K. Figure S4 shows the DRS of the MC at 200 K (black line) and after heating to 330 K (red line). A clear thermal

switching back to the SNO isomer takes place.

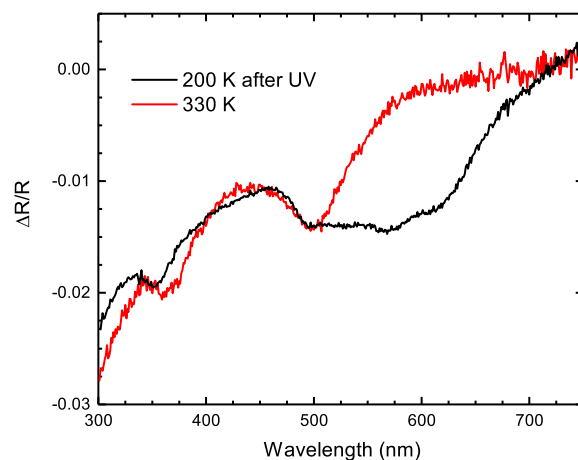


Figure S4: DRS of SNO on Au(111) after UV at 200 K and after the heating series as shown in Figure S3, measured at 330 K.

The spectrum at 330 K had to be scaled up by a factor of 2.2 since the molecules already started desorbing from the surface at this temperature. Differences of the 330-K SNO spectrum to the one at 200 K (*cf.* Figure 3 of the article) could occur from a temperature dependence of the organic-inorganic system, e.g., a rearrangement.

## References

- (S1) Nickel, F.; Bernien, M.; Kraffert, K.; Krüger, D.; Arruda, L. M.; Kipgen, L.; Kuch, W. Reversible Switching of Spiropyran Molecules in Direct Contact With a Bi(111) Single Crystal Surface. *Adv. Funct. Mater.* **2017**, *27*, 1702280.
- (S2) Hermann, K.; Pettersson, L. G. M.; Casida, M.; Daul, C.; Goursot, A.; Koester, A.; Proynov, E.; St-Amant, A.; Salahub, D. R. StoBe-deMon, Version 3.3. 2014.
- (S3) Guo, C. S.; Sun, L.; Hermann, K.; Hermanns, C. F.; Bernien, M.; Kuch, W. X-Ray Absorption from Large Molecules at Metal Surfaces: Theoretical and Experimental Results for Co-OEP on Ni(100). *J. Chem. Phys.* **2012**, *137*, 194703.



- (S4) Nickel, F.; Bernien, M.; Herder, M.; Wrzalek, S.; Chittas, P.; Kraffert, K.; Arruda, L. M.; Kipgen, L.; Krüger, D.; Hecht, S.; Kuch, W. Light-Induced Photoisomerization of a Diarylethene Molecular Switch on Solid Surfaces. *J. Phys.: Condens. Matter* **2017**, *29*, 374001.
- (S5) Piantek, M.; Miguel, J.; Krüger, A.; Navío, C.; Bernien, M.; Ball, D. K.; Hermann, K.; Kuch, W. Temperature, Surface, and Coverage-Induced Conformational Changes of Azobenzene Derivatives on Cu(001). *J. Phys. Chem. C* **2009**, *113*, 20307–20315.
- (S6) Piantek, M.; Schulze, G.; Koch, M.; Franke, K. J.; Leyssner, F.; Krüger, A.; Navío, C.; Miguel, J.; Bernien, M.; Wolf, M.; Kuch, W.; Tegeder, P.; Pascual, J. I. Reversing the Thermal Stability of a Molecular Switch on a Gold Surface: Ring-Opening Reaction of Nitrospiropyran. *J. Am. Chem. Soc.* **2009**, *131*, 12729–12735.
- (S7) Hammer, B.; Hansen, L. B.; Nørskov, J. K. Improved Adsorption Energetics within Density-Functional Theory Using Revised Perdew-Burke-Ernzerhof Functionals. *Phys. Rev. B* **1999**, *59*, 7413–7421.
- (S8) Perdew, J. P.; Burke, K.; Ernzerhof, M. Generalized Gradient Approximation Made Simple. *Phys. Rev. Lett.* **1996**, *77*, 3865–3868.
- (S9) Godbout, N.; Salahub, D. R.; Andzelm, J.; Wimmer, E. Optimization of Gaussian-Type Basis Sets for Local Spin Density Functional Calculations. Part I. Boron through Neon, Optimization Technique and Validation. *Can. J. Chem.* **1992**, *70*, 560–571.
- (S10) Slater, J. C.; Johnson, K. H. Self-Consistent-Field  $X\alpha$  Cluster Method for Polyatomic Molecules and Solids. *Phys. Rev. B* **1972**, *5*, 844–853.
- (S11) Slater, J. C. In *Statistical Exchange-Correlation in the Self-Consistent Field*; Löwdin, P.-O., Ed.; Academic Press, 1972; Vol. 6.

- (S12) Nickel, F.; Bernien, M.; Lipowski, U.; Kuch, W. Optical Differential Reflectance Spectroscopy for Photochromic Molecules on Solid Surfaces. *Rev. Sci. Instr.* **2018**, *89*, in press, <https://doi.org/10.1063/1.5019415> .
- (S13) Bernien, M.; Naggert, H.; Arruda, L. M.; Kipgen, L.; Nickel, F.; Miguel, J.; Hermanns, C. F.; Krüger, A.; Krüger, D.; Schierle, E.; Weschke, E.; Tuczek, F.; Kuch, W. Highly Efficient Thermal and Light-Induced Spin-State Switching of an Fe(II) Complex in Direct Contact with a Solid Surface. *ACS Nano* **2015**, *9*, 8960–8966.

# Bibliography

---

- [FN 1] F. Nickel, M. Bernien, M. Herder, S. Wrzalek, P. Chittas, K. Kraffert, L. M. Arruda, L. Kipgen, D. Krüger, S. Hecht, and W. Kuch: *Light-Induced Photoisomerization of a Diarylethene Molecular Switch on Solid Surfaces*. J. Phys.: Condens. Matter **29**, 374001 (2017), DOI: 10.1088/1361-648X/aa7c57.
- [FN 2] F. Nickel, M. Bernien, K. Kraffert, D. Krüger, L. M. Arruda, L. Kipgen, and W. Kuch: *Reversible Switching of Spiropyran Molecules in Direct Contact With a Bi(111) Single Crystal Surface*. Adv. Funct. Mater. **27**, 1702280 (2017), DOI: 10.1002/adfm.201702280.
- [FN 3] F. Nickel, M. Bernien, U. Lipowski, and W. Kuch: *Optical Differential Reflectance Spectroscopy for Photochromic Molecules on Solid Surfaces*. Rev. Sci. Instr. **89**, 033113 (2018), DOI: 10.1063/1.5019415.
- [FN 4] F. Nickel, M. Bernien, D. Krüger, J. Miguel, A. J. Britton, L. M. Arruda, L. Kipgen, and W. Kuch: *Highly Efficient and Bidirectional Photochromism of Spirooxazine on Au(111)*. J. Phys. Chem. C **122**, 8031 (2018), DOI: 10.1021/acs.jpcc.8b02220.
- [1] K. E. Drexler: *Engines of Creation: The Coming Era of Nanotechnology*. New York: Anchor (1987).
- [2] K. E. Drexler: “*There’s Plenty of Room at the Bottom*”, Richard Feynman, Pasadena, 29 December 1959, URL: <http://metamodern.com/2009/12/29/theres-plenty-of-room-at-the-bottom%E2%80%9Dfeynman-1959/>, Accessed: 2018/1/22.
- [3] S. Anthony: *IBM Unveils World’s First 5nm Chip*, Built with a new type of gate-all-around transistor, plus extreme ultraviolet lithography., URL: <https://arstechnica.com/gadgets/2017/06/ibm-5nm-chip/>, Accessed: 2018/1/22.
- [4] *The Nobel Prize in Chemistry 2016*, Nobel Media AB 2014, URL: [https://www.nobelprize.org/nobel\\_prizes/chemistry/laureates/2016/](https://www.nobelprize.org/nobel_prizes/chemistry/laureates/2016/), Accessed: 2018/1/21.
- [5] R. Eelkema, M. M. Pollard, J. Vicario, N. Katsonis, B. S. Ramon, C. W. M. Bastiaansen, D. J. Broer, and B. L. Feringa: *Molecular Machines: Nanomotor Rotates Microscale Objects*. Nature **440**, 163 (2006), DOI: 10.1038/440163a.

- [6] T. Kudernac, N. Ruangsapapichat, M. Parschau, B. Maciá, N. Katsonis, S. R. Harutyunyan, K.-H. Ernst, and B. L. Feringa: *Electrically Driven Directional Motion of a Four-Wheeled Molecule on a Metal Surface*. Nature **479**, 208 (2011), DOI: 10.1038/nature10587.
- [7] J. V. Barth, G. Costantini, and K. Kern: *Engineering Atomic and Molecular Nanostructures at Surfaces*. Nature **437**, 671 (2005), DOI: 10.1038/nature04166.
- [8] J. E. Green, J. Wook Choi, A. Boukai, Y. Bunimovich, E. Johnston-Halperin, E. Delonno, Y. Luo, B. A. Sheriff, K. Xu, Y. Shik Shin, H.-R. Tseng, J. F. Stoddart, and J. R. Heath: *A 160-Kilobit Molecular Electronic Memory Patterned at 1011 Bits per Square Centimetre*. Nature **445**, 414 (2007), DOI: 10.1038/nature05462.
- [9] M. Karimi, P. Sahandi Zangabad, S. Baghaee-Ravari, M. Ghazadeh, H. Mirshekari, and M. R. Hamblin: *Smart Nanostructures for Cargo Delivery: Uncaging and Activating by Light*. J. Am. Chem. Soc. **139**, 4584 (2017), DOI: 10.1021/jacs.6b08313.
- [10] R. S. Liu and A. E. Asato: *The Primary Process of Vision and the Structure of Bathorhodopsin: A Mechanism for Photoisomerization of Polyenes*. PNAS **82**, 259 (1985).
- [11] K. Palczewski, T. Kumasaka, T. Hori, C. A. Behnke, H. Motoshima, B. A. Fox, I. L. Trong, D. C. Teller, T. Okada, R. E. Stenkamp, M. Yamamoto, and M. Miyano: *Crystal Structure of Rhodopsin: A G Protein-Coupled Receptor*. Science **289**, 739 (2000), DOI: 10.1126/science.289.5480.739.
- [12] B. Osterby, R. D. McKelvey, and L. Hill: *Photochromic Sunglasses: A Patent-Based Advanced Organic Synthesis Project and Demonstration*. J. Chem. Educ. **68**, 424 (1991), DOI: 10.1021/ed068p424.
- [13] A. Aviram and M. A. Ratner: *Molecular Rectifiers*. Chem. Phys. Lett. **29**, 277 (1974), DOI: 10.1016/0009-2614(74)85031-1.
- [14] M. Irie: *Photochromism: Memories and Switches - Introduction*. Chem. Rev. **100**, 1683 (2000), DOI: 10.1021/cr980068l.
- [15] M. E. Gemayel, K. Börjesson, M. Herder, D. T. Duong, J. A. Hutchison, C. Ruzié, G. Schweicher, A. Salleo, Y. Geerts, S. Hecht, E. Orgiu, and P. Samorì: *Optically Switchable Transistors by Simple Incorporation of Photochromic Systems into Small-Molecule Semiconducting Matrices*. Nat. Commun. **6**, 6330 (2015), DOI: 10.1038/ncomms7330.

- [16] T. Leydecker, M. Herder, E. Pavlica, G. Bratina, S. Hecht, E. Orgiu, and P. Samorì: *Flexible Non-Volatile Optical Memory Thin-Film Transistor Device with over 256 Distinct Levels Based on an Organic Bicomponent Blend*. Nat. Nanotechnol. **11**, 769 (2016), DOI: 10.1038/nnano.2016.87.
- [17] F. Meng, Y.-M. Hervault, Q. Shao, B. Hu, L. Norel, S. Rigaut, and X. Chen: *Orthogonally Modulated Molecular Transport Junctions for Resettable Electronic Logic Gates*. Nat. Commun. **5**, 3023 (2014), DOI: 10.1038/ncomms4023.
- [18] T. Hugel, N. B. Holland, A. Cattani, L. Moroder, M. Seitz, and H. E. Gaub: *Single-Molecule Optomechanical Cycle*. Science **296**, 1103 (2002), DOI: 10.1126/science.1069856.
- [19] M. Elbahri, A. U. Zillohu, B. Gothe, M. K. Hedayati, R. Abdelaziz, H. J. El-Khozondar, M. Bawa'aneh, M. Abdelaziz, A. Lavrinenko, S. Zhukovsky, and S. Homaeigohar: *Photoswitchable Molecular Dipole Antennas with Tailored Coherent Coupling in Glassy Composite*. Light Sci. Appl. **4**, e316 (2015), DOI: 10.1038/lsa.2015.89.
- [20] M. R. Banghart, A. Mourot, D. L. Fortin, J. Z. Yao, R. H. Kramer, and D. Trauner: *Photochromic Blockers of Voltage-Gated Potassium Channels*. Angew. Chem. Int. Ed. **48**, 9097 (2009), DOI: 10.1002/anie.200904504.
- [21] A. H. Flood, J. F. Stoddart, D. W. Steuerman, and J. R. Heath: *Whence Molecular Electronics?* Science **306**, 2055 (2004), DOI: 10.1126/science.1106195.
- [22] M. del Valle, R. Gutiérrez, C. Tejedor, and G. Cuniberti: *Tuning the Conductance of a Molecular Switch*. Nat. Nanotechnol. **2**, 176 (2007), DOI: 10.1038/nnano.2007.38.
- [23] T. Ikeda and O. Tsutsumi: *Optical Switching and Image Storage by Means of Azobenzene Liquid-Crystal Films*. Science **268**, 1873 (1995), DOI: 10.1126/science.268.5219.1873.
- [24] Z. F. Liu, K. Hashimoto, and A. Fujishima: *Photoelectrochemical Information Storage Using an Azobenzene Derivative*. Nature **347**, 658 (1990), DOI: 10.1038/347658a0.
- [25] G. Ragazzon, M. Baroncini, S. Silvi, M. Venturi, and A. Credi: *Light-Powered Autonomous and Directional Molecular Motion of a Dissipative Self-Assembling System*. Nat. Nanotechnol. **10**, 70 (2015), DOI: 10.1038/nnano.2014.260.

- [26] D. A. Davis, A. Hamilton, J. Yang, L. D. Cremer, D. Van Gough, S. L. Pottisek, M. T. Ong, P. V. Braun, T. J. Martínez, S. R. White, J. S. Moore, and N. R. Sottos: *Force-Induced Activation of Covalent Bonds in Mechanoreponsive Polymeric Materials*. *Nature* **459**, 68 (2009), DOI: 10.1038/nature07970.
- [27] I. Cabrera, F. Shvartsman, O. Veinberg, and V. Krongauz: *Photocontraction of Liquid Spiropyran-Merocyanine Films*. *Science* **226**, 341 (1984), DOI: 10.1126/science.226.4672.341.
- [28] D. Duli, S. J. van der Molen, T. Kudernac, H. T. Jonkman, J. J. D. de Jong, T. N. Bowden, J. van Esch, B. L. Feringa, and B. J. van Wees: *One-Way Optoelectronic Switching of Photochromic Molecules on Gold*. *Phys. Rev. Lett.* **91**, 207402 (2003), DOI: 10.1103/PhysRevLett.91.207402.
- [29] N. Katsonis, T. Kudernac, M. Walko, S. J. van der Molen, B. J. van Wees, and B. L. Feringa: *Reversible Conductance Switching of Single Diarylethenes on a Gold Surface*. *Adv. Mater.* **18**, 1397 (2006), DOI: 10.1002/adma.200600210.
- [30] Y. Kim, T. J. Hellmuth, D. Sysoiev, F. Pauly, T. Pietsch, J. Wolf, A. Erbe, T. Huhn, U. Groth, U. E. Steiner, and E. Scheer: *Charge Transport Characteristics of Diarylethene Photoswitching Single-Molecule Junctions*. *Nano Lett.* **12**, 3736 (2012), DOI: 10.1021/nl3015523.
- [31] Straight S. D., Liddell P. A., Terazono Y., Moore T. A., Moore A. L., and Gust D.: *All-Photonic Molecular XOR and NOR Logic Gates Based on Photochemical Control of Fluorescence in a Fulgimide-Porphyrin-Dithienylethene Triad*. *Adv. Funct. Mater.* **17**, 777 (2007), DOI: 10.1002/adfm.200600802.
- [32] W. R. Browne, T. Kudernac, N. Katsonis, J. Areephong, J. Hjelm, and B. L. Feringa: *Electro- and Photochemical Switching of Dithienylethene Self-Assembled Monolayers on Gold Electrodes*. *J. Phys. Chem. C* **112**, 1183 (2008), DOI: 10.1021/jp0766508.
- [33] K. Smaali, S. Lenfant, S. Karpe, M. Oçafrain, P. Blanchard, D. Deresmes, S. Godey, A. Rochefort, J. Roncali, and D. Vuillaume: *High OnOff Conductance Switching Ratio in Optically-Driven Self-Assembled Conjugated Molecular Systems*. *ACS Nano* **4**, 2411 (2010), DOI: 10.1021/nn100295x.
- [34] O. Ivashenko, J. T. van Herpt, B. L. Feringa, P. Rudolf, and W. R. Browne: *UV/Vis and NIR Light-Responsive Spiropyran Self-Assembled Monolayers*. *Langmuir* **29**, 4290 (2013), DOI: 10.1021/la400192c.

- [35] T. Moldt, D. Brete, D. Przyrembel, S. Das, J. R. Goldman, P. K. Kundu, C. Gahl, R. Klajn, and M. Weinelt: *Tailoring the Properties of Surface-Immobilized Azobenzenes by Monolayer Dilution and Surface Curvature*. *Langmuir* **31**, 1048 (2015), DOI: 10.1021/la504291n.
- [36] M. Schulze, M. Utecht, A. Hebert, K. Rück-Braun, P. Saalfrank, and P. Tegeder: *Reversible Photoswitching of the Interfacial Nonlinear Optical Response*. *J. Phys. Chem. Lett.* **6**, 505 (2015), DOI: 10.1021/jz502477m.
- [37] T. Mosciatti, M. G. del Rosso, M. Herder, J. Frisch, N. Koch, S. Hecht, E. Orgiu, and P. Samorì: *Light-Modulation of the Charge Injection in a Polymer Thin-Film Transistor by Functionalizing the Electrodes with Bistable Photochromic Self-Assembled Monolayers*. *Adv. Mater.* **28**, 6606 (2016), DOI: 10.1002/adma.201600651.
- [38] T. Garling, Y. Tong, T. A. Darwish, M. Wolf, and R. K. Campen: *The Influence of Surface Potential on the Optical Switching of Spiropyran Self Assembled Monolayers*. *J. Phys.: Condens. Matter* **29**, 414002 (2017), DOI: 10.1088/1361-648X/aa8118.
- [39] M. Karcher, C. Rüdte, C. Elsässer, and P. Fumagalli: *Switching of Non-functionalized Spiropyran Thin Films on Single Crystalline MgO(100)*. *J. Appl. Phys.* **102**, 084904 (2007), DOI: 10.1063/1.2799090.
- [40] G. Schulze, K. J. Franke, and J. I. Pascual: *Induction of a Photostationary Ring-Opening–Ring-Closing State of Spiropyran Monolayers on the Semimetallic Bi(110) Surface*. *Phys. Rev. Lett.* **109**, 026102 (2012), DOI: 10.1103/PhysRevLett.109.026102.
- [41] M. Piantek, G. Schulze, M. Koch, K. J. Franke, F. Leyssner, A. Krüger, C. Navío, J. Miguel, M. Bernien, M. Wolf, W. Kuch, P. Tegeder, and J. I. Pascual: *Reversing the Thermal Stability of a Molecular Switch on a Gold Surface: Ring-Opening Reaction of Nitrospiropyran*. *J. Am. Chem. Soc.* **131**, 12729 (2009), DOI: 10.1021/ja901238p.
- [42] E. R. McNellis, C. Bronner, J. Meyer, M. Weinelt, P. Tegeder, and K. Reuter: *Azobenzene versus 3,3,5,5-Tetra-Tert-Butyl-Azobenzene (TBA) at Au(111): Characterizing the Role of Spacer Groups*. *Phys. Chem. Chem. Phys.* **12**, 6404 (2010), DOI: 10.1039/C001978J.
- [43] M. Piantek, J. Miguel, M. Bernien, C. Navío, A. Krüger, B. Priewisch, K. Rück-Braun, and W. Kuch: *Adsorption of Carboxymethylester-Azobenzene on Copper and Gold Single Crystal Surfaces*. *Appl. Phys. A* **93**, 261 (2008), DOI: 10.1007/s00339-008-4825-3.



- [44] M. Piantek, J. Miguel, A. Krüger, C. Navío, M. Bernien, D. K. Ball, K. Hermann, and W. Kuch: *Temperature, Surface, and Coverage-Induced Conformational Changes of Azobenzene Derivatives on Cu(001)*. J. Phys. Chem. C **113**, 20307 (2009), DOI: 10.1021/jp907641f.
- [45] F. Leyssner, S. Hagen, L. Óvári, J. Doki, P. Saalfrank, M. V. Peters, S. Hecht, T. Klamroth, and P. Tegeder: *Photoisomerization Ability of Molecular Switches Adsorbed on Au(111): Comparison between Azobenzene and Stilbene Derivatives*. J. Phys. Chem. C **114**, 1231 (2010), DOI: 10.1021/jp909684x.
- [46] M. Bazarnik, J. Henzl, R. Czajka, and K. Morgenstern: *Light Driven Reactions of Single Physisorbed Azobenzenes*. Chem. Commun. **47**, 7764 (2011), DOI: 10.1039/C1CC11578B.
- [47] C. Bronner, M. Schulze, S. Hagen, and P. Tegeder: *The Influence of the Electronic Structure of Adsorbate–substrate Complexes on Photoisomerization Ability*. New J. Phys. **14**, 043023 (2012), DOI: 10.1088/1367-2630/14/4/043023.
- [48] C. Bronner, B. Priewisch, K. Rück-Braun, and P. Tegeder: *Photoisomerization of an Azobenzene on the Bi(111) Surface*. J. Phys. Chem. C **117**, 27031 (2013), DOI: 10.1021/jp4106663.
- [49] C. Bronner and P. Tegeder: *Photo-Induced and Thermal Reactions in Thin Films of an Azobenzene Derivative on Bi(111)*. New J. Phys. **16**, 053004 (2014), DOI: 10.1088/1367-2630/16/5/053004.
- [50] M. Piantek: *Switchable Molecules on Metallic Surfaces Studied by Core-Level Spectroscopies*. PhD thesis. Freie Universität Berlin, Germany (2010).
- [51] F. Leyßner: *Analysis of Functional Organic Molecules at Noble Metal Surfaces by Means of Vibrational Spectroscopies*. PhD thesis. Freie Universität Berlin, Germany (2011).
- [52] A. Krüger: *Schaltbare Moleküle auf metallischen und nichtmetallischen Oberflächen*. PhD thesis. Freie Universität Berlin, Germany (2015).
- [53] A. Krüger, M. Bernien, C. F. Hermanns, and W. Kuch: *X-Ray-Induced Reversible Switching of an Azobenzene Derivative Adsorbed on Bi(111)*. J. Phys. Chem. C **118**, 12916 (2014), DOI: 10.1021/jp5029118.
- [54] L. Kipgen, M. Bernien, F. Nickel, H. Naggert, A. J. Britton, L. M. Arruda, E. Schierle, E. Weschke, F. Tuczek, and W. Kuch: *Soft-x-Ray-Induced Spin-State Switching of an Adsorbed Fe(II) Spin-Crossover Complex*. J. Phys.: Condens. Matter **29**, 394003 (2017), DOI: 10.1088/1361-648X/aa7e52.



- [55] S. M. Mendoza, M. Lubomska, M. Walko, B. L. Feringa, and P. Rudolf: *Characterization by X-Ray Photoemission Spectroscopy of the Open and Closed Forms of a Dithienylethene Switch in Thin Films*. J. Phys. Chem. C **111**, 16533 (2007), DOI: 10.1021/jp0751662.
- [56] R. Püttner, P. Schmidt-Weber, T. Kampen, C. Kolczewski, K. Hermann, and K. Horn: *Identification of Isomers in the Gas Phase and as Adsorbates by Near-Edge X-Ray Absorption Fine Structure Spectroscopy: Cis- and Trans-Stilbene*. J. Electron. Spectrosc. Relat. Phenom. **215**, 16 (2017), DOI: 10.1016/j.elspec.2016.11.014.
- [57] R. E. Hummel: *Differential Reflectometry and Its Application to the Study of Alloys, Ordering, Corrosion, and Surface Properties*. phys. stat. sol. (a) **76**, 11 (1983), DOI: 10.1002/pssa.2210760102.
- [58] D. E. Aspnes and A. A. Studna: *Anisotropies in the Above-Band-Gap Optical Spectra of Cubic Semiconductors*. Phys. Rev. Lett. **54**, 1956 (1985), DOI: 10.1103/PhysRevLett.54.1956.
- [59] H. Proehl, T. Dienel, R. Nitsche, and T. Fritz: *Formation of Solid-State Excitons in Ultrathin Crystalline Films of PTCDA: From Single Molecules to Molecular Stacks*. Phys. Rev. Lett. **93**, 097403 (2004), DOI: 10.1103/PhysRevLett.93.097403.
- [60] T. Dienel, C. Loppacher, S. C. B. Mannsfeld, R. Forker, and T. Fritz: *Growth-Mode-Induced Narrowing of Optical Spectra of an Organic Adlayer*. Adv. Mater. **20**, 959 (2008), DOI: 10.1002/adma.200701684.
- [61] T. Dienel, A. Krause, R. Alle, R. Forker, K. Meerholz, and T. Fritz: *Alkali Metal Doped Organic Molecules on Insulators: Charge Impact on the Optical Properties*. Adv. Mater. **22**, 4064 (2010), DOI: 10.1002/adma.201000891.
- [62] A. Baby, M. Gruenewald, C. Zwick, F. Otto, R. Forker, G. van Straaten, M. Franke, B. Stadtmüller, C. Kumpf, G. P. Brivio, G. Fratesi, T. Fritz, and E. Zojer: *Fully Atomistic Understanding of the Electronic and Optical Properties of a Prototypical Doped Charge-Transfer Interface*. ACS Nano **11**, 10495 (2017), DOI: 10.1021/acsnano.7b05828.
- [63] R. Forker, D. Kasemann, T. Dienel, C. Wagner, R. Franke, K. Müllen, and T. Fritz: *Electronic Decoupling of Aromatic Molecules from a Metal by an Atomically Thin Organic Spacer*. Adv. Mater. **20**, 4450 (2008), DOI: 10.1002/adma.200801112.

- [64] T. Moldt, D. Przyrembel, M. Schulze, W. Bronsch, L. Boie, D. Brete, C. Gahl, R. Klajn, P. Tegeder, and M. Weinelt: *Differing Isomerization Kinetics of Azobenzene-Functionalized Self-Assembled Monolayers in Ambient Air and in Vacuum*. *Langmuir* **32**, 10795 (2016), DOI: 10.1021/acs.langmuir.6b01690.
- [65] C. Weber, T. Liebig, M. Gensler, A. Zykov, L. Pithan, J. P. Rabe, S. Hecht, D. Bléger, and S. Kowarik: *Cooperative Switching in Nanofibers of Azobenzene Oligomers*. *Sci. Rep.* **6**, 25605 (2016), DOI: 10.1038/srep25605.
- [66] J. Stöhr: *NEXAFS Spectroscopy*. Berlin Heidelberg New York: Springer-Verlag (1992).
- [67] L. G. Parratt: *Electronic Band Structure of Solids by X-Ray Spectroscopy*. *Rev. Mod. Phys.* **31**, 616 (1959), DOI: 10.1103/RevModPhys.31.616.
- [68] T. G. Gopakumar, M. Bernien, H. Naggert, F. Matino, C. F. Hermanns, A. Bannwarth, S. Mühlenberend, A. Krüger, D. Krüger, F. Nickel, W. Walter, R. Berndt, W. Kuch, and F. Tuczek: *Spin-Crossover Complex on Au(111): Structural and Electronic Differences Between Mono- and Multilayers*. *Chem. Eur. J.* **19**, 15702 (2013), DOI: 10.1002/chem.201302241.
- [69] J. Stöhr and D. A. Outka: *Determination of Molecular Orientations on Surfaces from the Angular Dependence of Near-Edge x-Ray-Absorption Fine-Structure Spectra*. *Phys. Rev. B* **36**, 7891 (1987), DOI: 10.1103/PhysRevB.36.7891.
- [70] K. Hermann, L. G. M. Pettersson, M. Casida, C. Daul, A. Goursot, A. Koester, E. Proynov, A. St-Amant, and D. R. Salahub: *StoBe-deMon, Version 3.3*,
- [71] C. Kolczewski, R. Püttner, O. Plashkevych, H. Ågren, V. Staemmler, M. Martins, G. Snell, A. S. Schlachter, M. Sant'Anna, G. Kaindle, and L. G. M. Pettersson: *Detailed Study of Pyridine at the C1s and N1s Ionization Thresholds: The Influence of the Vibrational Fine Structure*. *J. Chem. Phys.* **115**, 6426 (2001), DOI: 10.1063/1.1397797.
- [72] C. Kolczewski, R. Püttner, M. Martins, A. S. Schlachter, G. Snell, M. M. Sant'Anna, K. Hermann, and G. Kaindle: *Spectroscopic Analysis of Small Organic Molecules: A Comprehensive near-Edge x-Ray-Absorption Fine-Structure Study of C6-Ring-Containing Molecules*. *J. Chem. Phys.* **124**, 034302 (2006), DOI: 10.1063/1.2139674.

- [73] R. Püttner, C. Kolczewski, M. Martins, A. S. Schlachter, G. Snell, M. Sant'Anna, J. Viefhaus, K. Hermann, and G. Kaindl: *The C 1s NEXAFS Spectrum of Benzene below Threshold: Rydberg or Valence Character of the Unoccupied -Type Orbitals*. Chem. Phys. Lett. **393**, 361 (2004), DOI: 10.1016/j.cplett.2004.06.053.
- [74] C. S. Guo, L. Sun, K. Hermann, C. F. Hermanns, M. Bernien, and W. Kuch: *X-Ray Absorption from Large Molecules at Metal Surfaces: Theoretical and Experimental Results for Co-OEP on Ni(100)*. J. Chem. Phys. **137**, 194703 (2012), DOI: 10.1063/1.4765373.
- [75] K. Diller, F. Klappenberger, F. Allegretti, A. C. Papageorgiou, S. Fischer, A. Wiengarten, S. Joshi, K. Seufert, D. Écija, W. Auwärter, and J. V. Barth: *Investigating the Molecule-Substrate Interaction of Prototypic Tetrapyrrole Compounds: Adsorption and Self-Metalation of Porphine on Cu(111)*. J. Chem. Phys. **138**, 154710 (2013), DOI: 10.1063/1.4800771.
- [76] K. Diller, F. Klappenberger, F. Allegretti, A. C. Papageorgiou, S. Fischer, D. A. Duncan, R. J. Maurer, J. A. Lloyd, S. C. Oh, K. Reuter, and J. V. Barth: *Temperature-Dependent Templated Growth of Porphine Thin Films on the (111) Facets of Copper and Silver*. J. Chem. Phys. **141**, 144703 (2014), DOI: 10.1063/1.4896605.
- [77] W. Koch and M. C. Holthausen: *A Chemist's Guide to Density Functional Theory, 2nd Edition*. Weinheim: Wiley-VCH Verlag GmbH (2001).
- [78] P. Hohenberg and W. Kohn: *Inhomogeneous Electron Gas*. Phys. Rev. **136**, B864 (1964), DOI: 10.1103/PhysRev.136.B864.
- [79] J. Kohanoff: *Electronic Structure Calculations for Solids and Molecules: Theory and Computational Methods*. Cambridge: Cambridge University Press (2006).
- [80] J. P. Perdew, K. Burke, and M. Ernzerhof: *Generalized Gradient Approximation Made Simple*. Phys. Rev. Lett. **77**, 3865 (1996), DOI: 10.1103/PhysRevLett.77.3865.
- [81] B. Hammer, L. B. Hansen, and J. K. Nørskov: *Improved Adsorption Energetics within Density-Functional Theory Using Revised Perdew-Burke-Ernzerhof Functionals*. Phys. Rev. B **59**, 7413 (1999), DOI: 10.1103/PhysRevB.59.7413.
- [82] M. Born, E. Wolf, A. B. Bhatia, P. C. Clemmow, D. Gabor, A. R. Stokes, A. M. Taylor, P. A. Wayman, and W. L. Wilcock: *Principles of Optics: Electromagnetic Theory of Propagation, Interference and Diffraction of Light*. Cambridge, New York: Cambridge University Press (1999).

- [83] F. Nickel: *Untersuchung von Photochromen Molekülen Auf Oberflächen Mit Differentieller Reflexions-Spektroskopie*. Master thesis. Freie Universität Berlin, Germany (2013).
- [84] O. S. Heavens: *Optical Properties of Thin Solid Films*. New York: Dover Books on Physics (1991).
- [85] W. N. Hansen: *Electric Fields Produced by the Propagation of Plane Coherent Electromagnetic Radiation in a Stratified Medium*. J. Opt. Soc. Am. **58**, 380 (1968), DOI: 10.1364/JOSA.58.000380.
- [86] J. D. E. McIntyre and D. E. Aspnes: *Differential Reflection Spectroscopy of Very Thin Surface Films*. Surface Science **24**, 417 (1971), DOI: 10.1016/0039-6028(71)90272-X.
- [87] R. Forker and T. Fritz: *Optical Differential Reflectance Spectroscopy of Ultrathin Epitaxial Organic Films*. Phys. Chem. Chem. Phys. **11**, 2142 (2009), DOI: 10.1039/B814628D.
- [88] R. Forker: *Electronic Coupling Effects and Charge Transfer between Organic Molecules and Metal Surfaces*. PhD thesis. Technische Universität Dresden, Germany (2010).
- [89] E. D. Palik: *Handbook of Optical Constants of Solids. Vol. 3*. London: Academic Press (1998).
- [90] M. Bernien, H. Naggert, L. M. Arruda, L. Kipgen, F. Nickel, J. Miguel, C. F. Hermanns, A. Krüger, D. Krüger, E. Schierle, E. Weschke, F. Tuczek, and W. Kuch: *Highly Efficient Thermal and Light-Induced Spin-State Switching of an Fe(II) Complex in Direct Contact with a Solid Surface*. ACS Nano **9**, 8960 (2015), DOI: 10.1021/acsnano.5b02840.
- [91] P. B. Johnson and R. W. Christy: *Optical Constants of the Noble Metals*. Phys. Rev. B **6**, 4370 (1972), DOI: 10.1103/PhysRevB.6.4370.
- [92] M. R. Weiss, R. Follath, K. J. S. Sawhney, F. Senf, J. Bahrtdt, W. Frentrup, A. Gaupp, S. Sasaki, M. Scheer, H. C. Mertins, D. Abramsohn, F. Schäfers, W. Kuch, and W. Mahler: *The Elliptically Polarized Undulator Beamlines at BESSY II*. Nuclear Instruments and Methods in Physics Research Section A: Accelerators, Spectrometers, Detectors and Associated Equipment **467-468**, 449 (2001), DOI: 10.1016/S0168-9002(01)00355-2.

- [93] K. J. S. Sawhney, F. Senf, M. Scheer, F. Schäfers, J. Bahrddt, A. Gaupp, and W. Gudat: *A Novel Undulator-Based PGM Beamline for Circularly Polarised Synchrotron Radiation at BESSY II*. Nuclear Instruments and Methods in Physics Research Section A: Accelerators, Spectrometers, Detectors and Associated Equipment **390**, 395 (1997), DOI: 10.1016/S0168-9002(97)00402-6.
- [94] Jens Als-Nielsen and D. McMorrow: *Elements of Modern Xray Physics*. Hoboken: John Wiley & Sons, Ltd (2011).
- [95] M. Bernien: *X-Ray Absorption Spectroscopy of Fe Complexes on Surfaces*. PhD thesis. Freie Universität Berlin, Germany (2010).
- [96] C. F. Hermanns: *X-Ray Absorption Studies of Metalloporphyrin Molecules on Surfaces*. PhD thesis. Freie Universität Berlin, Germany (2013).
- [97] M. Herder, M. Utecht, N. Manicke, L. Grubert, M. Pätzelt, P. Saalfrank, and S. Hecht: *Switching with Orthogonal Stimuli: Electrochemical Ring-Closure and Photochemical Ring-Opening of Bis(Thiazolyl)Maleimides*. Chem. Sci. **4**, 1028 (2013), DOI: 10.1039/C2SC21681G.
- [98] M. Herder, B. M. Schmidt, L. Grubert, M. Pätzelt, J. Schwarz, and S. Hecht: *Improving the Fatigue Resistance of Diarylethene Switches*. J. Am. Chem. Soc. **137**, 2738 (2015), DOI: 10.1021/ja513027s.
- [99] K. Heister, M. Zharnikov, M. Grunze, L. S. O. Johansson, and A. Ulman: *Characterization of X-Ray Induced Damage in Alkanethiolate Monolayers by High-Resolution Photoelectron Spectroscopy*. Langmuir **17**, 8 (2001), DOI: 10.1021/1a001101d.
- [100] P. Feulner, T. Niedermayer, K. Eberle, R. Schneider, D. Menzel, A. Baumer, E. Schmich, A. Shaporenko, Y. Tai, and M. Zharnikov: *Strong Temperature Dependence of Irradiation Effects in Organic Layers*. Phys. Rev. Lett. **93**, 178302 (2004), DOI: 10.1103/PhysRevLett.93.178302.
- [101] B. L. Feringa and W. R. Browne, eds. *Molecular Switches*. Weinheim: Wiley-VCH, 2011. DOI: 10.1002/9783527634408.
- [102] R. Klajn: *Spiropyran-Based Dynamic Materials*. Chem. Soc. Rev. **43**, 148 (2014), DOI: 10.1039/C3CS60181A.
- [103] E. Pottier, R. Dubest, R. Guglielmetti, P. Tardieu, A. Kellmann, F. Tfibel, P. Levoir, and J. Aubard: *Effets de Substituant, d'hétéroatome et de Solvant Sur Les Cinétiques de Décoloration Thermique et Les Spectres d'absorption de Photomérocyanines En Série Spiro[Indoline-Oxazine]*. Helv. Chim. Acta **73**, 303 (1990), DOI: 10.1002/hlca.19900730210.

- [104] A. K. Chibisov and H. Görner: *Photoprocesses in Spiropyran-Derived Merocyanines*. J. Phys. Chem. A **101**, 4305 (1997), DOI: 10.1021/jp962569l.
- [105] H. Görner: *Photoprocesses in Spiropyrans and Their Merocyanine Isomers: Effects of Temperature and Viscosity*. Chem. Phys. **222**, 315 (1997), DOI: 10.1016/S0301-0104(97)00205-X.
- [106] H. Görner: *Photochemical Ring Opening in Nitrospiropyrans: Triplet Pathway and the Role of Singlet Molecular Oxygen*. Chem. Phys. Lett. **282**, 381 (1998), DOI: 10.1016/S0009-2614(97)01256-6.
- [107] A. K. Chibisov and H. Görner: *Photochromism of Spirobenzopyranindolines and Spironaphthopyranindolines*. Phys. Chem. Chem. Phys. **3**, 424 (2001), DOI: 10.1039/B007713P.
- [108] H. Görner: *Photochromism of Nitrospiropyrans: Effects of Structure, Solvent and Temperature*. Phys. Chem. Chem. Phys. **3**, 416 (2001), DOI: 10.1039/B007708I.
- [109] N. A. Voloshin, A. V. Chernyshev, A. V. Metelitsa, I. M. Raskita, E. N. Voloshina, and V. I. Minkin: *Spiropyrans and Spirooxazines. 3. Synthesis of Photochromic 5-(4,5-Diphenyl-1,3-Oxazol-2-yl)-Spiro[Indoline-2,3-Naphtho[2,3-b]Pyran]*. Russ. Chem. Bull. **54**, 705 (2005), DOI: 10.1007/s11172-005-0308-2.
- [110] C. Bronner, G. Schulze, K. J. Franke, J. I. Pascual, and P. Tegeder: *Switching Ability of Nitro-Spiropyran on Au(111): Electronic Structure Changes as a Sensitive Probe during a Ring-Opening Reaction*. J. Phys.: Condens. Matter **23**, 484005 (2011), DOI: 10.1088/0953-8984/23/48/484005.
- [111] C. R. Ast and H. Höchst: *Fermi Surface of Bi(111) Measured by Photoemission Spectroscopy*. Phys. Rev. Lett. **87**, 177602 (2001), DOI: 10.1103/PhysRevLett.87.177602.
- [112] P. Hofmann: *The Surfaces of Bismuth: Structural and Electronic Properties*. Progress in Surface Science **81**, 191 (2006), DOI: 10.1016/j.progsurf.2006.03.001.
- [113] S. Xiao, D. Wei, and X. Jin: *Bi(111) Thin Film with Insulating Interior but Metallic Surfaces*. Phys. Rev. Lett. **109**, 166805 (2012), DOI: 10.1103/PhysRevLett.109.166805.
- [114] N. P. Ernstring and T. Arthen-Engeland: *Photochemical Ring-Opening Reaction of Indolinespiropyrans Studied by Subpicosecond Transient Absorption*. J. Phys. Chem. **95**, 5502 (1991), DOI: 10.1021/j100167a027.



- [115] F. Liu, Y. Kurashige, T. Yanai, and K. Morokuma: *Multireference Ab Initio Density Matrix Renormalization Group (DMRG)-CASSCF and DMRG-CASPT2 Study on the Photochromic Ring Opening of Spiropyran*. J. Chem. Theory Comput. **9**, 4462 (2013), DOI: 10.1021/ct400707k.
- [116] S. Prager, I. Burghardt, and A. Dreuw: *Ultrafast C-Spiro-O Dissociation via a Conical Intersection Drives Spiropyran to Merocyanine Photo-switching*. J. Phys. Chem. A **118**, 1339 (2014), DOI: 10.1021/jp4088942.
- [117] C. Slavov, N. Bellakbil, J. Wahl, K. Mayer, K. Rück-Braun, I. Burghardt, J. Wachtveitl, and M. Braun: *Ultrafast Coherent Oscillations Reveal a Reactive Mode in the Ring-Opening Reaction of Fulgides*. Phys. Chem. Chem. Phys. **17**, 14045 (2015), DOI: 10.1039/C5CP01878A.
- [118] G. Gliemeroth and K.-H. Mader: *Phototropic Glass*. Angew. Chem. Int. Ed. **9**, 434 (1970), DOI: 10.1002/anie.197004341.
- [119] J. C. Crano, T. Flood, D. Knowles, A. Kumar, and G. B. Van: *Photochromic Compounds: Chemistry and Application in Ophthalmic Lenses*. Pure Appl. Chem. **68**, 1395 (1996), DOI: 10.1351/pac199668071395.
- [120] A. K. Chibisov and H. Görner: *Photoprocesses in Spirooxazines and Their Merocyanines*. J. Phys. Chem. A **103**, 5211 (1999), DOI: 10.1021/jp984822i.
- [121] M. K. Siddiqui, G. Corthey, S. A. Hayes, A. Rossos, D. S. Badali, R. Xian, R. Scott Murphy, B. J. Whitaker, and R. J. Dwayne Miller: *Synchronised Photoreversion of Spirooxazine Ring Opening in Thin Crystals to Uncover Ultrafast Dynamics*. CrystEngComm **18**, 7212 (2016), DOI: 10.1039/C6CE01049K.





## DRS Setup Details

### A.1 Pictures of the Setup

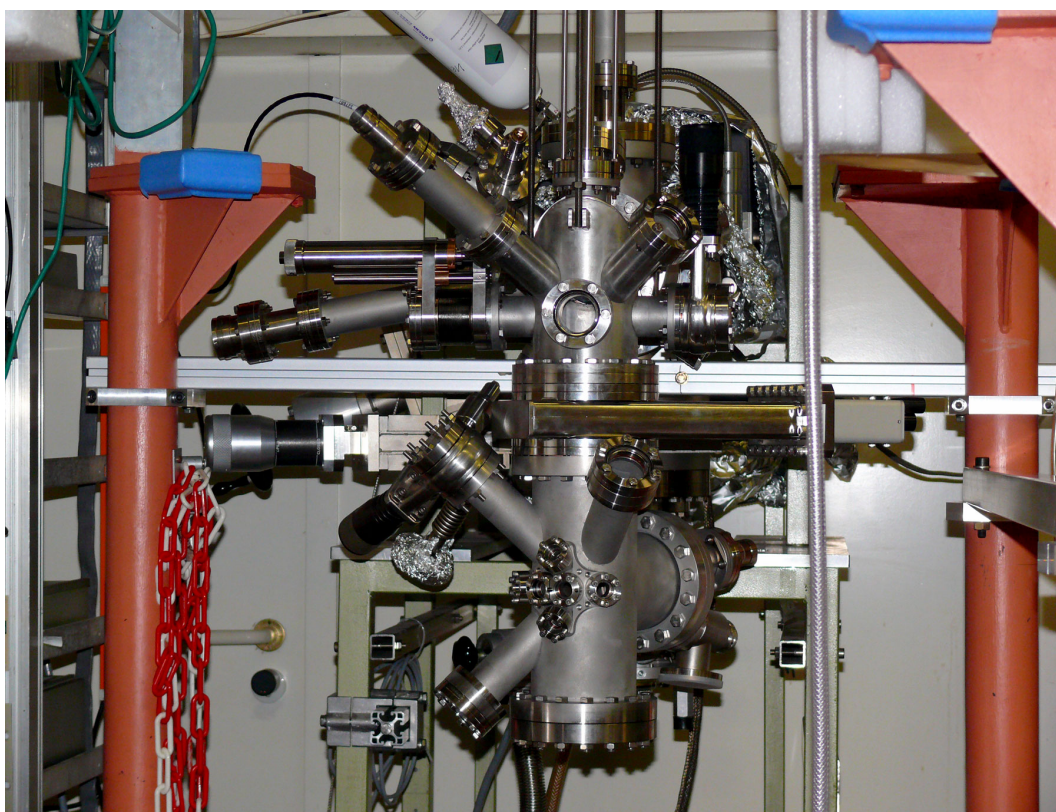


**Figure A.1:** Front view on the UHV chamber body. The top part enables preparation and sample exchange (only a sputter gun is mounted in this picture). The bottom part below a CF100 valve is the measurement part. Six CF16 windows point towards the measurement sample holder for a flexible setup of the optical components. Three additional CF40 flanges allow mounting of equipment such as evaporators. The sample holder base is inserted from the CF100 flange on the very bottom of the chamber.

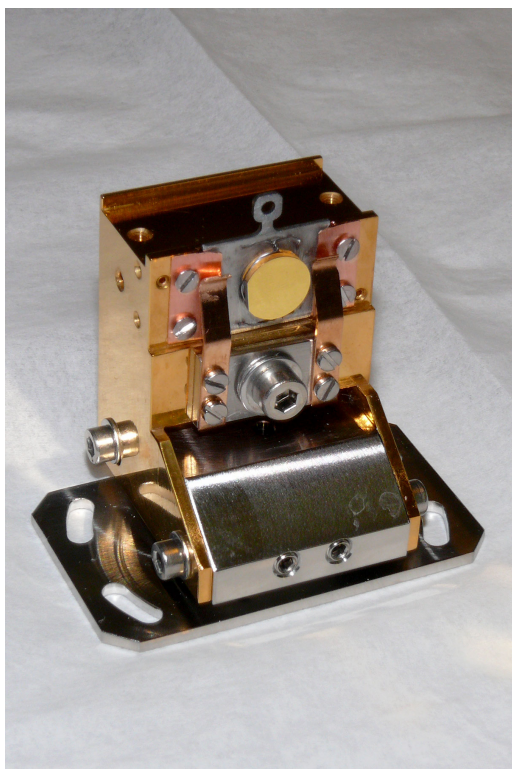


**Figure A.2:** Sample holder copper block with spring mechanism and no other functions mounted. A five axes (*ex situ*) manipulation is possible.

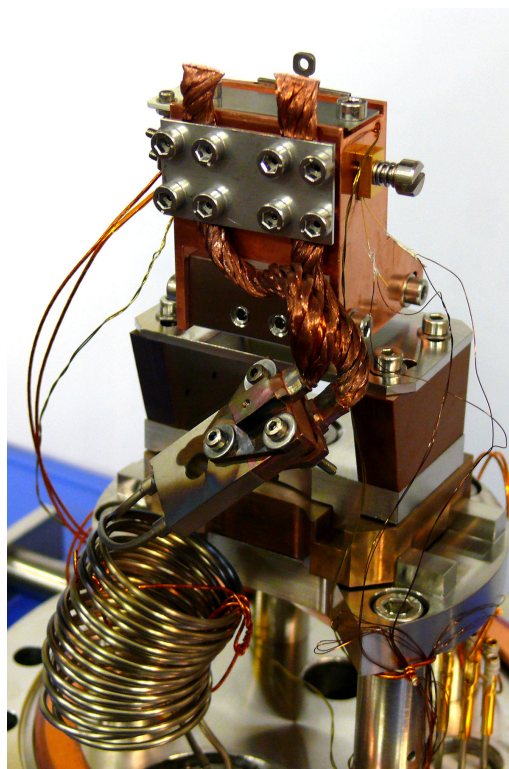


**Figure A.3:** Back-view on the fully-equipped sample holder. Temperature diode, heat exchanger with cooling strands, heating plate.

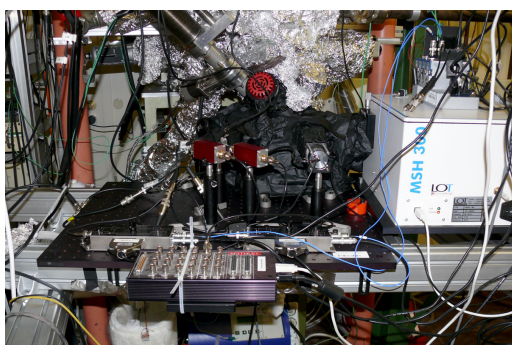


**Figure A.4:** Overview of measurement equipment. The optical components are in addition to a light-covering tube wrapped in black-anodized aluminum foil to block completely remaining light.



**Figure A.5:** Optical components on UHV chamber. Two LEDs (in red the high-power UV LED and on the left side the red-light LED) are equipped and both PMTs are connected.



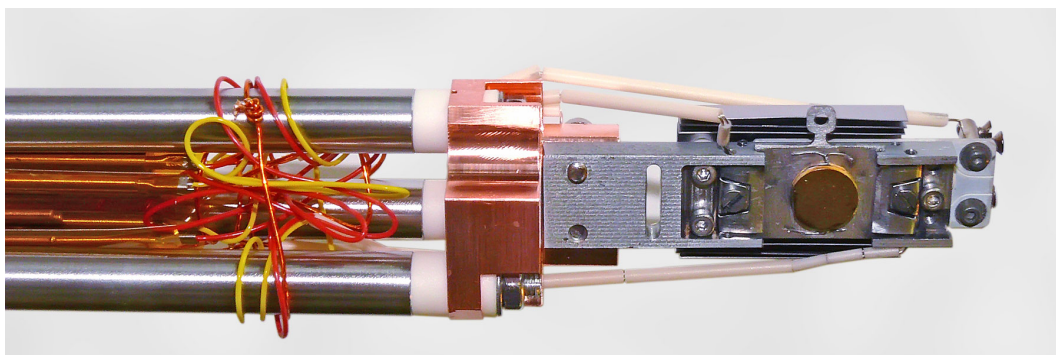


**Figure A.6:** Sample heater in the preparation part of the UHV chamber. It mainly consists of an Omicron sample-plate holder mounted in front of a boron nitride heater. Heating is achieved through thermal radiation and two thermocouples are mounted next to the holder. Temperatures above 900 K can be achieved. All connections are mounted on a CF16 military plug for an easy and stable usage.

The CAD drawings are available upon request at the AG Kuch. The figures above illustrate the UHV setup of the home-made main components, which have been built from scratch. Several additional hardware parts such as the construction to mount the optics or the load-lock are not shown.

## A.2 Software

The DRS setup is controlled by several LabView programs. These programs mostly operate independently, e.g., to log the temperature or the pressure. Through these *microservice-like* software infrastructures, independent debugging and the exchange of components is possible. Screenshots of the programs are provided in the following figures.

Special attention was paid to the automation of the setup. Due to the possibility of long measurement times, many variables had to be considered and led to a complex list of features, some examples of which are as follows:

- Measurements
  - Different measurement regions for spectra (e.g. different amplification)
  - Macros defined in text files
  - Ability of all possible measurements or commands to be used in macros
  - Full log, printable for lab book
  - Project and experiment organization (e.g., using the same settings for the full project such as a combination of molecule and substrate)
  - Live view of recorded data
  - Three measurement types:
    1. Wavelength-dependent spectrum
    2. Constant wavelength
    3. Measurement of single wavelength points
  - Integrated temperature control
  - Integrated LED control
  - Integrated PMT control
- Monochromator control
  - Full control over wavelengths and settings
  - Automatic selection of light source
  - Blocking the light when not needed
- PMT control

- Locally (through user interface) or globally (e.g., through measurement program) controllable
  - Ramping of control voltage while checking for overflow or exceedingly high currents
  - Control of Femto's amplification
- Temperature control
  - Flexible live view on temperature graph
  - Permanent logging
  - Readout of silicon temperature diode and two K-type thermocouples
  - PID control with variable PID parameters (necessary due to different heating and cooling powers at different temperatures)
  - Independent hardware- and software protection measures
- LED and shutter control
  - Control of two LED channels
  - Independent software protection measures to avoid operating LED and PMTs simultaneously (PMTs would be destroyed by this)
  - Shutters closed when no measurement is active
  - Customizable delay times for turning on the LED after shutter closure and vice versa.

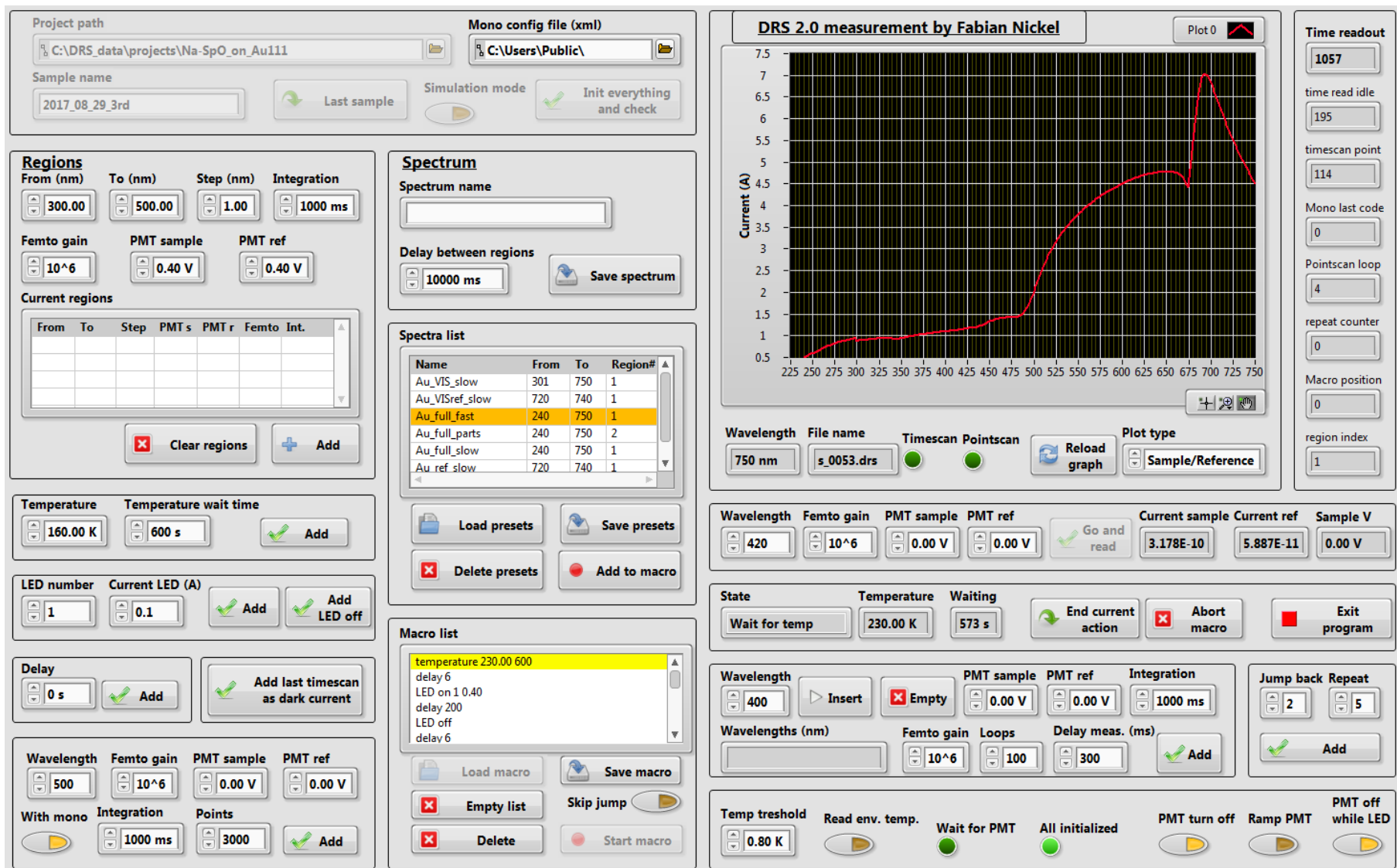
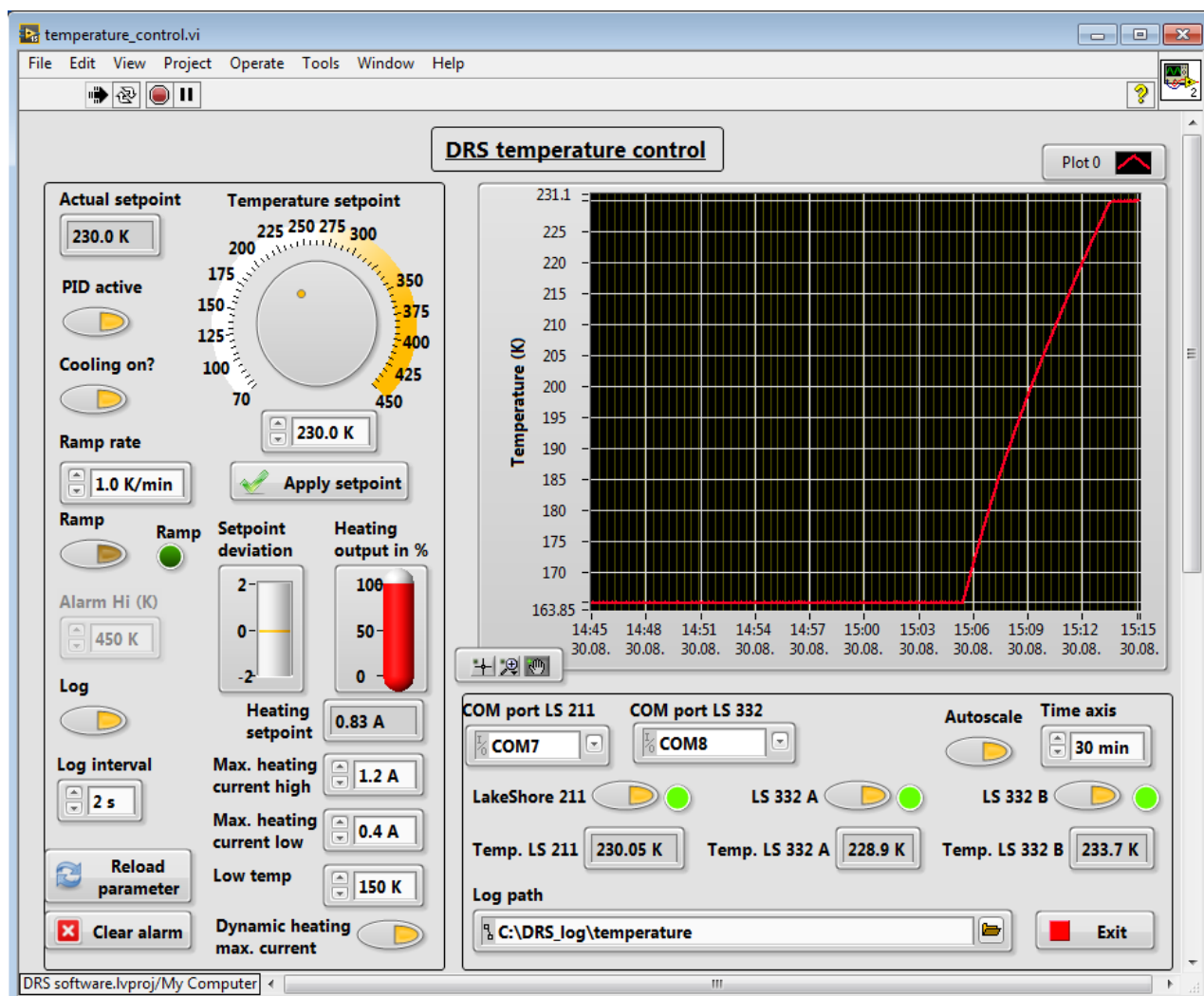
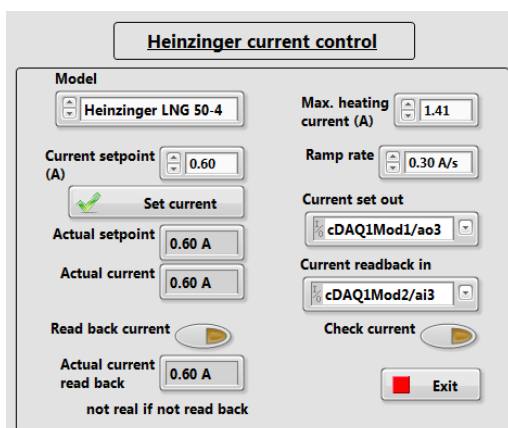


Figure A.7: LabView program to measure DRS. Features as described previously are included and a fully automatic control is achieved.



**Figure A.8:** LabView program to permanently control the sample holder temperature. Ramps, setpoints, logs, and protection measures are implemented.



**Figure A.9:** Control of the heating current of the Heinzinger analog power supply. A ramp of the current is automatically applied.

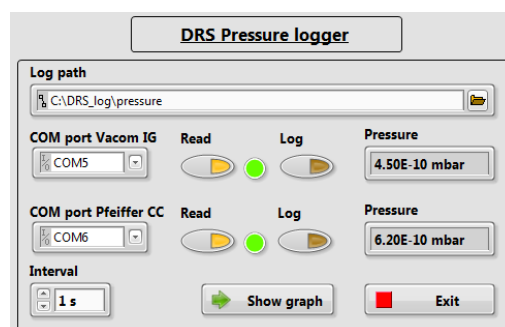


**Figure A.10:** Pressure logger for both UHV gauges inside the preparation and measurement chamber.

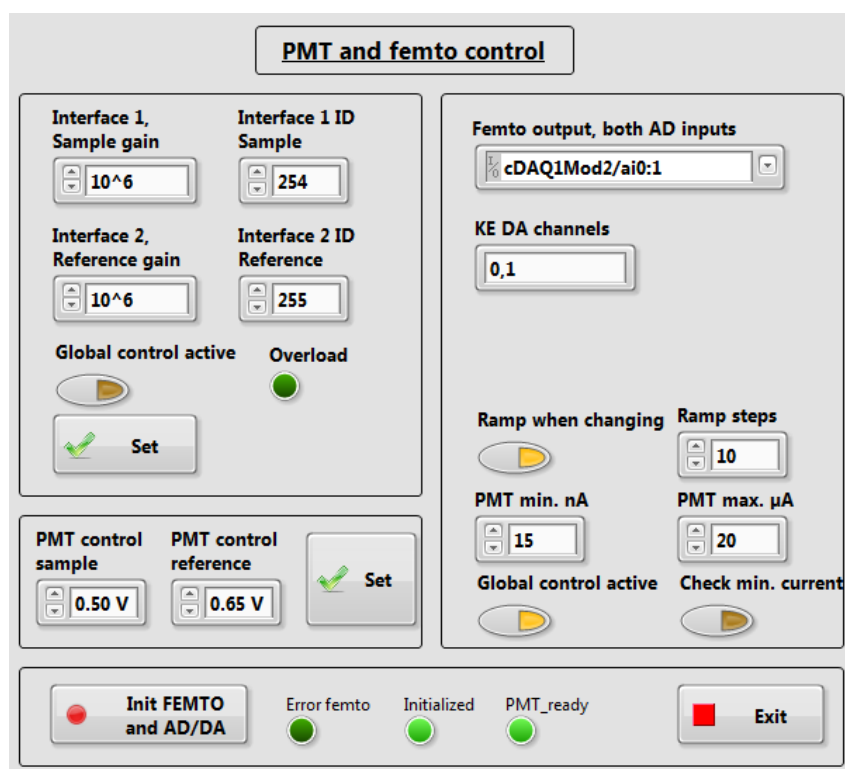


**Figure A.11:** Control of PMTs and Femto amplifier. Several protection measures are implemented to protect the PMTs.



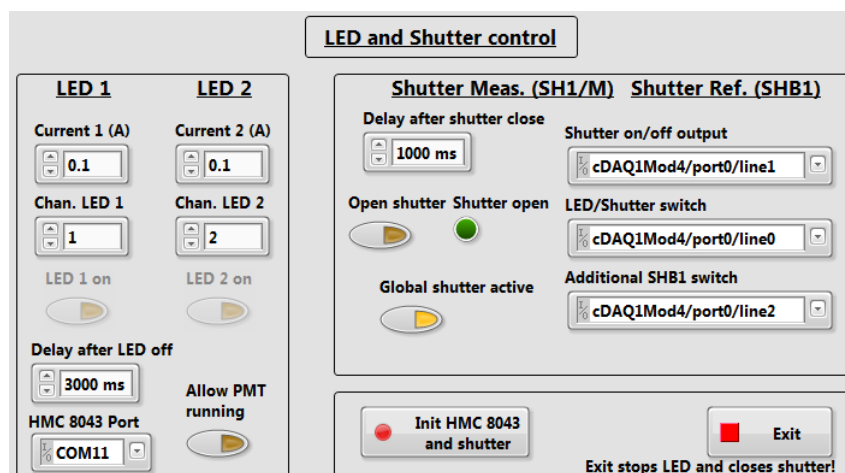


**Figure A.12:** Control of LEDs and shutters in front of both PMTs. There are several software protections (in addition to a hardware safety box) to ensure that no LED can be active while the shutters might be open.



## XA Measurement Software

### B.1 XA Measurement Program

The data acquisition of XA at the BESSY synchrotron in the past has been very slow. Many steps were performed manually. To save time and reduce the number of possible human errors, a measurement program was created for this work to control the beamline, chamber, and data acquisition.

The features include:

- Beamline control
  - Set photon energy directly
  - Control PSD (at dipole PM3)
  - Control offset and slope (for circular polarization on undulator beamlines)
- Spectra recording
  - Keithley settings accessible
  - Saving of spectrum presets
- Time-dependent spectra at static energy
  - Including record of temperature
- Recording of additional parameters
  - Temperature (before and after spectrum by self-built relay box)
  - Beamline properties as provided by BESSY EMC protocol
  - Saving of motor positions (see following section)
- Log
  - Queue for spectra to be recorded
  - Printable log for lab book

- Log viewer for quick access of logs
- Comments for attachment to the log
- Control of a home-made pneumatic shutter to reduce x-ray influence.

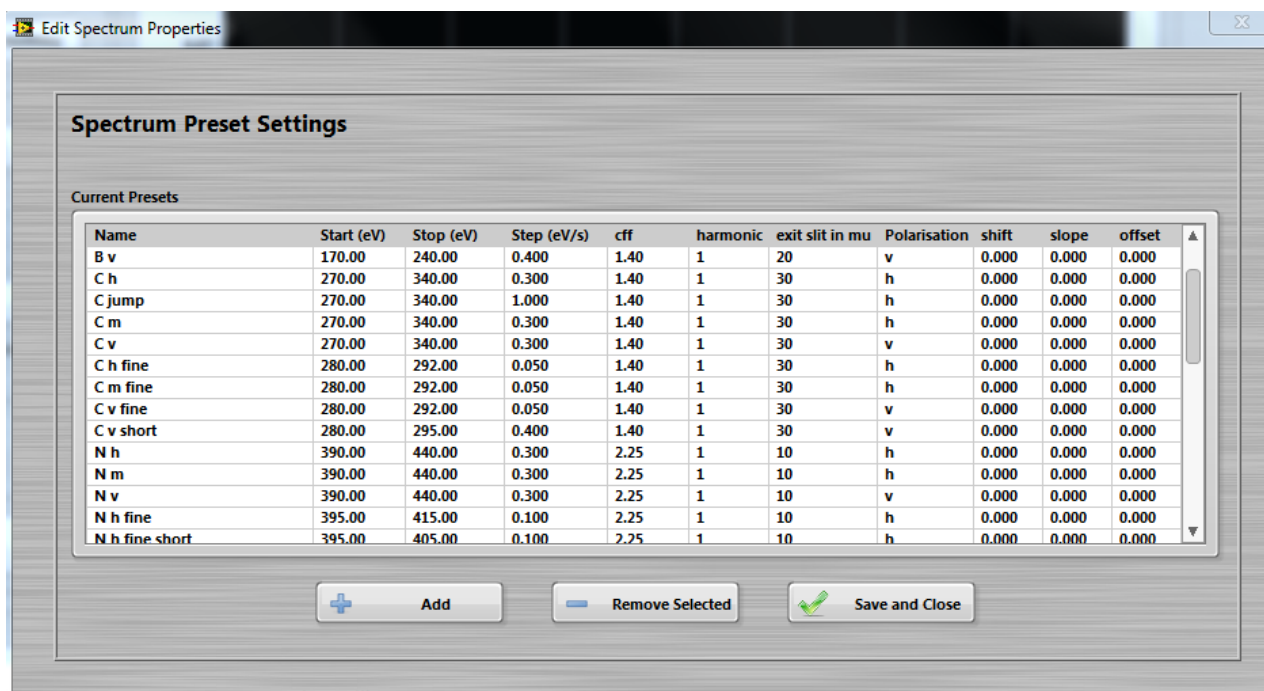


**Figure B.1:** Settings for the spectra presets to be selected in the main program for a measurement.

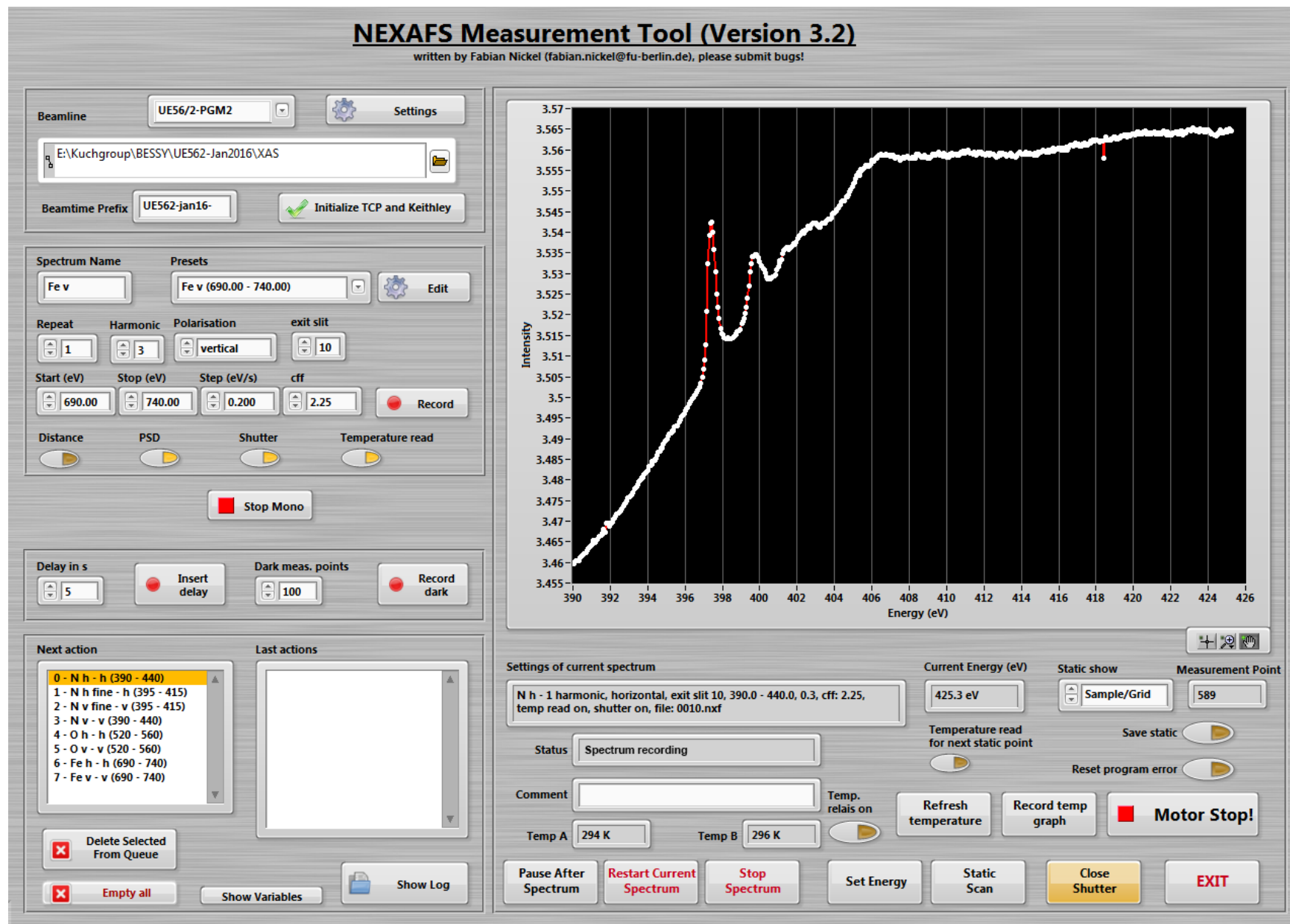


Figure B.2: Complete LabView program to measure XA on different beamlines at BESSY in a mostly automated way.

## B.2 Motor Control

As with the new XA measurement process, in order to improve reliability and efficiency, a new motor control for the described chamber used at the synchrotron radiation source was built. The controller SMCI35 from Nanotec Electronic GmbH & CO KG, assembled in a distinct housing for five axes, was used, which can be controlled by a self-made LabView program. Besides the lower price compared to solutions provided by the manipulator manufacturer, this new motor control has the advantage of easier integration with the previously-described LabView measurement program. For all measurements, the motor positions were recorded and (in principle, though without final integration) automatized control of the sample position through the measurement program became feasible. This recording enabled features such as the creation of maps of a sample by automatized scanning and evaluation of absorption edge jumps. The home-made x- and y-motor supports additionally use highly accurate gauges of type Mahr MarCator 1086 R to encode the exact position of the manipulator.

The features of the motor control are:

- Highly accurate control of motor positions
- Driving shortest way (for circular movement of manipulator)
- Persistent motor positions (no need for repeating reference drives and readouts)
- Automatic read-out and recalibration through x/y axes gauges
- Safety by reading sample current using a Keithley (stop when current overflows, occurs when the sample touches the chamber and the amplifier is in a sensitive range)
- Continuous logging of every motor position, saved among others by the measurement program.

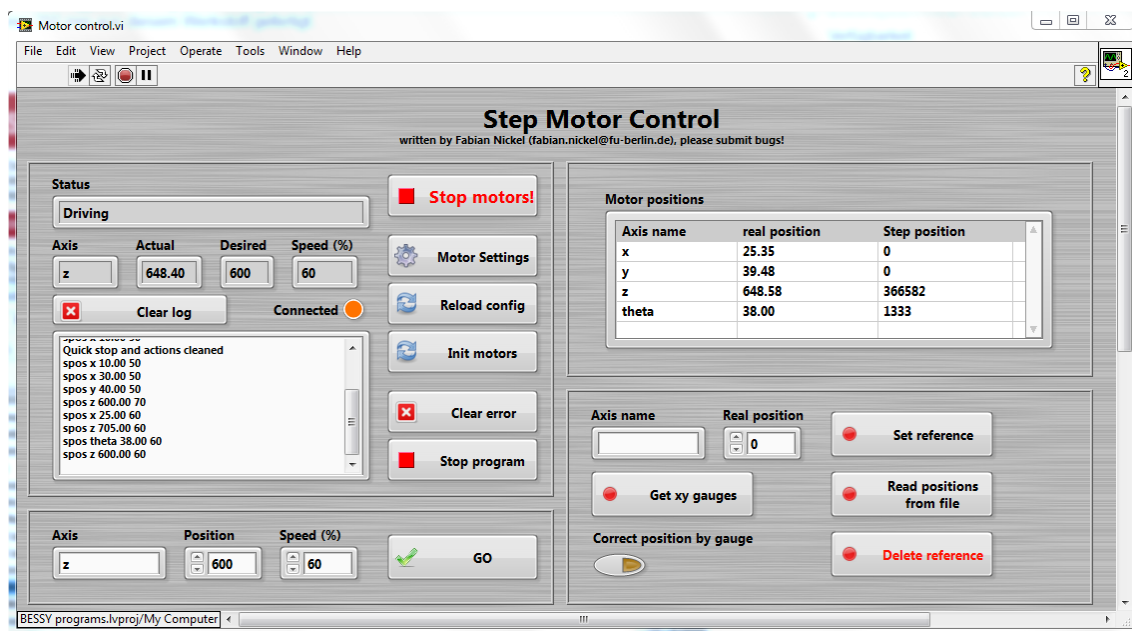


**Figure B.3:** Motor control LabView program used with the home-made UHV chamber to control all five axes.





# Acknowledgments

---

First and most important, I want to thank *Prof. Dr. Wolfgang Kuch* for supervising my thesis work. It has been a pleasure to receive this great support during the time of my work in your group. The possibility to build new equipment and even an entire experiment was exceptional to me and helped me greatly to gather knowledge in various fields.

I also thank *Prof. Dr. Martin Weinelt* for his willingness to co-assess this thesis and his kind interest in the topics addressed by my work.

I want to thank *Dr. Matthias Bernien* for his huge support during the whole time of my PhD work. I am indebted to him for all his great contributions to the fields covered in this thesis and to our hours of fruitful discussions. The sharing of his incredible knowledge about ultrahigh-vacuum and mathematica programming was fundamental to parts of my work.

Before, during, and after beamtimes has always been an intense time. I would like to thank all the people involved in preparations and executions of these beamtimes at BESSY, especially my PhD colleagues *Lucas Arruda and Lalminthang Kipgen*, with whom I shared most beamtimes. The help of *Dr. Andrew Britton and Dr. Jorge Miguel* during beamtime and in the lab was also important in order to succeed with the synchrotron measurements.

*Dennis Krüger, Kai Kraffert, Sandro Wrzalek, and Pantelis Chittas* have been wonderful students writing their bachelor or master theses in the field of x-ray studies of photochromic molecules on surfaces under my supervision and contributed to this work. Within the same topic, but using the differential reflectance setup, I would like to thank *Lukas Kemmler and Janina Drauschke* for their work in the lab, setting up and testing the new experiment and writing their bachelor theses about it. There have been numerous other students working in our group, especially during beamtimes, to whom I am also grateful.

For the sound collaboration about diaryethene switches on surfaces, I would like to thank *Dr. Martin Herder and Prof. Dr. Stefan Hecht*. I would like to thank *Holger Naggert* for doing hard work in the chemistry lab to provide great spin-crossover molecules and even attending in beamtimes. I also would like to thank *Prof. Dr. Felix Tuczek* and his group for their effort in providing great molecules. For proof-reading the most recent publications and discussions about their results and upcoming experiments, I

would like to thank *Ivar Kumberg*. I wish you and the new generation of PhD students prolific experiments! I am indebted to *Dr. Alex Krüger* and *Dr. Felix Hermanns* for their guidance to the field of adsorbed molecules on surfaces. I greatly enjoyed my time in the university, not least because of *Dr. Yasser Shokr*, with whom I shared an office for a long time. Our discussions in (at least perceived) all areas of life were legendary. I am also grateful to *Dr. Evangelos Golias*, who joined the office for the last year. I enjoyed discussions with you and learning about your work.

I would like to thank the whole AG Kuch for their continuous support and the pleasant working atmosphere. Thanks to *Oliver, Ismet, Tauqir, Jiaming, Till, Bin, Yin-Ming*, and many other guests and visiting scientists in the last years.

For the amazing work in designing UHV parts and contributing ideas to the work on the DRS, I would like to thank *Uwe Lipowski*. I would also like to thank *Detlef Müller*, representative of the team of the 'Feinwerktechnik'. Their quick and reliable manufacturing and consulting was essential to the buildup of the new experiment.

For the support at BESSY, I would like to thank all BESSY people who were involved! *Dr. Eugen Weschke* and *Dr. Enrico Schierle* provided great support for the many UE46-beamtimes and I would like to thank *Dr. Willy Mahler* and *Birgitt Zada* for their technical support during UE56/2 beam-times. I would also like to thank *Prof. Dr. Klaus Hermann* for his quick and administrable help with questions about the StoBe code.

For their non-scientific support in the AG Kuch and in the SFB 658 I would like to thank *Marion Badow, Irmhild Wegener, and Dr. Christian Frischkorn*. Marion, you always backed me up with all university issues and difficulties. I highly appreciate the sound support through the Sfb 658 during my studies. The many other service groups in the university, namely the *Elektronik, ZEDV of the department of physics, and ZEDAT (especially the HPC group!)*, contributed through their organized and quick help.

Finally, I would like to express my deepest gratitude to my parents *Kerstin and Wolfgang*, my brother *Clemens*, and my partner *Alina* for their extensive support over the duration of my studies and especially during the recent year of PhD work.

# Curriculum Vitae

---

Mein Lebenslauf wird aus Gründen des Datenschutzes in der elektronischen Fassung meiner Arbeit nicht veröffentlicht.

## Publications

1. L. Kipgen, M. Bernien, S. Ossinger, F. Nickel, A. J. Britton, L. M. Arruda, H. Naggert, Chen Luo, C. Lotze, H. Ryll, F. Radu, E. Schierle, E. Weschke, F. Tuczek, and W. Kuch:  
*Evolution of Cooperativity in the Spin Transition of an Fe(II) Complex on a Graphite Surface*  
Nat. Commun. 9, 2984 (2018). DOI: <https://doi.org/10.1038/s41467-018-05399-8>
2. F. Nickel, M. Bernien, D. Krüger, J. Miguel, A. J. Britton, L. M. Arruda, L. Kipgen, and W. Kuch:  
*Highly Efficient and Bidirectional Reversible Photochromism of Spirooxazine on Au(111)*  
J. Phys. Chem. C. 122, 8031 (2018). DOI: <https://doi.org/10.1021/acs.jpcc.8b02220>
3. F. Nickel, M. Bernien, U. Lipowski, and W. Kuch:  
*Optical differential reflectance spectroscopy for photochromic molecules on solid surfaces*  
Rev. Sci. Instrum. 89, 033113 (2018). DOI: <https://doi.org/10.1063/1.5019415>
4. F. Nickel, M. Bernien, K. Kraffert, D. Krüger, L. M. Arruda, L. Kipgen, and W. Kuch:  
*Reversible Switching of Spiropyran Molecules in Direct Contact With a Bi(111) Single Crystal Surface*  
Adv. Funct. Mater. 27, 1702280 (2017). DOI: <https://doi.org/10.1002/adfm.201702280>
5. L. Kipgen, M. Bernien, F. Nickel, H. Naggert, A. J. Britton, L. M. Arruda, E. Schierle, E. Weschke, F. Tuczek, and W. Kuch *Soft-x-ray-induced spin-state switching of an adsorbed Fe(II) spin-crossover complex*  
J. Phys.: Condens. Matter 29, 394003 (2017). DOI: <https://doi.org/10.1088/1361-648X/aa7e52>
6. F. Nickel, M. Bernien, M. Herder, S. Wrzalek, P. Chittas, K. Kraffert, L. M. Arruda, L. Kipgen, D. Krüger, S. Hecht, and W. Kuch *Light-induced photoisomerization of a diarylethene molecular switch on solid surfaces*  
J. Phys.: Condens. Matter 29, 374001 (2017). DOI: <https://doi.org/10.1088/1361-648X/aa7c57>

7. S. Ossinger, H. Naggert, L. Kipgen, T. Jasper-Toennies, A. Rai, J. Rudnik, F. Nickel, L. M. Arruda, M. Bernien, W. Kuch, R. Berndt, and F. Tuzcek *Vacuum-Evaporable Spin-Crossover Complexes in Direct Contact with a Solid Surface: Bismuth versus Gold* J. Phys. Chem. C 121, 1210 (2017). DOI: <https://doi.org/10.1021/acs.jpcc.6b10888>
8. P. Stoll, M. Bernien, D. Rolf, F. Nickel, Q. Xu, C. Hartmann, T. R. Umbach, J. Koppasch, J. N. Ladenthin, E. Schierle, E. Weschke, C. Czekelius, W. Kuch, and K. J. Franke *Magnetic anisotropy in surface-supported single-ion lanthanide complexes* Phys. Rev. B 94, 224426 (2016). DOI: <https://doi.org/10.1103/PhysRevB.94.224426>
9. M. Bernien, H. Naggert, L. M. Arruda, L. Kipgen, F. Nickel, J. Miguel, C. F. Hermanns, A. Krüger, D. Krüger, E. Schierle, E. Weschke, F. Tuzcek, and W. Kuch *Highly Efficient Thermal and Light-Induced Spin-State Switching of an Fe(II) Complex in Direct Contact with a Solid Surface* ACS Nano 9, 8960 (2015). DOI: <https://doi.org/10.1021/acsnano.5b02840>
10. H. Naggert, J. Rudnik, L. Kipgen, M. Bernien, F. Nickel, L. M. Arruda, W. Kuch, C. Näther, and F. Tuzcek *Vacuum-evaporable spin-crossover complexes: physicochemical properties in the crystalline bulk and in thin films deposited from the gas phase* J. Mater. Chem. C 3, 7870 (2015). DOI: <https://doi.org/10.1039/C5TC00930H>
11. T. R. Umbach, M. Bernien, C. F. Hermanns, L. L. Sun, H. Mohrmann, K. E. Hermann, A. Krüger, N. Krane, Z. Yang, F. Nickel, Y.-M. Chang, K. J. Franke, J. I. Pascual, and W. Kuch *Site-specific bonding of copper adatoms to pyridine end groups mediating the formation of two-dimensional coordination networks on metal surfaces* Phys. Rev. B 89, 235409 (2014). DOI: <https://doi.org/10.1103/PhysRevB.89.235409>
12. T. G. Gopakumar, M. Bernien, H. Naggert, F. Matino, C. F. Hermanns, A. Bannwarth, S. Mühlenberend, A. Krüger, D. Krüger, F. Nickel, W. Walter, R. Berndt, W. Kuch, and F. Tuzcek *Spin Crossover Complex on Au(111): Structural and Electronic Differences Between Mono- and Multilayers* Chem. Eur. J. 19, 15702 (2013). DOI: <https://doi.org/10.1002/chem.201302241>





# Selbstständigkeitserklärung

---

Hiermit versichere ich, die vorliegende Dissertation eigenständig und ausschließlich unter Verwendung der angegebenen Quellen und Hilfsmittel angefertigt zu haben. Die vorliegende Arbeit ist in dieser oder anderer Form zuvor nicht als Prüfungsarbeit zur Begutachtung vorgelegt worden.

Berlin, den

Fabian Nickel